The Role of the Aryl Hydrocarbon Receptor in *Helicobacter pylori* Infection

Supervised by

Dr Francesco Boccellato

This thesis has been submitted to the Nuffield Department of Medicine, University of Oxford in partial fulfilment of the requirements for the degree of Doctor of Philosophy in Clinical Medicine.

Jan Traulsen

Green Templeton College, University of Oxford

Michaelmas Term 2023

Declaration

I declare that this thesis is my own work, and except where otherwise stated, describes my own research. To the best of my knowledge, it contains no material that has been written by another person or previously submitted in the same form as academic work, to this or another university.

The results presented herein are derived from my own experiments, with the exception of Figure 7.1.1 from Dr Francesco Boccellato. Data presented in Chapter 3 were obtained from an experiment performed by Kirstin Hoffmann and Miriam Lohr at the Max Planck Institute for Infection Biology, Berlin, Germany under the supervision of Dr Francesco Boccellato. This includes pathological analysis of tissue samples by Anja Kühl, Charité Berlin. Images in Figure 3.2.3B were created by Miriam Lohr and adapted by me. RNA-sequencing for data presented in 3.2.2.1 was performed by the Oxford Genomics Centre and handling of the raw data of all RNA-sequencing experiments was performed by Dr Pakavarin Louphrasitthiphol, as indicated.

The cell line used to obtain data presented in Figure 4.2.26 was created in part by Sarah Andrews, who assisted in transduction and selection of the cells. The experiments shown in Figure 4.2.26 were performed by Antonia Voli.

Figure 1.1.2 was created by me as part of a published scientific paper (Traulsen, Zagami *et al.*, 2021) and has been included with permission of the co-authors.

Jan Traulsen

Green Templeton College

Michaelmas Term 2023

Acknowledgements

First and foremost, I want to thank Francesco Boccellato for his supervision and guidance throughout my DPhil, for pushing me when deadlines were looming and for supporting me when support was needed. I also want to thank him for the opportunity to conduct research in a stimulating environment, at the beginning of an important new chapter in both of our careers. I would also like to thank Professor Colin Goding for his co-supervision during my DPhil. I am very grateful to my present and former lab members, Antonella D'Amore, Diana Papp, George Maier, Ian McFarlane, Camilla Persi, Anisa Ashraf and Alice Daddi, for their scientific, moral and emotional support, for fun, fruitful discussions and constructive criticism and especially to Claudia Zagami, for always being happy to help, for telling me not to worry, to believe in myself more and for always saying that "it's going to work"! Thank you to all of you for making my time in Oxford so enjoyable, and for being friends both inside and outside the lab. I could not have wished for better colleagues.

I also want to thank Pakavarin Louphrasitthiphol for his collaboration on the RNA-sequencing, for his help and support and for sharing his wisdom and knowledge with me.
Thank you to Yilong Lian and Pedro Moura-Alves, for sharing their knowledge on AHR in particular and on science in general, as well as cell lines and plasmids.

Furthermore, I am very thankful to Professor Brigitta Stockinger and her lab members from the AhRimmunity Laboratory at the Francis Crick Institute, Anke Liebert and Nicola Diny, for generously supplying me with mouse stomach tissue and to Anke for offering her help with my primary cells. Without them, this project would not have been possible.

Sarah, it is impossible to express in a few sentences how much you have helped me, how amazing you have made my time here, how much I have learned from you and how much you have helped me grow as a person. Thank you for always believing in me, for helping me get through this DPhil and for always being there for me, no matter what. I truly could not have done it without you. I am grateful that we found each other.
To Heston and Poppy, for their unconditional love and for never judging me, and only occasionally getting impatient with me, I will always be thankful.

Finally, I want to thank my parents, my sister and my family and friends for their love, support and understanding, even when I decided to leave the country.

I want to especially thank my grandparents, who I wish could have seen me graduate, and who have never been anything but proud of me.

List of Abbreviations

7-ER	7-ethoxyresorufin
A_{560}	Absorption at 560 nm
ADP	Adenosine diphosphate
AHR	Aryl hydrocarbon receptor
AHR-OE	AHR-overexpressing
AHRR	Aryl hydrocarbon receptor repressor
AIP	AHR-interacting protein
ALPK1	Alpha-protein kinase 1
ANOVA	Analysis of variance
ARM	Ankyrin repeat motif
ARNT	AHR nuclear translocator
BHI	Brain-heart infusion
bHLH	Basic helix-loop-helix
BME	Basement membrane extract
bp	Base pairs
BSA	Bovine serum albumin
CagA	Cytotoxin-associated gene A
cagPAI	CAG pathogenicity island A
CD40L	Cluster of differentiation 40 ligand
cDNA	Complementary DNA
CFU	Colony forming units
Cgt	Cholesterol-α-glucosyltransferase
ChIP	Chromatin immunoprecipitation
cIAP	Cellular inhibitor of apoptosis protein
CLR	C-type lectin receptor
CORO1A	Coronin-1A
CPM	Counts per million
CRISPR	Clustered regularly interspaced short palindromic repeats
CUL4B	Cullin 4B
CYP1A1	Cytochrome P450, family 1, subfamily A, polypeptide 1
CYP1A2	Cytochrome P450, family 1, subfamily A, polypeptide 2
CYP1B1	Cytochrome P450, family 1, subfamily B, polypeptide
DEG	Differentially expressed gene
dH_2O	Deionised water
DMEM	Dulbecco’s Minimal Eagle Medium

DMSO	Dimethylsulfoxide
DNA	Deoxyribonucleid acid
DRE	Dioxin response element
dsRNA	Double-stranded ribonucleic acid
DTT	Dithiotreitol
ECM	Extracellular matrix
EDTA	Ethylenediaminetetraacetic acid
EF1a	Elongation factor 1-alpha
EGF	Epithelial growth factor
EGFR	Epithelial growth factor receptor
EMT	Epithelial-mesenchymal transition
ER	Estrogen receptor
EROD	Ethoxyresorufin-O-deethylase
FC	Fold change
FFPE	Formalin-fixed paraffin-embedded
FGF-10	Fibroblast growth factor-10
FHA	Forkhead-associated
FICZ	6-Formylindolo[3,2-*b*]carbazole
GFP	Green fluorescent protein
GLM	Generalised log-linear model
GO	Gene ontology
gRNA	Guide RNA
GSEA	Gene set enrichment analysis
H&E	Haematoxylin & eosin
H. pylori	*Helicobacter pylori*
hBD	Human beta-defensin
HEPES	4-(2-hydroxyethyl)-1-piperazineethanesulfonic acid
HIC	High-income countries
HIF1α	Hypoxia inducible factor 1 subunit alpha
HRP	Horseradish peroxidase
HSP90	Heat shock protein 90
I3C	Indole-3-carbinol
IARC	International Agency for Research on Cancer
ICZ	Indolo[3,2-b]carbazole
IDO1	Indoleamine 2,3-dioxygenase 1
IFNGR1	Interferon gamma receptor 1
IFNGR2	Interferon gamma receptor 2

IFN-γ	Interferon-gamma
IKKα	Inhibitor of nuclear factor kappa-B kinase subunit alpha
IKKβ	Inhibitor of nuclear factor kappa-B kinase subunit beta
IKKγ	Inhibitor of nuclear factor kappa-B kinase subunit gamma
IL-10	Interleukin-10
IL-18	Interleukin-18
IL-1β	Interleukin-1 beta
IL-2	Interleukin-2
IL-6	Interleukin-6
IL-8	Interleukin-8
iNOS	Inducible nitric oxide synthase
ITAC	Intestinal-type adenocarcinoma
IκBα	Nuclear factor kappa-light-chain enhancer of activated B-cells inhibitor, alpha
IκBβ	Nuclear factor kappa-light-chain enhancer of activated B-cells inhibitor, beta
IκBε	Nuclear factor kappa-light-chain enhancer of activated B-cells inhibitor, epsilon
kb	Kilobase
KLF6	Krüppel-like factor 6
KO	Knock-out
LMIC	Low and middle income countries
logFC	Log_2(fold change)
LPS	Lipopolysaccharide
LTβ	Lymphotoxin beta
MALT	Mucosa-associated lymphoid tissue
MCS	Multiple cloning site
MOI	Multiplicity of infection
MPIIB	Max Planck Institute for Infection Biology
mRNA	Messenger ribonucleid acid
MUC5AC	Mucin-5AC
MUC6	Mucin-6
MW	Molecular weight
N.B.	Nota bene
NADPH	Nicotinamide adenine dinucleotide phosphate, reduced form
NEB	New England Biolabs
NEMO	NF-kappa-B essential modulator

NES	Nuclear export sequence
NF-κB	Nuclear factor kappa-light-chain enhancer of activated B-cells
NI	Non-infected
NIK	NF-κB-inducing kinase
NK	Natural killer
NLR	NOD-like receptor
NLS	Nuclear localisation sequence
NOD1	Nucleotide-binding oligomerization domain-containing protein 1
NOD2	Nucleotide-binding oligomerization domain-containing protein 2
ns	Not significant
NT	Non-treated
OCT4	Octamer-binding transcription factor 4
OD_{550}	Optical density at 550 nm
OD_{600}	Optical density at 600 nm
p.i.	Post infection
PAMP	Pathogen-associated molecular pattern
PAS	PER-ARNT-SIM
PBS	Phosphate-buffered saline
PC	Principal component
PCA	Principal component analysis
PCR	Polymerase chain reaction
PD-L1	Programmed death-ligand 1
PEG	Poly(ethylene glycol)
PER	Period
PFA	Paraformaldehyde
PIV5	Parainfluenzavirus 5
PRR	Pattern recognition receptor
QL	Quasi-likelihood
qPCR	Quantitative polymerase chain reaction
RANKL	Receptor activator of nuclear factor kappa-B ligand
RelA	Transcription factor p65
RIG I	Retionoic acid-inducible gene I
RIN	Ribonucleic acid integrity number
RIPA	Radioimmunoprecipitation assay buffer
RIPK-2	Receptor-interacting serine/threonine-protein kinase 2
RLR	RIG-I-like receptor
RNA	Ribonucleic acid

ROS	Reactive oxygen species
RPMI	Roswell Park Memorial Institute
rRNA	Ribosomal RNA
RT	Room temperature
RT-qPCR	Reverse transcription quantitative polymerase chain reaction
SDS-PAGE	Sodium dodecyl sulfate polyacrylamide gel electrophoresis
SIM	Single-minded protein
siRNA	Small interfering RNA
SOCS2	Suppressor of cytokine signaling 2
SPF	Specific-pathogen-free
STAT1	Signal transducer and activator of transcription 1
STAT3	Signal transducer and activator of transcription 3
T4SS	Type IV secretion system
TAB2	Mitogen-activated protein kinase kinase kinase 7-interacting protein 2
TAD	Transactivation domain
TAE	Tris-acetate-EDTA
TAK1	Mitogen-activated protein kinase kinase kinase 7
TBS	Tris-buffered saline
TCDD	2,3,7,8-Tetrachlorodibenzo-*p*-dioxin
TDO	Tryptophan 2,3-dioxygenase
TEMED	*N*,*N*,*N'*,*N'*-Tetramethylethylenediamine
TFF1	Trefoil factor 1
tGFP	turboGFP
TGF-β	Transforming growth factor beta
TIFA	TRAF-interacting protein with FHA domain-containing protein A
TlpB	Methyl-accepting chemotaxis protein
TLR	Toll-like receptor
TLR2	Toll-like receptor 2
TLR3	Toll-like receptor 3
TLR5	Toll-like receptor 5
T_m	Melting temperature
TMM	Trimmed mean of M-values
TNFAIP3	Tumor necrosis factor, alpha-induced protein 3
TNFRS	Tumor necrosis factor receptor superfamily
TNF-α	Tumor necrosis factor, alpha
TRAF2	TNF receptor-associated factor 2
TRAF3	TNF receptor-associated factor 3

TRAF6	TNF receptor-associated factor 6
Treg	Regulatory T cell
VacA	Vacuolating cytotoxin A
WT	Wild-type
XRE	Xenobiotic response element

Table of contents

Table of contents

List of Figures

Table of contents

Table of contents

Table of contents

Table of contents

List of Tables

Abstract

The role of the Aryl Hydrocarbon Receptor in *Helicobacter pylori* Infection

Jan Traulsen, Green Templeton College

D.Phil. Clinical Medicine, Michaelmas Term 2023

The gastric pathogen *Helicobacter pylori* is a master of immune evasion and the main risk factor for developing non-cardia gastric cancer. The bacterium has evolved numerous strategies to evade the immune response launched by the infected host, enabling it to persist on the epithelium of the stomach for decades, despite chronic inflammation of the stomach mucosa. While many evasion mechanisms have been discovered, it is unknown as of yet, how the bacterium evades the strong NF-κB-driven inflammatory response that follows sensing of the bacterium by the gastric epithelium. The aryl hydrocarbon receptor is an important regulator of homeostasis and has been shown to modulate the inflammatory response by regulating pro-inflammatory signalling pathways such as the one mediated by NF-κB. We therefore hypothesized that activation of the AHR by *H. pylori* could lead to inhibition of the NF-κB-driven inflammatory response, which would enable a novel strategy to eradicate *H. pylori* without the use of antibiotics through inhibition of AHR. In this study we demonstrate that loss of AHR led to decrease of *H. pylori* burden in infected AHR-deficient mice, possibly preventing the progression of gastritis. AHR-deficient mice demonstrated reduction of bacteria and did not develop mucosal hyperplasia, as opposed to wild-type mice. We also demonstrate that *H. pylori* activates the AHR in human epithelial cells and leads to increased AHR expression in human corpus tissue. Additionally, we show that AHR-deficient murine epithelial cells displayed an increased pro-inflammatory response to infection compared to wild-type cells and that this was potentially mediated by TNF-α. When attempting to increase the epithelial NF-κB response through inhibition of AHR however, we found that this did not lead to an increase in NF-κB activation, but that this effect could still be obtained by knockout of AHR in a human epithelial cell line.

Chapter 1 - Introduction

1.1 *Helicobacter pylori* and the innate immune response

1.1.1 Introducing *Helicobacter pylori*

The gastric pathogen *Helicobacter pylori* is present in about 50% of the world's population, making it the most common bacterial infection in the world (Bauer and Meyer, 2011). Infection prevalence is skewed towards low and middle income countries (LMIC), where infection rates can be as high as 80%, which coincides with the incidence of gastric cancer (Crew and Neugut, 2006).

H. pylori is a Gram-negative, flagellated, microaerophilic bacterium with helical shape that colonizes the stomach epithelium and has developed strategies that allow it to persist in a part of the body that is a particularly harsh environment to live in, mainly due to its low pH.

It has been shown to have been associated with humans for over 100,000 years (Bauer and Meyer, 2011). Infection with *H. pylori* is thought to mainly occur during childhood, inversely correlated to socioeconomic status also within more economically developed countries (Feldman, Eccersley *et al.*, 1998; Malaty, Logan *et al.*, 2001). If transmission of *H. pylori* occurs mainly within the family or rather horizontally between individuals could be different between LMIC and developed, high income countries (HIC; Schwarz, Morelli *et al.*, 2008); it is therefore not entirely clear if infections are mainly transmitted from mother to child or rather between persons simply as a result of prolonged close contact.

1.1.2 *H. pylori* virulence factors

Several bacterial factors have been proposed to determine virulence of *H. pylori* strains, the most prominent ones being the cytotoxic proteins vacuolating cytotoxin A (VacA), cytotoxicity-associated gene A (CagA) and the gene locus cytotoxicity-associated gene pathogenicity island (*cag*PAI). VacA has been shown to induce vacuolization and apoptosis in epithelial cells (de Bernard, Arico *et al.*, 1997). CagA induces morphological changes, leading to the development of the "hummingbird"-phenotype. While around 60 – 70 % of western *H. pylori*

strains are *cag*PAI positive (termed Type I-strains), VacA can be found in all strains (Palframan, Kwok *et al.*, 2012). The *cag*PAI encodes CagA as well as proteins that make up a type IV secretion system (T4SS), which is required for translocation of CagA into the host cytosol.

The CagA effector protein as an activator of NF-κB and other pro-inflammatory signalling pathways has been described in numerous publications (reviewed in Backert and Naumann, 2010). While the consensus among them is that CagA is largely dispensable for activation of NF-κB, but rather requires a functional T4SS (Sharma, Tummuru *et al.*, 1998; Hirata, Maeda *et al.*, 2006; Schweitzer, Sokolova *et al.*, 2010), it has been reported that activation of NF-κB by CagA is indeed possible at later infection time points (>24 h p.i.) and the extent to which CagA is able to induce that effect depends on the specific sequence of the CagA EPIYA region, which can differ in different strains of *H. pylori* (Brandt, Kwok *et al.*, 2005). One publication suggests a rapid CagA-dependent activation of NF-κB (Lamb, Yang *et al.*, 2009), however Schweitzer and colleagues have doubted these findings and suggested that unintentional altering of the cagPAI was likely responsible for the observed results (Schweitzer, Sokolova *et al.*, 2010).

In general, all CagA-dependent mechanisms of NF-κB activation have been shown to also be T4SS-dependent (as discussed in Backert and Naumann, 2010); this is unsurprising, as the T4SS enables the translocation of bacterial factors into the infected host cell. Apart from CagA, it has been shown that bacterial peptidoglycan is also being translocated and that it is responsible for activation of NOD1 in the host cell (Viala, Chaput *et al.*, 2004), which could be important for activation of the inflammasome and subsequent cleavage of pro-IL1-β into its active, mature form. The T4SS is further required for the rapid, ADP-heptose-dependent activation of NF-κB by *H. pylori* (Pfannkuch, Hurwitz *et al.*, 2019; discussed further in 1.1.7). Lastly, the T4SS itself is able to directly induce activation of NF-κB by its CagL subunit; this is mediated by the interaction of TLR5 with the CagL D1-motif, which is similar to motifs found in flagellin of TLR5-activating bacteria (Pachathundikandi, Tegtmeyer *et al.*, 2019).

1.1.3 *H. pylori* is a causative agent for stomach cancer

Barry Marshall and J. Robin Warren postulated in 1983 that rather than stress or diet, infection with *H. pylori* could be the underlying cause of various gastrointestinal disorders such as gastritis, peptic ulcers and gastric adenocarcinoma (Warren and Marshall, 1983; Marshall and Warren, 1984), which Marshall famously demonstrated in a self-experiment in 1985, developing gastritis shortly after ingesting *H. pylori* (Marshall, Armstrong *et al.*, 1985). This shed light on the now established link between *H. pylori* infection and gastric cancer development (Uemura, Okamoto *et al.*, 2001) and allowed early, preventative treatment of these diseases by antibiotic eradication therapy. While other risk factors for gastric cancer are known, such as a high-salt diet, smoking, alcohol consumption and gastro-oesophageal reflux (Venerito, Link *et al.*, 2016; Smyth, Nilsson *et al.*, 2020), *H. pylori* is generally accepted to be the major cause of gastric cancers such as intestinal-type adenocarcinoma and mucosa-associated lymphoid tissue (MALT) lymphoma. Consequently, in 1994, *H. pylori* was added to the list of type I carcinogens by the International Agency for Research on Cancer (IARC, 1994). More recently, it has been suggested that infection with *H. pylori* could be responsible for 89% of all non-cardia gastric cancer cases worldwide and thereby 6.2% of the total global cancer burden (Plummer, Franceschi *et al.*, 2015).

However, all links between *H. pylori* infection and cancer development have been derived from epidemiological studies, for both adenocarcinoma (Parsonnet, Friedman *et al.*, 1991; Huang, Sridhar *et al.*, 1998; Eslick, Lim *et al.*, 1999; Lee, Chiang *et al.*, 2016; Yang, Kartsonaki *et al.*, 2021) and MALT lymphoma (Fischbach, Goebeler-Kolve *et al.*, 2004; Stathis, Chini *et al.*, 2009); a direct mechanism(s) by which *H. pylori* infection causes cancer is still outstanding as of now.

Generally, it is thought that only about 1-3% of all people infected with *H. pylori* will develop *H. pylori*-associated cancer in their lifetime (Peek and Crabtree, 2006).

One of the major problems in treating gastric cancer is its late detection; a retrospective analysis conducted in a Norwegian hospital concluded that patients undergoing resections of micro- or macroscopic tumours (stage IIIb or IV) had a five-year survival rate of 0 (Lello, Furnes

et al., 2007). While prophylactic screening of the whole population could potentially improve survival rates through early detection (Degiuli and Calvo, 2006), the costs for such an approach would probably be too high, especially in LMIC.

1.1.4 Treatment of *H. pylori* infection

Treatment of *H. pylori* infection is normally performed upon confirmation of active infection, using either a triple-therapy regimen, which includes 1) a proton pump inhibitor, 2) amoxicillin and 3) clarithromycin or metronidazole or a quadruple-therapy regimen also including bismuth subsalicylate (NICE, 2014).

As studies have suggested, general eradication of *H. pylori* could be a more worthwhile approach to reduce the incidence of gastric cancer (Uemura, Okamoto *et al.*, 2001; Pan, Zhang *et al.*, 2016; Wu, Lee *et al.*, 2019; Yan, Chen *et al.*, 2022), however a meta-analysis conducted in 2020 concluded that the results from many studies, primarily performed in Eastern Asia, might not be applicable to the global population (Ford, Yuan *et al.*, 2020). As Peek and Crabtree point out, the timepoint of intervention therapy is also critical for the successful prevention of gastric cancer; furthermore, antibiotic-based eradication therapy of huge parts of the global population poses the risk of emergence of antibiotic-resistant strains (Peek and Crabtree, 2006). This is already a problem without a global eradication program; reports show a rise in resistance to commonly used antibiotics in different parts of the world (Xia, Fan *et al.*, 1999; Krzyżek, Pawełka *et al.*, 2020).

Due to the aforementioned issues and due to the potential benefits, which a reduction in *H. pylori* prevalence could bring, development of a vaccine has been attempted several times (Michetti, Kreiss *et al.*, 1999; Flach, Mozer *et al.*, 2012; Zeng, Mao *et al.*, 2015; Li, Zeng *et al.*, 2016); a number of reviews have described advances and problems (Sutton and Chionh, 2013; Velin, Straubinger *et al.*, 2016; Sutton and Boag, 2019). Generally, vaccines, even when evoking an immune response, failed to eradicate *H. pylori* upon vaccination.

In summary, there is a clear potential benefit of targeting *H. pylori* infection to reduce the global gastric cancer burden, however an efficient and cost-effective way to do so, while avoiding obvious problems like antibiotic resistance still remains to be found.

1.1.5 The innate immune response to bacterial infections

If intact, the epithelium prevents most external, environmental microorganisms from entering the body. Apart from forming a tight physical barrier, this first line of host defence comprises chemical factors such as antimicrobial peptides, proteolytic enzymes and acidic or basic environments, which are not suitable for microbial growth (Basset, Holton *et al.*, 2003); a further layer of protection is provided by commensal microorganisms. If compromised by wounds such as ulcers, the epithelium cannot fulfil its protective role anymore and leaves the body exposed to infections by pathogens and so-called opportunistic pathogens, microorganisms that are normally part of a healthy microbiome, but can become pathogenic if the normal barrier function of the epithelium is compromised. Pathogens are also able to disrupt the epithelial barrier through interaction with epithelial cells, allowing them to colonise the epithelium. Some, like *Shigella flexneri*, *Listeria monocytogenes* or *Chlamydia trachomatis* reside in the epithelium within the host cell (Weddle and Agaisse, 2018; Stelzner, Vollmuth *et al.*, 2023); *H. pylori* instead attaches tightly to the outside of epithelial cells.

Apart from the defence mechanisms mentioned above, innate immune cells such as dendritic cells, macrophages, neutrophils and natural killer cells form an important part of the innate immune system.

Generally, sensing of microorganisms happens via so-called pattern recognition receptors (PRRs), allowing the immune system to employ an unspecific immune response (Janeway, 1989), compared to the adaptive immune system; innate immune mechanisms still vary depending on the type of microorganism. The idea that these receptors help the body to discriminate between self and non-self was supported by findings about an important protein called “Toll”, made in *Drosophila* (Lemaitre, Nicolas *et al.*, 1996). These findings could be replicated in humans, yielding the discovery of Toll-like receptors (TLRs; Medzhitov, Preston-Hurlburt *et al.*, 1997).

PRRs detect conserved cellular structures produced by microorganisms called pathogen associated molecular patterns (PAMPs). This group of microbial products comprises very different molecules, such as bacterial flagellin, lipopolysaccharide (LPS), double-stranded

RNA (dsRNA) and peptidoglycan. PRRs themselves can vary in structure and cellular localisation; toll-like receptors (TLRs), among the best-characterised membrane-bound PRRs, can reside on the cell membrane, where they recruit downstream adaptor molecules to induce an immune response, like TLR4 and TLR5, or they reside on endosomal surfaces and induce a response from inside the endosome upon ligand binding, like TLR3, TLR7 and TLR8 (Kopp and Medzhitov, 1999; Modlin, Brightbill *et al.*, 1999; Muzio and Mantovani, 2000; Uehata and Takeuchi, 2020). Other PRRs are localised in the cytosol, namely the ones belonging to the groups of RIG-I like receptors (RLRs), NOD-like receptors (NLRs) and C-type lectin receptors (CLRs; Akira, Uematsu *et al.*, 2006; Kawai and Akira, 2009). Recently, a novel PRR called alpha-kinase 1 (ALPK1), which can detect a heptose subunit of bacterial LPS found in the majority of Gram-negative bacteria, has been identified (Zhou, She *et al.*, 2018).

Upon binding of microbial PAMPs, a range of pro-inflammatory pathways are initiated downstream; this depends on the type of PAMP detected and the PRR that binds it. While some PAMPs, especially the ones stemming from viruses, activate an interferon-driven inflammatory response, the main responsible transcription factor in the initiation of pro-inflammatory response is the nuclear factor kappa-light-chain-enhancer of activated B cells (NF-κB). This activation then in turn leads to the expression of NF-κB target genes, which are important for cell survival, but also the expression of antimicrobial peptides, a class of molecules that possess antimicrobial activity (Ostaff, Stange *et al.*, 2013), and expression of immune cell-attracting chemokines like interleukin 8 (IL-8).

Subsequent activation of innate immune cells triggers inflammatory responses that comprise expression and secretion of chemokines and proinflammatory cytokines such as interleukin-6 (IL-6), IL-1β and tumor necrosis factor α (TNF-α), induction of apoptosis, vasodilation and an increase in the permeability of the local blood vessel (Medzhitov, 2007).

Another layer of defence that is present in all mucosal layers of the human body is the eponymous mucus. In the stomach, the main purpose of the mucus is to protect the epithelial lining from the gastric acid. It is composed of 93% water, 3% glycoproteins (mucins, such as MUC5AC or MUC6) and a number of low-molecular weight molecules; in the low pH of the

stomach lumen, these components form a network, resulting in a hydrogel-like, viscoelastic fluid (Bansil, Celli *et al.*, 2013). Trapped in the mucus are antimicrobial peptides and immunoglobulins, making the mucus not only a physical, but also a biochemical-immunological barrier to infection (McGuckin, Lindén *et al.*, 2011). In the stomach, this mucus is composed of two layers: a thick, adherent inner MUC5AC-dominant layer and a looser, MUC6-dominant outer layer; together, they can reach a total thickness of around 700 µm (Bansil, Celli *et al.*, 2013; Traulsen, Zagami *et al.*, 2021).

To make sure the inflammatory response is kept under control to limit tissue damage and dangerous systemic effects such as systemic inflammatory response syndrome (SIRS), the body is equipped with a range of anti-inflammatory mechanisms that can counteract pro-inflammatory processes. One such mechanism is the expression of the anti-inflammatory cytokine interleukin-10 (IL-10), that can inhibit the expression of pro-inflammatory cytokines such as IL-1β and TNF-α and is important in modulating autoimmune inflammation and inflammation induced by bacterial compounds (de Waal Malefyt, Abrams *et al.*, 1991). Another important regulatory factor is A20, that acts on pro-inflammatory, ubiquitin-dependent signalling such as the ones induced by TNF, IL-1β, TLRs and NOD1/2 and modulates their signalling through ubiquitin modification (Ma and Malynn, 2012), thereby regulating the activation of NF-κB.

1.1.6 Nuclear factor-κB (NF-κB) signalling

Nuclear factor-κB (NF-κB) signalling plays a central role in innate as well as adaptive immunity; it has been suggested to be involved in inflammation as well as in carcinogenesis (DiDonato, Mercurio *et al.*, 2012). It is exerted by members of the NF-κB/Rel family that form dimers, which are sequestered in the cytoplasm in their inactive state. Upon activation, dimers are translocated into the nucleus and act as transcription factors for multiple genes involved in inflammation and proliferation (Jost and Ruland, 2007). The NF-κB family is formed by five proteins, NF-κB1 (p105/p50) and NF-κB2 (p100/p52), RelA (p65), RelB and c-Rel. All five proteins contain a Rel homology domain (RHD) that mediates DNA binding and dimerization; RelA, RelB and c-Rel, who are part of the Rel subfamily, also have c-terminal transactivation

domains (TAD), which are responsible for gene activation upon binding to target genes. NF-κB1 and NF-κB2 on the other hand contain several ankyrin-repeat motifs (ARM); they have been proposed to exert repressor functions (Li and Verma, 2002). p50 and p52 are generated by proteolytic cleavage of the precursor molecules p105 and p100, respectively. Both a canonical and a non-canonical NF-κB signalling pathway have been described (Figure 1.1.1). In the canonical signalling pathway, TAD-containing proteins interact with inhibitor of NF-κB (IκB) proteins, IκBα, IκBβ and IκBε. IκB proteins retain the heterodimers made up out of RelA, c-Rel an p50 in the cytosol. Upon activation of upstream signalling molecules, IκB molecules are phosphorylated, which induces ubiquitination and subsequent proteasomal degradation of the inhibitors. The NF-κB heterodimer is released and translocated to the nucleus where it can activate NF-κB target genes. IκB molecules are phosphorylated by the IκB kinase complex, consisting of IκB kinases (IKKs) IKKα, IKKβ and NF-κB essential modifier (NEMO/IKKγ). Receptors that employ canonical NF-κB signalling are PRRs, including TLRs, NLRs and RLRs, and T-cell and B-cell receptors, and members of the TNF receptor superfamily (TNFRS). Target genes of NF-κB involved in pro-inflammatory responses include *CASP4*, *CXCL1*, *CXCL2*, *IL6*, *CXCL8* (IL-8), *SELE*, *SELP* and *ICAM1,* among many others (Newton and Dixit, 2012). In the last years, on the other hand, several publications have suggested an immunomodulatory role of NF-κB, which could mean that NF-κB is not solely responsible for the induction of proinflammatory signalling but might play a broader role in the regulation of inflammatory processes (Banerjee, Thamphiwatana *et al.*, 2014; O'Reilly, Putoczki *et al.*, 2018).

The non-canonical NF-κB signalling pathway is mediated by the activation of the p100/RelB heterodimer. In basal, unstimulated conditions, the inactive dimer is located in the cytoplasma. Its activator NF-κB-inducing kinase (NIK) is subjected to constant proteasome-mediated degradation, resulting in low cellular levels. Degradation is controlled through ubiquitination by a ubiquitin ligase complex of TNF receptor-associated factor 2 (TRAF2), TNF receptor-associated factor 3 (TRAF3) and cellular inhibitor of apoptosis 1 and 2 (cIAP1/2). Upon stimulation of TNFRS members by their respective ligands, such as lymphotoxin beta (LTβ),

cluster of differentiation factor 40 ligand (CD40L) or receptor activator of nuclear factor kappa-B ligand (RANKL), the cIAP-TRAF2-TRAF3 complex is recruited to the activated TNFR, resulting in the release of NIK. NIK then in turn induces phosphorylation of p100 and subsequent partial degradation by the proteasome, yielding the p52/RelB heterodimer, which is the main transcription factor associated with non-canonical NF-κB signalling. This pathway has been shown to be involved in regulation of B cell survival, lymphoid organ development and modulation of the adaptive immune response (Cildir, Low *et al.*, 2016; Sun, 2017).

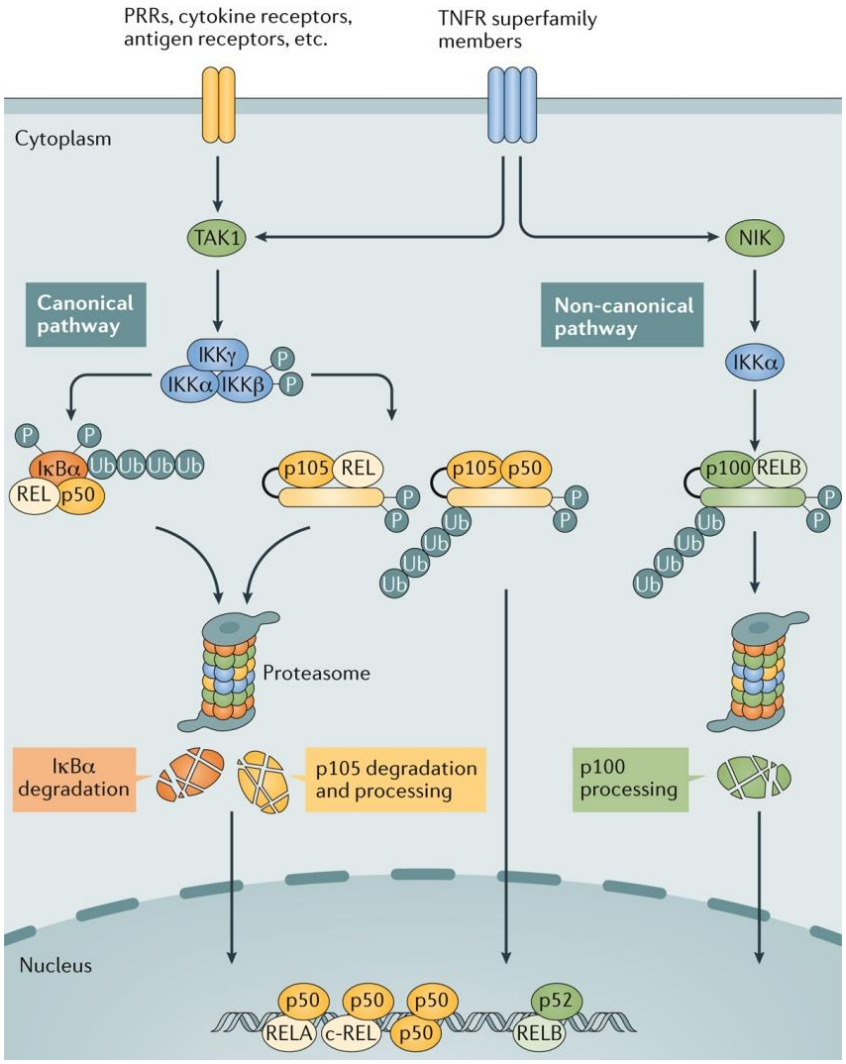

Figure 1.1.1 | Canonical and non-canonical NF-kB signalling pathways.
Canonical NF-κB signalling is initiated by activation of various immune receptors such as PRRs and cytokine receptors. This in turn leads to activation of TAK1, which then phosphorylates IKKβ, thereby inducing activation of the IKK complex. The activated complex in turn phosphorylates and thereby marks IκB family members and p105 for ubiquitin-mediated proteasomal degradation, inducing the release of sequestered NF-κB subunits. While IκB proteins are completely degraded, a cleavage product of p105, p50, is translocated into the nucleus where it acts as one monomer of the various heterodimeric NF-κB transcription factors. The non-canonical pathway is regulated by NIK, which is stabilised upon activation of TNFRS members, leading to phosphorylation, ubiquitination and partial proteasomal degradation of p100, yielding the activated p52/RelB heterodimeric transcription factor. Reproduced from Sun, 2017.

While *H. pylori* infection is generally associated with activation of the canonical signalling pathway, a number of recent publications have described non-canonical NF-κB signalling as being involved in the context of *H. pylori* infection, specifically via the activation of the lymphotoxin beta receptor, which resulted in increased gastritis *in vivo* (Mejias-Luque, Zoller *et al.*, 2017) and was found to be increased in *H.pylori*-associated gastritis in human patients (Feige, Vieth *et al.*, 2018).

1.1.7 The innate immune response to *Helicobacter pylori* infection

The innate immune response to *H. pylori* is driven by the gastric epithelium. While a number of publications have described the presence of immune cells in *H. pylori*-infected patients, such as neutrophils, macrophages, T cells, B cells, NK cells and dendritic cells (Nielsen and Andersen, 1992; Hatz, Meimarakis *et al.*, 1996; Elitsur, Jackman *et al.*, 1999; Yun, Lundgren *et al.*, 2005; Bimczok, Clements *et al.*, 2010), the epithelium acts as a sentinel of the immune system, detecting pathogens and recruiting immune cells to the location of infection. The main pro-inflammatory signalling factor in *H. pylori* infection is NF-κB, specifically the canonical NF-κB pathway, which gets induced when an epithelial cell encounters a bacterium, leading to the expression of interleukin (IL)-8 (Münzenmaier, Lange *et al.*, 1997). How exactly the epithelial cell senses the presence of *H. pylori* had long been unclear; several mechanisms have been proposed, such as recognition of bacterial CagA protein (Brandt, Kwok *et al.*, 2005; Lamb, Yang *et al.*, 2009), by activation of TLR2 and 5 (Torok, Bouton *et al.*, 2005), by detection of bacterial peptidoglycan through NOD1 (Viala, Chaput *et al.*, 2004), or by type 4 secretion system (T4SS)-mediated activation of TLR5 (Pachathundikandi, Tegtmeyer *et al.*, 2019). However, several recent publications have identified a novel receptor called alpha-kinase 1 (ALPK1), that detects ADP-heptose, an intermediate in the biosynthesis of LPS in gram-negative bacteria (Kneidinger, Marolda *et al.*, 2002). ADP-heptose is a potent activator of NF-κB, which is induced after the heptose binds to ALPK1. This is mediated by a signalling axis, which includes TRAF-interacting protein with FHA domain-containing protein A (TIFA), forming large oligomers upon activation (“TIFAsomes”).

Zimmermann and colleagues could show that during infection with *H. pylori* involvement of ALPK1 and TIFA is crucial for the activation of canonical NF-κB signalling. Furthermore, they could elucidate that TAK1-binding protein 2 (TAB2) and TRAF2 are associated with TIFAsomes upon stimulation by *H. pylori*. Additionally, they demonstrated that TIFAsome formation leads to downstream activation of transforming growth factor beta-associated kinase 1 (TAK1), which in turn activates the IKK complex, leading to canonical NF-κB signalling, and the expression of the proinflammatory cytokine IL-8 (Zimmermann, Pfannkuch *et al.*, 2017). Shortly after, ALPK1 was identified as the direct receptor for ADP-heptose from *Yersinia pseudotuberculosis* (Zhou, She *et al.*, 2018). Pfannkuch and colleagues finally demonstrated that ADP-heptose is present in *H. pylori* and a number of other Gram-negative bacteria, and that it is indeed the major activator of NF-κB signalling in *H. pylori* infection (Pfannkuch, Hurwitz *et al.*, 2019).

When NF-κB is activated in epithelial cells, this results in the expression of inflammation-associated cytokines and chemokines, such as TNF-α, IL-1β, IL-18 (Lehours and Ferrero, 2019) and IL-8, which recruits neutrophils and macrophages to the site of infection (Fehlings, Drobbe *et al.*, 2012; Traulsen, Zagami *et al.*, 2021). On top of that, the epithelium can express antimicrobial peptides (AMPs) to defend itself against invading pathogens. Several have been shown to be expressed during infection with *H. pylori*:

Cathelicidin (LL-37; Hase, Murakami *et al.*, 2003), Intelectin1 and Reg3γ (Sigal, Reines *et al.*, 2019) and human beta-defensin 2 (hBD2; Bauer, Wex *et al.*, 2013).

Both LL-37 and hBD2 are known target genes of NF-κB, suggesting that NF-κB plays a pivotal role in the epithelial response to *H. pylori*. In order to protect itself from damage caused by uncontrolled inflammation, the host will also employ immunomodulatory mechanisms that control the extent of the inflammatory response, for example, blocking the NF-κB-induced activation of STAT3 through TFF1 (Soutto, Bhat *et al.*, 2021).

1.1.8 Immune evasion mechanisms of *H. pylori*

H. pylori has developed strategies to evade innate and adaptive immune responses, allowing the bacterium to persist in the gastric mucosa for decades. These strategies target three

different layers of gastric immunity. An overview of various immune evasion mechanisms is given in Figure 1.1.2.

The first layer comprises the gastric lumen, mucus and the epithelial defense.

The main obstacle to overcome in the colonisation of the gastric mucosa is the gastric acid and the resulting low-pH environment. *H. pylori* has managed to overcome this barrier by expression of urease, an enzyme that converts epithelial urea into NH_3 and CO_2 (Bauerfeind, Garner *et al.*, 1997). This has a threefold effect: firstly, buffering the low pH locally and allowing the bacterium to survive exposure to gastric acid; secondly, creating a gradient of urea and pH towards the epithelium, which *H. pylori* is able to sense via its membrane receptor TlpB and use to localise the epithelium (Croxen, Sisson *et al.*, 2006; Huang, Sweeney *et al.*, 2015), particularly in the case of a damaged epithelium (Hanyu, Engevik *et al.*, 2019); and thirdly, by increasing the pH, altering the rheological properties of the mucus, thereby making it less viscous and enabling *H. pylori* to swim through it (Celli, Turner *et al.*, 2009; Su, Padra *et al.*, 2018).

As introduced before, pattern recognition receptors are responsible for the detection of external microorganisms. TLR4 for example is a key PRR for the detection of gram-negative bacteria, such as *H. pylori*. It detects the lipid A moiety of the bacterial lipopolysaccharide (LPS). *H. pylori* has adapted to this by developing a modified LPS, which displays lower toxicity compared to other bacteria (Cullen, Giles *et al.*, 2011). TLR5, responsible for the detection of bacterial flagellin, fails to sense *H. pylori*, as its flagellin is mutated in the region detected by TLR5 (Gewirtz, Yu *et al.*, 2004). Furthermore, *H. pylori* is able to inhibit the expression of important antimicrobial compounds: as opposed to the aforementioned hBD2, human beta-defensin 3 (hBD3), which is not detected in human biopsy samples (Nuding, Gersemann *et al.*, 2013) is repressed via CagA-mediated inactivation of EGFR signalling (Bauer, Pang *et al.*, 2012) and hBD1 via a mechanism that is dependent on the bacterial T4SS (Patel, Smith *et al.*, 2013).

The second layer comprises adaptive and innate immune cells.

H. pylori is able to not only induce, but also defend itself from reactive oxygen species (ROS) produced by antigen precenting cells, termed the respiratory burst. Specifically, Ramarao and colleagues were able to demonstrate that, while presence of *H. pylori* induced production of ROS by primary monocytes and polymorphonuclear neutrophils, it was ineffective in killing the bacteria. They found that the bacterial enzyme catalase is able to neutralise the bactericidal effect on bacteria present at the cell surface (Ramarao, Gray-Owen *et al.*, 2000). Targeting a similar host defence system, *H. pylori* inhibits the production of nitric oxide by macrophages by consumption of L-arginine through its arginase enzyme, which depletes the substrate of the macrophage enzyme inducible nitric oxide synthase (iNOS; Gobert, McGee *et al.*, 2001). Further mechanisms targeting macrophages are the interruption on phagosome maturation via the bacterial virulence factor VacA and recruitment of the host protein CORO1A (Zheng and Jones, 2003), and the induction of macrophage apoptosis (Menaker, Ceponis *et al.*, 2004). Apart from macrophages, *H. pylori* also targets the T cell-mediated immune response. VacA has been shown to inhibit IL-2 signalling and proliferation of CD4+ T cells (Gebert, Fischer *et al.*, 2003; Sundrud, Torres *et al.*, 2004). An interesting mechanism of immune cell inactivation is the induction of expression of programmed death-ligand 1 (PD-L1) on infected epithelial cells. This has been demonstrated to protect cells from CD8+ T cell-mediated cell death (Holokai, Chakrabarti *et al.*, 2019), as well as promoting the differentiation of regulatory T cells (Treg) from naïve T cells, which have an inhibitory effect on other activated T cells (Beswick, Pinchuk *et al.*, 2007). Promotion of Treg differentiation has also been shown to be induced by TGF-β, which is another effector expressed during *H. pylori* infection (Beswick, Pinchuk *et al.*, 2011).

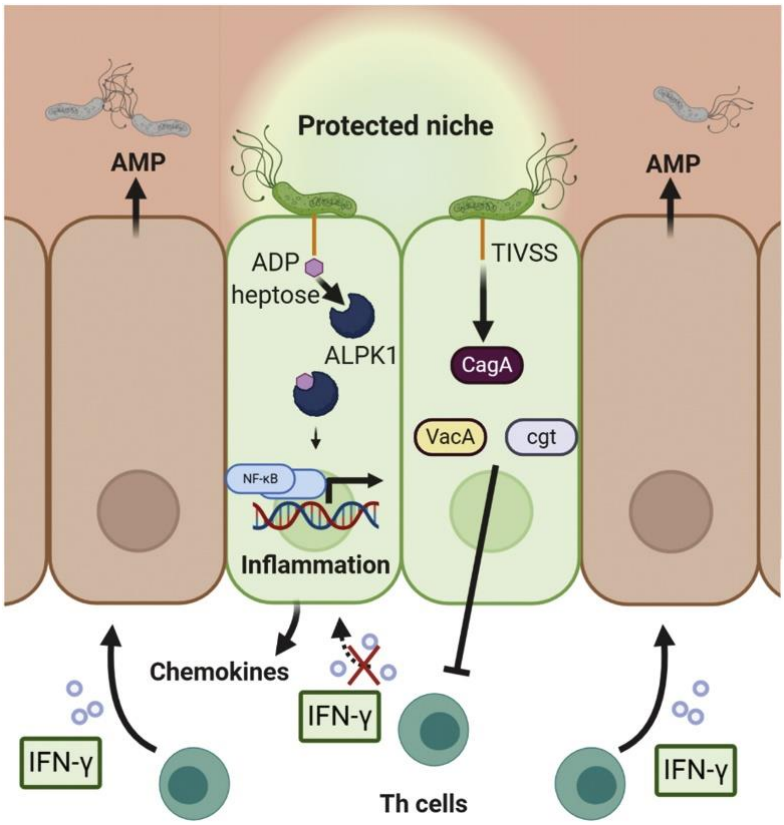

Figure 1.1.2 | Select immune evasion mechanisms of *H. pylori*.
ADP heptose, a bacterial intermediate of LPS, binds the intracellular receptor kinase ALPK1, thereby inducing NF-κB nuclear translocation and transcription of pro-inflammatory mediators including chemokines for the recruitment of immune cells and antimicrobials (AMP) for controlling the infection in the mucus. Among the immune cells, T helper type 1 cells play a critical role as they secrete IFN-γ. Interferon receptors are located on the epithelium and their activation contributes to the production of further cytokines and antimicrobial peptides. *H. pylori* has evolved strategies to hijack this defence mechanism. A bacterial virulence factor called cgt inhibits formation of IFN-γ receptors on the epithelial cells, while other important virulence factors, CagA and VacA can inhibit activation of T helper cells. From Traulsen, Zagami *et al.*, 2021

The third layer of gastric defence that is targeted by *H. pylori* is the communication between the epithelium and immune cells recruited to the place of infection.

This area of host-pathogen interaction has not been investigated as deeply as the two aforementioned ones. When immune cells are recruited to the site of infection, they express various pro-inflammatory cytokines, as introduced before. *H. pylori* infection has been shown to be accompanied by recruitment of Th1 helper cells and an increase in IFN-γ (Karttunen, Karttunen *et al.*, 1995; Serrano, Diaz *et al.*, 2007); still, the bacterium is able to persist in the inflamed gastric mucosa. Studies have suggested that the reason for this is an induced resistance to IFN-γ of the infected cells (Mitchell, Huynh *et al.*, 2004; Wang, Chen *et al.*, 2014),

thereby creating a protected niche at the point of infection. Recently, Morey and colleagues could show that the bacterium indeed induces resistance to IFN-γ in infected cells through cholesterol depletion via its enzyme cholesterol-α-glucosyltransferase (Cgt). This leads to the disruption of cholesterol-rich microdomains on the infected cell; these microdomains, called lipid rafts, enable the formation of the interferon gamma receptor heterodimer IFNGR1/IFNGR2. When cholesterol is extracted, the formation of the heterodimer is inhibited, effectively abrogating IFN-γ induced signalling within the epithelial cell (Morey, Pfannkuch *et al.*, 2018).

This intriguing mechanism explains in part why the bacterium can persist while at the same time evoking a chronic inflammatory response.

Still unexplained is the fact that in chronic infection, NF-κB is also activated (Isomoto, Miyazaki *et al.*, 2000; Isomoto, Mizuta *et al.*, 2000; van Den Brink, ten Kate *et al.*, 2000), yet *H. pylori* is still not efficiently cleared from the gastric epithelium; the existence of a bacterial mechanism that subverts the strong NF-κB response therefore seems likely. An interesting candidate for such a mechanism is the aryl hydrocarbon receptor, a ligand-activated transcription factor that has been shown to crosstalk with NF-κB signalling as well as to be involved in sensing of bacteria and control of bacterial infection.

1.2 The aryl hydrocarbon receptor

1.2.1 Regulation and structure of the AHR

The aryl hydrocarbon receptor (AHR) is a highly-conserved transcription factor of the basic helix-loop-helix (bHLH)/periodic circadian protein (PER)-AHR nuclear translocator (ARNT)-single-minded protein (SIM) family, sensing environmental toxins such as benzo[*a*]pyrene and 2,3,7,8-tetrachlorodibenzodioxin (TCDD) as well as endogenous compounds via its PER-ARNT-SIM (PAS) domain and inducing expression of detoxifying enzymes, most notably cytochrome P450, family 1, subfamily A, polypeptide 1 (CYP1A1) as well as CYP1A2 and CYP1B1. These enzymes break down AHR ligands, thereby regulating its induction.

Several distinct domains have been identified in the AHR: a DNA-binding bHLH domain, a PAS domain responsible for dimerization and ligand binding and a Q-rich domain that is involved in the transcriptional activation of target genes (Figure 1.2.1).

AhR is a cytosolic receptor, sequestered in the cytosol by p23, AhR-interacting protein (AIP), a 90 kDa heat-shock protein (HSP90) homodimer and c-Src (Src) in its inactive state (Gutierrez-Vazquez and Quintana, 2018). The HSP90 monomers bind to distinct regions of the AHR: one monomer binds to the PAS domain, the second one to another region in the PAS domain and to the bHLH region (Fukunaga, Probst *et al.*, 1995). These regions are involved in ligand binding and binding to its DNA target sequence, termed the dioxin response element (DRE) or xenobiotic response element (XRE).

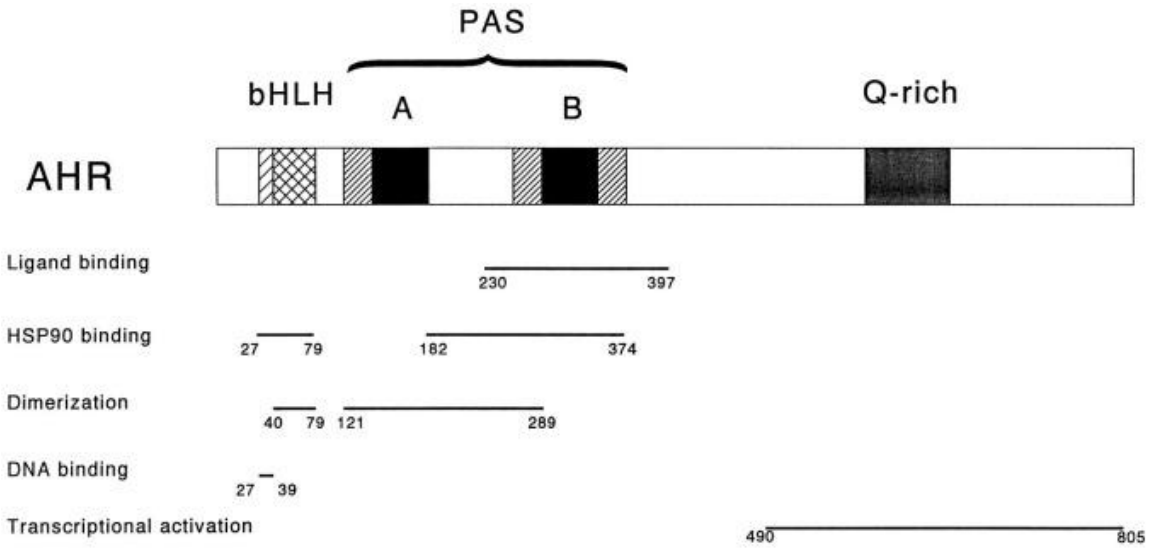

Figure 1.2.1 | Functional domains of the aryl hydrocarbon receptor.
The AHR contains several domains required for its distinct functions. As it contains both bHLH and PAS domains, it is classed as a member of the bHLH/PAS transcription factor family. The bHLH motif allows binding to DNA, binding to HSP90 when part of its cytosolic complex and binding to ARNT in the nucleus to form the heterodimeric AHR/ARNT transcription factor. Dimerization and binding to HSP90 is also supported by the PAS domains. The PAS-B domain specifically allows binding of ligands to the AHR. The glutamine-rich (Q-rich) domain located in the C-terminal region is required for transcriptional activation, specifically in recruitment on co-activators and transactivation. bHLH: basic helix-loop-helix. HSP90: 90 kDa heat-shock protein. PAS: Per-Arnt-Sim. Reproduced from Fukunaga, Probst *et al.*, 1995.

The AIP serves as a scaffolding protein by binding to both AHR and HSP90 (Carver and Bradfield, 1997; Meyer and Perdew, 1999) as well as regulating cytoplasmic localisation of AHR by inhibiting the interaction of AHR with importin-β, which is responsible for nuclear translocation of the activated AHR complex (Petrulis, Kusnadi *et al.*, 2003). Furthermore, it is also able to regulate cellular levels of AHR (Meyer, Petrulis *et al.*, 2000).

Src is a non-receptor tyrosine kinase of the Src kinase family. It is part of the cytosolic AHR receptor complex and gets released and activated upon ligand binding to AHR (Enan and Matsumura, 1996).

The final compound of the complex is the co-chaperone p23. It primarily protects the AHR from ubiquitination-mediated proteasomal degradation. It has been demonstrated that in the absence of p23, formation of the AHR-ARNT heterodimer does not require ligand binding to AHR, suggesting that p23 is important for the control of AHR transcriptional activity by requiring the presence of a ligand for activation (Kazlauskas, Poellinger *et al.*, 1999; Pappas, Yang *et al.*, 2018).

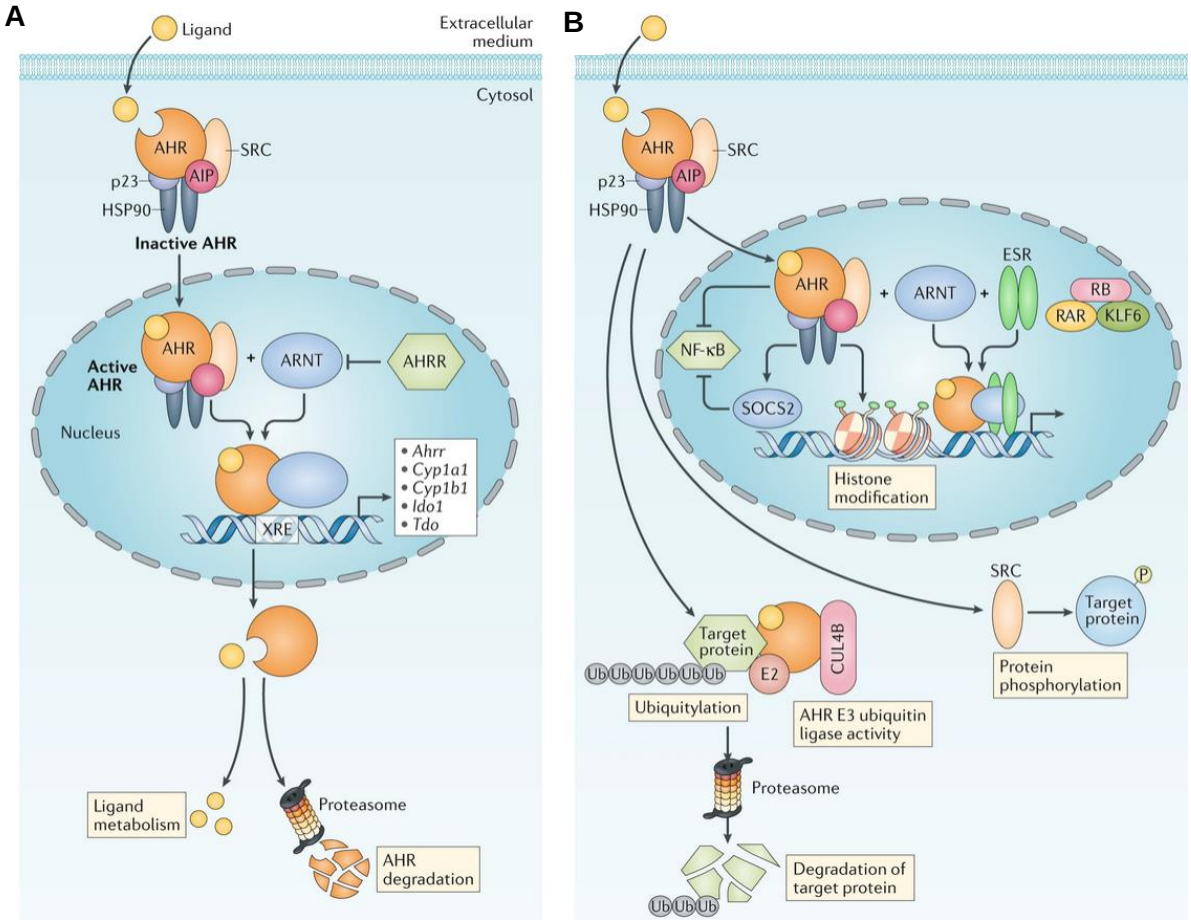

Figure 1.2.2 | Overview of canonical and non-canonical AHR signalling pathways
A: Canonical signalling pathway. In its inactive state, AHR is sequestered in a complex of proteins in the cytosol. Upon ligand binding, it is translocated into the nucleus, released from its complex and forms a heterodimer with ARNT. The heterodimer binds to the xenobiotic response element (XRE) and induces expression of target genes. B: Non-canonical signalling pathways. Reproduced from Rothhammer and Quintana, 2019. Note that the AIP here is still depicted as part of the AHR complex after nuclear translocation, however, release of AIP from the complex is necessary to initiate translocation.

1.2.2 AHR signalling pathways

Upon binding of a ligand, AhR undergoes a conformational change, which causes the release of AIP from the cytosolic complex.

This releases the nuclear localisation sequence (NLS; Ikuta, Eguchi *et al.*, 1998; Kudo, Hosaka *et al.*, 2018) and induces subsequent nuclear translocation of the AHR-p23-HSP90 complex in an importin-β-mediated process, as mentioned above. The complex then disassociates and AHR binds to ARNT, forming the transcriptionally active AHR-ARNT-heterodimer.

In the canonical signalling pathway, AHR-ARNT acts as a transcription factor, binding to the dioxin response element (XRE) in target gene promoters (Figure 1.2.2A), which harbours the

consensus sequence 5'-TNGCGTG-3' (Yao and Denison, 1992; Swanson, Tullis *et al.*, 1993). Target genes include CYP1A1, CYP1A2, AhR repressor (AHRR), indoleamine 2,3-dioxygenase 1 (IDO1) and tryptophan 2,3-dioxygenase (TDO). The AHRR competes with activated AHR for ARNT binding, thereby working as a negative regulator of AHR signalling (Sakurai, Shimizu *et al.*, 2017). Further control of AHR signalling is provided by the CYP family target genes, which break down AHR-activating ligands. Once ligands are removed from the AHR, it is then exported from the nucleus and targeted for proteasomal breakdown by ubiquitination.

Ligands for the AhR typically are planar, aromatic hydrocarbons. They can be

a) exogenous such as environmental pollutants like Benzo[a]pyrene or 2,3,7,8-tetrachlorodibenzo-p-dioxin (TCDD) or certain drugs, such as omeprazole or
b) produced endogenously, either by the organism itself, such as 6-Formylindolo[3,2-b]carbazole (FICZ) or kynurenine or by the microbiota, such as tryptamine or indole or
c) dietary compounds taken up with food, such as Indolo[3,2-b]carbazole (ICZ) or Indole-3-carbinol (I3C; Torti, Giovannoni *et al.*, 2021).

Apart from the canonical signalling mechanism, AHR is also involved in various non-canonical signalling pathways (Figure 1.2.2B). It has been shown to control the expression of NF-κB target genes directly by interacting with members of the NF-κB family (Vogel, Sciullo *et al.*, 2007; Vogel and Matsumura, 2009; Vogel, Khan *et al.*, 2014) or indirectly through interaction with the NF-κB modulator suppressor of cytokine signalling 2 (SOCS2; McBerry, Gonzalez *et al.*, 2012; Yeste, Takenaka *et al.*, 2016), and similar mechanisms have been reported for its interaction with signal transducer and activator of transcription (STAT) signalling (Quintana, Murugaiyan *et al.*, 2010).

Binding to transcription factors and regulating expression of genes that do not contain an XRE has been described for various transcription factors such as estrogen receptor (ER; Ohtake, Takeyama *et al.*, 2003), Krüppel-like factor (KLF) 6 (Wilson, Joshi *et al.*, 2013) and c-Myc (Kim, Gazourian *et al.*, 2000). Further transcriptional control is exerted by AHR through modulation of chromatin remodelling via post-translational modifications of histone, namely acetylation,

methylation and phosphorylation (Schnekenburger, Peng *et al.*, 2007; Chang, Sue *et al.*, 2014), and regulation of epigenetic effectors such as microRNAs and long non-coding RNAs (Hanieh and Alzahrani, 2013; Garcia, Goodale *et al.*, 2017; Grimaldi, Rajendra *et al.*, 2018; Liu, Xia *et al.*, 2018). Additionally, AHR has been shown to regulate gene expression by binding to regulatory regions of genes, leading to repression or induction of gene expression (Shah, Maradana *et al.*, 2022).

An additional important non-canonical AHR signalling process is ubiquitination; specifically, AHR has been shown to associate with the cullin 4B ubiquitin ligase complex (CUL4B), thereby forming a CUL4B-AHR complex, where it acts as an E3 ubiquitin ligase (Ohtake, Baba *et al.*, 2007). This complex is then responsible for the ubiquitination and subsequent proteasomal degradation of different transcription factors, such as octamer-binding transcription factor 4 (OCT4), Hypoxia-inducible factor 1-alpha (HIF1α), ER and p65 (Bunaciu and Yen, 2011; Mejia-Garcia, González-Barbosa *et al.*, 2015; Domínguez-Acosta, Vega *et al.*, 2018). Another potential mechanism of transcriptional regulation is the sequestration of transcription factors in the nucleus; this has been described for p65 and STAT1, which were hindered to translocate into the nucleus by formation of an AHR-p65-STAT1 complex (Kimura, Naka *et al.*, 2009). Lastly, as mentioned before, activation of AHR results in the release of c-Src from the cytosolic AHR complex; c-Src can then phosphorylate target proteins and thereby regulate further signalling pathways (Matsumura, 2009; Bessede, Gargaro *et al.*, 2014).

Taken together, the AHR is not only able to regulate expression of its target genes via the canonical AHR signalling pathway, but can exert control over gene transcription by a wide range of mechanisms: the regulation of epigenetic effectors, direct interaction with transcription factors, regulation of specific inhibitors of signalling pathways, modulation of chromatin remodelling through post-translational modification of histones, binding to regulatory elements of genes, altering subcellular localisation of transcription factors and modulating transcription factor half-life through ubiquitination. Overall, many of these regulatory mechanisms result in

the modulation or inhibition of signalling pathways, suggesting the role of AHR as a regulator of homeostasis.

1.2.3 The role of AHR in inflammation and immunity

The AHR has been described as a regulator of the inflammatory response in various contexts. As mentioned above, the AHR seems to be important in regulating homeostasis, particularly in regulating the inflammatory response to infection and injury. This has been demonstrated in specific tissues and organs, but also on a systemic level.

It has been shown to regulate the severity of inflammation in autoimmune conditions, for example in skin in psoriasis, influencing expression of antimicrobial peptides and chemokines (Di Meglio, Duarte *et al.*, 2014), and in the brain in autoimmune encephalomyelitis (Abdullah, Maged *et al.*, 2019). In a mouse model of inflammatory bowel disease, dextran sodium sulfate-induced colitis, activation of AHR was shown to induce Treg cells and ameliorate the severity of colitis (Abron, Singh *et al.*, 2018).

Systemically, AHR was shown to induce tolerance to bacterial LPS, protecting the host from immunopathology caused by exposure to LPS (Bessede, Gargaro *et al.*, 2014). This effect was mediated through the enzymes indoleamine 2,3-dioxygenase 1 (IDO1) and transforming growth factor-β (TGF-β). IDO1 is a target gene of AHR and has also been implicated in mechanisms promoting immune evasion of cancer (as reviewed in Meireson, Devos *et al.*, 2020). Additionally, activation of the AHR has been shown to promote generation of Treg cells, which can play an immunomodulatory role in autoimmune conditions (Yoshimatsu, Sujino *et al.*, 2022; Zhang, Zhu *et al.*, 2023). Another publication described that activation of AHR prevented septic shock in mice caused by *S. enterica* but that this also caused long-term persistence of bacteria, as well as posing the risk of chronic inflammation (Fueldner, Riemschneider *et al.*, 2022).

Activation of AHR has been demonstrated in various viral infections such as influenza (Vaidyanathan, Chaudhry *et al.*, 2017), coronaviruses (Grunewald, Shaban *et al.*, 2020; Thomas, Stefanoni *et al.*, 2020) and Zika (Giovannoni, Bosch *et al.*, 2020). Generally, this has been linked to poorer outcomes because the activation of AHR seems to be beneficial to viral

infection in many cases, either through inhibition of the interferon-mediated antiviral response (Yamada, Horimoto *et al.*, 2016) or by modulation of cytokine expression (Grunewald, Shaban *et al.*, 2020).

In the case of many bacterial infections, however, the AHR seems to be necessary to control the infection and protect the host. Infection with the murine intestinal pathogen *Citrobacter rodentium* for example was shown to be exacerbated when AHR was absent and the infected mice succumbed to infection (Schiering, Wincent *et al.*, 2017). Mice infected with the opportunistic lung pathogen *Pseudomonas aeruginosa* showed impaired response to infection when treated with antibiotics because of decreased AHR expression; supplementation with AHR ligands reversed the observed effect and increased ROS production and clearance of bacteria (Tsay, Chen *et al.*, 2019). Similarly, activation of AHR through dietary ligands was shown to be important for defence against infection with the intestinal parasite *Cryptosporidium tyzzeri* (Maradana, Marzook *et al.*, 2023). And finally, a seminal paper by Moura-Alves and colleagues described for the first time AHR as a sensor of bacterial pigmented virulence factors, which led to activation of AHR and subsequent regulation of host defence against *P. aeruginosa* and *Mycobacterium tuberculosis* to control infection in the lung (Moura-Alves, Fae *et al.*, 2014).

Overall, the role of AHR in regulating inflammation and immunity is diverse and dependent on the type of inflammatory response, the pathogen inducing it and the location. While its function in autoimmune conditions seems to be modulatory to decrease inflammation, in bacterial infections it appears to be important for control of infection and regulating an effective immune response, but it has also been shown to dampen the pro-inflammatory response to systemic bacterial infection to protect the host. In many viral infections, activation seems to have a rather detrimental effect. Systemically, it has been shown to induce tolerance to potentially dangerous bacterial LPS. Taken together, the mechanisms by which AHR regulates inflammation and the immune response are numerous and complex, with AHR being able to induce immune defence against pathogens on one hand and modulate inflammation to protect from tissue damage on

the other; therefore, the question which role it plays in *H. pylori* infection needs to be investigated.

1.3 Summary and aims

The gastric pathogen *H. pylori* is the major risk factor for developing non-cardia gastric cancer. While its prevalence is on a steady decline in HIC, it is still highly prevalent in many areas of the world, with one in two people infected globally, on average. Late detection of gastric cancer means that a majority of patients have a low 5-year survival rate. Tackling this by routine screening of the population poses a major financial hurdle, especially in LMIC. Country-wide or even global eradication of *H. pylori* has therefore been proposed, but using an antibiotic-driven approach risks global emergence of antibiotic-resistant strains of *H. pylori* and other bacteria, which is already becoming a problem, even without such an approach. Vaccines, on the other hand, promise a safe way to protect from *H. pylori* infection, however so far, no efficient immunisation could be developed. This is not least because *H. pylori* is a master of immune evasion, and while it causes chronic inflammation in infected patients, which has been linked to the development of pre-cancerous conditions and gastric cancer (Correa and Piazuelo, 2012), it is still able to persist in the inflamed mucosa for decades. The gastrointestinal mucosa is able to mount a strong immune response to infection, comprising the recruitment of innate and adaptive immune cells and the production of antimicrobial peptides by the epithelium. Several immune evasion mechanisms of *H. pylori* have been discovered, but how the bacterium avoids the strong NF-κB-driven immune response it evokes is still unknown.

Several mechanisms of modulation of NF-κB signalling are known to date, but none have been linked to *H. pylori* infection. One intriguing candidate for such a regulation is the aryl hydrocarbon receptor. It is able to regulate gene transcription and activation of signalling pathways through a variety of mechanisms. Specifically, it has been shown to be able to modulate the NF-κB response in various cell types. Furthermore, it has also been recognised as a novel receptor of bacteria that senses their presence by detecting bacterial pigments, but is potentially able to recognise other bacterial compounds that are typical AHR ligands, namely planar aromatic hydrocarbons. Presence of the AHR has been linked to successful control of bacterial infections, but the result of activation of AHR seems to be dependent not only on the

ligand but also on the tissue and cell type and can evoke opposite effects in different contexts. While it is not clear if or how the AHR is involved in the modulation of the immune response to infection with *H. pylori*, we hypothesized that activation of the AHR through the bacterium is a possible mechanism, by which *H. pylori* is able to locally dampen the NF-κB-driven inflammatory response, thereby creating a protected niche that allows the bacterium to persist on the surface of the mucosa.

We found the main AHR target genes *CYP1A1*, *CYP1A2*, *CYP1B1* and *AHRR* to be significantly upregulated in primary human gastric epithelial cells infected with *H. pylori* for 3 days, with *CYP1A1* being among the ten highest upregulated genes overall, suggesting that AHR signalling is being activated in epithelial cells as a result of *H. pylori* infection (see chapter 4, Figure 4.2.1 and appendix, Figure 7.1.1).

The first part of the thesis will therefore investigate the effect of AHR on antibacterial defence to infection with *H. pylori*. To this end, an *in vivo* infection experiment was performed utilising an AHR-deficient mouse model and the mouse-adapted *H. pylori* strain PMSS1 to compare the immune response in wild-type and AHR-knockout mice by histological and microbiological methods and transcriptomic profiling via RNA-sequencing, assessing if underlying differences in immune response led to differences in colonisation and tissue morphology. The aim of this part is to answer the question if AHR signalling is relevant to the inflammatory response to *H. pylori* infection.

The second part of the thesis will specifically focus on the role of AHR in the epithelial inflammatory response via NF-κB to understand if activation or inhibition of AHR can drive changes in NF-κB signalling and if findings made in infected mice can be replicated in human cells. Primary human and murine epithelial cultures as well as human cancer cell lines were used to study their response to *H. pylori* infection *in vitro* with active or inactive AHR signalling, using biochemical and molecular biology approaches, such as knock-out and overexpression of AHR and measurement of enzymatic activity of the AHR target gene CYP1A1.

Transcriptomic profiling of murine wild-type and AHR-deficient cells was performed to analyse if inflammatory signalling pathways showed differential activity due to differences in genotype. This part specifically focusses on NF-κB signalling in order to identify differentially regulated key factors, which could provide a link between AHR and NF-κB signalling. The aim of the second part is to investigate if inhibition of AHR is a viable strategy to initiate an efficient proinflammatory response to facilitate eradication of *H. pylori* and which part of the NF-κB-driven response is modulated by the AHR in the context of *H. pylori* infection.

Chapter 2 - Materials & methods

2.1 Primary cell culture

2.1.1 Human cells

Primary human gastric epithelial cells had previously been isolated from stomach tissue obtained from gastric sleeve resection surgeries (Boccellato, Woelffling *et al.*, 2019). As these are healthy, non-immortalised primary cell lines, culture conditions have to be chosen so that the cultures retain their stemness potential to allow for long-term cultivation of stem cell-driven cultures. Cells were either cultured as gastric organoids (Barker, Huch *et al.*, 2010), or as gastric mucosoid cultures (Boccellato, Woelffling *et al.*, 2019).

2.1.1.1 Organoid culture

To obtain organoid cultures of primary gastric epithelial cells, single cells were grown in Cultrex basement membrane extract (BME; Bio-Techne) or Matrigel (Corning), which are solubilized extracellular matrices (ECM) purified from Engelbreth-Holm-Swarm murine tumours (in the following paragraphs referred to as “ECM”). Culturing epithelial cells in these ECM allows for the formation of organoids. Both ECM polymerize at 37 °C and are liquid when kept at around 4 °C. ECM was thawed and kept on ice while working with it to ensure it stayed liquid. All glass and plasticware that would get in contact with primary cells was coated with a sterile, ice-cold 1% (w/v) solution of BSA in PBS by filling once and then removing the coating solution to minimise cells sticking to any surfaces.

Per well of a 24-well cell culture plate, $5x10^4$ cells were suspended in 50 µL of pure ECM and the cell suspension carefully placed in the middle of the well to form a dome of ECM. The plate was then carefully transferred to a humidified incubator and left to polymerize for at least 25 min at 37 °C. Once polymerized, the dome was then overlaid with 500 µL of warm human organoid culture medium (Table 1). Cultures were generally kept for 10 days at 37 °C, with medium changes every 3-4 days. Every 10 days, organoid cultures were passaged to ensure continued growth of the cultures.

To passage the organoids, the ECM was dissolved first by removing the culture medium and then adding 300 µL of ice-cold Cultrex Organoid Harvesting Solution (Bio-Techne) or Cell Recovery Solution (Corning) to each well, breaking up the ECM dome. Plates were then transferred to an orbital shaker and shaken at 150 rpm for 30 min at 4 °C. Cell suspensions were then collected in microcentrifuge tubes and centrifuged at 700x *g* for 5 min at 4 °C. Supernatants containing the dissolved ECM were removed and 700 µL of Gibco TrypLE Express Enzyme (Thermo Scientific) added to each tube. Organoids were then sheared using 150 mm glass Pasteur pipettes (VWR) with a narrowed tip (as described in Bartfeld and Clevers, 2015) by passing the organoid suspension through the tip 7-8 times. The tubes were then placed in a water bath and incubated for 7 min at 37 °C. Following incubation, 300 µL of Dulbecco's Modified Eagle Medium (DMEM) containing 10% fetal bovine serum (FBS) were added to each tube to inhibit the TrypLE enzyme. The cell suspension was then passed through a new glass pipette, again 7-8 times to break up remaining organoid fragments. Cells were then centrifuged at 300x *g* for 5 min, supernatants removed and fresh ECM added to each tube. Generally, cells were split 1:4, so that per original dome collected in one single tube, 200 µL of ECM were added to the cell pellet, resuspended and then divided into four new domes.

2.1.1.2 Mucosoid culture

Millicell cell culture inserts (12 mm, 0.4 µm, Millipore) were coated with 150 µL of a 1% (v/v) solution of bovine collagen I (Gibco) in 0.02 M acetic acid i.e., a total amount of 12.5 µg/cm^2. Coating was carried out for 45 min at 37 °C in a humidified incubator. Inserts were then washed twice with warm 1x PBS and stored at 37 °C covered with PBS or washed once with warm water and air-dried if not used within 24 h. For initial seeding of mucosoid cultures, inserts were transferred to a new 24-well cell culture plate and 3x10^5 viable cells suspended in 200 µL of human mucosoid culturing medium (hiROCK; Table 2) were added to each insert. 400 µL of medium were added to each well and cells cultured in a humidified incubator at 37 °C for 72 h. To start air-liquid interface culture, medium was removed from the inside of the insert and

the surrounding medium replaced with 500 µL of human mucosoid culturing medium (lowROCK).

Cultures were passaged every 4-8 weeks. For passaging, inserts were washed three times with 1x PBS from both sides and then placed in 500 µL warm 0.05% Trypsin-ethylenediaminetetraacetic acid (EDTA; Gibco). 200 µL of warm trypsin were added on top of each insert. Cultures were then placed into a humidified incubator at 37 °C for 30 min. Every 10 min, the trypsin on top of each insert was pipetted up and down several times to facilitate detachment of cells from the insert. The progress of detachment was assessed using a microscope. After 30 min, trypsin containing the cells was removed and added to 5 mL of cell culture medium containing 10% FBS to inhibit the trypsin. Inserts were washed by addition of 300 µL of 1x PBS, which was then added to the same tube. If all cells were detached from the insert, live cell counts were determined by addition of 10 µL trypan blue solution to 10 µL of cell suspension and cells counted using a TC20 automated cell counter (Bio-Rad) and the proprietary cell counting slides. Following counting, suspensions were centrifuged (300x *g*, 5 min), supernatants removed and cells resuspended in fresh mucosoid medium (hiROCK) to a cell count of $3x10^5$ live cells per 200 µL medium. Cells were then seeded onto new, coated cell culture inserts as described above. Every 3-4 days after starting air-liquid interface culture, half of the surrounding medium was replaced with fresh medium (lowROCK). Once a week, the liquid accumulating on top of the cells was removed. Once the liquid was colourless, cell cultures were considered confluent.

Table 1 | Organoid medium

Compound	Final concentration
Advanced DMEM/F12 + 10% FBS + 1x GlutaMAX + 1x HEPES	N/A
R-spondin1	25%
Wnt surrogate	20 ng/mL
B-27	1x
N-2	1x
Epithelial growth factor	50 ng/mL
Y-27632 2HCl	9 µM

FGF-10	150 ng/mL
Noggin	150 ng/mL
N-acetyl cysteine	1 mM
Gastrin	10 nM
Nicotinamide	100 mM
A83-01	1 µM

Table 2 | Mucosoid medium

Advanced DMEM/F12 + 10% FBS + 1x GlutaMAX + 1x HEPES	N/A
R-spondin1	25%
Wnt surrogate	20 ng/mL
B-27	1x
N-2	1x
Epithelial growth factor	50 ng/mL
Y-27632 2HCl	9 µM (hiROCK)/1.8 µM (lowROCK)
FGF-10	150 ng/mL
Noggin	150 ng/mL
Gastrin	10 nM
Nicotinamide	100 mM
A83-01	1 µM

R-spondin1 is produced in-house by the group as R-spo1 conditioned medium, using an Rspo1-overexpressing cell line.

2.1.2 Murine cells

2.1.2.1 Epithelial cell isolation

Murine gastric epithelial cells were isolated from the corpus region of stomachs from *Ahr*$^{-/-}$ and wild-type C57BL/6 mice; tissue was collected from both male and female mice between 6-14 weeks of age. Mice of different genotypes were not littermates and not cohoused (Weighardt, Shapiro *et al.*, 2024).

The *Ahr*$^{-/-}$ mouse strain was originally described in Schmidt, Su *et al.*, 1996 and mice were found to have various hepatic defects, including reduced liver weight. The strain is available

from The Jackson Laboratory, strain number 002727; homozygous females have small litters and mating of heterozygous siblings is recommended for strain maintenance (https://www.jax.org/strain/002727).

Stomachs were obtained from Gitta Stockinger's group (AhRimmunity laboratory, The Francis Crick Institute, London) from animals that were being sacrificed for unrelated projects. Stomachs were opened by cutting along the greater curvature (Figure 2.1.1A). Contents were removed, tissue washed twice in 1x PBS and then stored in FBS with 1% DMSO on ice for transport to Oxford. The following procedure was carried out within 6 h of harvesting of the stomachs:

The tissue was placed on a piece of Whatman paper (GE Healthcare) and carefully spread out flat. The corpus (or "body") region of the stomach was dissected carefully, ensuring that no tissue from the antrum was collected in the process. Dark regions of the tissue between the forestomach and the duodenum were considered corpus, with the antral region being markedly lighter (Figure 2.1.1B). Tissue pieces were collected in 1x PBS in 15 mL centrifuge tubes and once all pieces were collected, tubes were briefly spun down using the "short" setting of the centrifuge to collect tissue pieces at the bottom of the tube. The supernatant was removed and replaced with fresh 1x PBS to wash off any remaining FBS/DMSO and food particles. The PBS was then replaced by 12 mL of freshly prepared 1x PBS containing 0.05 mM dithiotreitol (DTT) and 3 mM EDTA (isolating solution) to disrupt cell-cell adhesions mediated either by cation-dependent proteins (EDTA) or by disulfide bonds (DTT). Tubes were wrapped in aluminium foil, placed on a tube roller and incubated for 90 min at room temperature. Following incubation, isolating solution was removed, tissue pieces washed in ice-cold 1x PBS and tubes shaken vigorously for 1 min to release epithelial glands from the tissue. Glands were pelleted by centrifugation (400x *g*, 6 min, 4 °C) and resuspended in 50-100 µL of ice-cold ECM. 50 µL cell suspension was added per well of a 24-well cell culture plate. ECM was polymerised at 37 °C for 30 min and then overlaid with 500 µL of warm mouse organoid medium (Figure 2.1.1C).

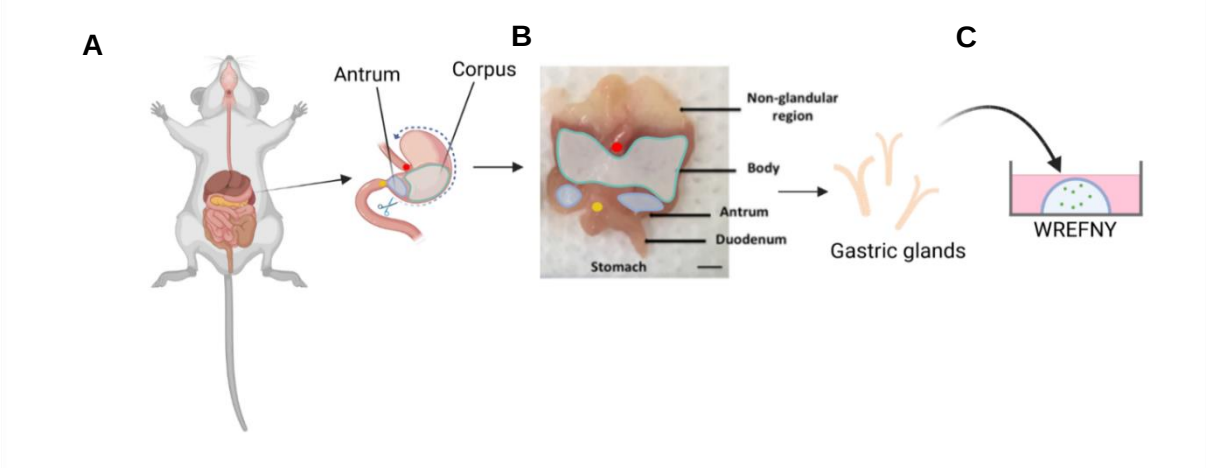

Figure 2.1.1 | Schematic depicting the isolation and culturing of murine primary gastric epithelial cells.
A: Schematic of a mouse GI tract and the location of antrum and corpus, indicating the procedure of opening the stomach along the greater curvature. B: Opened mouse stomach with the distinctive regions of the stomach and uppermost part of the duodenum. Gastric glands are released from epithelial tissue. Adapted from D'Costa, Chonwerawong *et al.*, 2018. C: Schematic of an organoid culture grown in an ECM matrix dome and primary cell medium containing Wnt (W), Rspondin (R), EGF (E), FGF-10 (F), Noggin (N) and Y-27632 (Y). Created with BioRender.

2.1.2.2 Organoid culture

Cells were cultivated as organoids for 7 days before being passaged, with medium changes every 3 days. For passaging of the organoid cultures, medium was removed and 300 µL cell recovery solution or organoid harvesting solution added to each well, breaking the ECM dome. Plates were then incubated on an orbital shaker (30 min, 150 rpm, 4 °C). All plasticware that would get in contact with the cells was previously coated as described in Organoid culture. Following incubation, organoid suspensions were collected in microcentrifuge tubes on ice and centrifuged (700x *g*, 5 min, 4 °C). Organoids were sheared into smaller pieces by passing them through a P10 pipette tip, which was attached to a P1000 filter pipette tip three times. Tubes were then centrifuged again (300x *g*, 5 min), supernatants removed and fresh, ice-cold ECM added. Organoids were split in a 1:2 ratio, meaning that from each original dome two new domes were created.

Cells were grown in human organoid medium (Table 1).

2.1.2.3 Mucosoid-like culture

To create murine liquid-liquid interface (mucosoid-like) cultures, organoids from 8-10 wells were collected as described in *Organoid culture*. After removing the supernatant containing

the dissolved ECM, pellets were resuspended in 700 µL TrypLE Express enzyme solution. Organoids were sheared as described above and tubes subsequently placed in a waterbath at 37 °C and incubated for 1 min. 300 µL of cell culture medium containing 10% FBS were added to each tube. Organoids were sheared three more times and then live cell counts determined as described in Mucosoid culture. $3x10^5$ viable cells were seeded on a Millicell cell culture insert, which had been coated as described in Mucosoid culture, using bovine collagen IV instead of collagen I as murine cells did not adhere to cell culture inserts when coated with collagen I. When using collagen IV, cells adhered to inserts for the duration of the experiment. Cells were kept in liquid-liquid interface culture with medium changes every 3-4 days for 14 days. New cultures were always made from organoids and never propagated from mucosoid to mucosoid.

Cells were grown in human mucosoid medium (Table 2).

2.2 Human cancer cell line culture

2.2.1 AGS cells

AGS, a gastric adenocarcinoma cell line (Barranco, Townsend *et al.*, 1983; Barranco, Townsend *et al.*, 1983) was used to carry out experiments and to create AHR-knockout and AHR-overexpressing cell lines. Since commercially available AGS cell lines can be infected with parainfluenza virus 5 (PIV5; Young, Carlos *et al.*, 2007), a PIV5-free AGS cell line, termed AGSo, was used in this project. Throughout this thesis, these cells will be referred to as “AGS cells”.

AGS cells were routinely cultured in Roswell Park Memorial Institute 1640 medium (RPMI), which was supplemented with 10%(v/v) fetal bovine serum (FBS; from here on referred to as “complete RPMI”). Cells were cultured in cell culture flasks (Corning or Sarstedt) in a humidified incubator at 37 °C and 5% CO_2 until 80-90% confluency before passaging. For passaging, growth medium was removed, cells washed once with an equal volume of sterile phosphate-buffered saline (PBS, pH 7.4) and then 2 mL (for a T75 flask) or 5 mL (for a T175 flask) of 0.05% Trypsin-EDTA (Gibco) were added to the cells, respectively. Cells were normally

incubated for around 10 min or until completely detached, before 8 mL or 5 mL of complete RPMI was added to inactivate the trypsin. The cell suspension was then centrifuged for 3 min at 500x *g*, the supernatant removed and the cells resuspended in complete medium. For routine culturing, subcultivation was normally performed at a ratio of 1:10.

2.2.2 Caco-2 cells

Caco-2 is a colorectal adenocarcinoma cell line (Fogh, Fogh *et al.*, 1977). Caco-2 cells were routinely cultured in Dulbecco's Modified Eagle Medium (DMEM), which was supplemented with 10%(v/v) FBS (from here on referred to as “complete DMEM”). Culturing and passaging conditions were the same as for AGS cells.

2.2.3 HEK293T cells

HEK293T is a human embryonic kidney cell line (Graham, Smiley *et al.*, 1977). HEK293T cells were routinely cultured in complete DMEM. Culturing and passaging conditions were the same as for AGS cells.

2.3 Bacterial cell culture

2.3.1 *Helicobacter pylori* culture

Bacteria were grown from frozen glycerol stocks on GC agar (36 g/L) selection plates supplemented with 100 µg/mL vancomycin, 10% horse serum, 1% vitamin mix, 1 µg/mL nystatin and 5 µg/mL trimethoprim for two passages in a humidified incubator at 37 °C, 10% CO_2 and 5% O_2. For infection experiments, after the first passage bacteria were transferred onto four new plates using a single cotton swab and cultured over night to obtain bacteria growing at different densities.

Table 3 | Vitamin mix for *H. pylori* plates

Compound	Final concentration
D(+)-Glucose	100 g/L
L-Glutamine	10 g/L
L-Cysteine hydrochloride monohydrate	26 g/L

Thiamine pyrophosphate	100 mg/L
Iron(III) nitrate nonahydrate	20 mg/L
Thiamine hydrochloride	3 mg/L
4-aminobenzoic acid	13 mg/L
Nicotinamide adenine dinucleotide	250 mg/L
Vitamin B12, 0.1% in mannitol	10 mg/L
L-Cystine	1.1 g/L
Adenine hemisulfate	1 g/L
Guanine hydrochloride	30 mg/L
L-Arginine hydrochloride	150 mg/L
Uracil	500 mg/L

2.3.2 *Escherichia coli* culture

Bacteria were grown on Luria-Bertani (LB) agar plates for one passage overnight in an incubator at 37 °C to form colonies. Liquid cultures were grown in LB broth in a shaking incubator over night at 37 °C and 200 rpm. Both LB broth and agar plates were supplemented with 100 µg/mL ampicillin if antibiotic selection was required.

2.4 Cryopreservation of bacterial cells

2.4.1 *Helicobacter pylori*

Bacteria were grown as described in 2.3.1. After two passages, bacteria were collected in PBS, pelleted by centrifugation at 3250x *g* for 10 min and resuspended in 1 mL/plate of brain-heart infusion (BHI) broth (36 g/l) supplemented with 10% FBS. Sterile glycerol (86%) was added to bacterial suspensions for a final concentration of 20%, mixed thoroughly and then immediately frozen on dry ice. Frozen stocks were stored at -80 °C.

2.4.2 *Escherichia coli*

Bacteria were grown in liquid culture as described in 2.3.2. Sterile glycerol (86%) was added to bacterial suspensions for a final concentration of 20%, mixed thoroughly and then immediately frozen on dry ice. Frozen stocks were stored at -80 °C.

2.5 *H. pylori* infections

If not otherwise specified, all incubation steps were carried out in a humidified incubator at 37 °C and 5% CO_2. Infections of human cells were conducted using *H. pylori* strain P12 (Haas, Meyer *et al.*, 1993). The strain was chosen as it possesses a functional cagPAI and expresses the cagPAI-encoded T4SS (Odenbreit, Püls *et al.*, 2000), has been shown to successfully induce NF-κB activation in human epithelial cells (Pfannkuch, Hurwitz *et al.*, 2019) and a number of isogenic deletion mutant strains were available in the lab. Infections of murine cells were conducted using *H. pylori* strain PMSS1 as this strain is one of few *H. pylori* strains that can successfully infect mice long-term and possesses a functional cagPAI (Arnold, Lee *et al.*, 2011). It was also the strain chosen to infect mice *in vivo* and was therefore used for *in vitro* infection experiments. Several isogenic deletion mutant strains were available in the lab.

2.5.1 Preparation of *H. pylori* suspensions

Bacteria were grown as described in 2.3.1. On the day of the infection, bacteria from four different plates (passage 2) were collected using a cotton swab and each plate resuspended separately in warm BHI medium. For infections of AGS cell lines, bacteria were resuspended in warm, FBS-free RPMI medium (or DMEM, for infections of Caco-2 cells). 150 µL of each bacterial suspension were added to 500 µL of the respective medium in a 24 well cell culture plate and the plate was placed in an incubator at 37 °C for 10 min. Bacteria were then assessed for fitness via observation of motility (i.e., proportion of bacteria displaying directed movement) using a bright field microscope at 400x total magnification. The suspension of bacteria that displayed the highest fitness was chosen for infection.

The suspension was diluted to optical density at 550 nm (OD_{550}) 1 in case of RPMI medium or OD_{600} 1 in case of BHI medium using a spectrophotometer to obtain a bacterial count of 10^8

cells/mL. If using BHI medium, the diluted suspensions were then washed twice in PBS to remove potential AHR ligands present in the BHI medium. For infections of cell lines using RPMI medium, this step was skipped as the bacteria were resuspended in the same medium the cells were cultured in, meaning no additional compounds were added to the cells through the medium.

Preparation of suspensions was identical for both *H. pylori* strains P12 and PMSS1.

2.5.2 Infection of cell lines

AGS or Caco-2 cells were seeded on 24-well cell culture plates the previous day, cultured overnight and used for infection experiments at 70% confluency. On the day of the infection, cell culture medium with 10% FBS was replaced with 500 µL of the respective FBS-free cell culture medium 2 h before infection. Bacterial suspensions were prepared as described in Preparation of *H. pylori* suspensions. Cells were infected at a multiplicity of infection (MOI) of 100 or 10, meaning that per eukaryotic cell, 100 or 10 bacterial cells were added to each well, respectively. For a 24-well cell culture plate, the MOI was calculated assuming a confluent well contains $4x10^5$ cells. For one well an MOI of 100 is equivalent to $4x10^7$ bacterial cells or 400 µL of an OD_{550} 1 suspension. To reduce the required volume, the OD_{550} 1 suspension was pelleted and subsequently resuspended in 30% of the initial volume of FBS-free RPMI to obtain a more concentrated suspension. 120 µL of the concentrated suspension were then added per each infected well. In case of an infection performed with an MOI of 10, 40 µL of the initial, non-concentrated suspension were directly added to each infected well.

If not otherwise specified, cells were infected for 24 h and motility of the bacteria checked 1 h post infection. Infections were stopped by removal of infection medium, carefully washed by addition and removal of 500 µL warm PBS to each well and finally addition of lysis buffer, exact buffer and volume depending on the subsequent analysis.

2.5.3 Infection of murine organoid cultures

Bacterial suspensions were prepared as described in Preparation of *H. pylori* suspensions, using BHI medium. Organoids were cultured as described in 2.1.2.2. For infections, Cultrex

BME was removed and organoids were harvested as described in 2.1.2.2. Organoids were roughly sheared by passing through a coated 10 µL pipette tip attached to a 1000 µL filtered pipette tip using a P1000 pipette once to obtain large organoid fragments. Fragments were subsequently resuspended in organoid medium with a volume of bacterial suspension that corresponded to an MOI of 50 for a total volume of 300 µL. The resulting suspension was incubated for 1 h at 37 °C and then centrifuged at 1000x *g* for 1 min. Supernatant was removed and pelleted organoid fragments were then resuspended in 100 µL ice-cold BME and 50 µL each added to two wells of a 24-well cell culture plate, creating a dome in the middle of each well. Cells were incubated at 37 °C for 30 min to induce polymerisation of BME. Once polymerised, 500 µL of warm mouse organoid culture medium were added to each well and cells incubated overnight at 37°C (adapted from Sepe, Hartl *et al.*, 2020). After 24 h, cells were lysed by addition of 350 µL RLT lysis buffer per well.

2.5.4 Infection of human mucosoid cultures

Human mucosoid cultures were used for infection experiments 21 days after seeding if producing clear mucus that did not contain any medium (indicative of an incompletely formed monolayer). Cells from a single culture were detached for counting as described in Mucosoid culture and MOI were calculated based on the total cell count. If not otherwise specified, cells were infected for 24 h with an MOI of 50. Bacterial suspensions were prepared as described in Preparation of *H. pylori* suspensions using BHI medium. Bacterial cells were resuspended in 100 µL PBS and added on to the apical side of the mucosoid culture. In the case of non-infected controls 100 µL of PBS were added to the cultures. Infections were stopped by removal of infection medium, carefully washed by addition and removal of 500 µL warm PBS to each well and finally addition of lysis buffer, exact buffer and volume depending on the subsequent analysis (adapted from Boccellato, Woelffling *et al.*, 2019)

2.5.5 Infection of murine mucosoid cultures

Murine mucosoid cultures were used for infection experiments 14 days after seeding if producing clear mucus that did not contain any medium (indicative of an incompletely formed monolayer). Infection was performed as described for human mucosoid cultures.

2.6 Preparation of *H. pylori* lysates

Bacteria were cultured as described in *Helicobacter pylori culture* and prepared as described in Preparation of *H. pylori* suspensions. Suspensions were washed twice by centrifugation at 3250x *g* for 10 min and bacterial pellets subsequently resuspended in 10% of the original volume of dH_2O to enhance bacterial lysis and transferred to screw-cap tubes. Suspensions were snap-frozen in liquid nitrogen and then thawed in a water bath heated to 37 °C three times in total. Suspensions were then transferred to a microcentrifuge tube and sonicated using a Bioruptor sonication device (Diagenode) on high setting twice for 15 min at 4 °C.

Of the resulting lysate, 100 µL were plated on a *Helicobacter* culture plate (see *Helicobacter pylori culture*) and cultured for two days to confirm lysates contained no viable bacteria.

2.7 RNA isolation

RNA isolation was performed using the RNeasy Mini kit (Qiagen) and the GeneJET RNA purification kit (Thermo Scientific) according to the respective instructions. Isolated RNA was quantified using a Nanodrop 2000 spectrophotometer (Thermo Scientific) and absorbance values at 230 nm, 260 nm and 280 nm compared to assess the quality of isolated RNA. For RNA samples intended for RNA-sequencing an additional on-column DNase treatment step was performed using an RNase-free DNase kit during isolation with the RNeasy Mini kit (both Qiagen).

Adherent cells cultured in cell culture plates and primary cells grown in organoid or mucosoid cultures were lysed for RNA isolation by addition of 350 µL of the kit's respective lysis buffer per well of a 24-well cell culture plate i.e., to one dome of BME/Matrigel or one mucosoid

transwell, or directly onto the adherent cells in the case of cell lines. Prior to lysis, cells were washed once with room-temperature PBS.

To isolate RNA from mouse stomach tissue, the snap-frozen tissue was first ground up into fine particles in a microcentrifuge tube using a disposable polypropylene pestle (Bel-Art), while the tube was submerged in liquid nitrogen to keep the tissue frozen. 350 µL of the respective kit's lysis buffer were added to the tissue at room temperature and the tissue homogenized by passing it through a syringe and 21G needle 15-20 times. Homogenates were then left for further cell lysis for 10 minutes at room temperature.

2.8 Reverse transcription - quantitative polymerase chain reaction

Reverse transcription - quantitative polymerase chain reaction (RT-qPCR) was carried out in a two-step format. Firstly, synthesis of cDNA was performed on a Veriti 96-well Fast Thermal cycler (Applied Biosystems) using the Tetro cDNA synthesis kit (meridian Bioscience) according to manufacturer's instructions, using oligo $(dT)_{18}$ primers. If not specified otherwise, 500 ng of RNA were used per sample. Following cDNA synthesis, samples were diluted 1:10 in nuclease-free water.

Secondly, qPCR was performed on a StepOnePlus Real-Time PCR system or a QuantStudio 3 Real-Time PCR system (both Applied Biosystems) using the SensiMix SYBR Hi-ROX kit (for the StepOnePlus) or the SensiMix SYBR Low-ROX kit (for the QuantStudio 3), respectively (both Meridian Bioscience). For each well, 12.5 ng of cDNA in 5 µL were added to 10 µL of 2x master mix, 4 µL of nuclease-free water and 1 µL of 10 µM primer mix, containing 10 pmol each of forward and reverse primer. Reactions were performed in technical triplicates.

The qPCR was carried out as follows: An initial denaturation step at 95 °C was performed for 10 minutes to denature DNA and activate the hot start polymerase, followed by 40 cycles of 1) denaturation at 95 °C for 15 s, 2) annealing at 60 °C for 30 s and 3) extension at 72 °C for 30 s. After 40 cycles, melt curve analysis was performed by first increasing the temperature to 95 °C for 15 s and then starting gradual dissociation of the PCR product by stepwise increase of the temperature from 60 °C to 95 °C in increments of 0.3 °C/s, holding the temperature for 5 s

per step and measuring fluorescence. The resulting fluorescence profile was then plotted as the derivative of the fluorescence intensity against the temperature. Signals were considered specific if one clear fluorescence peak could be observed for each investigated gene. Additional peaks were considered to be signal if they reached 10% of the intensity of the main peak.

C_T values were calculated by the respective qPCR cycler software, where the threshold was manually set to 0.2 ΔR_n for experiments performed on the StepOnePlus cycler or 0.03 on the QuantStudio 3 cycler, respectively, to allow comparability and calculation of relative gene expression values between separate plates. Baselines were set automatically by the respective software. C_T values obtained from qPCR experiments run on one cycler were only compared to C_T values obtained from the same cycler. For human cells, *C1orf43* was used as the reference gene, for murine cells small ribosomal subunit protein uS13 (*Rps18*).

Quantification of gene expression was performed in Microsoft Excel using the $2^{-\Delta\Delta C_T}$ method (Livak and Schmittgen, 2001), where

$$\Delta C_T = C_T(\text{gene of interest}) - C_T(\text{reference gene})$$

for a given sample and

$$\Delta\Delta C_T = \Delta C_T(\text{sample}) - \Delta C_T(\text{biological reference sample}).$$

For experiments performed in duplicates or triplicates, the median of the ΔC_T values of the biological reference sample from each experimental replicate was used as ΔC_T(biological reference sample) for all calculations. The fold change (FC) or relative change of the expression of the gene of interest in a given condition compared to the biological control was then calculated as

$$FC = 2^{-\Delta\Delta C_T}.$$

Statistical analyses were performed on the $\log_2$ of the FC values and plots produced using GraphPad Prism versions 9.0.0 and 10.0.0.

2.9 Primer design

Primers for qPCR were designed using the NCBI Primer-BLAST tool with the following modifications to the default settings:

PCR product size range was set to 70-300 bp; primer T_m range was set to 59 °C (min) – 60 °C (opt) – 61 °C (max), with a max. T_m difference of 2 °C; exon-junction span was set to "primer must span an exon-exon junction", organism was set to either "Homo sapiens" or "Mus musculus" depending on the experiment; GC clamp was set to 1; primers were required to have at least 4 total mismatches to unintended targets, including at least 3 mismatches within the last 3 bps at the 3' end.

Of the up to 10 returned primer pairs, the one with the lowest self-complementarity and self 3'-complementarity values were chosen.

2.10 Selection of housekeeping gene for mouse qPCR

One antrum RNA sample obtained from mice used in the *in vivo* infection experiment was used per condition. Seven commonly used reference genes (*Rps18*, *Gapdh*, *Rplp0*, *Tubb5*, *Tbp*, *Ywhaz*, *B2m*) were selected as candidates for reference genes and their expression measured across all RNA samples by RT-qPCR. The expression values were then used to calculate an overall comprehensive gene stability score using the RefFinder tool (Xie, Xiao *et al.*, 2012, Xie, Wang *et al.*, 2023).

2.11 Western blotting

2.11.1 Protein quantification

Protein quantification was performed prior to SDS-PAGE/Western blotting when specific amounts of protein were needed to be used for either assay. Cells were lysed by addition of 1x radioimmunoprecipitation assay (RIPA) buffer, followed by a 30 min incubation on ice, with a 15 s vortexing step every 10 min. Cell lysates were then centrifuged at 13000x *g* and 4 °C for 15 min. Supernatants were transferred to a new microcentrifuge tube and 10 µL per sample used to determine protein concentration with a Pierce BCA protein assay kit (Thermo Scientific)

according to the manufacturer's instructions using a pre-made BSA standard dilution series included in the kit. Absorbance was measured at 560 nm on a CLARIOstar microplate reader (BMG Labtech) and absorbance values of the BSA standards plotted against the protein concentration. If the absorbance of the protein sample was in the linear range of the standard curve, slope and intercept of the curve were used to calculate the concentration of the protein sample from its measured absorbance at 560 nm.

$$A_{560} = m \cdot c + n \Leftrightarrow c = \frac{A560 - n}{m}$$

where m = slope, n = intercept, c = concentration and A_{560} = absorbance at 560 nm.

Table 4 | RIPA buffer (2x)

Compound	Final concentration
Sodium chloride	300 mM
NP-40	2% (v/v)
Sodium deoxycholate	1% (v/v)
SDS	0.2% (v/v)
Tris, pH 8.0	100 mM

2.11.2 Sodium dodecyl sulphate - polyacrylamide gel electrophoresis

In preparation for western blotting, proteins were size-separated by sodium dodecyl sulphate - polyacrylamide gel electrophoresis (SDS-PAGE). Cells were lysed in 1x Laemmli buffer (Laemmli, 1970) or, if protein quantification was to be carried out first, in RIPA buffer and then subsequently diluted to the desired concentration using water and 4x Laemmli buffer (Table 5).

Separation of proteins was achieved using a polyacrylamide gel consisting of a stacking part at the top (Table 7) and a separation part at the bottom (Table 6). Gels were prepared using Mini-PROTEAN short plates, spacer plates (1 mm), casting frames and casting stands (all Bio-Rad), where one spacer plate and one short plate were clamped together in a casting frame, which was then held in place and sealed at the bottom by a casting stand (in combination called a "casting station"). The resolving gel was prepared with a final concentration of 10%

acrylamide for optimal resolution of AHR (MW = 96 kDa). The prepared solution was added to the gel casting station until it was about 80% filled. The resolving gel was then overlaid with isopropanol to create a smooth, even edge and remove any bubbles that formed on top of the gel. The gel was then left to polymerise and, once polymerised was overlaid with a second gel with 3.75% acrylamide, to which a comb was added to create pockets to hold the protein samples. When a 15-well comb was used, 10 µL of sample were added, for a 10-well comb 20 µL. To be able to estimate the molecular weight of proteins, a Precision Plus Dual Color Standard ("ladder"; Bio-Rad) was added to at least one empty lane of each gel. Samples were heated to 95 °C for 5 min before being loaded onto the gel for denaturation. Gels were placed into a Mini-PROTEAN Tetra cell vertical tank (Bio-Rad) filled with ice-cold 1x running buffer before addition of samples. Runs were carried out at 20 mA for 2 h.

Table 5 | Laemmli buffer (4x)

Compound	**Final concentration**
Tris base	250 mM
SDS	8% (v/v)
Glycerol	40% (v/v)
2-mercaptoethanol	20% (v/v)
Bromophenol blue	0.005% (v/v)

Table 6 | Resolving gel

Compound	**Final concentration**
Acrylamide-Bisacrylamide (37.5:1)	10% (v/v)
Tris	125 mM
SDS	0.1% (v/v)
APS	0.17% (v/v)
TEMED	0.083% (v/v)

Table 7 | Stacking gel

Compound	Final concentration
Acrylamide-Bisacrylamide (37.5:1)	3.75% (v/v)
Tris	125 mM
SDS	0.1% (v/v)
APS	0.17% (v/v)
TEMED	0.083% (v/v)

2.11.3 Immunoblotting

If not otherwise specified, western blots were carried out after completing SDS-PAGE as described in Sodium dodecyl sulphate - polyacrylamide gel electrophoresis. Following the run, the gel was carefully removed from the spacer plate, placed onto an Amersham Protran 0.45 µm nitrocellulose blotting membrane (Cytiva) sandwiched between two foam pads and four layers of Whatman filter paper (GE Healthcare), held together in a gel holder cassette. The cassette was then submerged in ice-cold 1x transfer buffer. Transfer of proteins was carried out overnight (18 - 20 h) at 4 °C and a voltage of 20 V using a wet-transfer Criterion blotting system (Bio-Rad). Following transfer, membranes were briefly washed in 1x TBS to remove methanol and then blocked in 5% (w/v) skim milk (Marvel) in 1x TBS at room temperature for 30 min. After blocking, membranes were briefly rinsed in 1x TBS twice before being incubated with primary antibody diluted either in a) 5% skim milk in 1x TBS with 0.1% Tween-20 (TBS-T) or in b) 5% (w/v) bovine serum albumin (BSA) in 1x TBS-T containing 0.02% (w/v) sodium azide, depending on the antibody. Primary antibody incubation was carried out overnight at 4 °C on a tube roller. The following day, antibody solutions were removed, membranes briefly rinsed in 1x TBS-T and then washed in twice for 5 min and twice for 10 min in 1x TBS-T, with the washing buffer being replaced after each incubation. This step was followed by incubation with species-specific, horseradish peroxidase (HRP)-conjugated secondary antibody, diluted 1:7000 in 5% (w/v) skim milk in 1x TBS-T, for 1 h at room temperature. Membranes were then washed again as described before, transferred to a ChemiDoc MP imaging system (Bio-Rad)

and overlaid with 1 mL of Amersham ECL Select Western Blotting Detection Reagent (Cytiva). Ladder bands were visualized with the colorimetric imaging mode and protein bands using the chemiluminescence mode.

2.12 Bulk RNA-sequencing

RNA sequencing was carried out in two separate experiments: the first one on murine RNA samples collected from the antrum was performed by the Oxford Genomics Centre (OGC) as a service. RNA samples were submitted to the OGC after quantification using a Nanodrop 2000 and quality control using a 2100 Bioanalyzer system (Agilent). One sample was recovered from FFPE tissue and analysed using a separate, specific workflow for FFPE samples by the OGC. Libraries were prepared using a Lexogen QuantSeq 3‘ mRNA-Seq Library Prep Kit (FWD) for Illumina. Libraries were pooled and run on a NextSeq 500 sequencer (Illumina) using the NextSeq 500/550 High Output Kit, 75 cycles (Illumina). Subsequently, raw, demultiplexed fastq files were supplied by the OGC for further analysis.
The second experiment was performed by the candidate using murine corpus RNA samples and murine mucosoid epithelial cell samples. The workflow for the second experiment was carried out as described below.

2.12.1 RNA isolation

RNA was isolated from snap-frozen stomach tissue using the RNeasy Mini kit (QIAGEN) or the AllPrep DNA/RNA Mini Kit (QIAGEN) in case of murine antrum tissue samples. First, tissue was ground to a powder using a plastic pestle and a microcentrifuge tube. To avoid thawing of the tissue, the tube was repeatedly submerged in liquid nitrogen. 350 µL of RLT buffer were then added to the tube and the tissue was further homogenised by passing it through a 21G needle into a clean 1 mL syringe for 10-20 times, until no obvious tissue pieces were present in the lysate. RNA was then extracted following the kit manufacturer’s instructions. Extracted RNA was quantified using a Nanodrop 2000 (Thermo Fisher Scientific).

2.12.2 RNA quality control

Quality of extracted RNA was tested using a 2100 Bioanalyzer instrument (Agilent) and an RNA 6000 Pico kit (Agilent). RNA was diluted to the appropriate range in nuclease-free water and then loaded onto an RNA 6000 Pico chip, following the manufacturer's instructions. The loaded and prepared chip was then analysed on the Bioanalyzer instrument. RNA integrity was assessed by electrophoresis, determined by degradation of 18S and 28S rRNA and reported as RNA integrity number (RIN). Samples with a RIN>6 were used for library preparation.

2.12.3 Library preparation

cDNA libraries were prepared from RNA using the 3' mRNA-Seq V2 Library Prep Kit FWD with Unique Dual Indices (12nt) (Lexogen) in a two-step process: first, libraries were generated by 1) oligo(dT)-primed reverse transcription, 2) removal of RNA template, 3) second strand synthesis using random primers and 4) purification of tagged, double-stranded cDNA libraries. Secondly, libraries were amplified by endpoint PCR, after an intermediate step to determine the optimal cycle number by qPCR using the PCR Add-on and Reamplification Kit (Lexogen) and SYBR Green I, 10000X (Thermo Fisher Scientific).

The optimal cycle number was determined as the number of cycles needed to reach half-maximal fluorescence minus 3; 14 cycles were used for the final endpoint PCR. Endpoint PCR amplification was also used to attach i5 and i7 indices to each individual library, as well as Illumina sequencing adapters.

Amplified cDNA libraries were quality checked and quantified using a 4150 Tapestation (Agilent) with the high sensitivity D1000 reagents (Agilent). Libraries were pooled equimolarly to a final concentration of 650 pM and the library pool quantified using a Qubit 3 fluorometer (Invitrogen).

2.12.4 RNA sequencing

20 µL of the library pool were loaded into the reagent cartridge according to the manufacturer's instructions. RNA sequencing was carried out on a NextSeq 2000 sequencer using the NextSeq 2000 P3 Reagents (100 Cycles; Illumina). The run was set up using the Illumina

basespace environment. Following completion of the run, data were demultiplexed using the BCL Convert App on the basespace environment.

2.12.5 Data analysis

The following data handling steps were carried out by Dr Pakavarin Louphrasitthiphol (Goding group, Ludwig Institute for Cancer Research, University of Oxford).

Demultiplexed raw fastq reads for each sample were stitched using UNIX, quality controlled using fastqc (v0.11.9), then adaptor-, poly-A-, and 2 colour-trimmed as paired-end reads using trim_galore (v0.6.5; running python-base v.3.6.10, cutadapt v.2.10, java v.17.0.1, fastqc v.0.11.9, and pigz v.2.4). Processed fastq results were mapped against the Mus musculus (UCSC/mm10) igenomes STAR index using rna-star (v2.7.8a) using two-pass mapping with quantMode enabled, allowing for soft-clipping (Nmin = 0.2) and splicing (min 20 bp).

The following data analysis steps were carried out by the candidate.

Data analysis was performed using R (v4.2.2) base and Bioconductor packages. Basic data manipulation was carried out using R base commands and the tidyverse package (v2.0.1). ENTREZ IDs and Gene names were retrieved using AnnotationDbi (v1.60.2) and org.Mm.eg.db (v3.16.0). PCA analysis was performed and plots produced using PCAtools (v2.10.0). Count normalisation, differential gene expression analysis and statistical analyses were performed and plots produced with edgeR (v3.40.2). Normalisation was carried out by calculation of counts per million reads (CPM) values and normalisation for composition bias by performing the TMM method (Robinson and Oshlack, 2010). Comparisons were set up, calculating an F statistic, with pairwise comparisons between conditions. Quasi-likelihood (QL) negative binomial generalised log-linear models (GLM) were fit to the data and differentially expressed genes determined using the glmQLFTest() function to perform QL F-tests.

GSEA analysis was carried out and enrichment plots produced using fgsea (v1.24.0). Ranks were calculated as follows:

$$\text{sign}(\text{logFC}) * -\log10(\text{p-value})$$

GO enrichment and overexpression analysis was carried out and plots produced using DOSE (v3.24.2), clusterProfiler (v4.6.2) and enrichplot (v1.18.4) with p-value cutoff of 0.05. for GO

enrichment analysis and p-value cutoff of 0.05 and q-value cutoff of 0.05 for GO overrepresentation analysis. Heatmaps were produced with ComplexHeatmap (v2.14.0) and pheatmap (v1.0.12). Unless otherwise specified, all other plots were produced using R base commands, ggplot2 (v3.4.3) and cowplot (v1.1.1).

All code used to generate data and figures can be found at:

https://github.com/j4yt33/RNA-seq_PhD

2.13 Haematoxylin and eosin staining (H&E)

Tissues were de-paraffinized using xylene washes followed by stepwise rehydration in a series of ethanol solutions (100%, 100%, 90%, 70%) and water. Tissues were then stained with haematoxylin for 5 min at RT, followed by 5 min washing in running tap water and 1 min of differentiation in acidic ethanol. Differentiated tissues were washed for 5 min in dH_2O and then placed in Scot's water for 1 min to induce blueing of the haematoxylin. Slides were then washed for 5 min in dH_2O before being stained with 1% (w/v) Eosin-Y (Sigma Aldrich) in 70% ethanol and 0.5% (v/v) glacial acetic acid for 3.5 min. Slides were then washed in running tap water for 5 min and dehydrated in the opposite order as described for rehydration, incubated in Histo-Clear and mounted using VectaMount (Vector Laboratories).

After drying overnight at RT, slides were imaged using a NanoZoomer S-210 slide scanner (Hamamatsu) in semi-automatic acquisition mode.

2.14 Ethoxyresorufin-O-deethylase assay

To measure enzymatic activity of human cytochrome P450, family 1, subfamily A, polypeptide 1 (CYP1A1), ethoxyresorufin-O-deethylase (EROD) assay was performed (Burke and Mayer, 1974). Cells were cultured in black, clear-bottom cell culture plates (Greiner); $4x10^4$ cells were plated in each well and incubated overnight at 37 °C. The following day, cells were treated as necessary for the respective experiment. 1 h before the end of the experiment, 0.5 nmol 7-ethoxyresorufin (7-ER) were added to each well (4 µM). To reduce the inhibitory activity of NADPH oxidoreductase, 1.25 nmol of dicoumarol were added to the reaction mix (10 µM), as

suggested by Rodrigues and Prough, 1991. Cells were incubated for 1 h before media were removed, cells washed once in 1x PBS and then overlaid with warm 1x PBS for fluorescence measurement. Measurements were performed at 530 nm and 590 nm using a CLARIOstar microplate reader (BMG Labtech), using the top optic measurement setting. Experiments were performed in technical triplicates i.e., three wells per condition. Fluorescence values were then divided by the median of the fluorescence values of non-treated controls from three independent experiments to calculate the fold change for each individual well. Fold changes for each condition were then averaged by calculating the mean. Mean fold changes were compared between conditions.

2.15 Generation of lentiviral particles

Lentiviral particles were produced by transfection of HEK293T cells with 10 µg target DNA plasmid, 7.5 µg of psPAX2 packaging plasmid and 2.5 µg of pMD2.G VSV-G envelope expressing plasmid per 100 mm cell culture plate of 5 - 6x10^6 cells. Plasmids were combined with 62.5 µmol CaCl2 and UltraPure nuclease-free distilled water (Invitrogen) to a total volume of 500 µL. The resulting solution was combined with 500 µL of 2x HEPES-buffered saline (HBS; Sigma Aldrich) and incubated for 20 min at RT.

Volumes were scaled up depending on the number of plates used for transfection.

After incubation, 1 mL of transfection mix were added to each plate of HEK293T cells. Cells were incubated overnight at 37 °C for not longer than 18 h.

The following day, medium was changed to remove transfection mix. After another overnight incubation, lentivirus-containing supernatants were collected and replaced with fresh cell culture medium. The collected supernatants were combined, centrifuged (300x *g*, 5 min, 4 °C) and filtered sterile using a 0.22 µm syringe filter. 0.25 volumes of ice-cold, sterile 40% (w/v) poly(ethylene glycol) 8000 with 0.9% (w/v) NaCl (PEG-8000) were added to the supernatant and then stored at 4 °C. The following day, supernatants were collected again, centrifuged and sterile filtered mixed with 0.25 volumes PEG-8000 and stored at 4 °C. After 3-4 days, both lentivirus-containing supernatants were centrifuged (2500x *g*, 30 min, 4 °C), supernatants

removed and pellets resuspended in 0.5% of the original volume of ice-cold 1x PBS. Solutions were then aliquoted and stored at -80 °C.

2.16 Delivery of plasmid DNA *via* lentiviral transduction

For delivery of plasmid DNA into eukaryotic cells, cells were plated on a 6-well cell culture plate and incubated overnight at 37 °C and 5% CO_2. The following day, transduction medium was prepared by addition of 8 µg of Polybrene infection/transfection reagent (Sigma Aldrich) to 1 mL of cell culture medium. The cell culture medium on the cells was replaced with transduction medium and 20 µL concentrated lentivirus solution (see Generation of lentiviral particles) added to the well and mixed by gentle swirling of the plate. Cells were then incubated for 20 h at 37 °C before the lentivirus-containing transduction medium was replaced with normal cell culture medium. Cells were incubated for further 24 h and then selection was started using the appropriate selection antibiotic.

2.17 Gene knockout using CRISPR/Cas9

AHR knockout was performed using the clustered regularly interspaced short palindromic repeats (CRISPR)-Cas9 gene editing system (Jinek, Chylinski *et al.*, 2012). A lentiviral expression plasmid containing a U6 promotor-driven sgRNA expression cassette as well as a EF1a-driven polycistronic expression cassette expressing Cas9, puromycin resistance gene and turbo green fluorescent protein (tGFP) was used (U6-gRNA:ef1a-puro-2A-Cas9-2A-tGFP; LV01, Sigma Aldrich). The plasmid was obtained from Dr Pedro Moura-Alves (i3S Institute, University of Porto, Portugal) and contained a gRNA targeting the sequence 3'-TCGCCGTATCTCTGGCTGA-5' (- strand) in exon 2 of the human AHR gene.

The system was delivered into cells via lentiviral transduction (see *Delivery of plasmid DNA*).

2.17.1 Generation of clonal cell lines

Transduced and non-transduced cells were selected for 3 days using 2 µg/mL puromycin (InvivoGen) until all non-transduced cells had died. Successful selection was confirmed by epifluorescence microscopy, observing only GFP-positive cells. Selection was continued for

another 4 days with a reduced puromycin concentration of 1 µg/mL. The pool of cells was then sorted into single cells using a MA900 cell sorting system (Sony). Gates were set for viable, GFP+ cells. Sorting was adjusted to the highest stringency, meaning never more than one cell was sorted into each individual well. Cells were cultured in Roswell Park Memorial Institute (RPMI) 1640 medium (Gibco) with 10% (v/v) FCS and 100 U/mL penicillin/streptomycin (Gibco) at 37 °C for 14 days. Wells displaying growth of single colonies were marked and kept for expansion.

Successful knock-out of AHR was assessed by Western blotting. Cells were lysed by addition of 1x Laemmli buffer, lysates collected in microcentrifuge tubes and boiled at 95 °C for 10 min. Lysates were then used for Western blotting as described in One antrum RNA sample obtained from mice used in the *in vivo* infection experiment was used per condition. Seven commonly used reference genes (*Rps18*, *Gapdh*, *Rplp0*, *Tubb5*, *Tbp*, *Ywhaz*, *B2m*) were selected as candidates for reference genes and their expression measured across all RNA samples by RT-qPCR. The expression values were then used to calculate an overall comprehensive gene stability score using the RefFinder tool (Xie, Xiao *et al.*, 2012, Xie, Wang *et al.*, 2023).

Western blotting, testing for the presence of full-length AHR protein, using a C-terminal binding α-AHR antibody (Santa Cruz Biotechnology). Clones showing no band at 100 kDa were assumed to be potentially AHR-deficient.

2.18 Overexpression of AHR

Plasmids for preparation of an AHR-overexpression plasmid were obtained from addgene as bacterial stabs: a lentiviral expression plasmid N174-MCS (#81061) and a plasmid containing the human AHR coding sequence cDNA, pIGAhRC (#112510). The multiple cloning site (MCS) in the expression plasmid contains the unique cutters NsiI and MluI, which were chosen as the AHR cDNA does not contain restriction sites for these enzymes. Cloning primers for AHR were designed so that they would allow amplification of the AHR cDNA sequence from the pIGAhRC plasmid and contain restriction sites for NsiI and MluI on the 5’- and the 3’-end, respectively.

2.18.1 Plasmid preparation and purification

Plasmids were purified from *E. coli* after bacteria were plated on LB agar selection plates containing 100 µg/mL ampicillin (see *Escherichia coli culture*) from bacterial stabs obtained by addgene. Individual bacterial colonies were collected after overnight culture and transferred to 5 mL LB medium containing 100 µg/mL ampicillin. Liquid cultures were incubated overnight as described in *Escherichia coli culture*. Bacteria were pelleted by centrifugation (3500x *g*, 15 min) and plasmid DNA isolated from the pellet using a QIAprep Spin Miniprep kit (Qiagen) according to manufacturer's instructions. Isolated DNA was eluted in ultrapure nuclease-free water and quantified using a NanoDrop 2000 spectrophotometer (Thermo Scientific).

For large-scale purification (i.e., for lentiviral particle preparation), bacteria were grown on LB agar selection plates as described above, then transferred to 5 mL of LB selection medium, incubated on a shaking incubator at 37 °C and 200 rpm for 5 h and then transferred to 500 mL of LB selection medium and incubated overnight as described. The following day, plasmid DNA was isolated using a Plasmid Maxi kit (Qiagen) according to manufacturer's instructions. Isolated DNA was eluted in ultrapure nuclease-free water and quantified using a NanoDrop 2000 spectrophotometer (Thermo Scientific).

2.18.2 Agarose gel electrophoresis

Agarose gel electrophoresis was used to confirm the size of plasmids and DNA fragments and to resolve them by size. Agarose type I (Merck) was dissolved in 1x TAE buffer (Table 8) to a final concentration of 1% (w/v) by boiling the solution in a microwave. Once dissolved, the solution was cooled down under running water to 50 °C and then 3 µL of peqGREEN (Peqlab) per 50 mL of gel were added for visualisation of DNA. Gels were then cast using a Sub-Cell GT horizontal electrophoresis system (Bio-Rad) and a 15-well comb added to form wells. Gels were allowed to solidify at RT for 30 min. The tank was then filled with 1x TAE, thereby overlaying the agarose gel with 1 cm buffer. DNA samples were mixed with 0.2 volumes of 6x Gel loading dye, purple (no SDS, New England Biolabs) and loaded into the wells of the gel. For molecular weight estimation, Quick-Load Purple 1kb DNA ladder or Quick-Load Purple 100 bp DNA ladder (both NEB) were added to one well of the gel, depending on the molecular

weight of the DNA. Electrophoresis was carried out at 100 V for 1.5 - 2 h. Bands were visualized on a ChemiDoc MP imaging system (Bio-Rad) using the SYBR Green setting in Auto Rapid acquisition mode.

Table 8 | TAE buffer (50x)

Compound	Final concentration
Tris	2 M
Glacial acetic acid	1 M
EDTA (0.5 M, pH 8.0)	0.05 M

2.18.3 Polymerase chain reaction

AHR cDNA was amplified and restriction sites added by PCR, which was performed using Phusion High-Fidelity PCR master mix with HF buffer (NEB) to ensure high-fidelity DNA amplification. For each reaction, 25 pmol each of forward and reverse primer and 10 ng of pIGAhRC were combined with 25 µL of 2x Phusion master mix and nuclease-free water to a final volume of 50 µL. PCR was carried out on a Veriti 96-well Fast Thermal cycler (Applied Biosystems). Ideal annealing temperature for the specific primers and master mix used was determined with the NEB Tm Calculator tool (https://tmcalculator.neb.com/#!/main, accessed last on 29/06/2023). An initial denaturation step was performed at 98 °C for 30 s, followed by 25 amplification cycles of denaturation at 98 °C for 10s, annealing at 69 °C for 20 s and extension at 72 °C for 57 s. Amplification cycles were followed by a final extension step at 72 °C for 10 min.

2.18.4 Restriction enzyme digestion and ligation

Restriction digestion was performed using NsiI-HF and MluI-HF restriction enzymes (both NEB). Reactions were carried out with plasmid and insert in separate tubes. 1 µg of plasmid DNA was combined with 5 µL 10x rCutSmart buffer (NEB), 20 U of each enzyme and nuclease-free water to a final volume of 50 µL. For the insert, 0.5 µg of DNA was combined with 5 µL 10x rCutSmart buffer, 10 U of each enzyme and nuclease-free water to a final volume of 50

µL. DNA was digested on a Veriti 96-well Fast Thermal cycler (Applied Biosystems) at 37 °C for 15 min. Digestion was stopped and DNA purified using the Monarch PCR & DNA cleanup kit (NEB). Molecular weights of the digestion products were checked by agarose gel electrophoresis as described above.

Ligation of vector and insert was carried out with a molar ratio of 1:3 (vector:insert), meaning that for 100 ng of vector, 87.51 ng of insert were used. Calculations were performed using the NEB ligation calculator tool (https://nebiocalculator.neb.com/#!/ligation, accessed last on 03/07/2023). Ligation was performed using the Instant sticky-end Ligase master mix (NEB). 5 µL of master mix were combined with plasmid and insert DNA and nuclease-free water to a final volume of 10 µL, mixed 10 times by pipetting and then frozen for transformation.

2.18.5 Generation of chemically competent *E. coli*

E. coli TOP10F' (Invitrogen) were plated on an LB agar plate and cultured overnight to obtain single colonies (see *Escherichia coli culture*). The following day, 5 single colonies were picked and 5 separate tubes of 20 mL LB medium were inoculated with one colony per tube. Bacteria were incubated at 37 °C and 120 rpm on a shaking incubator until cultures reached an OD_{600} of 0.6. Cultures were centrifuged (3500x *g*, 10 min, 4 °C), supernatants discarded and pellets resuspended in 5 mL of 0.1 M $MgCl_2$, combining all 5 pellets. Bacteria were centrifuged again (3500x *g*, 10 min, 4 °C), supernatant discarded, pellet resuspended in 10 mL 0.1 M $CaCl_2$ and incubated on ice for 1 h. Bacteria were then centrifuged once more (3500x *g*, 10 min, 4 °C), supernatant discarded and pellet resuspended in 7 mL of 0.085 M CaCl2 with 15% (v/v) glycerol. Suspensions were aliquoted, frozen on dry ice and stored at -80 °C.

2.18.6 Transformation of competent *E. coli*

100 ng of plasmid DNA were added to 100 µL of suspension of competent *E. coli* bacteria and placed on ice for 1 h. Following incubation, the tube containing bacteria and DNA was placed in a 42 °C water bath and incubated for 3 min and then moved back on ice for another 2 min. As the transformed plasmid contained an ampicillin resistance selection marker, transformed bacteria were immediately plated on an LB agar selection plate (100 µg/mL ampicillin) and

incubated overnight at 37 °C. Single colonies were picked the following day and used for large-scale plasmid preparation (see *Plasmid preparation and purification*).

2.18.7 Generation of cell lines

Isolated plasmid was used to create lentiviral particles (see Generation of lentiviral particles). AGS cells were transduced as described in Delivery of plasmid DNA *via* lentiviral transduction. 48 h after transduction, 500 µg/mL of G418 were added to transduced and non-transduced cells to start selection of cells and selection was carried out for 7 days, until all non-transduced AGS cells had died. Following selection, a western blot for AHR was performed (see One antrum RNA sample obtained from mice used in the *in vivo* infection experiment was used per condition. Seven commonly used reference genes (*Rps18, Gapdh*, *Rplp0, Tubb5, Tbp*, *Ywhaz*, *B2m*) were selected as candidates for reference genes and their expression measured across all RNA samples by RT-qPCR. The expression values were then used to calculate an overall comprehensive gene stability score using the RefFinder tool (Xie, Xiao *et al.*, 2012, Xie, Wang *et al.*, 2023).

Western blotting) to confirm overexpression of AHR protein.

2.19 *In vivo* infection experiment

The *in vivo* infection experiment was carried out by Kirstin Hoffmann and Miriam Lohr at the animal facility of the Max Planck Institute for Infection Biology, Berlin (MPIIB), Germany.

Mice had a C57BL/6 background and were either wild-type (n= 24) or *Ahr*$^{-/-}$ (n = 22); animals were between 4-8 weeks old and all male. Mice were specific-pathogen-free, born and housed at the MPIIB animal facility. Infections were set up as follows:

Genotype	Treatment	Number of mice
Ahr$^{+/+}$	Not infected	4
	Infected 2 weeks	6
	Infected 8 weeks	14

Ahr$^{-/-}$	Not infected	4
	Infected 2 weeks	4
	Infected 8 weeks	14

2.19.1 Preparation of *H. pylori* suspension

H. pylori PMSS1 were prepared for infection from frozen glycerol stocks by plating on two *H. pylori* culture plates (see 2.3.1) and incubating for 48 h at 5% O_2 and 10% CO_2 at 37 °C in a humidified incubator. After 48 h, one plate was selected based on the macroscopic appearance of bacterial colonies and bacteria were transferred onto two new *H. pylori* culture plates using an inoculation loop after resuspension in BHI broth. Plates were then incubated for 24 h at the aforementioned conditions. Following incubation, bacteria from one plate were resuspended in BHI medium, optical density at 550 nm (OD_{550}) determined using a spectral photometer and three liquid cultures with volumes of 22 mL, 10 mL and 7 mL were prepared, respectively, to an OD_{550} of 0.02. Liquid cultures were incubated on a shaker incubator overnight. Following incubation, motility of the bacteria was determined using a phase-contrast light microscope. Liquid cultures were diluted to OD_{550} = 0.22 and centrifuged (4000 rpm, 5 min). Supernatant was discarded and bacteria resuspended in 239 µL co-culture medium (DMEM, 5% FBS, 10% Brucella broth). The resulting suspension had a theoretical OD_{550} of 45 and was assumed to contain 10^8/µL bacteria. Serial dilution of the suspension in PBS was performed and dilutions 10^{-6}, 10^{-7} and 10^{-8} were plated on *H. pylori* culture plates and cultured for 6 d at conditions mentioned above before colony counting.

2.19.2 Infection and sample collection

Mice were infected by oral gavage of 10 µL infection suspension.

After 2 or 8 weeks of infection, respectively, mice were sacrificed by cervical dislocation. Stomachs were harvested, opened along the smaller curvature, forestomachs removed and the tissue dissected as follows: part of the glandular stomach (corpus + antrum) was retained for pathological analysis and fixed in 4% PFA for 24 h at 4 °C; parts of the corpus were

transferred to 500 µL BHI broth for colony counting; parts of antrum and corpus were collected separately for nucleid acid extraction and snap-frozen in microcentrifuge tubes in liquid nitrogen before storage at -80 °C. Samples fixed in PFA were washed twice in PBS following fixation and stored in PBS at 4 °C.

For colony counting, collected samples were weighed out individually, homogenised using a tissue homogeniser and each homogenate diluted 1:5, 1:25 and 1:125, respectively. 100 µL of each dilution were plated on blood agar plates and incubated as described above for 7 days. Colonies were counted and CFU/mg calculated based on dilution and weight of collected tissue. As the lowest dilution was 1:5, a single colony observed would result in a CFU value of 5, which was therefore determined to be the limit of detection for this assay.

2.19.3 Pathological analysis

Pathology scoring was carried out by Anja Kühl at the iPATH.Berlin – Core Unit Immunopathology for Experimental Models at Charité Berlin and severity of pathology scored from none (0) to marked (4) using a modified Sydney Score (Dixon, Genta *et al.*, 1996), which was used to assess *H. pylori*-induced gastritis based on the following: presence of *Helicobacter*, hyperplasia, metaplasia, atrophy and level of leukocyte infiltration. Assessments were made on H&E and PAS-stained FFPE tissue sections.

Scoring was carried out in a single blinded manner, where the pathologist was blinded to ensure unbiased assessment of pathology.

2.20 Quantification of gland height

Length (height) of gastric glands in murine stomach sections was determined using QuPath 0.3.2 (Bankhead, Loughrey *et al.*, 2017). Gland length was measured for 7 individual glands per mouse using the line annotation tool and the mean value was reported as mean gland height for each mouse.

2.21 Statistics

When determining if two unmatched sample sets were significantly different, non-parametric distribution of data was assumed and a Mann-Whitney U test performed.

For analysis of bacterial load (Figure 3.2.4), data were tested for lognormality using the Shapiro-Wilk test. To each normalised CFU value, 0.1 was added before $\log_2$ transformation. Statistical significance was then tested on transformed data using Student's t-test.

For experiments comprising more than two groups, one-way or two-way ANOVA were performed, followed by Tukey's post-hoc test to determine differences between groups when every group was compared to every other group.

When groups were compared to one reference group only, Dunnett's test was performed instead following the ANOVA.

Statistical tests were performed using GraphPad Prism version 9.0.0 and 10.0.0 for Windows, (GraphPad Software, Boston, Massachusetts, USA).

Statistical analysis of RNA-sequencing data was performed using the egdeR package, version 3.40.2 (Robinson, McCarthy *et al.*, 2010, McCarthy, Chen *et al.*, 2012, Chen, Lun *et al.*, 2016).

2.22 Ethics

Primary human gastric epithelial cells were derived from patient samples collected with approval of the ethics committee of Charité University Medicine, Berlin, reference number EA1/129/12.

The *in vivo* infection experiment described in chapter 3 was approved by the ethics commission "Ethik-Kommission des Landes Berlin" of the Regional Office for Health and Social Affairs Berlin (LaGeSo), reference number G0239/18.

Mouse stomachs were obtained from Gitta Stockinger's group (AhRimmunity laboratory, The Francis Crick Institute, London) from animals that were being sacrificed for unrelated projects. Animals were bred and maintained according to protocols approved by the UK Home Office and the Francis Crick Institute ethics committee (AWERP), PPL number PP0858308.

Human cDNA samples described in chapter 4.2.3, Figure 4.2.6 were obtained from Alexander

Link, Otto-von-Guericke University Magdeburg, Germany. Samples were collected with approval of the ethics board of the Otto-van-Guericke University Magdeburg, study number 80/11.

2.23 Materials

All instruments used in this study are listed in the table below.

Table 9 | Instruments

Instrument	Name	Manufacturer
Slide scanner	NanoZoomer S-210	Hamamatsu
PCR cycler	Veriti 96-well Fast Thermal Cycler	Applied Biosystems
Real-time PCR cycler	StepOnePlus Real-Time PCR System	Applied Biosystems
Real-time PCR cycler	QuantStudio 3 Real-Time PCR System	Applied Biosystems
Sequencer	NextSeq 2000	Illumina
cDNA analyser	4150 TapeStation	Agilent
RNA analyser	2100 BioAnalyzer	Agilent
Nucleic acid quantification	Nanodrop 2000	Thermo Fisher Scientific
Nucleic acid quantification	Qubit 3 Fluorometer	Invitrogen
Microscope	ECLIPSE Ts2	Nikon
Microplate reader	CLARIOstar Plus	BMG Labtech
Imaging system	ChemiDoc MP	Bio-Rad

All kits used in this study are listed in the table below.

Table 10 | Kits

Name	Supplier	Catalogue No.
GeneJET RNA Purification Kit	Thermo Fisher Scientific	K0732
RNeasy Mini Kit	QIAGEN	74106
Monarch PCR & DNA Cleanup Kit	New England Biolabs	T1030S
QIAPrep Spin Miniprep Kit	QIAGEN	27104
QIAGEN Plasmid Maxi Kit	QIAGEN	12162
QIAQuick Gel Extraction Kit	QIAGEN	28704
Lexogen QuantSeq 3’ mRNA-Seq V2 Library Prep Kit FWD with UDI 12 nt Set B1, 96 preps	Cambridge Bioscience	192.96
PCR Add-on and Reamplification Kit V2	Cambridge Bioscience	208.96
AllPrep DNA/RNA Mini Kit	QIAGEN	80204
RNA 6000 Pico Kit	Agilent	5067-1513
Pierce BCA Protein Assay Kit	Thermo Fisher Scientific	A55864

All reagents used in this study are listed in the table below.

Table 11 | Reagents and specific consumables

Name	Supplier	Catalogue No.
Instant Sticky-end Ligase Master Mix	New England Biolabs	M0370S
Meridian Bioscience SensiMix SYBR Low-ROX Kit	Scientific Laboratory Supplies	QT625-05
Meridian Bioscience SensiMix SYBR Hi-ROX Kit	Scientific Laboratory Supplies	QT605-05
Meridian Bioscience Tetro cDNA Synthesis Kit	Scientific Laboratory Supplies	BIO-65043
DreamTaq Hot Start Green PCR Master Mix	Thermo Fisher Scientific	K9021
Phusion® High-Fidelity PCR Master Mix with HF Buffer	New England Biolabs	M0531S
NextSeq 2000 P3 Reagents (100 Cycles)	Illumina	20040559
High Sensitivity D1000 Reagents	Agilent	5067-5585
High Sensitivity D1000 ScreenTape	Agilent	5067-5584
Quick-Load® Purple 100 bp DNA Ladder	New England Biolabs	N0551S
Quick-Load® Purple 1 kb DNA Ladder	New England Biolabs	N0552S
peqGREEN	Peqlab	732-2960
6x Gel loading dye, purple (no SDS)	New England Biolabs	B7025S
10x rCutSmart buffer	New England Biolabs	B6004S
SYBRGreen I – 10000X	Thermo Fisher Scientific	S7563
Millicell® Standing Cell Culture Inserts	Merck	PIHP01250
Cultrex Reduced Growth Factor Basement Membrane Extract, Type 2, Select	Bio-Techne	3536-005-02
DMEM	Thermo Fisher Scientific	10566016
RPMI 1640	Thermo Fisher Scientific	61870036
Advanced DMEM/F-12	Thermo Fisher Scientific	12634010
Cell Recovery Solution	Corning	354253
Cultrex Organoid Harvesting Solution	Bio-Techne	3700-100-01
Trypsin-EDTA (0.25%)	Thermo Fisher Scientific	25200056
TrypLE Express	Thermo Fisher Scientific	12604013
Cryo-SFM	PromoCell	C-29912
Precision Plus Dual Color Standard	Bio-Rad	1610374

All antibodies used in this study are listed in the table below.

Table 12 | Antibodies

Antibody	Catalogue No.	Supplier	Dilution
α-AHR (A-3) mouse monoclonal	sc-133088	Santa Cruz Biotechnology	1:300
α-β-Actin-HRP (AC-15)	A3854	Sigma Aldrich	1:2000
Goat anti-Mouse IgG (H/L):HRP	STAR207P	Bio-Rad	1:10000

All plasmids used in this study are listed in the table below.

Table 13 | Plasmids

Name	Description	Source
N174-MCS	Lentiviral vector for constitutive gene expression (empty backbone)	Adam Karpf (addgene #81061)
pIGAhRC	Plasmid containing human AHR and ARNT coding sequences	Charles Miller (addgene #112510)
MISSION LV01_AHR	Lentiviral vector expressing Cas9 and gRNA targeting AHR; tGFP and puromycin selection markers	Pedro Moura-Alves
N174_EF1a-AHR_PGK-NeoR	Lentiviral vector for AHR overexpression; AHR in N174-EF1a with neomycin resistance cassette	Prepared by the candidate
psPAX2	Packaging plasmid	Pedro Moura-Alves
pMD2.G	VSV-G envelope expressing plasmid	Pedro Moura-Alves

All oligonucleotides used in this study were purchased from Integrated DNA Technologies (Leuven, Belgium) and are listed in the table below.

Table 14 | Oligonucleotides

Application	Name	Sequence (5'->3')
qPCR	Human *AHR* gene, forward	CAAATCCTTCCAAGCGGCATA
qPCR	Human *AHR* gene, reverse	CGCTGAGCCTAAGAACTGAAA G
qPCR	Human *CYP1A1* gene, forward	ACATGCTGACCCTGGGAA A
qPCR	Human *CYP1A1* gene, reverse	GGTGTGGAGCCAATTCGGAT
qPCR	Human *GAPDH* gene, forward	GGTATCGTGGAAGGACTCATGAC
qPCR	Human *GAPDH* gene, reverse	ATGCCAGTGAGCTTCCCGTTCAG
qPCR	Human *IL8* gene, forward	ACACTGCGCCAACACAGAAAT
qPCR	Human *IL8* gene, reverse	ATTGCATCTGGCAACCCTACA
qPCR	Human *TNF* gene, forward	TGAAAGCATGATCCGGGACG
qPCR	Human *TNF* gene, reverse	CAGCTTGAGGGTTTGCTACAAC
qPCR	Human *C1orf43*, forward	GGTGAATGTCGTGCTGGTG
qPCR	Human *C1orf43*, reverse	GGATCTCAGAGGTACGAATGG
qPCR	Human *IRF7*, forward	GAGCTGTGCTGGCGAGAAG
qPCR	Human *IRF7*, reverse	TTGGTTGGGACTGGATCTGC
qPCR	Murine *Rps18*, forward	CTTTTGGGGCCTTCGTGTC
qPCR	Murine *Rps18*, reverse	TCTTGGATACACCCACAGTTCG
qPCR	Murine *Gapdh*, forward	TCACCATCTTCCAGGAGCG
qPCR	Murine *Gapdh*, reverse	AAGCAGTTGGTGGTGCAGG
qPCR	Murine *Rplp0*, forward	TCCCACTTACTGAAAAGGTCAAGG
qPCR	Murine *Rplp0*, reverse	GGTTGCTTTGGCGGGATTAG

qPCR	Murine *Tubb5*, forward	ACAACTTCGTTTTCGGTCAGTC
qPCR	Murine *Tubb5*, reverse	AGTCAACCAACTCAGCTCCC
qPCR	Murine *Tbp*, forward	CAGTGCCCAGCATCACTATTTC
qPCR	Murine *Tbp*, reverse	AAGCCCTGAGCATAAGGTGG
qPCR	Murine *Ywhaz*, forward	TGTTCTAGCCTGTTTCCCCG
qPCR	Murine *Ywhaz*, reverse	CATAACTGGATATTCTTCTGGCTGC
qPCR	Murine *B2m*, forward	GACCGTCTACTGGGATCGAG
qPCR	Murine *B2m*, reverse	CATTGCTATTTCTTTCTGCGTGC
qPCR	Murine *Cyp1a1*, forward	TGG TCG TGT CAG TAG CCA AT
qPCR	Murine *Cyp1a1*, reverse	GGA TGT GGC CCT TCT CAA ATG
qPCR	Murine *Cxcl1*, forward	CCAAACCGAAGTCATAGCCAC
qPCR	Murine *Cxcl1*, reverse	CTCCGTTACTTGGGGACACC
Cloning	AHR-FW-NsiI-TAAGCA	TAAGCAATGCATATGAACAGCAGCAGC
Cloning	AHR-RV-MluI-TAAGCA	TGCTTAACGCGTTTACAGGAATCCACTGG

All chemicals used in this study are listed in the table below.

Table 15 | Chemicals

Name	Supplier	Catalogue No.
2,3,7,8-Tetrachlorodibenzo-*p*-dioxin	Agilent	RPE-029S-1
4-(2-hydroxyethyl)-1-piperazineethanesulfonic acid	Thermo Fisher Scientific	15630056
4-Aminobenzoic acid	Sigma Aldrich	100536
6-Formylindolo[3,2-*b*]carbazole	Sigma Aldrich	SML1489
A83-01	Merck	616454
Acrylamide-Bisacrylamide	Severn	20.2100-10
Adenine	Sigma Aldrich	A2786
Agarose	Fisher Scientific	BP1356
Ammonium persulfate	Sigma Aldrich	A3678
Ampicillin	Thermo Fisher Scientific	J66972.AB
B-27	Life Technologies	17504044
Brain-Heart Infusion Broth	Sigma Aldrich	53286
Calcium chloride	Merck	21115
CH223191	Merck	C8124
Ciprofloxacin	Sigma Aldrich	17850
Collagen I, bovine	Life Technologies	A1064401
Dicoumarol	Sigma Aldrich	287897
Dimethylsulfoxide	Sigma Aldrich	D2650
DL-Dithiotreitol	Sigma Aldrich	3860
Epithelial growth factor	Life Technologies	PHG0311
Ethylenediaminetetraacetic acid	Sigma Aldrich	E4884
Fetal bovine serum	Gibco	10500-064
Fibroblast growth factor-10	Peprotech	100-26
G418	Invivogen	ant-gn-1
Gastrin	Merck	G9145
GlutaMAX	Thermo Fisher Scientific	35050038

Glycerol	Sigma Aldrich	G5516
GNF351	Cambridge Bioscience	HY-102023
Guanine hydrochloride	Alfa Aesar	A11532
HEPES-buffered saline (2x)	Thermo Fisher Scientific	J62623.AK
Horse serum	Merck	H1138
Iron (III) nitrate nonahydrate	Sigma Aldrich	254223
L-Arginine monohydrate	Sigma Aldrich	A5131
LB Broth Base (Lennox)	Invitrogen	12780052
L-Cysteine	Alfa Aesar	A13762
L-Glutamine	Merck	100289
N,*N*,*N'*,*N'*-Tetramethylethylenediamine	Sigma Aldrich	T9281
N-2	Life Technologies	17502048
N-acetyl cysteine	Sigma Aldrich	A9165
Nicotinamide	Sigma Aldrich	N3376
Noggin, human	Peprotech	120-10C
Nonidet P40 Substitute	Sigma Aldrich	74385
Nystatin	Gibco	15340-029
Oxoid GC Agar Base	Thermo Fisher Scientific	CM0367B
Poly(ethylene glycol) 8000	Sigma Aldrich	P2139
Primocin	Invivogen	ant-pm-1
Puromycin	Invivogen	ant-pr-1
Resorufin ethyl ether	Merck	46121
Skimmed milk powder	Marvel	N/A
Thiamine hydrochloride	Sigma Aldrich	T4625
Thiamine pyrophosphate	Sigma Aldrich	C8754
Trimethoprim	Alfa Aesar	J63053
Tris	Thermo Fisher Scientific	17926
Triton X-100	Merck	112298
Tween-20	Thermo Fisher Scientific	3005
UltraPure Water	Invitrogen	10977-035
Uracil	Alfa Aesar	A15570
Vancomycin hydrochloride	Sigma Aldrich	SBR00001
Vitamin B12, 0.1% in mannitol	MP Biomedicals	103278
WNT Surrogate-Fc Fusion Protein	Immunoprecise Antibodies	N001

All restriction enzymes used in this study are listed in the table below.

Table 16 | Restriction enzymes

Name	**Supplier**	**Catalogue No.**
NsiI-HF	New England Biolabs	R3127S
MluI-HF	New England Biolabs	R3198S

Chapter 3 – Loss of AHR improves clearance of *H. pylori in vivo* through differential pro-inflammatory response

3.1 Introduction

H. pylori is universally accepted as the main risk factor for the development of gastric pathologies such as gastritis, peptic ulcers and intestinal-type adenocarcinoma (ITAC). It has developed the remarkable ability to persist in the harsh environment of the stomach, not only shielding itself from gastric acid but also avoiding clearance by the host immune system. How the bacterium is able to survive in the stomach acid through production of urease and local buffering of the pH is now well-understood (Sachs, Scott *et al.*, 2011).

Over the last 20 years, research has been focussed on answering the still open question of how exactly the bacterium is able to also escape the immune response (Traulsen, Zagami *et al.*, 2021). Generally, immune response to infection is mediated through interferon or NF-κB signalling. Recently, it has been demonstrated that *H. pylori* can extract cholesterol from human cell membranes, thereby disrupting lipid raft integrity and inhibiting formation of the IFN-γR1/IFN-γR2 heterodimer, ultimately making the infected cell unresponsive to IFN-γ (Morey, Pfannkuch *et al.*, 2018). While this satisfies the question of how *H. pylori* evades the type II IFN signalling-mediated immune response, a comparable mechanism is not known for NF-κB-induced inflammatory responses. *H. pylori* is known to strongly activate NF-κB, posing the question why the bacterium is still able to persist in the gastric epithelium. As the aryl hydrocarbon receptor has been implicated in the regulation of epithelial inflammation, we hypothesized that AHR might play a role in the epithelial response to *H. pylori* infection.

In 2014, AHR was described as a sensor of bacterial compounds for the first time, namely pigments found in *Pseudomonas aeruginosa* and *Mycobacterium tuberculosis* (Moura-Alves, Fae *et al.*, 2014); the authors could show here that loss of AHR resulted in an increased susceptibility of mice to infections with both pathogens. Given that AHR has also been shown to interact with NF-κB signalling (Vogel, Sciullo *et al.*, 2007; Vogel and Matsumura, 2009;

Vogel, Khan *et al.*, 2014), a potential role of AHR signalling seems intriguing in the search for a mechanism, through which *H. pylori* can evade the NF-κB-driven immune response even in the context of chronic inflammation of the stomach.

This chapter aims to investigate the role of AHR in the proinflammatory response to *H. pylori* infection. To do this, we first infected wild-type and *Ahr*-deficient mice with *H. pylori* to identify differences in the immune response.

After infection, tissue samples were collected from the stomach to assess AHR-dependent morphological and phenotypic differences.

Following this, transcriptomic analysis was performed to identify underlying differences in gene expression upon infection in both glandular regions of the stomach and if these are related to NF-κB signalling.

3.2 Results

3.2.1 *Ahr*-deficient mice display differential response to *H. pylori* PMSS1 infection

The AHR has been suggested as a regulator of the inflammatory response in a variety of contexts. To understand if this regulation might be potentially beneficial for *H. pylori* persistence *in vivo*, an infection experiment in *Ahr*-proficient and deficient mice was performed using the mouse-adapted *H. pylori* PMSS1 strain. At two time points, two- and eight- weeks post-infection (p.i.), mice were sacrificed and samples collected (Figure 3.2.1).

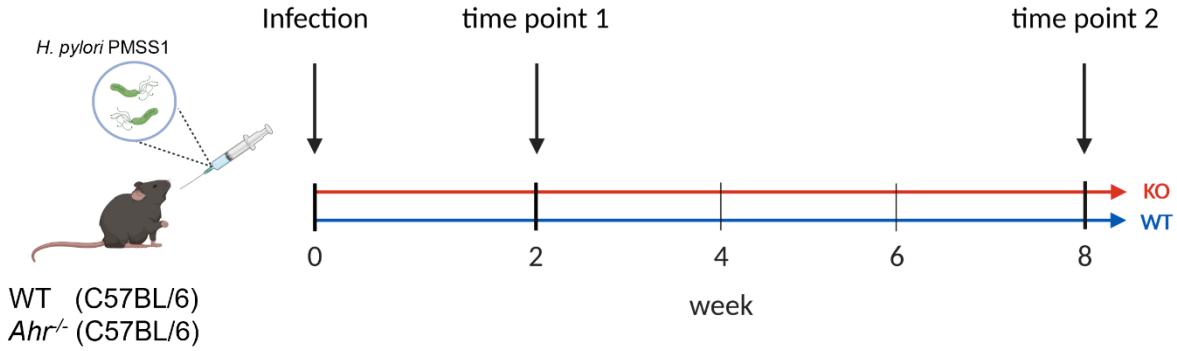

Figure 3.2.1 | Schematic of the *in vivo* infection experiment.
Wild type and *Ahr*$^{-/-}$ C57BL/6 mice were infected with the mouse-adapted *H. pylori* strain PMSS1 by oral gavage for a duration of 2 or 8 weeks. At either time point, mice were sacrificed and samples collected.

The aim of this experiment was to investigate if the absence of AHR would cause a difference in the murine response to infection. Analyses were performed on the tissue (mucosal thickness, pathology score, presence of immune cells) and the bacterial load at each time point, comparing the two genotypes.

First, a pathology score (from 0 - 4) was determined according to a modified Updated Sydney System (Dixon, Genta *et al.*, 1996) for tissue collected from the antrum and corpus region of the stomach. At two weeks p.i., the pathology score in the corpus tissue was 0 in both wild-type and *Ahr*$^{-/-}$ mice, except for two wild-type mice displaying slightly increased pathology. At 8 weeks p.i., a majority of mice were classified as displaying an increased pathology, between 1 and 2, with a few mice showing slightly higher or lower pathology. There was no significant difference between genotypes (Figure 3.2.2A).

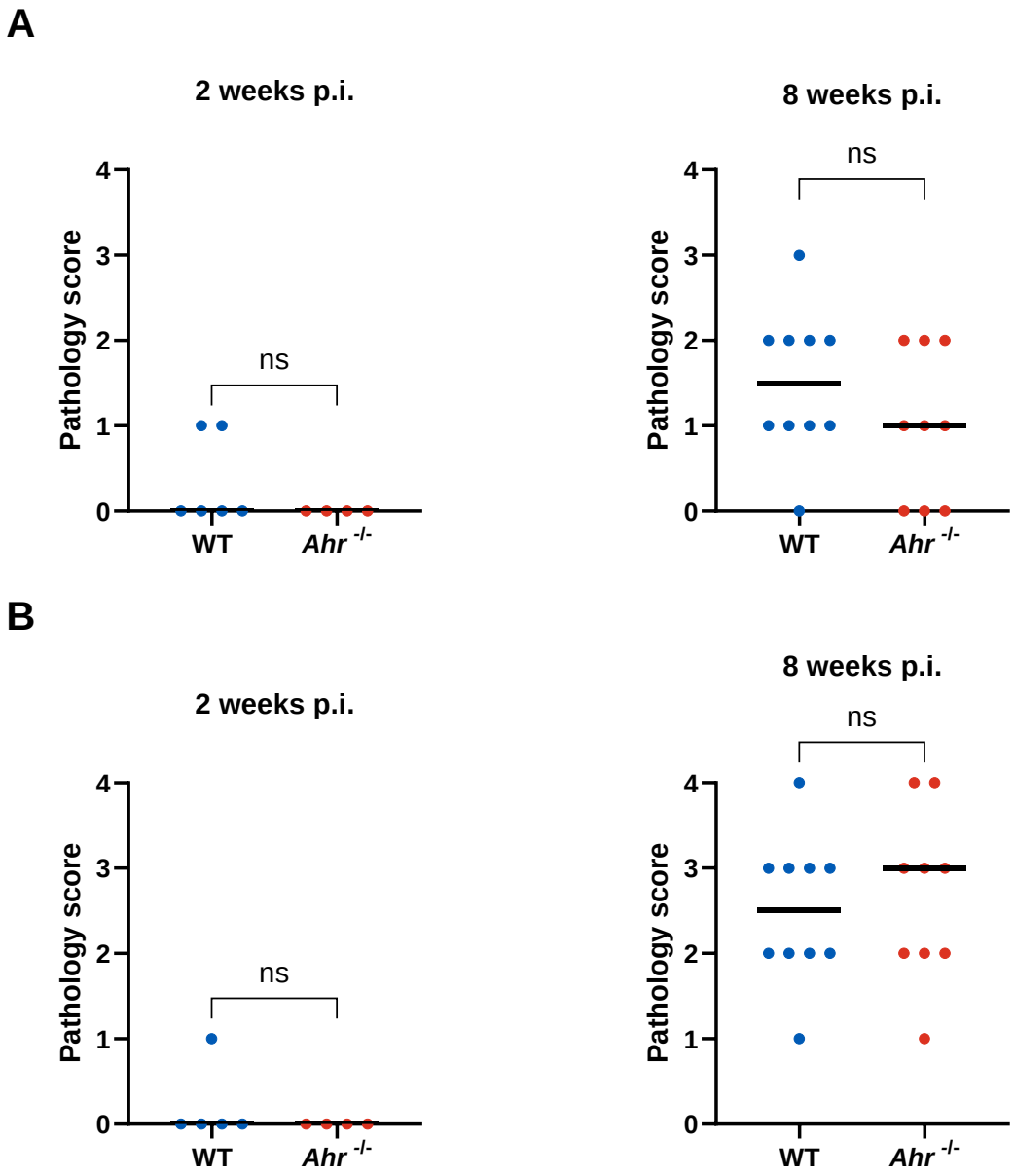

Figure 3.2.2 | Pathology scoring of the corpus region of infected mice.
Pathology scores at both timepoints were not different between genotypes within each respective region of the stomach. A: Pathology scores for tissue collected from the corpus. B: Tissue collected from the antrum. One data point represents one individual mouse (n=4-10). Horizontal bars represent the median of each group. Pathology scores were determined according to the updated Sydney System. Differences were tested for statistical significance by Mann-Whitney U test. ns: non-significant.

In tissue collected from the antrum, at two weeks p.i., all of the mice except for one wild-type mouse displayed no observable pathology, whereas after eight weeks of infection, pathology was markedly increased in both genotypes, with a majority of mice being scored as either 2 or 3 with a few outliers with higher or lower pathology (Figure 3.2.2B). Again, the difference between genotypes was not significant.

As the pathology scoring combines several indicators of pathological response to infection, more nuanced differences or differences in only few of the criteria might be missed. One key response to *H. pylori* infection is the thickening of the mucosa, or hyperplasia. Therefore, the thickness of the mucosa was determined by measuring the height of glands in the corpus region of individual mice and comparing median gland heights (Figure 3.2.3; N.B.: "gland height" refers to the total length of the gland plus the foveola). In non-infected mice, the median gland length was about 290 µm in wild-type mice and about 340 µm in *Ahr*$^{-/-}$ mice, with a variation of about 100 µm in each of the genotypes; a similar difference could be observed at 2 weeks p.i., albeit with a lower variation between mice. After 8 weeks of infection, the median gland height had increased in both phenotypes, to 400 µm in wild-type and 350 µm in *Ahr*$^{-/-}$ mice. When comparing median gland heights within time points, differences were not significant; however, when comparing gland heights in infected mice to values from non-infected mice, a significant increase was found between non-infected wild-type mice and wild-type mice that had been infected with *H. pylori* for 8 weeks. This is a typical morphological change that the stomach epithelium undergoes upon infection and was thus an expected result. Surprisingly, such an increase could not be observed in *Ahr*$^{-/-}$ mice.

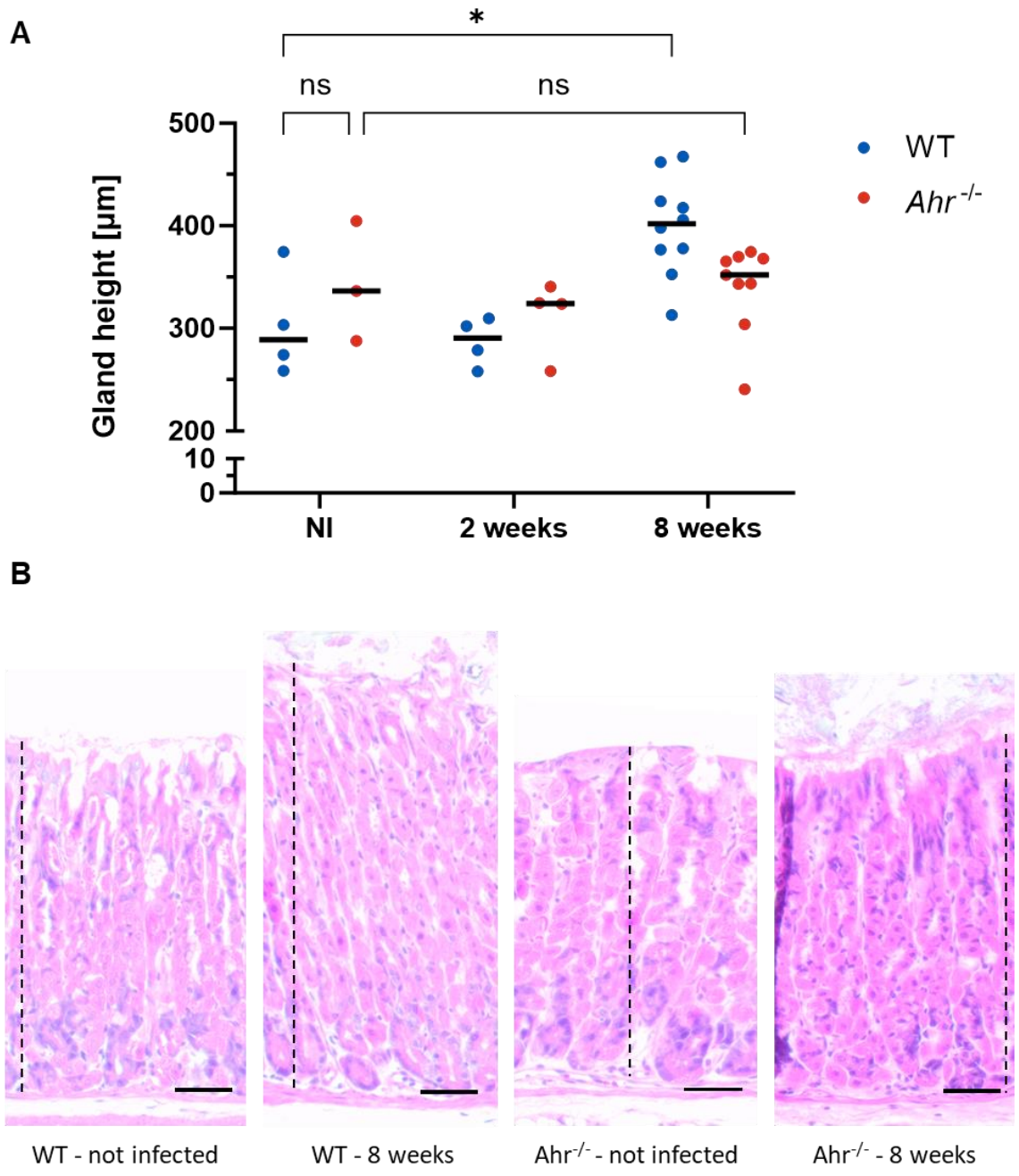

Figure 3.2.3 | Gland heights measured in the corpus region of infected and non-infected mice. Wild-type mice displayed a significant increase in mucosal thickness in line with mucosal hyperplasia observed in chronically infected patients. Hyperplasia was not observed in *Ahr*-deficient mice over the course of the experiment. A: Gland height measurements. Each data point represents one mouse, with seven quantifications performed on each mouse. Horizontal bars represent the median of each group. Differences between groups were tested for statistical significance by two-way ANOVA with Tukey's post-hoc correction (n=3-10). B: Selected images of H&E-stained corpus tissue sections illustrating the differences in mucosal thickness. Vertical dashed lines demonstrate the height of the respective epithelium. Scale bar: 50 µm. ns: non-significant. *: p<005.

As the focus of this experiment was to understand the role of the AHR in the response to bacterial infection, the bacterial load of each infected mouse was determined by analysis of

the number of colony-forming units (CFU) in a piece of stomach tissue, normalised to the weight of the respective piece of tissue and reported as CFU/mg stomach tissue (Figure 3.2.4).

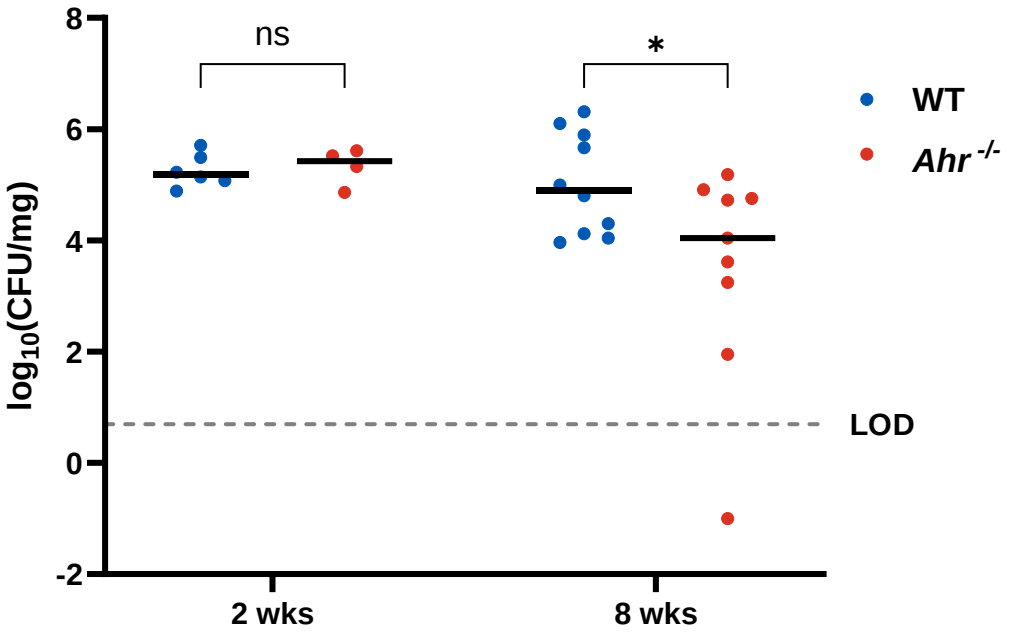

Figure 3.2.4 | Bacterial load in corpus of infected mice 2 weeks and 8 weeks p.i.
After eight weeks of infection, *Ahr*-deficient mice showed a significantly decreased bacterial load compared to wild-type mice. Bacteria were isolated from mouse tissue samples and cultivated on *H. pylori* culture plates (n = 4-10). Numbers of CFUs were normalised to the weight of the respective tissue sample bacteria were isolated from. One data point represents one individual mouse. Horizontal bars represent the median of each group. Differences were tested on log-transformed data using Student's two-sided t-test. A value of 0.1 was added to each count before log-transformation. LOD: Limit of detection (5 CFU/mg). ns: non-significant. *: $p<0.05$.

At two weeks p.i., bacterial load was similar in both genotypes; 10^5 to $3x10^5$ median CFU were detected per milligram stomach tissue, with the counts varying by a factor of about 1000 within both genotypes. At eight weeks however, the range in CFU/mg had increased notably, to about 10^4 in the wild type and 10^6 in the *Ahr*$^{-/-}$ mice. Crucially, comparison of bacterial counts in wild-type to *Ahr*$^{-/-}$ mice showed a significant difference, i.e., a marked decrease in bacterial colonisation in the *Ahr*$^{-/-}$ mice, with one of the mice completely eradicating all bacteria.

3.2.2 Transcriptome analysis of the stomach reveals differences in inflammatory response

Having observed differences in bacterial clearance, we aimed to further understand underlying differences in the transcriptional profile in wild-type and *Ahr*$^{-/-}$ mice. 3'-mRNA sequencing was

performed using RNA samples isolated from the antrum and corpus region of the mouse stomachs.

3.2.2.1 Transcriptome analysis – Antrum

The following number of samples was used for this experiment:

Genotype	Treatment	Number of samples
Ahr$^{+/+}$	Not infected	3
	Infected 2 weeks	5
	Infected 8 weeks	5
Ahr$^{-/-}$	Not infected	3
	Infected 2 weeks	3
	Infected 8 weeks	6

First, a principal component analysis (PCA) was performed using the *PCAtools* package (Blighe and Lun, 2023). The first 12 principal components (PCs) were sufficient to explain 80% of the observed variation (Figure 3.2.5A). Pairwise comparison of PCs was done using biplots to compare the clustering of samples (Figure 3.2.5C and D show biplots for the first four PCs as an example). While none of the PCs was able to completely separate samples by genotype or treatment, PC2 showed the best separation of *Ahr*$^{-/-}$ and wild-type samples (Figure 3.2.5B), while 8 weeks infection samples were mostly separated from the other samples by PC3 (Figure 3.2.5E). The top 0.5% of genes mainly contributing to clustering by PC2 and 3 are shown in Figure 3.2.5F.

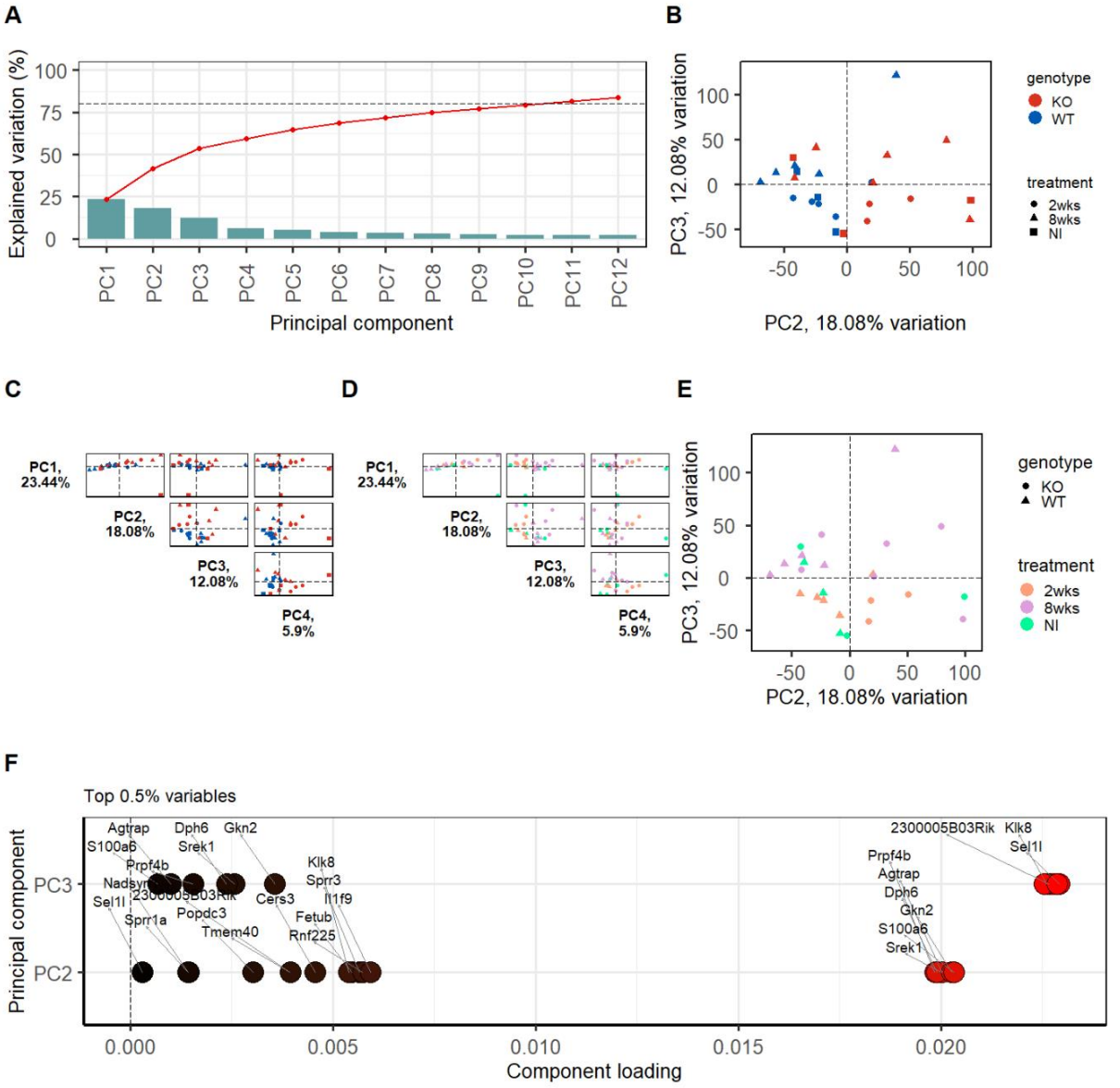

Figure 3.2.5 | Principal component analysis (antrum).
Principal component analysis was performed for dimensionality reduction of the dataset in order to identify clustering of data based on technical variability rather than biological effects. A: Scree plot of principal components 1-12 showing explained variation for each principal component (columns) and cumulative explained variation (red points) of 80%. B: PC2 showed best separation of samples by genotype, explaining 18.1% of observed variation. C, D: Pairs plots giving an overview of PCs to identify most informative PCs. Samples coloured by genotype (C) and treatment (D). Due to size limitation, only the most relevant PCs (1-4) are shown. E: PC3 showed best separation of samples by treatment, explaining 12.1% of observed variation. F: Top 0.5% of genes contributing to variation explained by PC2 and PC3. Higher loading means bigger contribution.

Hierarchical clustering was performed using Pearson correlation values (Figure 3.2.6). Generally, samples did not form clusters based on genotype or treatment, suggesting the data set was not of good quality. It did help identify samples that were markedly different than the

rest of the data set, namely “KO_NI_R3” (one of three non-infected *Ahr*$^{-/-}$ mice) and, to a lesser degree, “wild-type_8wks_R5” and “KO_8wks_R1”. The latter two samples posed less of a problem as the respective groups contained 5 and 6 samples, respectively. The former being an extreme outlier however, meant that results from any analysis using this sample group were potentially unreliable.

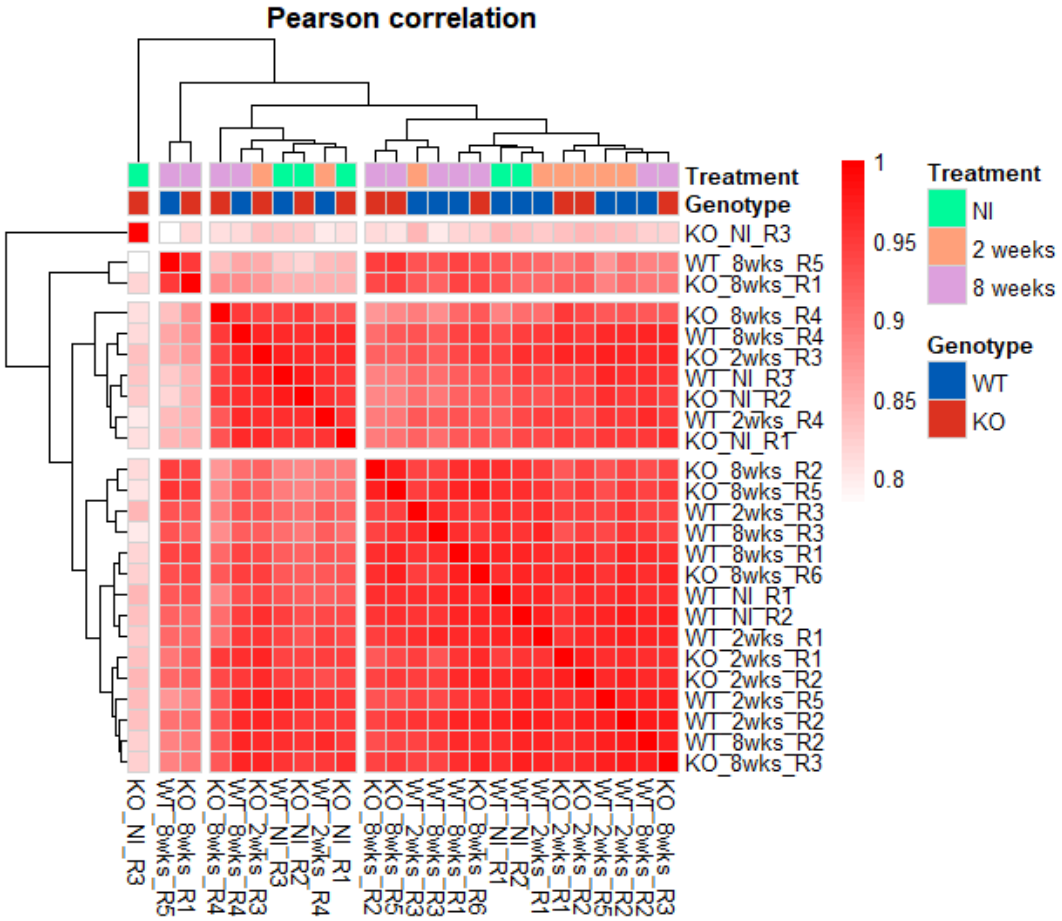

Figure 3.2.6 | Pearson correlation heatmap.
Hierarchical clustering of samples based on Pearson correlation. This approach identified one outlier (replicate 3 of non-infected AHR-KO mice), which shows distinctly lower correlation compared to the rest of the dataset. Generally, no distinct clusters based on genotype or treatment could be observed. Red: Pearson correlation.

Hierarchical clustering was also performed using the top 250 most variable genes across all samples (Figure 3.2.7). Again, no distinct clusters could be observed, and only two of the three non-infected KO samples clustered closely together.

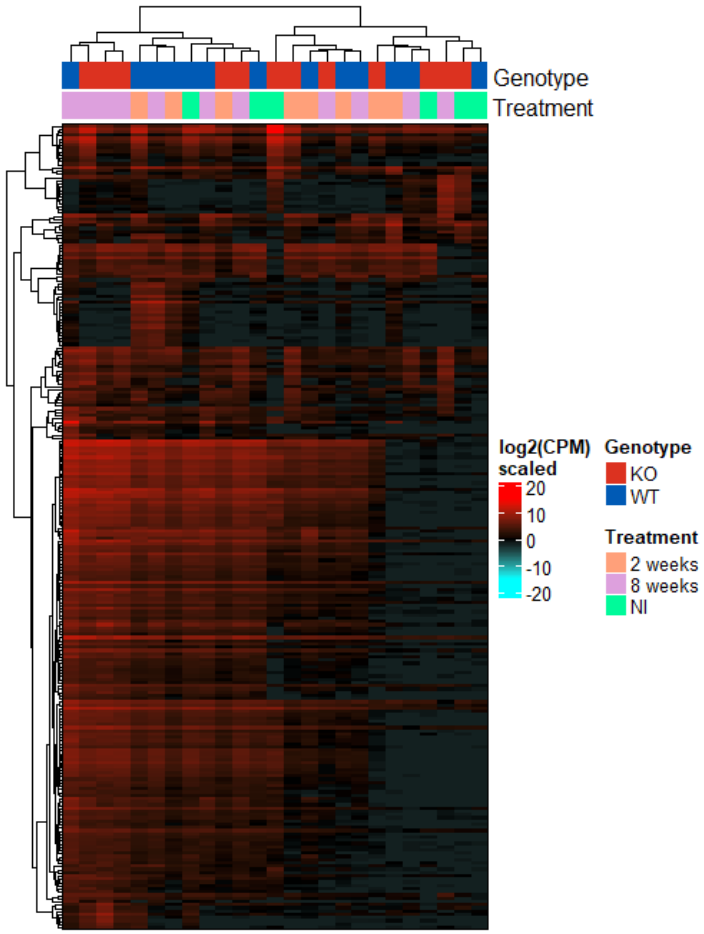

Figure 3.2.7 | Heatmap of the 250 most variable genes across all conditions (antrum).
The most variable genes were used to perform hierarchical clustering of samples. Again, no clusters based on genotype or treatment could be observed. Shown are log2 values of normalised counts. Columns were clustered by Euclidean distances, rows by Pearson distance using the complete linkage method.

First, expression of Ahr was analysed as Zhu and colleagues had shown downregulation of AHR in *H. pylori*-infected patients (Zhu, Gao et al., 2018).

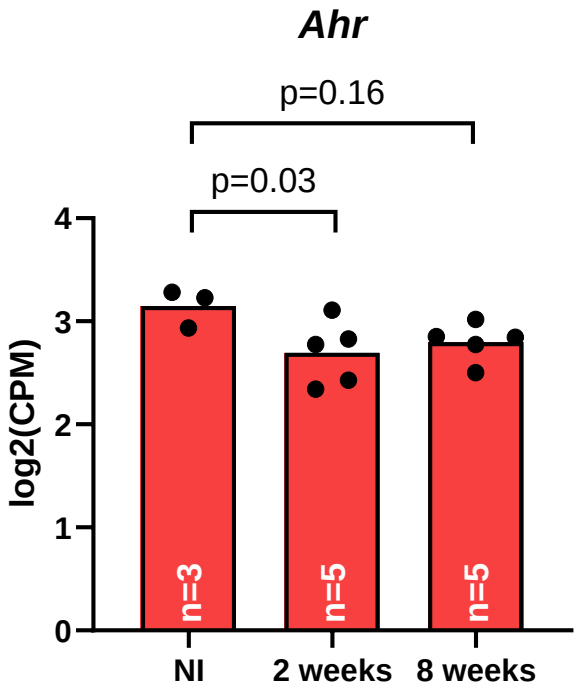

Figure 3.2.8 | Average expression of *Ahr* in wild-type mouse antrum.
Shown are TMM-normalised logCPM values for each condition. Values were tested for differential expression by fitting a negative binomial generalized log-linear model (GLM) to the data set, followed by a quasi-likelihood F-test and pairwise comparison between conditions.

Comparing normalised count values across all conditions, only a low difference in expression could be observed among wild-type mice (Figure 3.2.8). While the difference in expression after 2 weeks of infection was statistically significant, the effect size i.e., $\log_2$(fold change) (logFC) was of low magnitude (-0.5 x logFC) and below the predefined, arbitrary logFC cut-off (>0.6 or <-0.6). After 8 weeks of infection, the difference in *Ahr* expression reduced further to -0.31 x logFC and was not statistically significant.

To investigate the differences in response to infection between wild-type and *Ahr*$^{-/-}$ mice, differential gene expression analysis was performed. Specifically, samples were analysed in order to identify differentially expressed genes (DEGs) when comparing different experimental conditions and genotypes. This analysis was carried out using the *edgeR* package (Robinson, McCarthy *et al.* (2010), McCarthy, Chen *et al.*, 2012, Chen, Lun *et al.*, 2016). Comparisons were set up, calculating an F statistic, with pairwise comparisons between conditions. The *edgeR* package calculates differential gene expression using negative binomial generalized

log-linear models (GLM). It offers different options to fit such models to the data, either gene-wise negative binomial GLMs or quasi-likelihood (QL) negative binomial GLMs. When using the second method, DEGs are determined by performing QL F-tests instead of the likelihood ratio tests used in the first option. The authors of these packages suggest that using the latter method yields more conservative results while providing better control over the type I error rate (Lun, Chen *et al.*, 2016); it was therefore chosen for the identification of DEGs.

Having identified DEGs between experimental conditions and genotypes, libraries were next analysed for enrichment of pre-defined gene sets using the gene set enrichment analysis (GSEA) method as described by Subramanian, Tamayo *et al.*, 2005, in order to understand high-level differences in response to infection and in basal gene expression between genotypes. This analysis allows for the identification of patterns in the data as opposed to comparing expression of individual genes of interest between samples.

The GSEA was performed using the *fast gene set enrichment* (*fgsea*) package (Korotkevich, Sukhov *et al.*, 2021), looking at mouse-specific MSigDB hallmark gene sets (MH collection).

First, non-infected wild-type and *Ahr*$^{-/-}$ mice were compared (Figure 3.2.9). The comparison revealed, that at basal level, no gene sets linked to inflammation were enriched in the knockout mice, apart from “IL2-STAT5 signalling”. wild-type mice, on the other hand, showed enrichment of “TNFA signalling via NFKB”.

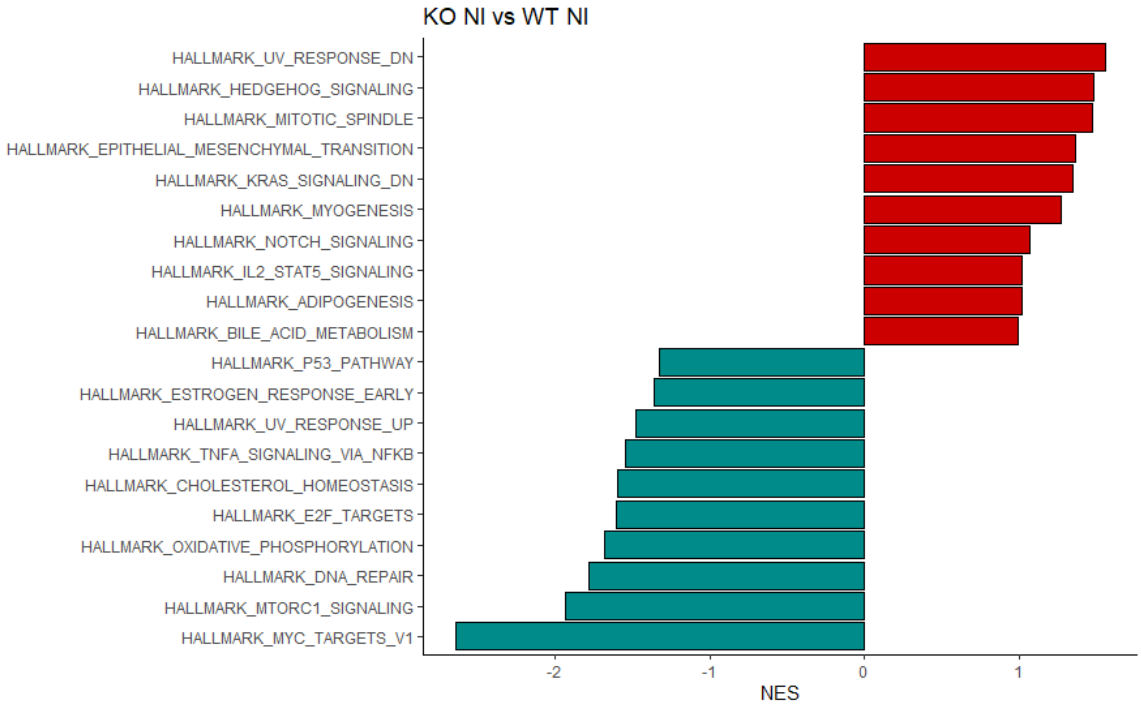

Figure 3.2.9 | GSEA result comparing non-infected wild-type and non-infected *Ahr*$^{-/-}$ mice.
GSEA was performed using the fgsea package, using mouse-specific MSigDB hallmark gene sets.

Next, samples of mice infected for 2 weeks were compared (Figure 3.2.10). In contrast to the comparison at baseline, *Ahr*$^{-/-}$ mice now showed enrichment of the gene sets “Inflammatory response”, “TNFA signalling via NFKB”, IL6-JAK-STAT3 signalling” and “Interferon Gamma response”, which are all linked to inflammation. Wild-type mice on the other hand showed no enrichment of any inflammation-linked gene sets; the most enriched gene set there was “Xenobiotic metabolism”, which is linked to AHR signalling. Interestingly, gene sets related to cell proliferation and cell cycle control were also more highly enriched in *Ahr*$^{-/-}$ mice, such as “E2F targets”, “G2M checkpoint” and “MYC targets”, with the exception of “p53 pathway”, which was found to be more enriched in wild-type mice. “Epithelial-mesenchymal transition” was the most highly enriched gene set in *Ahr*$^{-/-}$ mice.

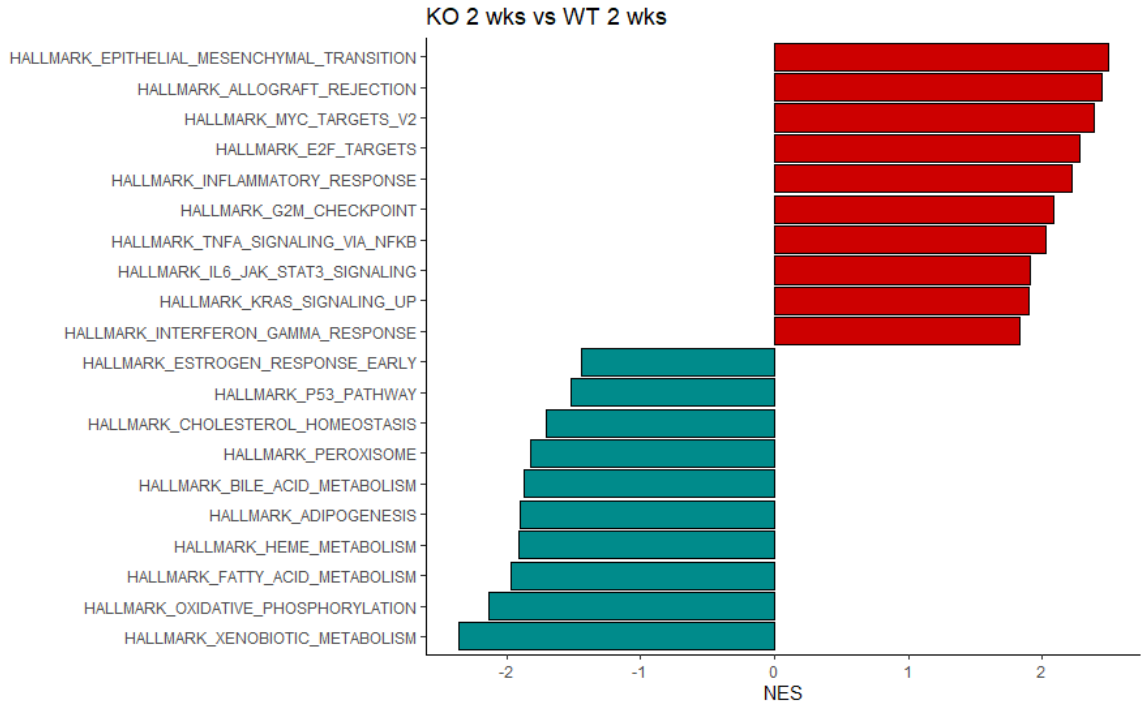

Figure 3.2.10 | GSEA result comparing wild-type and *Ahr*$^{-/-}$ mice after two weeks of infection. GSEA was performed using the fgsea package, using mouse-specific MSigDB hallmark gene sets.

Following this, mice infected for 8 weeks were compared as well (Figure 3.2.11). Again, “IL6-JAK-STAT3 signalling” and “Interferon Gamma response”, as well as “Interferon Alpha response” were enriched in *Ahr*$^{-/-}$ mice, while wild-type mice showed no enrichment of any inflammation-related gene sets.

“E2F targets”, “G2M checkpoint”, “MYC targets” and “Epithelial-mesenchymal transition” were found to be highly enriched in *Ahr*$^{-/-}$ mice again, as well as “Unfolded protein response”.

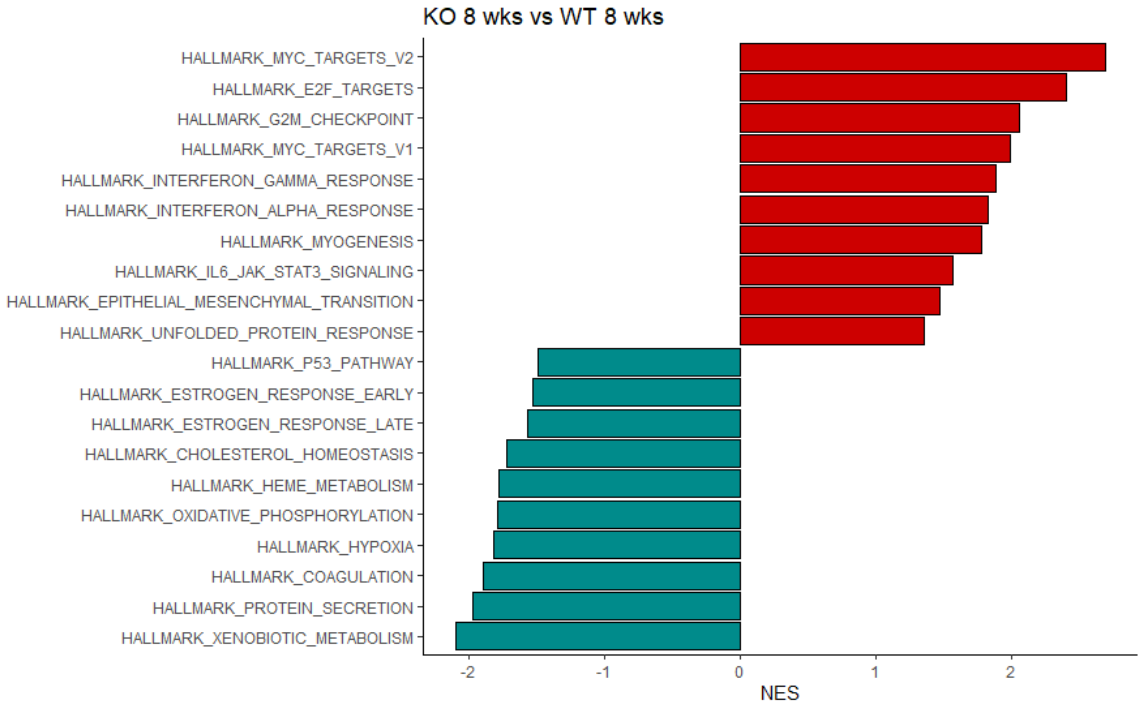

Figure 3.2.11 | GSEA result comparing wild-type and *Ahr*$^{-/-}$ mice after eight weeks of infection. GSEA was performed using the fgsea package, using mouse-specific MSigDB hallmark gene sets.

Notably, the “Inflammatory response” gene set did not show up as significantly enriched in the *Ahr*$^{-/-}$ mice anymore, and “TNFA signalling via NFKB” did not do so, either. This very likely means that a sufficient number of genes comprised by these gene sets were at equal expression in both genotypes after 8 weeks of infection.

Taken together, these results suggest that some pro-inflammatory genes, like those related to NF-κB signalling, were being upregulated earlier in the antrum of *Ahr*$^{-/-}$ mice before their expression in wild-type reached similar levels at 8 weeks. Others, such as those related to interferon (IFN)-α and IFN-γ-induced signalling, stayed consistently higher expressed in the *Ahr*$^{-/-}$ mice.

In addition to this, cell proliferation or cell turnover also seemed to be potentially enhanced in *Ahr*$^{-/-}$ mice.

3.2.2.2 Transcriptome analysis – Corpus

As the analysis of the bacterial burden was performed using corpus tissue, 3'-mRNA sequencing was performed also on RNA isolated from the corpus region. The following number of samples was used for this experiment:

Genotype	Treatment	Number of samples
Ahr$^{+/+}$	Not infected	3
	Infected 2 weeks	6
	Infected 8 weeks	13
Ahr$^{-/-}$	Not infected	4
	Infected 2 weeks	4
	Infected 8 weeks	7

Like before, a principal component analysis was performed first to identify if samples clustered together based on biological differences or due to the influence of technical variability. 12 PCs were found to be sufficient to explain 80% of observed variability (Figure 3.2.12A). Comparing the clustering of samples was done by pairwise comparison of PCs using biplots (biplots shown for the first 4 PCs, Figure 3.2.12C and D). None of the PCs were able to fully separate samples by genotype or treatment, however PC1 explained the variation based on genotype the best, whereas PC2 showed separation of samples by treatment, with mice infected for 8 weeks showing a more distinct cluster as compared to non-infected and 2 weeks infected mice (Figure 3.2.12B and E). The top 0.5% of genes mainly contributing to clustering by PC1 and 2 are shown in Figure 3.2.12F.

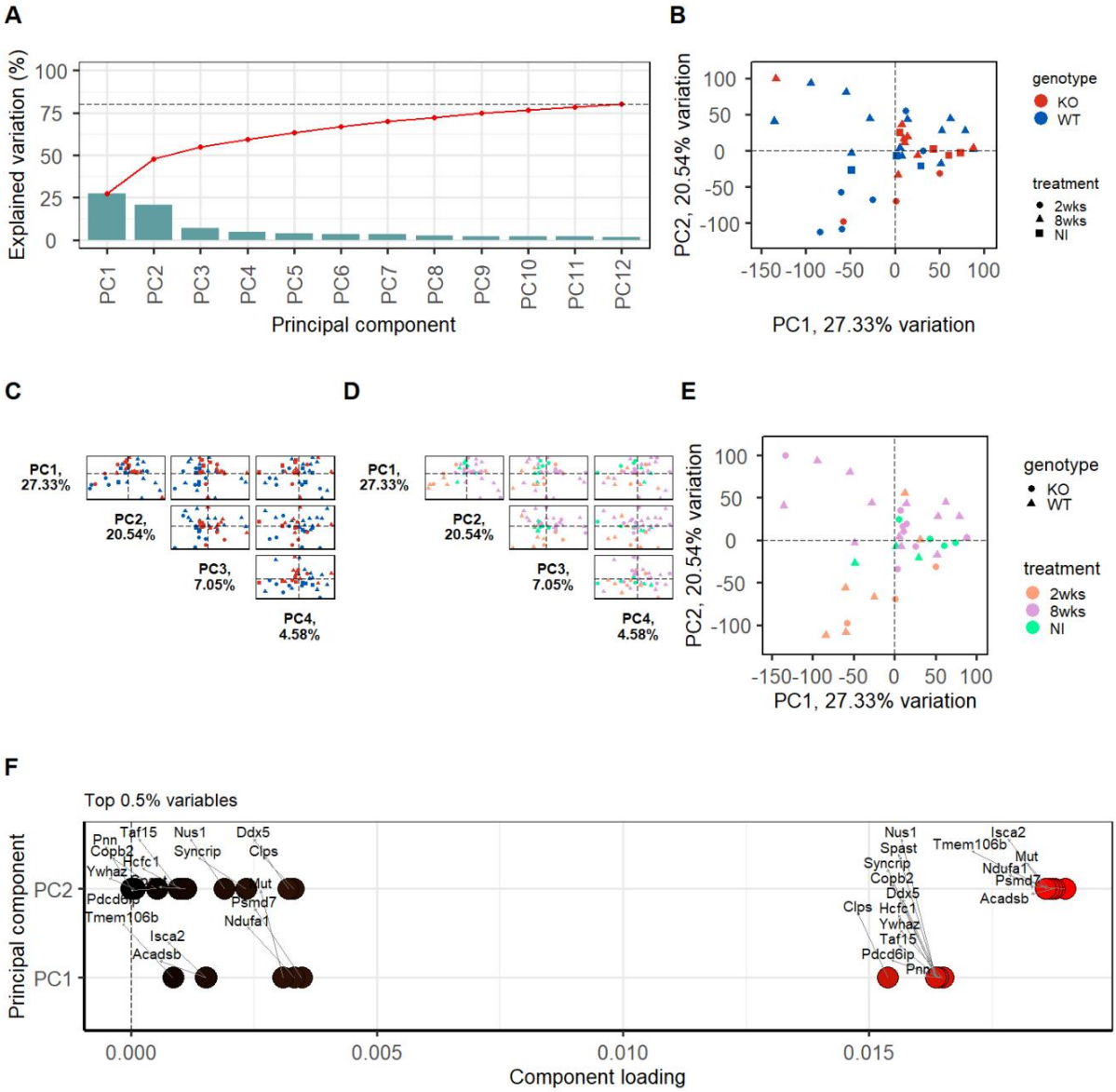

Figure 3.2.12 | Principal component analysis (corpus).
Principal component analysis was performed for dimensionality reduction of the dataset in order to identify clustering of data based on technical variability rather than biological effects. A: Scree plot of principal components 1-12 showing explained variation for each principal component (columns) and cumulative explained variation (red points) of 80%. B: PC1 showed best separation of samples by genotype, explaining 27.3% of observed variation. C, D: Pairs plots giving an overview of PCs to identify most informative PCs. Samples coloured by genotype (C) and treatment (D). Due to size limitation, only the most relevant PCs (1-4) are shown. E: PC2 showed best separation of samples by treatment, explaining 20.5% of observed variation. F: Top 0.5% of genes contributing to variation explained by PC1 and PC2. Higher loading means bigger contribution.

Next, hierarchical clustering by Pearson correlation coefficients was performed, confirming that different treatment led to more distinct clustering than genotype (Figure 3.2.13). This analysis made more obvious the fact that some of the mice showed more similar response within their

respective treatment group than others; a distinct clustering of non-infected mice in comparison to infected mice would have been expected.

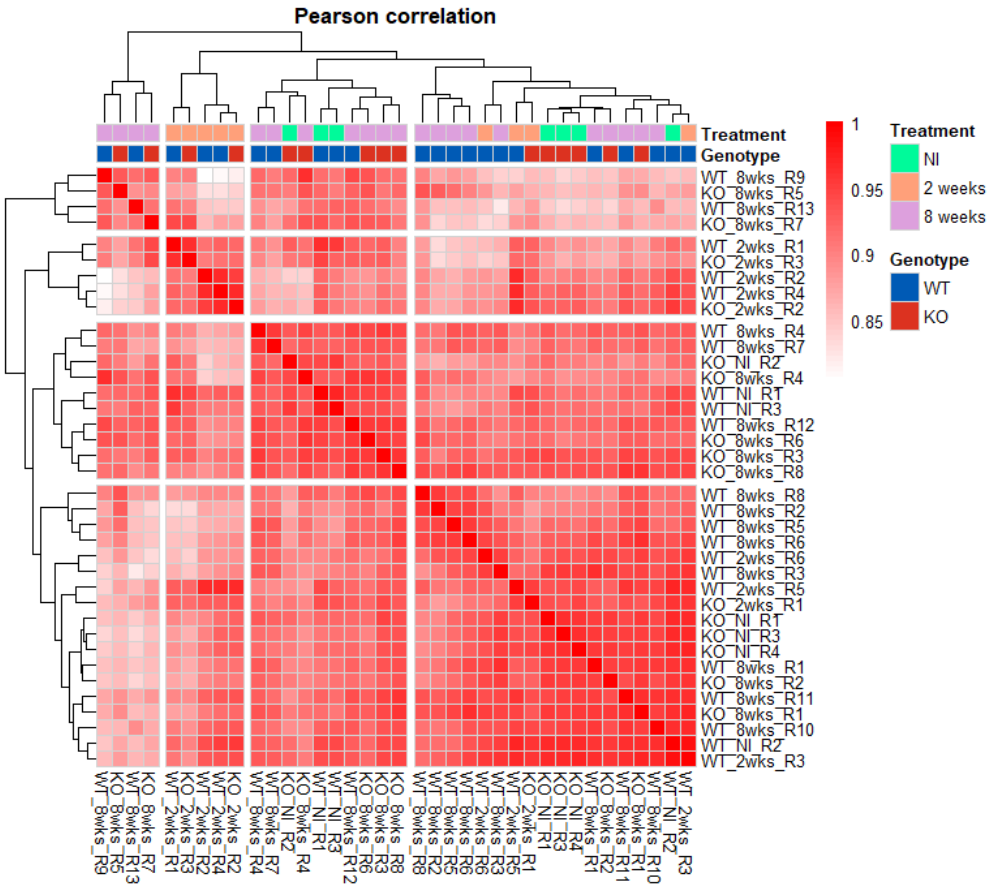

Figure 3.2.13 | Pearson correlation heatmap (corpus).
Hierarchical clustering of samples based on Pearson correlation. This approach identified no obvious outliers. Generally, no distinct clusters based on genotype or treatment could be observed but samples showed more clustering within treatment groups than within genotype groups. Red: Pearson correlation.

Generally, both clustering analyses showed that the treatment seemed to have had a higher impact on overall gene expression than the difference in genotype.

As in the antrum samples, expression of *Ahr* was compared among wild-type mice to see if it changed over the course of the experiment (Figure 3.2.14).

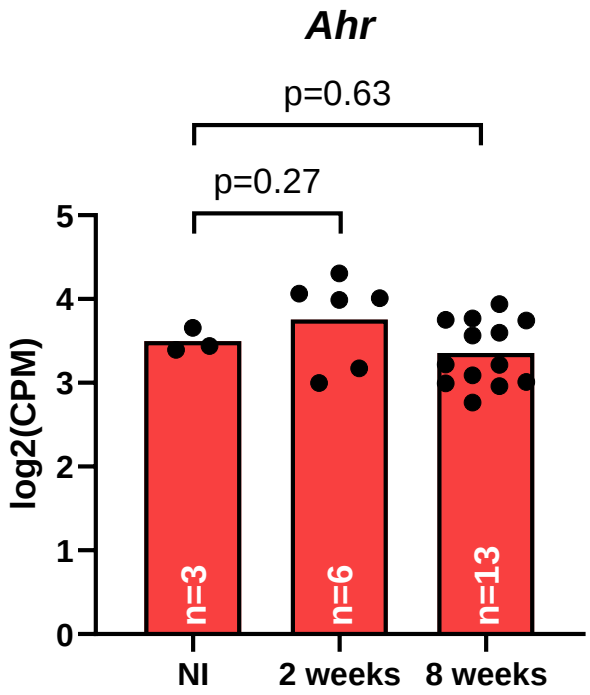

Figure 3.2.14 | Average expression of *Ahr* in wild-type mouse corpus.
Shown are TMM-normalised logCPM values for each condition. Values were tested for differential expression by fitting a negative binomial generalized log-linear model (GLM) to the data set, followed by a quasi-likelihood F-test and pairwise comparison between conditions.

Comparing normalised count values across all conditions, no significant difference in expression could be observed among wild-type mice.

As before, DEGs were identified using the *edgeR* package and GSEA was performed using the *fgsea* package.

First, a comparison of the baseline differences between non-infected *Ahr*$^{-/-}$ and wild-type mice was carried out (Figure 3.2.15). More detailed GSEA plots can be found under 7.1.2. In the absence of *H. pylori*, samples showed, among others, an enrichment of gene sets associated with Myc, upregulation of KRAS signalling and Epithelial-mesenchymal transition (EMT), but none related to inflammation, apart from the “Coagulation” gene set. In comparison, gene sets enriched in wild-type mice (shown here as having a negative normalised enrichment score (NES) due to the direction of the comparison) were ones related to metabolism (“Cholesterol homeostasis”, “mTORC1 signalling”) as well as cellular stress (“Apoptosis”, “PI3K-AKT-MTOR

signalling"). Interestingly, wild-type mice showed stronger enrichment for interferon (IFN) α and γ response as well as NF-κB signalling.

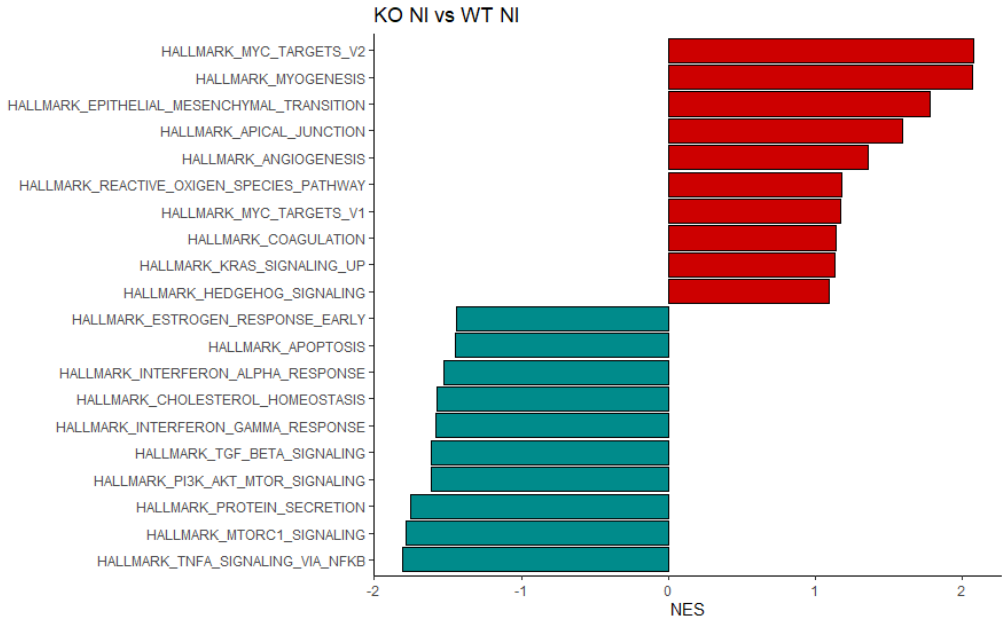

Figure 3.2.15 | GSEA results comparing non-infected *Ahr*$^{-/-}$ to non-infected wild-type mice. GSEA was performed using the fgsea package, using mouse-specific MSigDB hallmark gene sets.

Next, both wild-type mice infected for 2 weeks (Figure 3.2.16) and 8 weeks (Figure 3.2.17) were separately compared to the non-infected wild-type mice. As expected, gene sets related to inflammation and response to infection (IFN-α and γ signalling, IL-6/JAK/STAT3 signalling, "inflammatory response", "TNFA signalling via NFKB") were enriched in the infected mice, suggesting that the infection was successful.

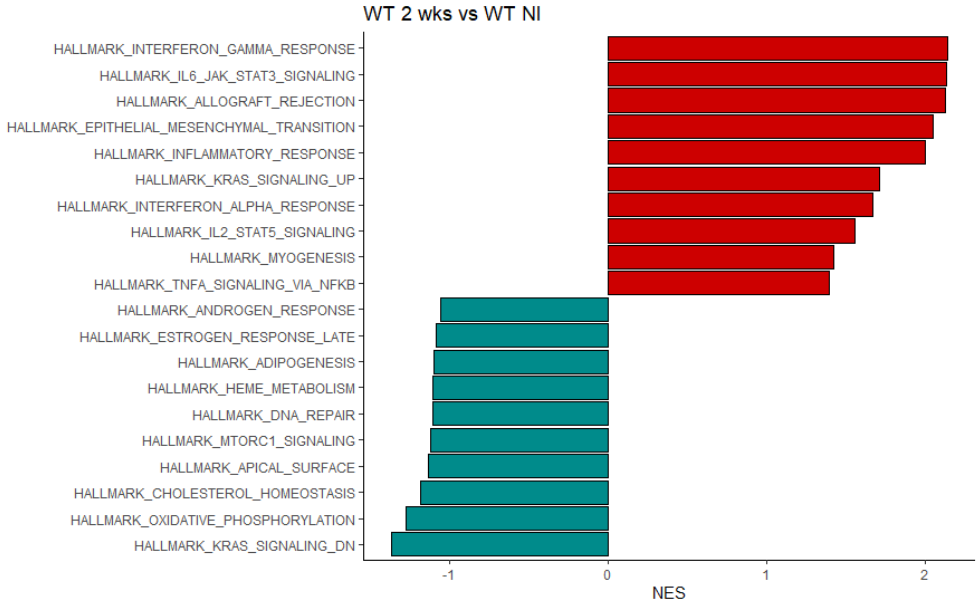

Figure 3.2.16 | GSEA result comparing wild-type mice after two weeks of infection to non-infected wild-type mice.
GSEA was performed using the fgsea package, using mouse-specific MSigDB hallmark gene sets.

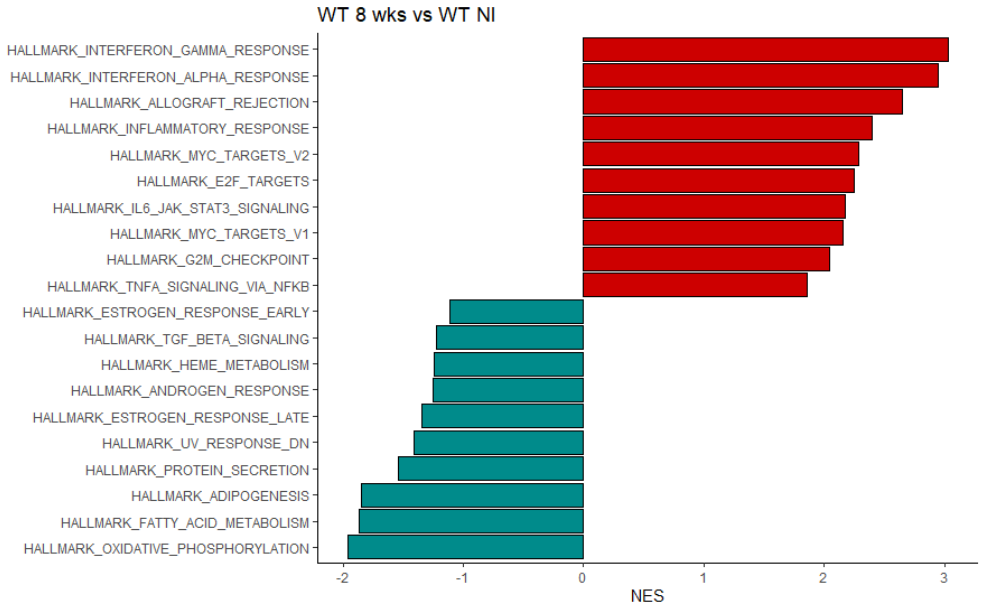

Figure 3.2.17 | GSEA result comparing wild-type mice after eight weeks of infection to non-infected wild-type mice.
GSEA was performed using the fgsea package, using mouse-specific MSigDB hallmark gene sets.

The same was done for the *Ahr*$^{-/-}$ mice (Figure 3.2.18 and Figure 3.2.19). Again, gene sets related to inflammation and infection were enriched in infected mice, however, interferon signalling gene sets were not enriched at 2 weeks p.i. (Figure 3.2.18) and only appeared at 8

weeks p.i. (Figure 3.2.19). In comparison, “TNFA signalling via NFKB” was the top enriched gene set at 2 weeks p.i., where it only appeared at the bottom of the positively enriched gene sets in the wild-type mice.

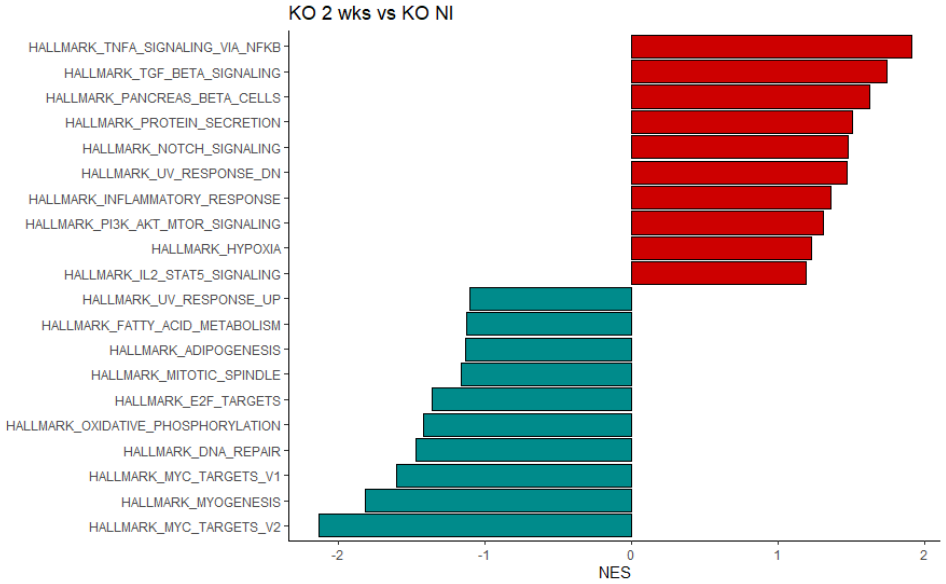

Figure 3.2.18 | GSEA result comparing *Ahr*$^{-/-}$ mice after two weeks of infection to non-infected *Ahr*$^{-/-}$ mice.
GSEA was performed using the fgsea package, using mouse-specific MSigDB hallmark gene sets.

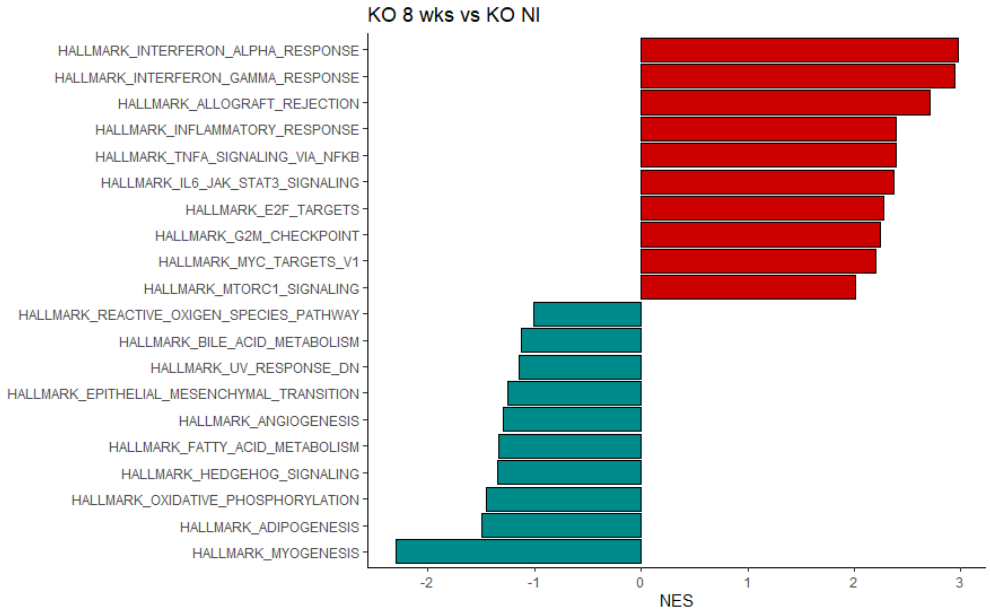

Figure 3.2.19 | GSEA result comparing *Ahr*$^{-/-}$ mice after eight weeks of infection to non-infected *Ahr*$^{-/-}$ mice.
GSEA was performed using the fgsea package, using mouse-specific MSigDB hallmark gene sets.

Finally, a direct comparison between infected wild-type and *Ahr*$^{-/-}$ mice was set up for both infection time points. At 2 weeks p.i., NF-κB signalling was more strongly enriched in the *Ahr*$^{-/-}$ mice, whereas IFN-α and IFN-γ signalling were among the most strongly enriched gene sets in the infected wild-type mice (Figure 3.2.20).

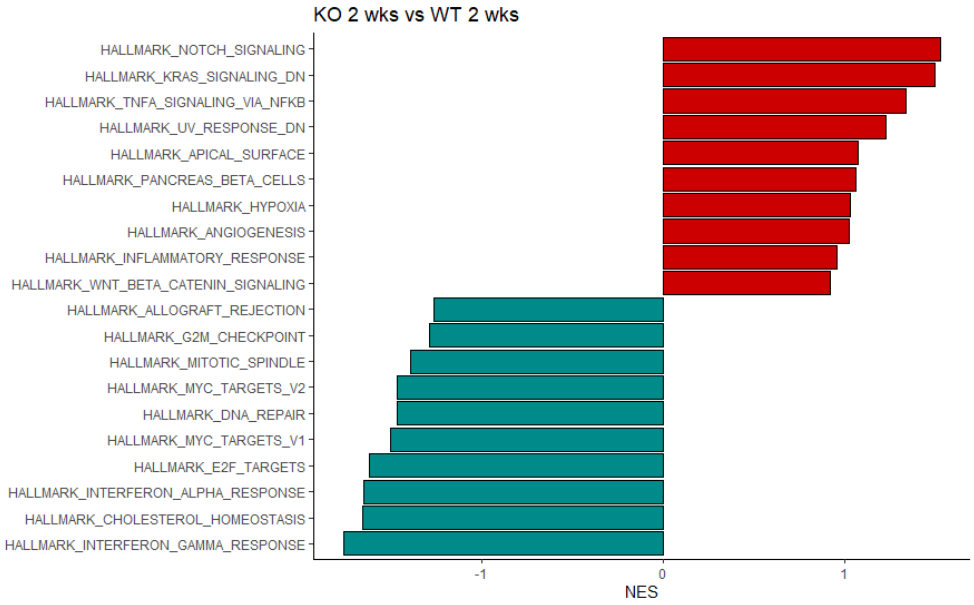

Figure 3.2.20 | GSEA result comparing *Ahr*$^{-/-}$ mice to wild-type mice after two weeks of infection. GSEA was performed using the fgsea package, using mouse-specific MSigDB hallmark gene sets.

Similar findings were made in samples from 8 weeks infected mice, NF-κB signalling was the most prominent inflammation-related gene set in *Ahr*$^{-/-}$ mice, and interferon signalling in wild-type mice (Figure 3.2.21).

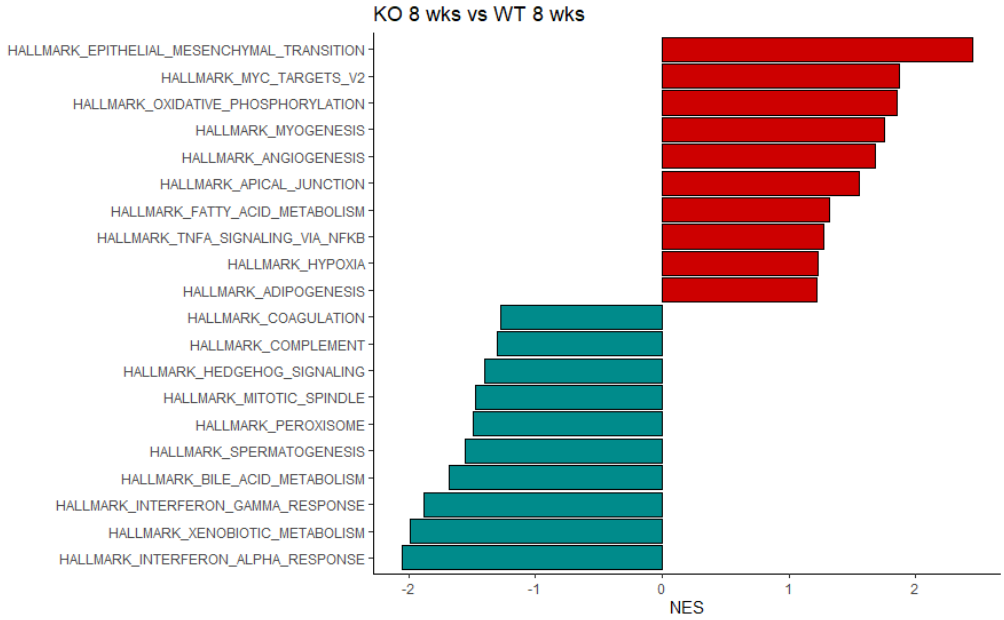

Figure 3.2.21 | GSEA result comparing *Ahr*$^{-/-}$ mice to wild-type mice after eight weeks of infection. GSEA was performed using the fgsea package, using mouse-specific MSigDB hallmark gene sets.

An interesting finding here was that unlike in the antrum, *Ahr*$^{-/-}$ mice did not show an increased enrichment of gene sets related to cell proliferation or cell turnover upon infection.

In summary, transcriptomic analysis of the corpus suggested that while a higher baseline expression of genes associated with inflammation seemed to be present in wild-type mice in absence of *H. pylori* infection, both genotypes responded differently to the infection, with IFN-α and IFN-γ signalling being the predominant response in wild-type mice, while it was not found enriched in *Ahr*$^{-/-}$ mice, which showed an NF-κB-dependent response.

3.3 Discussion

Several studies have shown AHR to be a regulator of inflammation in general (Rothhammer, Borucki *et al.*, 2018) and the immune response to infection in particular (Metidji, Omenetti *et al.*, 2018, Torti, Giovannoni *et al.*, 2021, Zhu, Luo *et al.*, 2018), as well as its link to NF-κB signalling (Vogel, Sciullo *et al.*, 2007; Vogel and Matsumura, 2009; Vogel, Khan *et al.*, 2014). If this crosstalk is of relevance in the immune response to *H. pylori* infection is unknown as of yet.

We undertook an *in vivo* infection experiment of wild-type and *Ahr*-deficient mice, infecting them for a duration of 2 or 8 weeks, respectively. Following this, we performed histological analysis of the gastric tissue to identify differences in morphology and bacterial load, identifying an increase in mucosal thickness in the corpus of wild-type mice only as well as a reduction in bacteria in the *Ahr*-deficient mice. Furthermore, analysis of the gastric transcriptome by bulk RNA-sequencing of corpus and antrum tissue identified underlying differences in the inflammatory response to infection. Specifically, GSEA suggested that interferon signalling was not consistently different between genotypes upon infection, but was rather found to be relatively higher in infected wild-type corpus tissue, but conversely relatively higher in infected *Ahr*$^{-/-}$ antrum tissue when compared to the other genotype, respectively. NF-κB signalling, on the other hand was found to be more strongly active upon infection in the *Ahr*$^{-/-}$ mice throughout the stomach, although in the antrum the difference disappeared at 8 weeks. Notably, it was generally more active in the wild-type mice in the absence of infection. Finally, results also suggested that cell turnover could be greater upon infection in *Ahr*$^{-/-}$ mice, however this effect was restricted to the antrum region.

Overall, the most consistent difference in inflammatory response to infection was an altered regulation of NF-κB signalling in *Ahr*-deficient mice.

As non-infected wild-type mice showed stronger activity of NF-κB signalling compared to non-infected *Ahr*-deficient mice, the question arose how this effect can be explained under the assumption that AHR signalling inhibits the NF-κB mediated immune response. In that case, *Ahr*-deficient mice would have been expected to show a consistently higher expression of NF-κB-related genes.

One possible explanation for this is that the AHR is necessary to maintain a certain basal level of NF-κB activity and in turn modulates its activation in the context of an infection. If true, mice lacking AHR would have lower NF-κB baseline activity, when infected however, there would be no inhibition of the inflammatory response. One previous study suggests such a mechanism exists in bronchial epithelial cells, specifically in the context of treatment of the cells with known NF-κB activators (Øvrevik, Låg *et al.*, 2014). The authors suggest a possible mechanism,

where AHR inhibits inhibitor of κB kinases (IKK)-mediated phosphorylation of p65 at S536 but does not influence basal activity of p65. Further investigations to understand if this effect is also present in the context of *H. pylori* infection might be a possible future direction.

As the mice used for this experiment were SPF, but not gnotobiotic, the presence of other microorganisms in the mouse stomach is a potential confounding factor. It is conceivable that the presence or absence of AHR could have an effect on the gastric microbiome and thereby predispose non-infected mice towards a differential inflammatory response, depending on their genotype. It has been shown, however, that in mice infiltration and colonization of gastric glands by *H. pylori* is necessary to elicit gastric pathology (Sigal, Rothenberg *et al.*, 2015). If potential differences in the stomach microbiota are responsible for the observed differences in non-infected mice, is therefore difficult to determine.

Nonetheless, this factor should be taken into consideration, as it has been shown that the preinfection host microbiota can shape the inflammatory response to *H. pylori* infection in mice (Rolig, Cech *et al.*, 2013).

The datasets obtained from RNA-sequencing were analysed for quality using PCA and hierarchical clustering analyses. Both tests showed that the dataset obtained from antrum samples was of poor quality and did not reflect differences in treatment or genotype. While the corpus dataset showed a clearer effect of the treatment, it was stronger than the effected caused by the genotype, which was unexpected. When comparing the obtained library sizes, the analysis showed that for both antrum and corpus, the median library sizes were very similar after normalization, even though for sequencing of corpus samples, a flow cell with much bigger capacity was used (see Figure 7.1.2 and Figure 7.1.3). This is very likely due to a technical error and would bias the obtained gene counts towards more highly expressed genes. If genes differentially expressed due to genotypical differences were less abundant, they could have possibly been detected only at a low level or not detected at all. Conclusions drawn from the RNA-sequencing experiments are therefore limited and likely to be unreliable.

The difference observed in mucosal thickening between the genotypes could be explained by the sustained infection of wild-type mice. In response to sustained infection, the epithelium is expected to display hypertrophy, in humans described as the initial step in the pre-cancerous cascade leading up to development of gastric adenocarcinoma, also known as Correa's cascade (Correa and Piazuelo, 2012). *Ahr*-deficient mice were able to reduce, and in one case completely eradicate, *H. pylori* found in the stomach after 8 weeks. It is therefore likely that these mice did not display mucosal hypertrophy because the infection was not able to successfully establish, avoiding the progression of gastric disease as observed in wild-type mice. As only three or four mice were available for each non-infected group, the experiment was underpowered and any conclusions drawn from these results should be investigated further by repeating the experiment using an equal number of mice for each condition.

In general, the infection experiment should be repeated with a greater, and equal number of mice per condition to ensure that the observed effects are reproducible and that a more robust analysis of gene expression and mucosal hyperplasia can be performed.

Overall, we were able to show that *Ahr*-deficient mice were better able to suppress, and in one instance clear, *H. pylori* infection as opposed to wild-type mice. The exact mechanism is still unknown but these results suggest that this improved clearance of infection could be mediated through a differential NF-κB mediated immune response.

Chapter 4 – Loss of AHR drives increased NF-κB-dependent, pro-inflammatory response to infection in gastric epithelial cells

4.1 Introduction

The stomach is generally known as an uninhabitable organ of the human body due to the presence of gastric acid and a resulting low pH environment. Furthermore, the healthy stomach does not possess organised gut-associated lymphoid tissues, such as Peyer's patches or isolated lymphoid follicles, although the latter have been described to be present in cases of *H. pylori* infection (Genta, Hamner *et al.*, 1993; Isaacson, 1994; Carney, 2010). This suggests that the epithelium is the first and main line of defence against infections by pathogens.

How the epithelium interacts with *H. pylori* and its specific response to infection have been of particular interest since the Nobel prize was awarded to Marshall and Warren in 1985 for their discovery that *H. pylori* is the main causative agent of stomach disease. Since then, a number of publications have aimed to characterise the immune response to infection, which has been shown to be mainly driven by NF-κB, specifically upon epithelial detection of the bacterial compound ADP-heptose, a precursor of bacterial lipopolysaccharide (Pfannkuch, Hurwitz *et al.*, 2019).

As demonstrated in the previous chapter, AHR is a potential regulator of the NF-κB-driven immune response to *H. pylori* infection. Because the epithelium is very likely to be the main driver of immune response to this infection, we hypothesized that differences observed in the clearance of bacteria in mice might be due to an altered NF-κB response in the epithelium.

This chapter aims to investigate if AHR signalling is relevant in the epithelial response to *H. pylori* and if this is due to differential regulation of NF-κB signalling upon infection. To do this, we used human and murine gastric primary cell models as well as human cell lines. First, the response of human cell lines to live bacteria and bacterial lysates was investigated in the presence or absence of AHR inhibitors. Following this, patient samples were analysed to uncover potential differences in AHR signalling in the antrum and corpus region of the stomach. Infection experiments were then performed using murine primary wild-type and *Ahr*$^{-/-}$ cell

models, followed by transcriptome profiling to understand underlying differences in their response to infection, specifically focussing on NF-κB signalling. Finally, infection experiments on human wild-type, *AHR*$^{-/-}$ and AHR-overexpressing cell lines were performed to understand if findings made in murine cells could be replicated and therefore applied to human epithelial cells.

4.2 Results

4.2.1 *H. pylori* activates AHR signalling in human cells

In order to understand the epithelial response to *H. pylori* infection, human mucosoid cultures were infected with *H. pylori* P12 for 3 days. Following infection, RNA was extracted and a microarray analysis of gene expression performed. Among the top 10 upregulated genes was the main AHR target gene *CYP1A1* (Figure 7.1.1). Upon further analysis, four of the major AHR target genes, *CYP1A1, CYP1A2, CYP1B1* and *AHRR* were found to be significantly upregulated following infection with *H. pylori* (Figure 4.2.1).

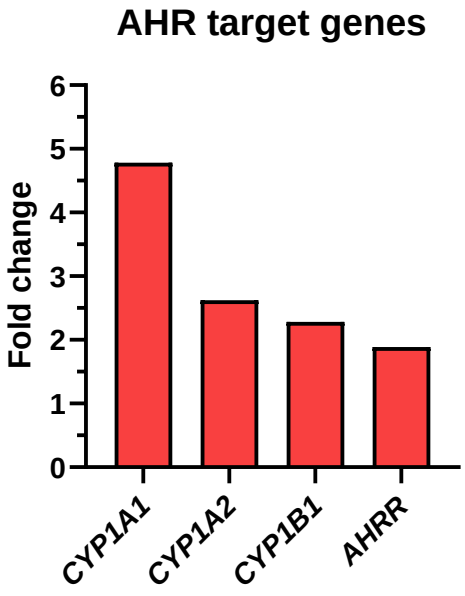

Figure 4.2.1 | Microarray analysis of AHR target gene expression in human primary mucosoid cultures infected with *H. pylori*.
Cells were infected with *H. pylori* P12 for 3 days with an initial MOI of 100. After 24 hours, non-attached bacteria were removed from the cells. The major AHR target genes *CYP1A1*, *CYP1A2*, *CYP1B1* and *AHRR* were found to be upregulated upon infection as compared to the non-infected control. Fold change was calculated as ratio of gene expression after infection to gene expression in non-infected cells. Differences in gene expression between infected and non-infected cells were tested for statistical significance by paired t-test. All genes shown passed the threshold of $p<0.05$.

Human epithelial cancer cell lines were used to study induction of AHR and activity of CYP1A1 during *H. pylori* infection. First, the gastric epithelial AGS cell line was tested for its ability to induce AHR signalling when treated with commonly used AHR ligands. Intestinal epithelial Caco-2 cells were also tested to understand if activation of AHR signalling by *H. pylori* is specific to the stomach epithelium or a more general response to bacterial infection. AGS and Caco-2 cells were first treated with TCDD or FICZ in different concentrations in the presence or absence of the AHR inhibitor CH223191 to confirm functional AHR signalling. Following treatment, an ethoxyresorufin-o-demethylase (EROD) assay was performed to measure activity of CYP1A1. To perform the assay, cells were treated with 7-ethoxyresorufin (7-ER) and dicoumarol (see 2.14). The EROD assay detects the conversion of 7-ER to resorufin by CYP1A1 through fluorescence measurement. When sufficiently high amounts of 7-ER are supplied, the reaction occurs at near-maximal rate, which means that concentration of CYP1A1 is proportional to the measured fluorescence intensity (Petrulis, Chen *et al.*, 2001). An increase in CYP1A1 activity compared to the non-treated (NT) control indicates activation of the AHR signalling pathway.

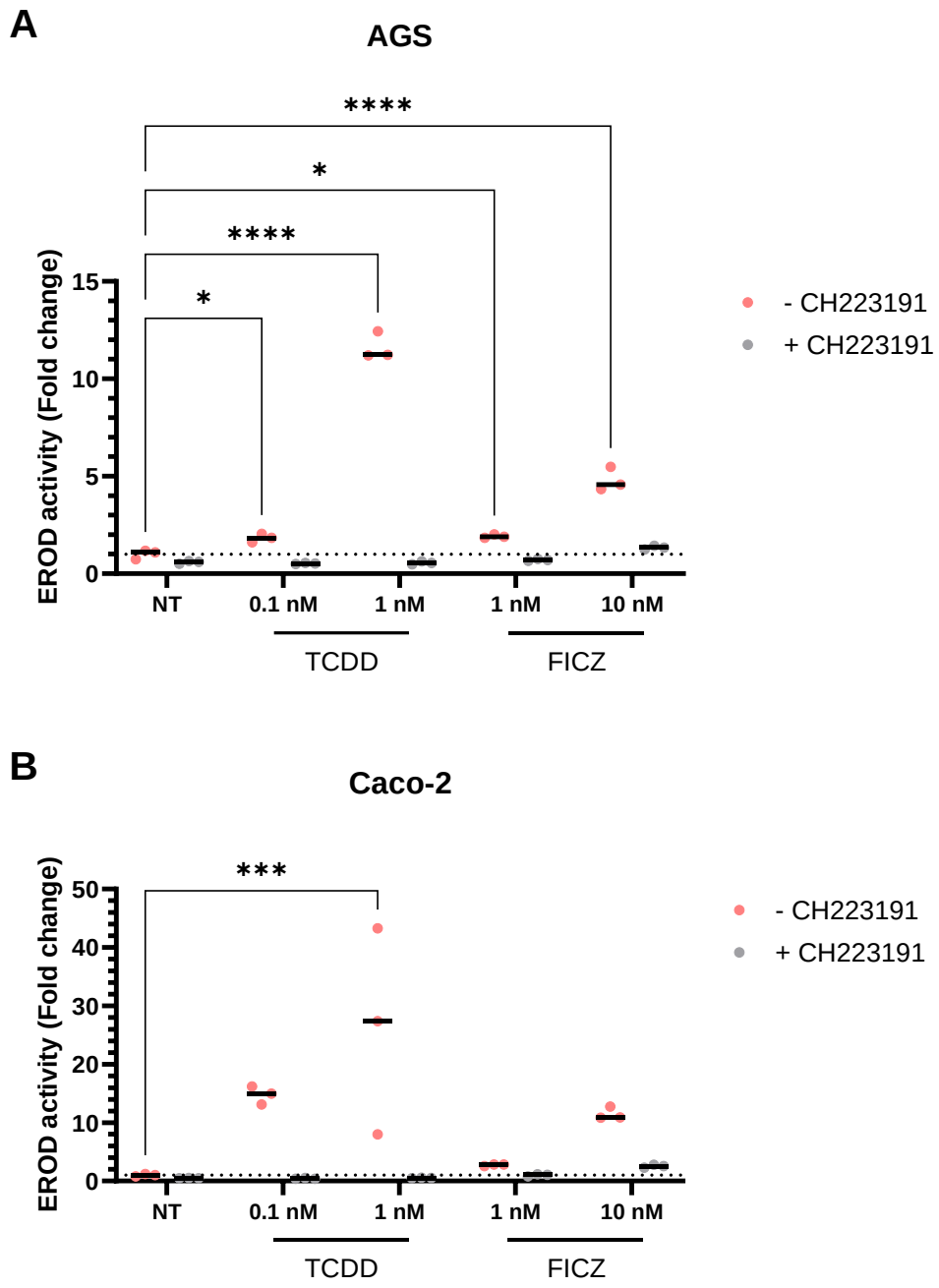

Figure 4.2.2 | Human epithelial cell lines AGS and Caco-2 activate AHR upon ligand stimulation. Activity of CYP1A1 in human AGS and Caco-2 cell lines, measured via EROD assay, increased after treatment with AHR agonists TCDD and FICZ, while concurrent treatment with AHR inhibitor CH223191 abrogated activation of AHR signalling. Cells were treated with different concentrations of AHR agonists for 4 h and with 7-ethoxyresorufin and dicoumarol for 1h. A: AGS cells. B: Caco-2 cells. One data point corresponds to one independent experiment (n=3). Differences in activity were tested for statistical significance by two-way ANOVA with Tukey's post-hoc correction. *: $p<0.05$, ***: $p<0.001$, ****: $p<0.0001$.

Treatment of AGS cells with 1 nM TCDD induced an 11-fold increase in fluorescence compared to the NT control, which signified the strongest induction of AHR signalling in this cell line across all tested conditions. The AHR inhibitor CH223191 induced a decrease in

EROD activity to the baseline level when given in combination with the ligands. Notably, treatment of the cells with CH223191 had a seemingly lower inhibitory effect on EROD activity when given in combination with the higher concentration of FICZ, even though activation capacity of 10 nM FICZ alone was lower than that of 1 nM TCDD alone (Figure 4.2.2A). Similar results were observed when the same experiment was carried out using Caco-2 cells. The overall effect of AHR activation was stronger in Caco-2 cells compared to AGS cells; 1 nM TCDD led to the highest induction of EROD activity. Again, the difference between 10 nM FICZ with and without CH223191 was smaller compared to 1 nM TCDD with and without CH223191. Having confirmed that both cell lines have a functioning AHR signalling system and that activation of AHR signalling can be tested via EROD assay, cells were then exposed to viable *H. pylori* to test activation of AHR by the bacteria. As the potential level of activation by the bacteria was not known and the Caco-2 cells had displayed a stronger activation of AHR signalling when exposed to ligands, co-culture experiments were carried out using this cell line. Cells were exposed to an increasing multiplicity of infection (MOI) i.e., number of bacterial cells per eukaryotic cell to test if a higher bacterial burden would correlate with an increase in EROD activity (Figure 4.2.3). Indeed, when exposed to an increasing MOI, EROD activity increased accordingly, which was confirmed by a test for linear trend after ANOVA comparing the mean values across all MOIs (R^2=0.7172, excluding TCDD). While an MOI of 50 was not sufficient to activate AHR signalling, higher MOIs did induce a significant increase in EROD activity, which was 5-fold higher than the non-infected (NI) control when an MOI of 200 was used. The activation induced by TCDD was stronger, with about 15-fold versus non-infected on a similar level to what was observed in the previous experiment.

To control for changes in EROD activity caused by differential expression of *CYP1A1* following AHR activation, RT-qPCR was performed to measure CYP1A1 expression levels. Indeed, a similar trend in *CYP1A1* expression to CYP1A1 activity could be observed, however variability between samples meant that none of the changes in gene expression were statistically significant.

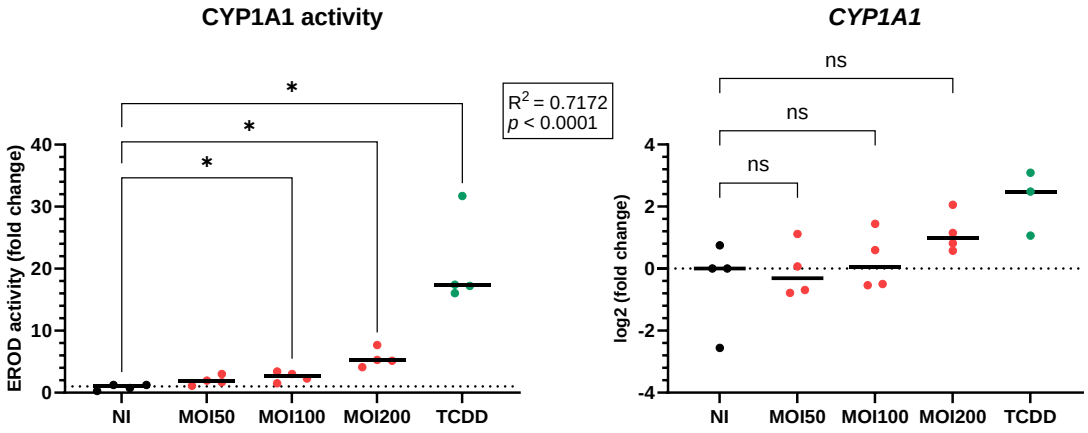

Figure 4.2.3 | Infection of Caco-2 cells with *H. pylori* induces activation of AHR in a dose-dependent manner.
Activity of CYP1A1 in Caco-2 cells, measured via EROD assay, increased after infection with increasing numbers of bacteria per cell and treatment of cells with AHR agonist TCDD (left). Changes in expression of CYP1A1 were controlled for by measuring expression of *CYP1A1* via RT-qPCR (right). Cells were infected with *H. pylori* P12 for 4 h and treated with 7-ethoxyresorufin and dicoumarol for 1h. Inset box: Results of test for linear trend between EROD activity and MOI (excluding TCDD). One data point corresponds to one independent experiment (n=4). Differences between treated and non-infected cells were tested for statistical significance by one-way ANOVA with Dunnett's post-hoc correction. ns: non-significant. *: p<0.05.

Since the cells showed a good, dose-dependent response to exposure to live bacteria, cells were next treated with *H. pylori* lysates (Figure 4.2.4) to understand if activation of the AHR required viable bacteria which are able to actively transport molecules into the eukaryotic cell e.g., through their type IV secretion system (T4SS). Again, the lysate with the highest concentration, prepared from a number of bacteria, equivalent to an MOI of 400, resulted in the strongest EROD activity. The lower MOI lysates did not lead to a significant increase of EROD activity over the NI control, although an upwards trend was observed and again, increase in EROD activity correlated with an increase in lysate concentration, confirmed by a test for linear trend (R^2=0.6608, excluding TCDD). Overall, the level of EROD activity was lower compared to the activities observed with viable bacteria, and remained within the same

order of magnitude between lysate concentrations. The positive control however displayed a markedly lower activation capacity in this set of experiments.

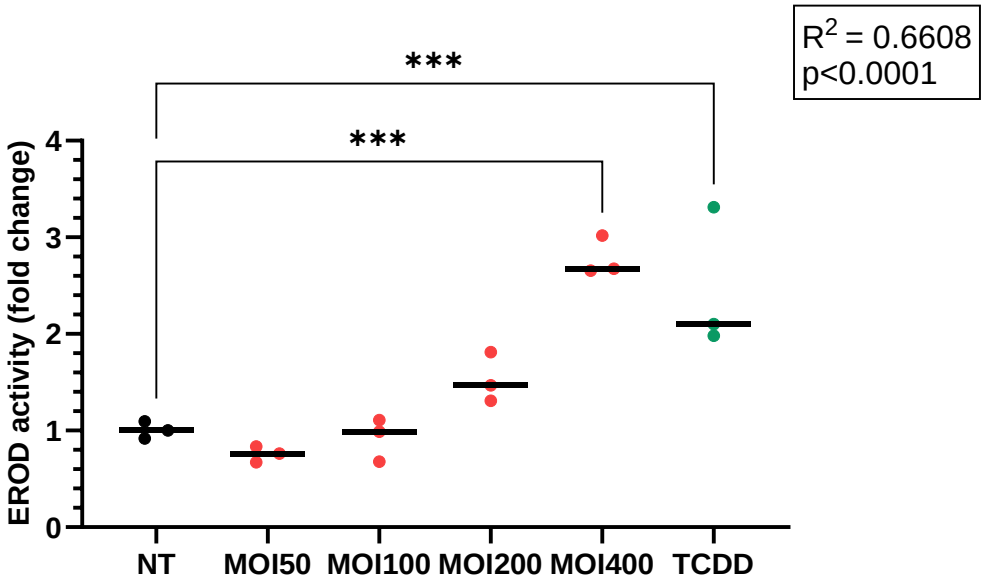

Figure 4.2.4 | Treatment of Caco-2 cells with *H. pylori* lysates induces activation of AHR in a dose-dependent manner.
Activity of CYP1A1 in Caco-2 cells, measured via EROD assay, increased after infection with increasing numbers of bacteria per cell and treatment of cells with AHR agonist TCDD. Cells were infected with *H. pylori* P12 for 4 h and treated with 7-ethoxyresorufin and dicoumarol for 1h. Inset box: Results of test for linear trend between EROD activity and MOI (excluding TCDD). One data point corresponds to one independent experiment (n=3). Differences between treated and non-infected cells were tested for statistical significance by one-way ANOVA with Dunnett's post-hoc correction. ***: p<0.001.

Taken together, these experiments confirmed activation of the AHR in human cell lines following infection with or exposure to viable *H. pylori* or bacterial lysates.

4.2.2 *H. pylori* does not activate AHR through inhibition of CYP1A1

While activation of AHR signalling was observed after infection of epithelial cell lines and of human primary epithelial cells (Figure 7.1.1), it was not known if this activation was a direct result of binding of an *H. pylori*-derived factor to the AHR or rather an indirect effect. Apart from direct ligand binding, the AHR can also be activated through an indirect mechanism, where the inhibition of CYP1A1 leads to accumulation of AHR ligands, which are not metabolised by CYP1A1 anymore, which in turn causes activation of AHR signalling; this effect has been demonstrated *in vitro* (Wincent, Bengtsson *et al.*, 2012) as well as *in vivo* (Yoda, Tochitani *et al.*, 2022). This is an intriguing mechanism as AHR ligands are likely to be abundant in the body. To test this hypothesis, Caco-2 cells were infected with *H. pylori* or treated with the AHR

ligand FICZ or both in the presence or absence of AHR inhibitor CH223191 and activity of CYP1A1 measured by EROD assay (Figure 4.2.5).

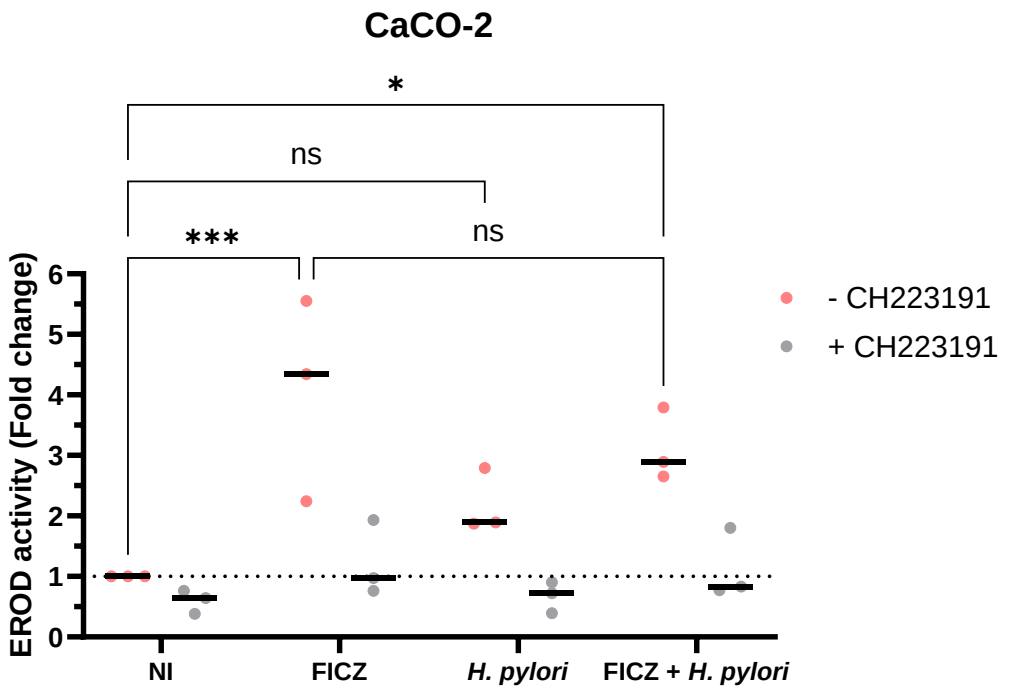

Figure 4.2.5 | *H. pylori* does not induce activation of AHR through inhibition of CYP1A1. Activity of CYP1A1 in Caco-2 cells, measured via EROD assay, increased after treatment of cells with AHR agonist TCDD. Cells were infected with *H. pylori* P12 or treated with FICZ for 4 h and treated with 7-ethoxyresorufin and dicoumarol for 1h. One data point corresponds to one independent experiment (n=3). Differences between treated and non-infected cells were tested for statistical significance by two-way ANOVA with Tukey's post-hoc correction. ns: non-significant. *: $p<0.05$. ***: $p<0.001$.

Testing for CYP1A1 inhibition by measuring EROD activity was confounded by the fact that inhibition of CYP1A1 would lead to activation of AHR and therefore higher expression of CYP1A1, thereby potentially increasing the total EROD activity above the level of the NI control. To account for this, cells were also treated with FICZ at the same time as infection with *H. pylori*. An inhibition of CYP1A1 activity would be visible as a decrease in EROD activity compared to FICZ treatment alone. FICZ was chosen as AHR activator for this experiment as the strong induction of EROD activity by TCDD could have masked small decreases in EROD activity induced by *H. pylori*. Both FICZ only and FICZ + *H. pylori* induced a significant increase compared to the NI control. However, no significant difference in EROD activity could be observed between treatment with *H. pylori* and FICZ and FICZ alone, suggesting that inhibition of CYP1A1 is not responsible for the AHR activation observed during *H. pylori* infections.

4.2.3 AHR expression is increased in *H. pylori*-positive human gastritis patients in the corpus but not in the antrum

AHR has been suggested to be downregulated in *H. pylori*-positive human gastritis patients (Zhu, Gao *et al.*, 2018). As observed in RNA-sequencing experiments in mice, loss of AHR caused more or less pronounced phenotypes in regards to the inflammatory response, depending of the region of the stomach the samples were collected from i.e., corpus tissue seemed to show a more pronounced increase in inflammatory response to infection when AHR was absent, as compared to the antrum. We therefore hypothesized that *H. pylori* infection might cause a downregulation of AHR expression in only the antrum, thereby making the difference between the wild-type and the knock-out less pronounced. To answer this question, qPCR was performed on cDNA samples collected from human patients (described in Link, Langner *et al.*, 2017) to analyse *AHR* gene expression (Figure 4.2.6).

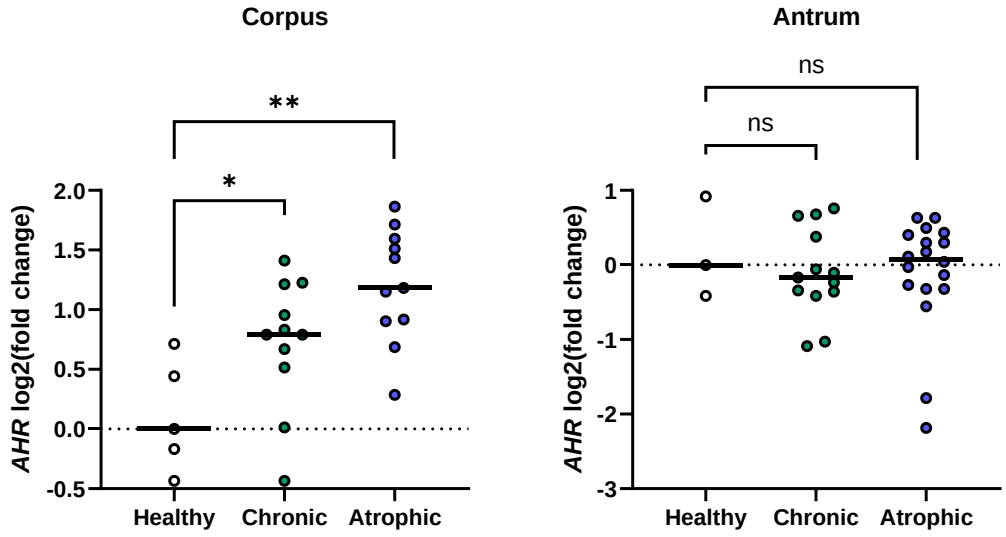

Figure 4.2.6 | Expression of *AHR* in *H. pylori*-positive gastritis patients.
Gastritis induces increased *AHR* expression in the corpus, but not the antrum region of the stomach. Shown are $\log_2$(fold change) values of *AHR* expression in *H. pylori*-positive patients exhibiting chronic or atrophic gastritis, respectively, compared to healthy, *H. pylori*-negative patients. Vertical bars show the median. Statistical significance was determined by Mann-Whitney U test. *: $p<0.05$. **: $p<0.01$.

Surprisingly, the data showed increased expression of *AHR* in corpus samples in *H. pylori*-positive gastritis patients when compared to samples from healthy, *H. pylori*-negative patients. The difference was visible in both chronic and atrophic gastritis patient groups, with cDNA

extracted from the corpus showing an about 1.5 to 2-fold increase in *AHR* expression compared to average expression in healthy patients. There was no change in gene expression in the antral region of the stomach compared to the control group for either chronic or atrophic gastritis patients.

While the data seemingly contradict findings published by Zhu, Gao *et al.*, 2018, they still fit the assumption that a difference in AHR expression in antrum vs. corpus in infected mice could explain the different phenotypes observed when analysing gene expression in *Ahr*$^{-/-}$ mice in corpus and antrum.

4.2.4 Murine organoids lacking AHR display higher baseline expression of pro-inflammatory markers

Mouse organoids were cultivated from freshly harvested mouse stomachs. As these cells were obtained from mice with the same genetic background as the mice used in the infection experiment described in 3.2, they were considered a good model of the epithelial response of these mice to pro-inflammatory stimuli including exposure to *H. pylori*. To identify a suitable reference gene for any following gene expression analyses in murine cells by RT-qPCR, one sample of the RNA obtained from mice used in the *in vivo* infection experiment was used per condition. Seven commonly used reference genes were selected as candidates for reference genes and their expression measured across all RNA samples. The expression values were then used to calculate an overall comprehensive gene stability score using the RefFinder tool (Xie, Xiao *et al.*, 2012, Xie, Wang *et al.*, 2023), identifying *Rps18* as the least variable gene across all tested conditions (Figure 7.1.4).

Having identified a suitable reference gene, mouse organoids were co-cultured with *H. pylori* PMSS1 or treated with FICZ as positive control for 24 h and gene expression measured *via* RT-qPCR (Figure 4.2.7). While FICZ induced a strong AHR activation as indicated by the 50-fold upregulation of *Cyp1a1* expression in the wild-type cells, co-culture with *H. pylori* failed to elicit AHR activation. Likewise, there was no upregulation of *Cxcl1* following *H. pylori* co-culture. The *Ahr*$^{-/-}$ cells exhibited decreased expression of *Cyp1a1* compared to the wild-type cells in all conditions. While there was no increase in *Cxcl1* expression in *Ahr*$^{-/-}$ cells when

comparing *H. pylori*-cocultured cells to non-treated cells, the expression of *Cxcl1* was significantly higher in the *Ahr*$^{-/-}$ cells in all conditions compared to wild-type cells, indicating that there is a higher baseline expression of this gene in the *Ahr*$^{-/-}$ cells.

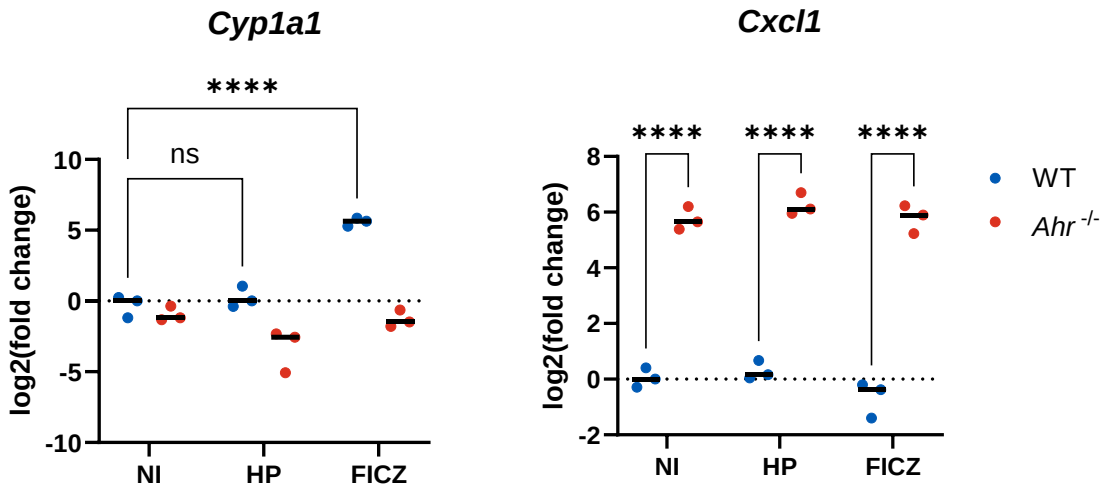

Figure 4.2.7 | Expression of *Cyp1a1* and *Cxcl1* in murine organoids after co-culture with *H. pylori* PMSS1.
Co-culture of primary murine gastric epithelial cells with *H. pylori* did not elicit activation of AHR or NF-κB signalling pathways as indicated by expression of target genes *Cyp1a1* and *Cxcl1*; treatment with AHR agonist FICZ successfully activated AHR signalling. Cells were cultured as organoids, co-cultured with *H. pylori* for 1 h (MOI50), washed and then plated and co-cultured for a further 24 h. One data point corresponds to one independent experiment (n=3). Differences between conditions were tested for statistical significance by two-way ANOVA with Tukey's post-hoc correction. ns: non-significant. ****: $p<0.0001$.

As there was no activation of NF-κB signalling indicated by the lack of *Cxcl1* upregulation following infection, organoids were assumed not to be appropriate to model primary murine cell infection. Instead, murine cells were used to create mucosoid-like monolayers, which were kept in liquid-liquid interface culture. After 7 days, mucosoids were infected with *H. pylori* for 24 h and once the experiment was finished, RNA was extracted, and then used for 3'-mRNA sequencing.

4.2.5 *Ahr*-deficient mouse mucosoids display higher baseline inflammatory signalling but difference is lost during infection

As the initial hypothesis was that the effect of AHR loss in mice was driven by the epithelium, primary murine epithelial cells, both AHR deficient and proficient, were infected with *H. pylori* to investigate differential gene expression.

Three samples per treatment and genotype were used for sequencing. First, unsupervised clustering was performed to assess which samples cluster together, indicating which samples are more similar to one another and that the major source of variation between the samples is the experimental condition rather than technical or biological variability. To show the effect of treatment and genotype on gene expression, principal component analysis (PCA) was performed (Figure 4.2.8). PCA identified 12 principal components (PC); PCs were considered relevant when their eigenvalues were greater than 1, which was the case for PC 1-11. The number of optimal PCs was defined as the number of PCs needed to explain over 80% of the variation observed in the dataset, for which six PCs were sufficient (Figure 4.2.8A). Comparing the first 4 PCs for clustering of genotype (Figure 4.2.8C) and treatment (Figure 4.2.8D) showed that PC1 and PC4 capture the variation caused by infection status and genotype, respectively

(Figure 4.2.8B). Notably, PC3 revealed a clustering of samples by replicate, suggesting that part of the overall data variation is due to a technical reason (Figure 4.2.8E).

As three replicates are generally considered a minimal number of data points to perform statistical analyses, replicate 2 was still carried forward for further analysis. The top 0.5% of genes contributing to clustering by PCs 1 and 4 are shown in Figure 4.2.8.

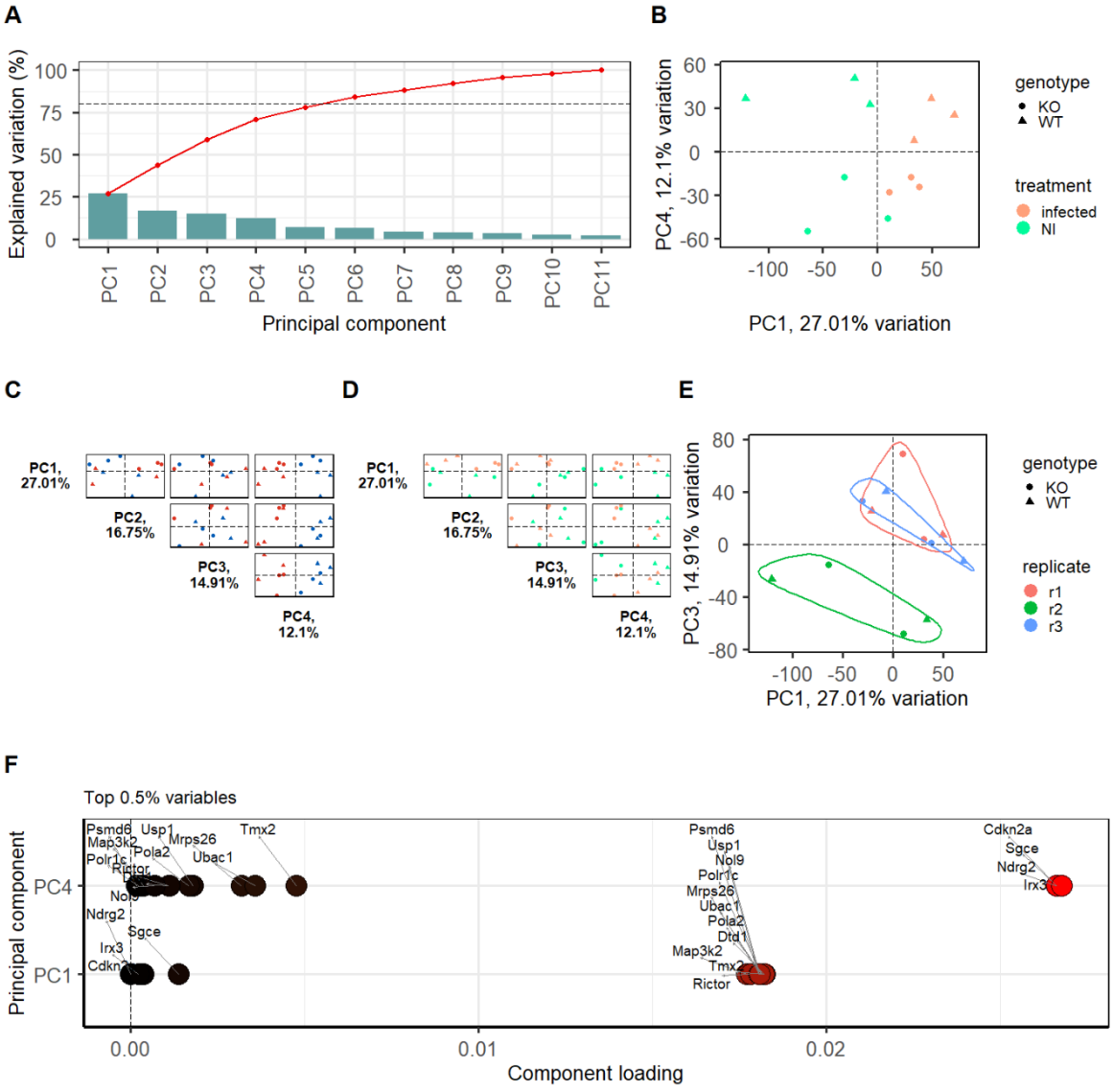

Figure 4.2.8 | Principal component analysis (murine mucosoids).

Principal component analysis was performed for dimensionality reduction of the dataset in order to identify clustering of data based on technical variability rather than biological effects. A: Scree plot of principal components 1-12 showing explained variation for each principal component (columns) and cumulative explained variation (red points) of 80%. PCs 1-6 were sufficient to explain >80% of observed variation. B: PC1 showed best separation of samples by treatment, explaining 27% of observed variation. PC4 showed best separation of samples by genotype, explaining 12.1% of variation observed in the dataset. C, D: Pairs plots giving an overview of PCs to identify most informative PCs. Samples coloured by genotype (C) and treatment (D). Due to size limitation, only the most relevant PCs (1-4) are shown. E: Biplot of PC1 and PC3 identified a cluster of samples based on replicate, suggesting technical variation caused observed variation in data. PC3 explained 14.9% of variation. F: Top 0.5% of genes contributing to variation explained by PC1 and PC4. Higher loading means bigger contribution.

Calculating Pearson correlation between samples (Figure 4.2.9) and performing hierarchical clustering of the 250 most variable genes (Figure 4.2.10) gave a similar result; the majority of the samples clustered by treatment and genotype and most correlation values lay above the expected value of 0.9, which indicates acceptable variability between samples (Figure 4.2.9). However, three of the four samples from the second replicate formed separate clusters, while still matching the respective genotype.

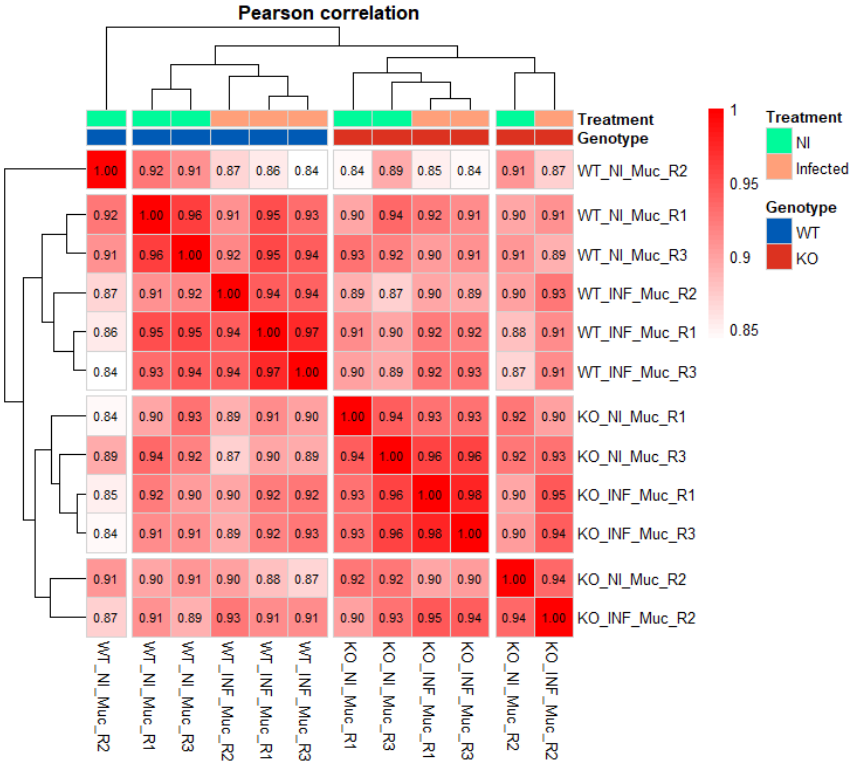

Figure 4.2.9 | Hierarchical clustering of samples by Pearson correlation values.

Hierarchical clustering of samples based on Pearson correlation. This approach identified no obvious outliers based on correlation values. Samples clustered by genotype as expected, as well as by treatment within genotypes. One exception was one non-infected knock-out cell sample. Red: Pearson correlation.

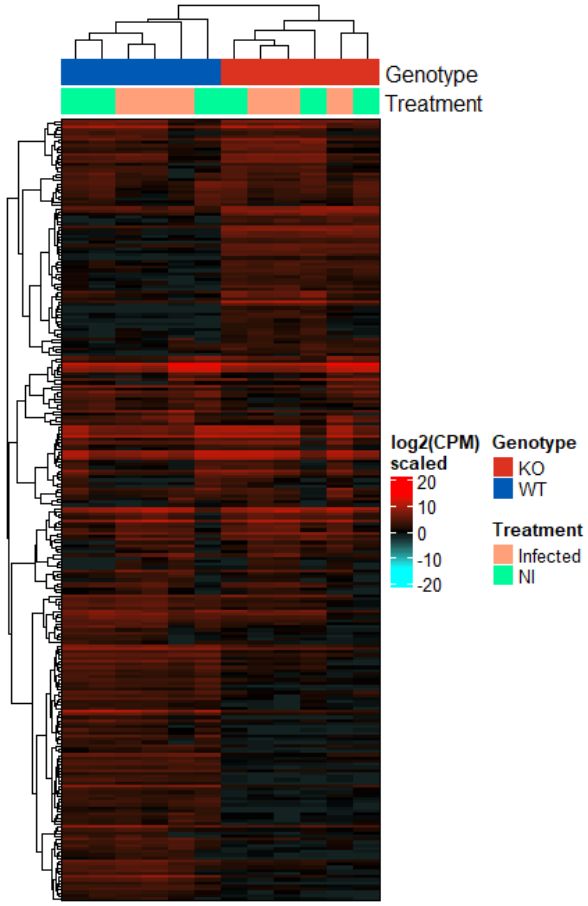

Figure 4.2.10 | Heatmap of the 250 most variable genes across all conditions (mouse mucosoids). The most variable genes were used to perform hierarchical clustering of samples. This approach confirmed clustering of samples by genotype, however clustering by treatment was inconsistent. Shown are log2 values of normalised counts. Columns were clustered by Euclidean distances, rows by Pearson distance using the complete linkage method.

Ahr expression was found not to be significantly different upon infection with *H. pylori* (Figure 4.2.11).

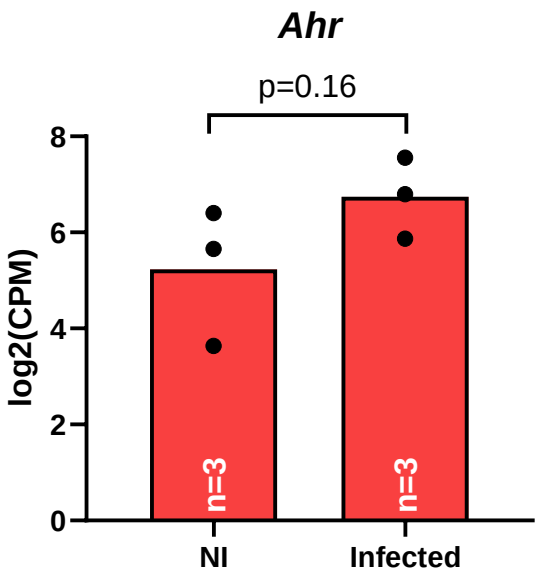

Figure 4.2.11 | Average expression of *Ahr* in wild-type murine mucosoids.
Shown are TMM-normalised logCPM values of *Ahr* for each wild-type sample. Values were tested for differential expression by fitting a negative binomial generalized log-linear model (GLM) to the data set, followed by a quasi-likelihood F-test and pairwise comparison between conditions.

Next, gene set enrichment analysis was performed. More detailed GSEA plots can be found under 7.1.3. At the baseline, i.e., in non-infected cells, *Ahr*$^{-/-}$ cells already showed a marked enrichment of gene sets correlated with inflammation, such as “TNFA signalling via NFκB”, “Complement”, “Inflammatory Response” and “IL6 JAK STAT3 signalling” (Figure 4.2.12); this fit the observations made in mouse organoids which showed a significantly increased expression of the NF-κB target gene *Cxcl1* in the absence of bacteria (Figure 4.2.7). On the other hand, gene sets relating to cell proliferation and cell cycle control (*MYC Targets*, *E2F Targets*, *P53 Pathway*) were more strongly enriched in the wild-type cells.

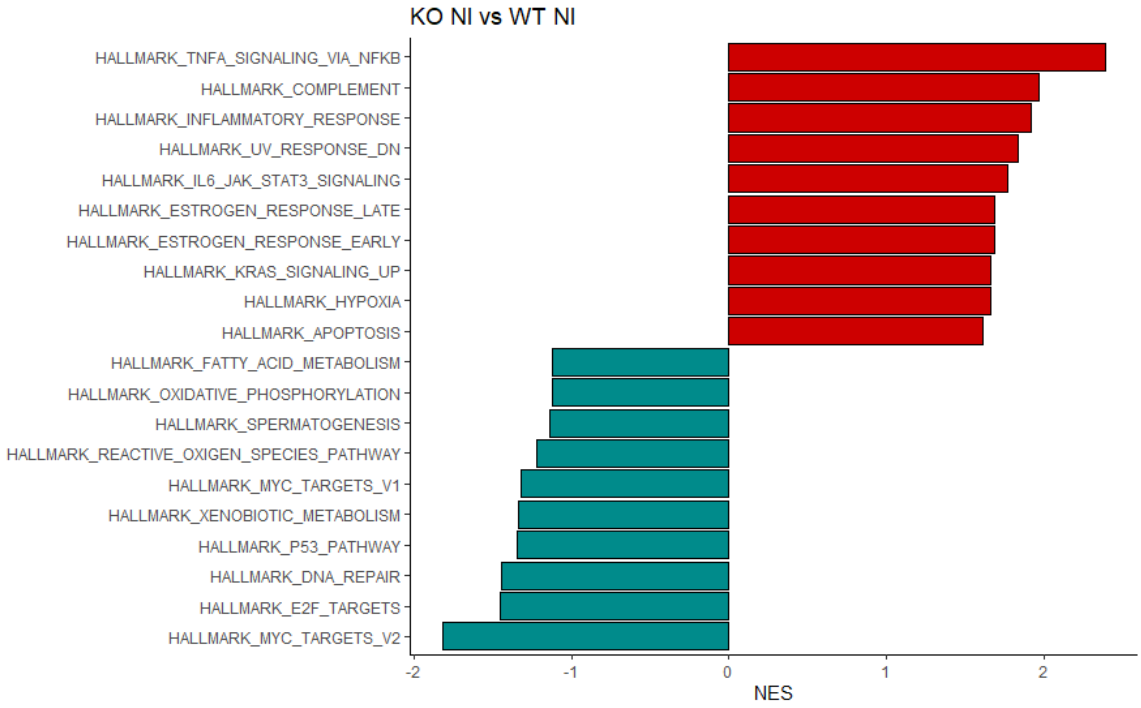

Figure 4.2.12 | GSEA results comparing non-infected *Ahr-/-* to wild-type cells.
GSEA was performed using the fgsea package, using mouse-specific MSigDB hallmark gene sets. Red: Gene sets with stronger enrichment in *Ahr*$^{-/-}$ cells. Teal: Gene sets with stronger enrichment in wild-type cells.

Infected wild-type cells, compared to non-infected wild-type cells showed a similar pattern of gene set enrichment (Figure 4.2.13). As expected, inflammation-related gene sets were enriched in the infected cells, confirming successful infection of the cells. Notably, any gene sets related to IFN signalling were not found to be enriched in the epithelial cells, as opposed to the results obtained from bulk tissue from infected mice (Figure 3.2.16, Figure 3.2.17).

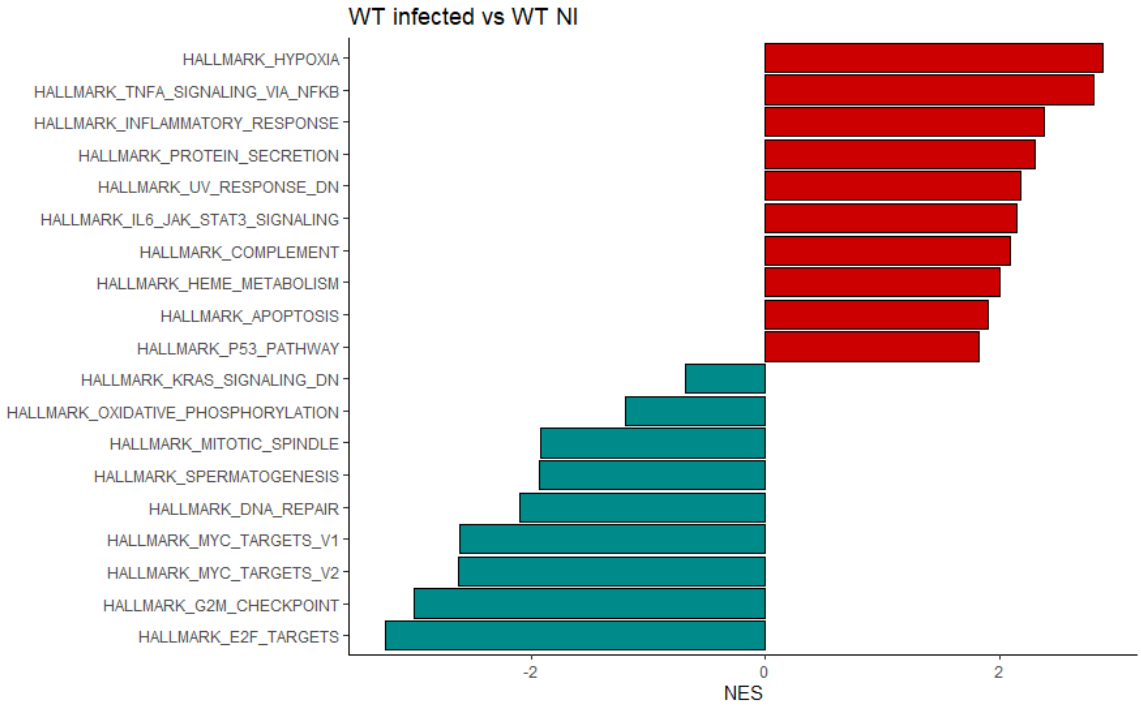

Figure 4.2.13 | GSEA results comparing infected to non-infected wild-type cells.
GSEA was performed using the fgsea package, using mouse-specific MSigDB hallmark gene sets. Red: Gene sets with stronger enrichment in *Ahr*$^{-/-}$ cells. Teal: Gene sets with stronger enrichment in wild-type cells.

Similarly, proliferation and cell cycle-related gene sets were more strongly enriched in non-infected wild-type cells. When comparing infected to non-infected *Ahr*$^{-/-}$ cells, a comparable pattern could be observed (Figure 4.2.14). Again, NF-κB signalling was found among the highest enriched gene sets in infected cells.

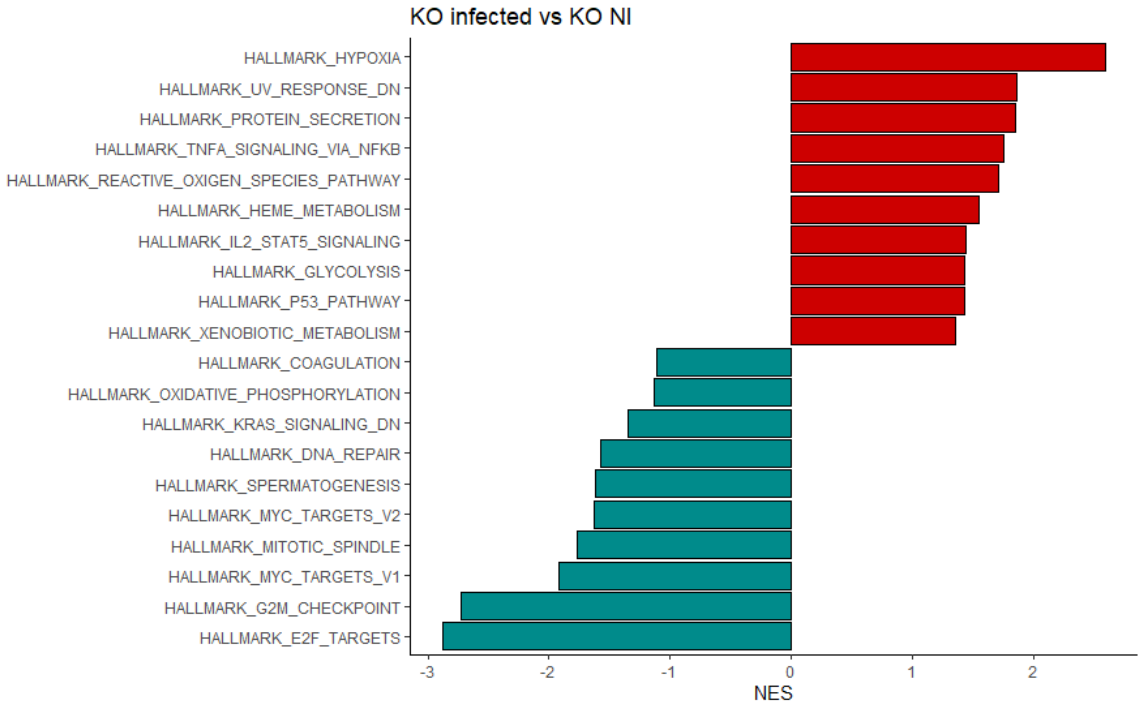

Figure 4.2.14 | GSEA results comparing infected to non-infected *Ahr-/-* cells.
GSEA was performed using the fgsea package, using mouse-specific MSigDB hallmark gene sets. Red: Gene sets with stronger enrichment in *Ahr*$^{-/-}$ cells. Teal: Gene sets with stronger enrichment in wild-type cells.

Taken together, these analyses suggest an expression of inflammation-related gene sets in infected wild-type and *Ahr*$^{-/-}$ cells, as was expected. Secondly, even in the absence of infection, *Ahr*$^{-/-}$ cells displayed increased expression of inflammation-related genes compared to wild-type cells, an effect that was already observed in murine gastric organoids.

Finally, infected *Ahr*$^{-/-}$ cells were compared to infected wild-type cells to assess differences in the inflammatory response (Figure 4.2.15). As infected *Ahr*$^{-/-}$ mice showed an increased enrichment of NF-κB related gene sets (Figure 3.2.20, Figure 3.2.21), a similar result was expected when comparing the infected epithelial cells. However, in the direct comparison, gene sets related to inflammatory response or response to infection were completely absent, suggesting that in infected mucosoids, the level of inflammatory response was similar in wild-type and *Ahr*$^{-/-}$ cells.

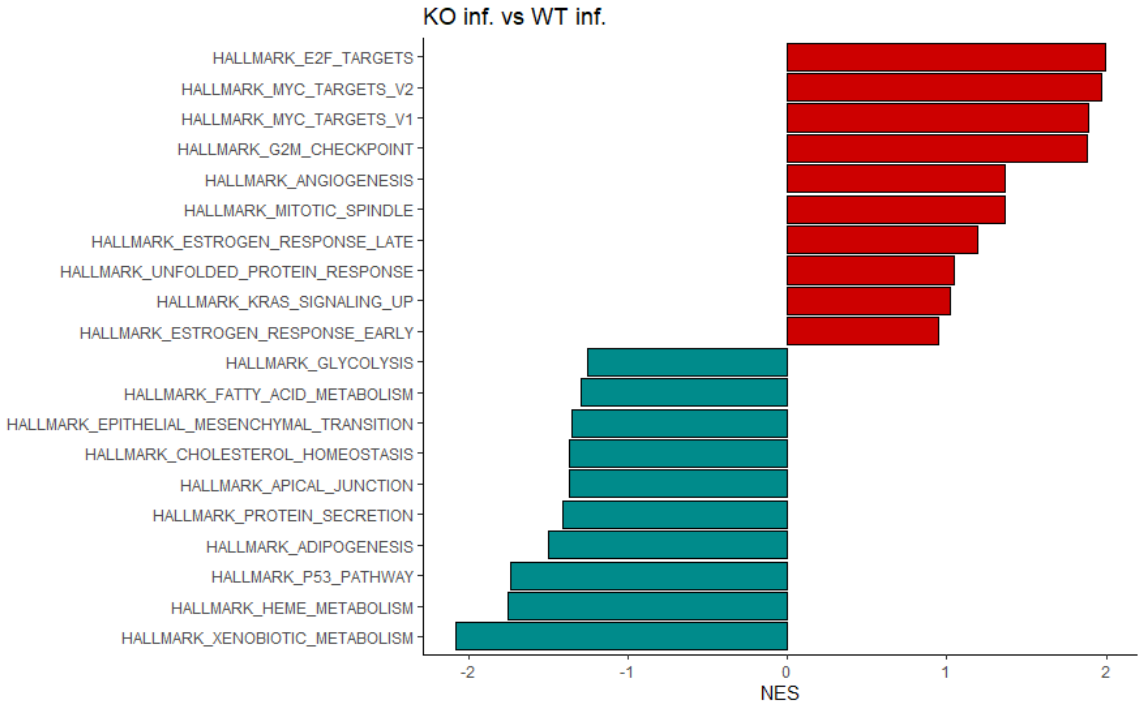

Figure 4.2.15 | GSEA results comparing infected *Ahr-/-* to infected wild-type cells.
GSEA was performed using the fgsea package, using mouse-specific MSigDB hallmark gene sets. Red: Gene sets with stronger enrichment in *Ahr*$^{-/-}$ cells. Teal: Gene sets with stronger enrichment in wild-type cells.

Next, DEGs were analysed using the clusterProfiler package (Wu, Hu *et al.*, 2021) to identify gene ontology (GO) terms enriched in the DEG lists for individual comparisons of conditions. First, a GO enrichment analysis was performed comparing non-infected *Ahr*$^{-/-}$ and wild-type cells (Figure 4.2.16A). With a cut-off q-value set to 0.05, only one term, “animal organ development” could be identified. Comparing infected *Ahr*$^{-/-}$ to wild-type cells yielded four enriched terms, as seen in Figure 4.2.16B. As a difference in NF-κB signalling between wild-type and *Ahr*$^{-/-}$ was observed in non-infected cells, GO terms related to the inflammatory response were expected to also show up in this analysis, however for neither of the comparisons any relevant GO terms could be identified.

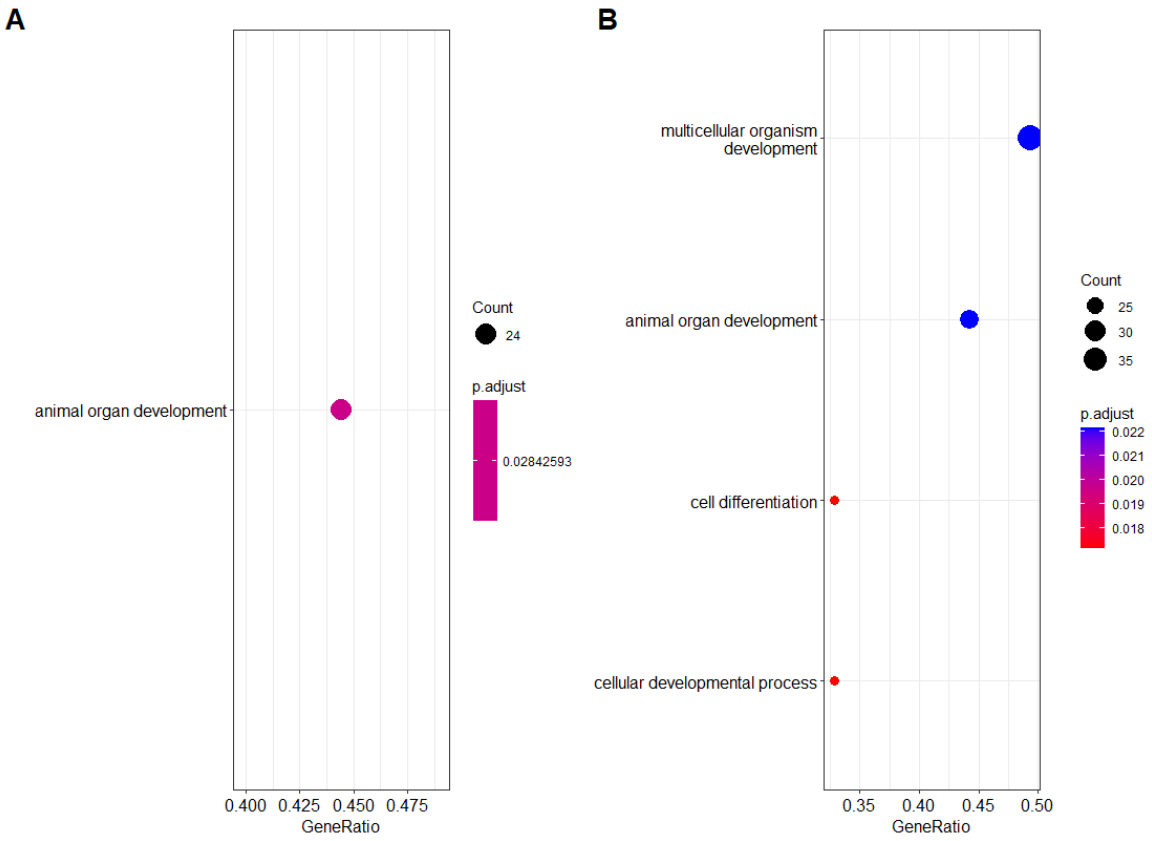

Figure 4.2.16 | GO terms enriched in non-infected and infected AHR-KO cells compared to wild-type cells.
A: Terms enriched in non-infected KO cells vs non-infected wild-type cells. B: Terms enriched in infected KO cells vs infected wild-type cells.

Additionally, GO overrepresentation analysis was performed for the same comparisons. While this analysis yielded more significantly overrepresented GO terms, again, none of them were related to the inflammatory response to infection, neither for the comparison of non-infected cells (Figure 4.2.17) nor infected cells (Figure 4.2.18).

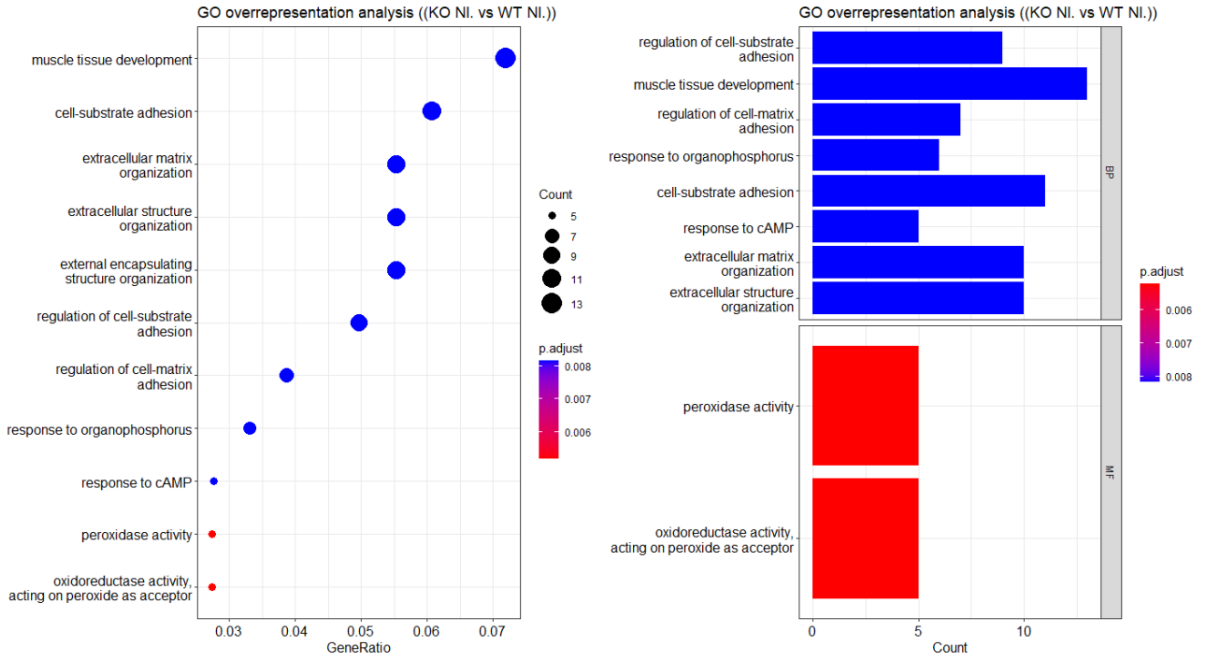

Figure 4.2.17 | GO overrepresentation analysis comparing non-infected *Ahr*$^{-/-}$ to non-infected wild-type cells.
Terms overrepresented in non-infected KO cells vs non-infected wild-type cells.

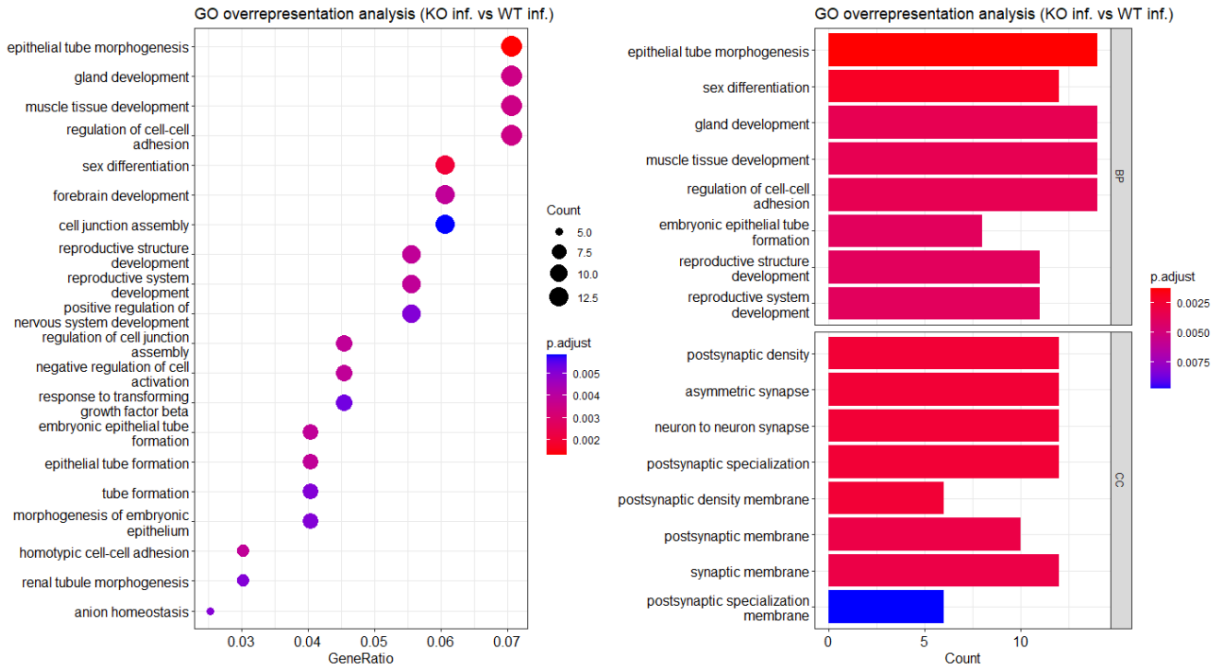

Figure 4.2.18 | GO overrepresentation analysis comparing infected *Ahr*$^{-/-}$ to infected wild-type cells.
Terms overrepresented in non-infected KO cells vs non-infected wild-type cells.

Looking directly at the comparisons between infected and non-infected for each genotype, no GO terms related to infection or inflammation could be observed (see Figure 7.1.22 and Figure 7.1.23).

Taken together, GO term analysis did not reveal any further insight into the differences in the inflammatory response.

While the GSEA found no differences in enrichment of inflammation-related gene sets, this is a high-level analysis that can potentially miss more nuanced differences, meaning that relevant individual genes might still be differentially regulated. To investigate further, NF-κB target genes (list and categories obtained from Dr Thomas Gilmore's lab, Boston University; https://www.bu.edu/nf-kb/gene-resources/target-genes/) were individually analysed for changes in expression in presence or absence of *H. pylori*. Figure 4.2.19 shows log-fold changes of genes differentially expressed between *Ahr*$^{-/-}$ and wild-type cells.

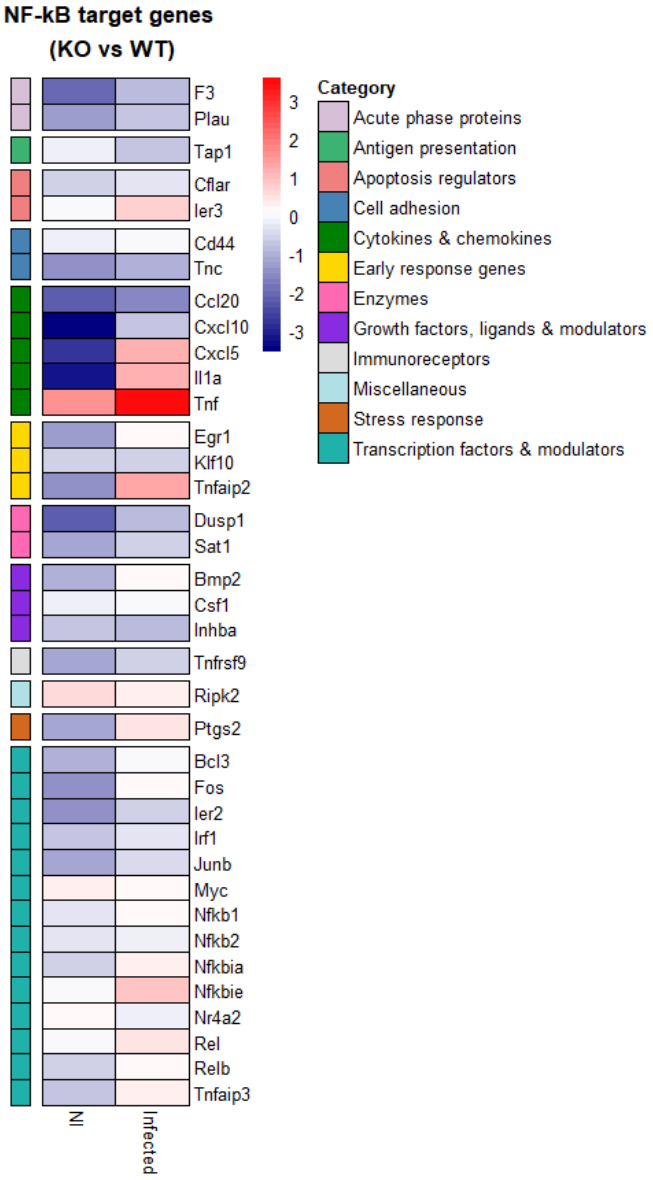

Figure 4.2.19 | Expression of NF-κB target genes in non-infected and infected murine musocoids. Comparison of NF-κB target gene expression between *Ahr*$^{-/-}$ and wild-type cells revealed that expression of many genes was increased in wild-type cells, particularly in absence of infection. Shown are the $\log_2$(fold changes) of differentially expressed genes between *Ahr*$^{-/-}$ and wild-type cells. Red: upregulated in *Ahr*$^{-/-}$ cells. Blue: downregulated in *Ahr*$^{-/-}$ cells.

Most genes were found to be less expressed in *Ahr*$^{-/-}$ in the absence of infection, which seems to contradict the findings made by GSEA. One noticeable exception was *Tnf*, which encodes the Tumour necrosis factor (TNF)-α protein, a major pro-inflammatory cytokine. Its expression in *Ahr*$^{-/-}$ cells was about two times higher than in the wild-type cells at baseline. During infection, the difference in expression increased to about 6-fold. Other pro-inflammatory cytokines, *Cxcl5*

and *Il1a*, were also found to be more expressed in *Ahr*$^{-/-}$ cells upon infection, however not at the baseline level. *Cxcl10* and *Ccl20*, in turn, were both found to be downregulated at baseline and upon infection. *Nfkbia* and *Nfkbie*, coding for the regulators of NF-κB signalling IκBα and IκBε, respectively, were upregulated during infection, indicating activated NF-κB signalling. NF-κB family members *Nfkb1*, *Rel* and *Relb* were slightly upregulated in *Ahr*$^{-/-}$ cells upon infection. Expression of *Ripk2* was found to be increased in *Ahr*$^{-/-}$ cells in both conditions. Lastly, the TNF-α-induced genes *Tnfaip2* and *Tnfaip3* were also found to be more strongly upregulated in *Ahr*$^{-/-}$ cells upon infection.

Overall, while expression of many NF-κB target genes was found to be lower in *Ahr*$^{-/-}$ cells, a number of genes showed differential expression, as they were either higher expressed in *Ahr*$^{-/-}$ cells in general or upon infection, i.e, *Cxcl5*, *Tnfaip2*, *Tnfaip3* and *Ripk2*, which are all induced by TNF-α and involved in activation or regulation of NF-κB signalling. *Tnf* and *Il1α* were also found to be upregulated, suggesting an activation of NF-κB signalling, potentially induced via TNF-α.

4.2.6 Absence of AHR rather than lack of AHR signalling drives inflammatory phenotype *in vitro*

Human primary epithelial cells were grown as mucosoid cultures, which are a long-term, low-maintenance culture system that enables access to both apical and basal side of an epithelial, polarised monolayer and facilitates infection experiments, as unlike organoids, mucosoids allow direct addition of bacterial suspensions to eukaryotic cells without the need for microinjection that is being used for organoid infection experiments (Bartfeld, Bayram *et al.*, 2015). Furthermore, as the expansion of mucosoid cultures is limited spatially by the dimension of the cell culture insert serving as substrate for each individual culture, the number of cells in two cultures of the same age from the same patient is very similar. This allows for a much more precise estimation of multiplicity of infection i.e., the number of bacterial cells per eukaryotic cell used for a given infection experiment, compared to organoid cultures.

To investigate the effect of lack of AHR signalling on the human inflammatory response to infection, human antral mucosoids were infected with *H. pylori* for 24 h in the presence or

absence of the AHR inhibitor CH223191. Following infection, expression of *CYP1A1* and *IL8* were analysed by RT-qPCR (Figure 4.2.20). Infection induced significant upregulation of CYP1A1, while treatment with the inhibitor abolished AHR signalling as indicated by the expression of CYP1A1, which was the same as in non-infected cells (Figure 4.2.20A). Surprisingly, while infection with *H. pylori* induced a strong upregulation of *IL8* of about 32-fold, inhibition of AHR had no effect on *IL8* expression (Figure 4.2.20B).

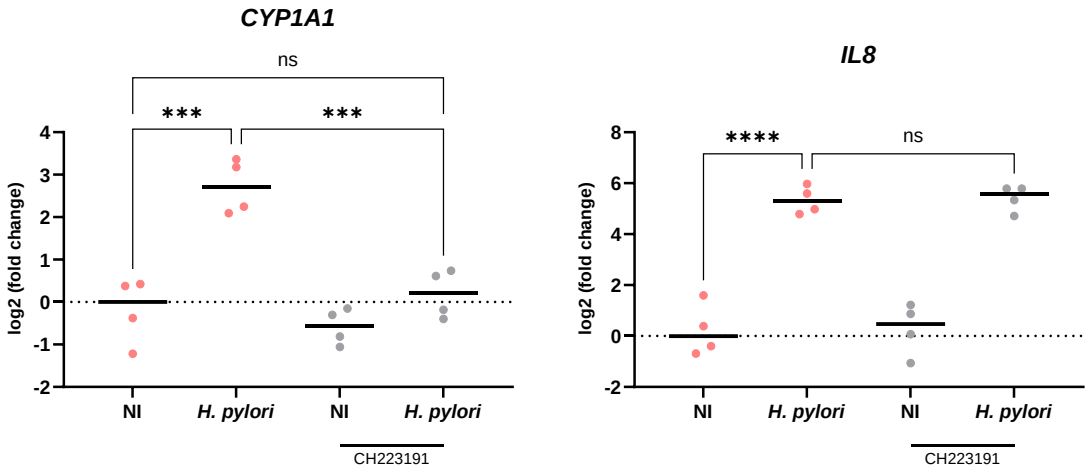

Figure 4.2.20 | Activation of AHR and NF-κB signalling in human antral mucosoids after infection. *CYP1A1* and *IL8* expression were increased upon infection with *H. pylori* P12 but inhibition of AHR signalling did not affect activation of NF-κB signalling. Mucosoids were infected for 4 h at MOI50 and half of the mucosoids were treated with the AHR antagonist CH223191 (grey points), the other half were not (red points). Shown are log2 values of fold changes compared to non-infected, non-treated controls. One data point corresponds to one independent experiment (n=4). Statistical significance was tested using a two-way ANOVA with Tukey's post-hoc correction. ns: non-significant. ***: $p<0.001$. ****: $p<0.0001$.

Likewise, a second set of experiments conducted using the same conditions revealed that, like NF-κB signalling, type I interferon signalling (IFN I) was not influenced by inhibition of AHR, indicated by the level of the IFN I marker gene *IRF7* (Figure 4.2.21).

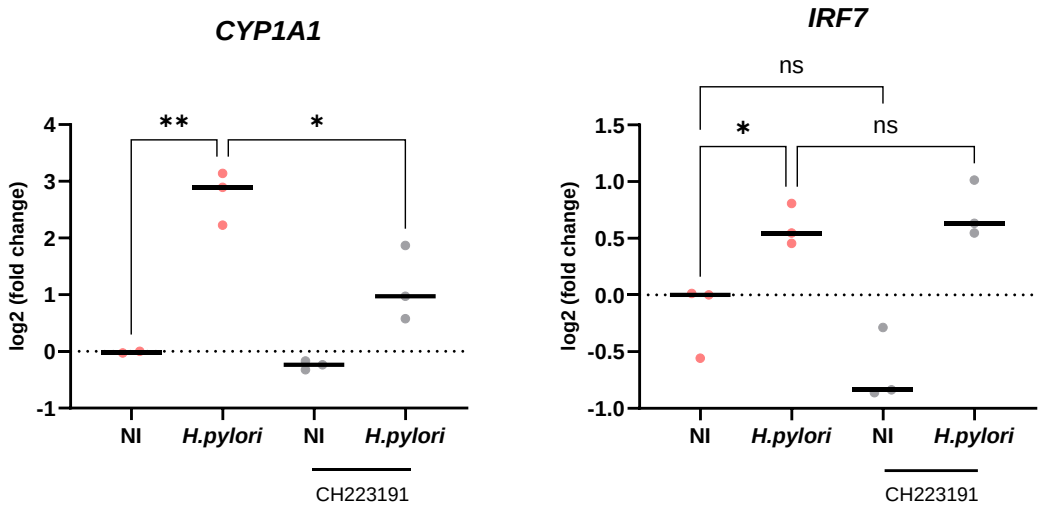

Figure 4.2.21 | Activation of AHR and type I interferon signalling in human antral mucosoids after infection.
CYP1A1 and *IRF7* expression were increased upon infection with *H. pylori* P12 but inhibition of AHR signalling did not affect activation of type 1 interferon signalling. Mucosoids were infected for 4 h at MOI50 and half of the mucosoids were treated with the AHR antagonist CH223191 (grey points), the other half were not (red points). Shown are log2 values of fold changes compared to non-infected, non-treated controls. One data point corresponds to one independent experiment (n=3). Statistical significance was tested using a two-way ANOVA with Tukey's post-hoc correction. ns: non-significant. *: $p<0.05$. **: $p<0.01$.

As human, *H. pylori*-positive gastritis patients were shown to have increased expression of AHR in the corpus, but not the antrum (4.2.3), another set of infection experiments was performed on mucosoid cultures derived from the corpus region of the stomach. This time, GNF351 was used to inhibit AHR as it specifically inhibits the ligand binding and to make sure the choice of inhibitor did not determine the phenotype observed in primary antral cells. Furthermore, to ensure the correct time point was not being missed by only looking at 24 h p.i., an infection time course was performed (Figure 4.2.22). Again, inhibition of AHR did not have an influence on NF-κB signalling as indicated by expression of *IL8*, which did not change between cells treated with GNF351 and cells without at any of the time points.

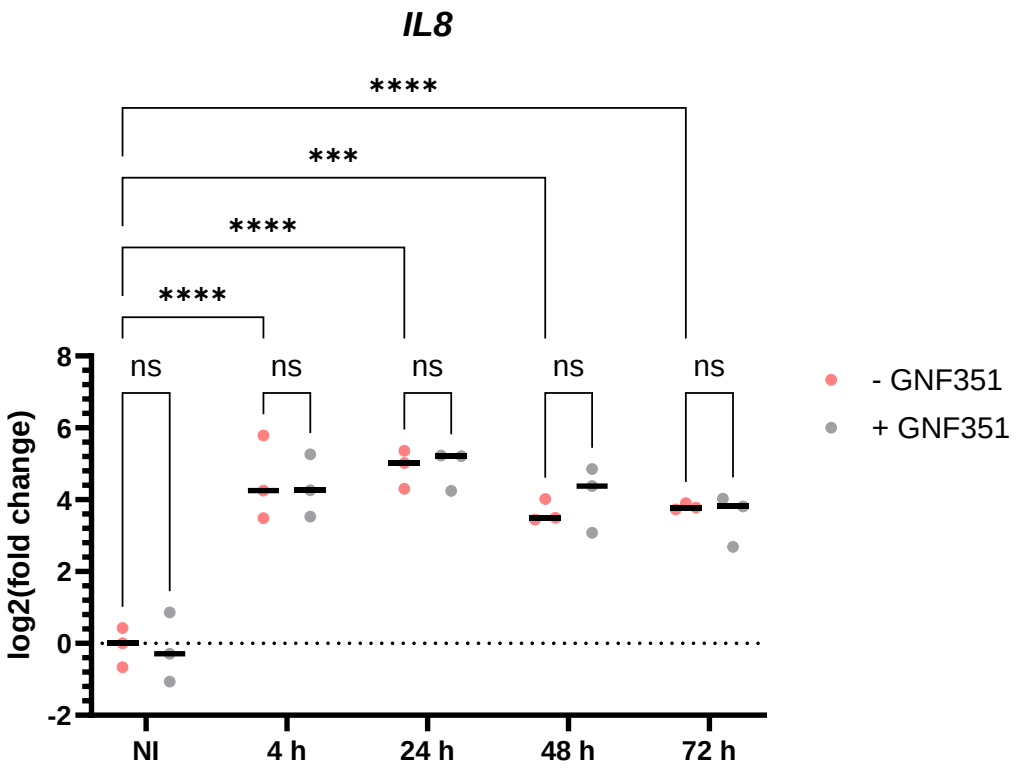

Figure 4.2.22 | Activation of NF-κB signalling in human corpus mucosoids during infection time course in the presence or absence of AHR inhibitor.
IL8 expression was increased upon infection with *H. pylori* P12 but inhibition of AHR signalling did not affect activation of NF-κB signalling. Mucosoids were infected for different durations at MOI50 and half of the mucosoids were treated with the AHR antagonist GNF351 (grey points), the other half were not (red points). Shown are log2 values of fold changes compared to non-infected, non-treated controls. One data point corresponds to one independent experiment (n=3). Statistical significance was tested using a two-way ANOVA with Tukey's post-hoc correction. ns: non-significant. ***: $p<0.001$. ****: $p<0.0001$.

These results suggested that, while *H. pylori* is able to activate AHR in gastric epithelial cells during an infection, this activation did not play a direct role in the epithelial pro-inflammatory response to the infection. As a difference was observed in *Ahr*$^{-/-}$ mice, however, this led us to develop the hypothesis that it is the presence of AHR, rather than its activation, that influences the epithelial pro-inflammatory response to infection.

To test this hypothesis, the CRISPR/Cas9 system was utilised to create clonal *AHR*$^{-/-}$ AGS cell lines, which were validated by immunoblotting for AHR (Figure 4.2.23).

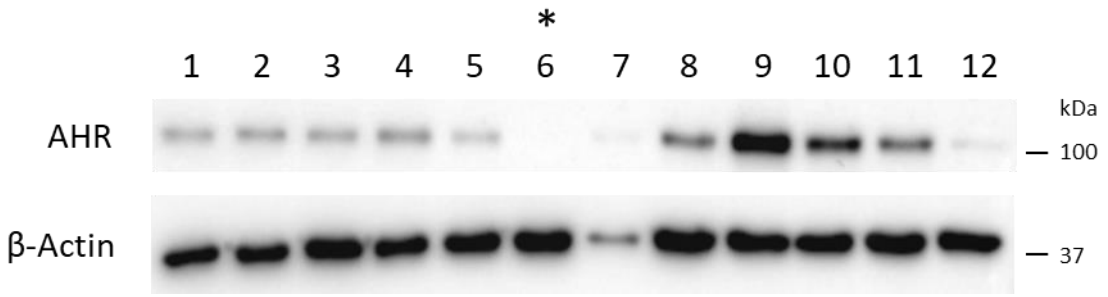

Figure 4.2.23 | Immunoblot of AGS cell clones expressing AHR after treatment with CRISPR/Cas9.
Shown are AHR and the loading control, β-Actin. AHR bands were always detected slightly above 100 kDa and β-Actin bands at around 45 kDa. No signal for AHR was detected in clone 6 (*), therefore this clone was chosen for the following experiments.

Clonal cell lines were tested for expression of AHR and three cell lines selected for subsequent experiments. Cells were infected with a high MOI of 100 for 4 h or a low MOI of 10 for 4 h. Expression of *CYP1A1* and *IL8* was analysed by RT-qPCR. To compare the effect of a loss of AHR to inhibition of AHR signalling, cells were treated in parallel with GNF351. As a control for activation of AHR signalling, cells were treated with 100 nM FICZ for 4 h (Figure 4.2.24). Infection with *H. pylori* for 4 h resulted in an *IL8* expression increase of about 200-fold in the non-GNF351 treated wild-type cells and about 550-fold in the *AHR*$^{-/-}$ cells, and similarly in the cells treated with GNF351, however, the differences were not statistically significant. When infected with a lower MOI for 24 h, the expression of *IL8* in the wild-type cells was lower compared to the 4 h treatment, at about 50-fold above the non-infected control. In the *AHR*$^{-/-}$ cells, *IL8* expression was also reduced compared to the earlier time point, however, it remained significantly higher than in the wild-type cells at around 380-fold above the NI control. When comparing wild-type cells treated with GNF351 and not treated with GNF351, there was no difference in IL8 expression, suggesting that inhibition of AHR was not able to alter expression of NF-κB signalling as indicated by the marker gene *IL8.* Interestingly, when wild-type and *AHR*$^{-/-}$ cells were treated with GNF351 during infection, there was no significant difference anymore between the two genotypes, neither at the 4 h nor at the 24 h time point.
Notably, *AHR*$^{-/-}$ cells already displayed a higher base line expression of *IL8* i.e., in non-infected control cells.

Expression of *CYP1A1* was not significantly increased or decreased between wild-type and *AHR*$^{-/-}$ cells in any of the tested conditions; infection or treatment with FICZ failed to significantly increase *CYP1A1* expression as well.

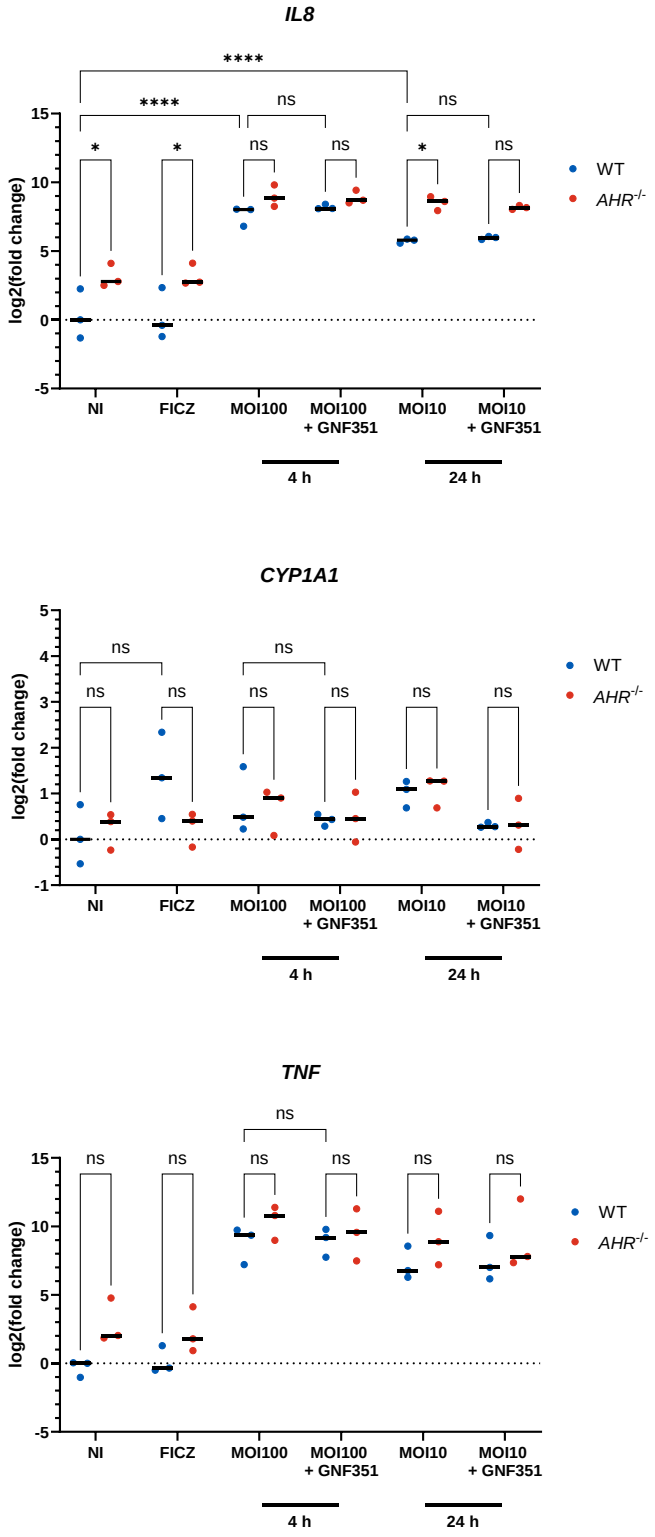

Figure 4.2.24 | Comparison of NF-κB and AHR activation in AHR-deficient and AHR inhibitor-treated AGS cells.

IL8 expression was increased upon infection with *H. pylori* P12 after 4 h and 24 h but inhibition of AHR signalling did not affect activation of NF-κB signalling at either time point. Loss of AHR however did lead to increased expression of *IL8* upon infection. Cells were infected for 4 h at MOI100 or for 24 h at MOI10 and half of the infected mucosoids were treated with the AHR antagonist GNF351. AHR activation control cells were treated with 100 nM FICZ for 4 h. Shown are log2 values of fold changes compared to non-infected, non-treated controls. One data point corresponds to one independent experiment (n=3). Statistical significance was tested using a two-way ANOVA with Tukey's post-hoc correction. ns: non-significant. *: p<0.05. ****: p<0.0001

Finally, expression of *TNF* was compared between different conditions as it had been found to be significantly increased in *Ahr*-deficient mice compared to wild-type mice (see Figure 4.2.19). While a trend could be observed suggesting increased expression in AHR-deficient cells after 24 h of infection, the high variability meant that any differences observed were not significant.

Given these findings, we decided to test if increased expression of AHR would have the opposite effect, i.e., if cells overexpressing AHR would react to *H. pylori* infection with decreased *IL8* expression, compared to wild-type AGS cells. Therefore, an AHR-overexpressing (AHR-OE) AGS cell line was created (Figure 4.2.25).

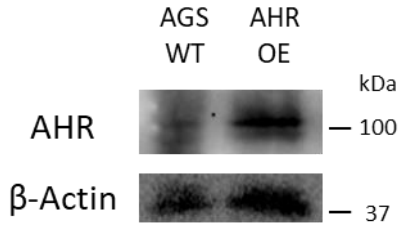

Figure 4.2.25 | AHR-overexpressing AGS cells.
Left: AGS parental cells. Right: AHR-overexpressing AGS cells (pool). β-Actin was used as loading control.

Cells were infected with *H. pylori*, under the same conditions as in the previous experiment except for inhibitor treatment and including treatment with FICZ for 4 h and 24 h (Figure 4.2.26). While expression of *CYP1A1* was significantly increased in AHR-overexpressing cells after 4 h of treatment with FICZ, infection with *H. pylori* failed to elicit the same effect at either time point; while a trend towards higher *CYP1A1* expression was observed in the AHR-overexpressing cells, the increase was not significant. At 24 h, *CYP1A1* expression was not

different between wild-type and overexpressing cells in either treatment. No significant difference in expression of *IL8* could be observed between wild-type and AHR-OE cells in any of the conditions.

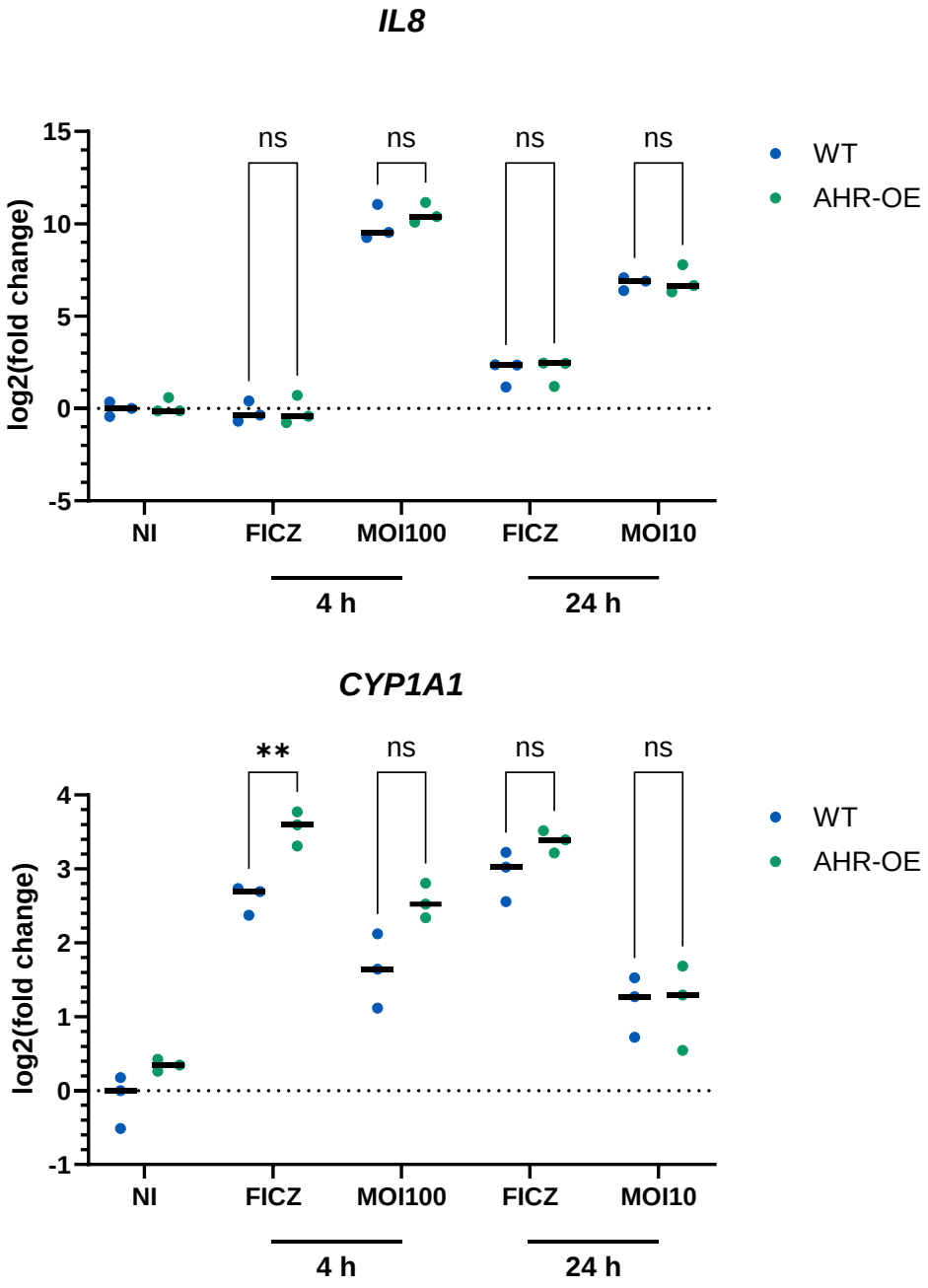

Figure 4.2.26 | Comparison of NF-κB activation in AHR-overexpressing and wild-type AGS cells. Overexpression of AHR did not lead to a difference in *IL8* expression compared to wild-type cells. Cells were infected with *H. pylori* P12 for 4 h at MOI100 or for 24 h at MOI10. AHR activation control cells were treated with 100 nM FICZ for 4 h or 24 h. Shown are log2 values of fold changes compared to non-infected, non-treated wild-type controls. One data point corresponds to one independent experiment (n=3). Statistical significance was tested using a two-way ANOVA with Tukey's post-hoc correction. *: $p<0.01$. ns: non-significant.

In summary, these results are supporting the hypothesis that presence of AHR, rather than its activation is the key factor for its inhibitory effect on NF-κB signalling during infection with *H. pylori*. Results from RNA-sequencing suggest that this effect might be mediated through TNF-α induced NF-κB signalling.

4.3 Discussion

The AHR is a ligand-activated transcription factor and has been implicated in the regulation of inflammatory signalling in the epithelium. As demonstrated in previous publications, the AHR is able to sense bacterial compounds and the presence of AHR is important for the host to be able to mount an effective immune response to infection in different organs (Moura-Alves, Fae *et al.*, 2014; Metidji, Omenetti *et al.*, 2018; Moura-Alves, Puyskens *et al.*, 2019). We observed a differential response to infection with *H. pylori* PMSS1 in wild-type and *Ahr*-deficient mice, in that the mice lacking AHR demonstrated a lowered bacterial burden after two months of infection, as well as potentially milder pathology. This difference seemed to be driven by increased NF-κB signalling in the *Ahr*-deficient mice.

We therefore set out to investigate a potential role of AHR in the regulation of the epithelial response to *H. pylori* infection, as the epithelium is the compartment of the mucosa that comes into direct contact with the bacteria and orchestrates the response to infection through induction of the pro-inflammatory signalling response. Our hypothesis was that by activating the AHR, *H. pylori* is able to induce an inhibitory effect on inflammatory signalling, specifically NF-κB mediated pathways.

First, activation of the AHR signalling pathway in epithelial cells was confirmed using EROD assays and RT-qPCR. We investigated, if activation of the AHR could be caused by inactivation of CYP1A1. While the results showed no significant effect supporting this hypothesis, the variability was relatively high, so that such a mechanism cannot be definitely excluded. We then analysed the expression of AHR in human antrum and corpus derived from patients that were diagnosed as *H. pylori*-positive or *H. pylori* -negative, respectively. This

analysis revealed an increased expression of AHR in corpus samples, but not in antrum samples of *H. pylori*-positive patients. As there were only few samples from *H. pylori*-negative, healthy patients available as control, the experiment was likely underpowered in that the numbers of patients in each group were very different. While for the original publication, patients that were *H. pylori*-positive but showed no signs of gastritis were included in the control group, they were not included in the analysis presented herein, to avoid *H. pylori* infection potentially confounding the experiment. Again, this should be taken into account when deriving conclusions from this dataset and a similar experiment should be repeated comprising a larger number of patients in the control group to improve statistical power.

To understand if the increased NF-κB signalling observed in *Ahr*-deficient mice could be confirmed in epithelial cells, we co-cultured murine gastric organoids from wild-type and *Ahr*-deficient mice with *H. pylori* PMSS1; while co-culture of organoids with *H. pylori* specifically did not lead to increased expression of the NF-κB target gene *Cxcl1* or the AHR target gene *Cyp1a1* in either genotype, gene expression analysis showed an increased expression of *Cxcl1* in *Ahr*-deficient cells in general when compared to wild-type organoids. An NF-κB positive control should have been included in this experiment to understand if the lack of increase of *Cxcl1* expression was due to the conditions used for organoid infection. The included control for AHR signalling, FICZ, did indeed induce increased *Cyp1a1* expression in the organoids, whereas *H. pylori* did not, which was unexpected.

As we could not determine if infection of murine organoids was successful, we set up a liquid-liquid interface culture of primary murine gastric epithelial cells to allow infection with *H. pylori* in a more controlled manner. 3'-mRNA sequencing was performed after 24 h of infection and subsequent differential gene expression analysis revealed an underlying difference in expression of genes involved in NF-κB signalling. While samples obtained from wild-type bulk stomach tissue showed a higher expression of NF-κB genes in absence of infection compared to *Ahr*-deficient tissue and an increased expression during infection in *Ahr*-deficient tissue, analysis of epithelial cells showed an almost inverse result; at basal level, in the absence of *H. pylori*, the *Ahr*-deficient cells displayed higher enrichment of NF-κB signalling pathway genes,

but when infected, this difference disappeared. This could be explained by the absence of any other cell compartments in this experimental setting, which means that in the whole tissue, stromal cells, immune cells and other cell types contribute to the gene expression analysed by bulk RNA-sequencing.

The proportion of infected epithelial cells of the total RNA captured is unknown and it is possible that the effects of loss of *Ahr* in other cell compartments outweigh the effects observed in epithelial cells. Several publications have attempted to understand how and how many bacteria present in infected patients are attaching to the epithelium and it has been suggested, that only around 20% of bacteria might actually be in contact with the epithelium (Hessey, Spencer *et al.*, 1990; Tan, Tompkins *et al.*, 2009). Assuming the situation is somewhat comparable in infected mice, one can attempt to roughly calculate the number of potentially infected cells:

For *Ahr*-deficient mice, the median number of CFU/mg stomach tissue was 10^4 (see Figure 3.2.4). Karam and Leblond counted the number of cells in the zymogenic gastric unit (i.e., corpus gland) and found 194.2 cells per gland, on average (Karam and Leblond, 1992). Attempting to identify the density of gastric glands of human gastric tissue, Kurbel and colleagues found a number of 135 glands/mm^2 (Kurbel, Kurbel *et al.*, 2001). Assuming that one mg of murine stomach tissue has an area of roughly 5 mm^2, the total number of epithelial cells per mg would be around $1.3x10^5$, neglecting differences in the gland density between human and murine stomach tissue. If only 20% of the 10^4 viable bacteria detected would be in contact with the epithelium, only 2000, or 2% of epithelial cells might have been infected, assuming that only one bacterium infected one epithelial cell and every contact between bacterium and cell lead to induction of NF-κB signalling. It is therefore possible that only a relatively small number of infected epithelial cells have actually contributed to the results of the bulk RNA-sequencing experiment.

Infecting an epithelial cell model with an MOI of 50 could therefore yield very different results. Investigating the changes in expression of differentially expressed NF-κB target genes revealed that the majority of genes were actually higher expressed in uninfected wild-type cells

and the expression got more similar between wild-type and *Ahr*-deficient cells upon infection for many NF-κB target genes (Figure 4.2.19). This contradicts some findings made by GSEA (Figure 4.2.12). One possible explanation for this is that the gene set used for GSEA ("Hallmark TNFA signalling via NF-κB" from MSigDB) is not the same as the NF-κB target genes shown in Figure 4.2.19 because that not all genes included in the hallmark gene set are NF-κB target genes. One striking finding was that *Tnf*, the gene encoding TNF-α, was higher expressed both in the presence and absence of infection in *Ahr*-deficient cells. While TNF-α is mainly known as a cytokine expressed by activated macrophages and T cells, it is a potential driver of the increased immune response in *Ahr*-deficient epithelium. Hou and colleagues demonstrated a regulation of TNF-α and lL-8 expression by AHR in human sebocytes (Hou, Chen *et al.*, 2019). As mentioned before, a number of genes linked to TNF-α were also found to be upregulated in *Ahr*-deficient cells. While *Cxcl5* and *Tnfaip2* seem to simply be TNF-α-responsive genes (Sarma, Wolf *et al.*, 1992; Zhou, Xia *et al.*, 2019), the role of *Tnfaip3* and *Ripk2* might be more complex: Receptor-interacting serine/threonine-protein kinase 2 (RIPK-2), the protein encoded by *Ripk2*, is an important adaptor for the Nucleotide-binding oligomerization domain-containing protein (NOD) 1 and NOD2-induced activation of NF-κB (Inohara, Koseki *et al.*, 2000; Girardin, Tournebize *et al.*, 2001); its expression is regulated by NF-κB and increased expression leads to induction of NF-κB through a positive feed-back loop (McCarthy, Ni *et al.*, 1998; Yin, Krikorian *et al.*, 2010). *Tnfaip3* encodes the protein Tumor necrosis factor alpha-induced protein 3 (TNFAIP3), or A20, which is also induced by TNF-α. A20 has been shown to have an inhibitory effect on NF-κB signalling (Song, Rothe *et al.*, 1996). Specifically, it inhibits NF-κB by deubiquitination of RIPK-1 and RIPK-2 polyubiquitin chains (Wertz, O'rourke *et al.*, 2004) and subsequent degradation, as well as through inhibition of TRAF2 and TRAF6-mediated NF-κB signalling (Heyninck and Beyaert, 1999; Heyninck, De Valck *et al.*, 1999), and by targeting TRAF2 for proteasomal degradation (Li, Soetandyo *et al.*, 2009); TRAF2 has been shown to be involved in the ALPK1-TIFA-mediated detection of *H. pylori* (Zimmermann, Pfannkuch *et al.*, 2017). It is therefore unclear, if changes in expression of these genes during infection are simply a result of increased TNF-α signalling, or if increased expression of

specifically *Tnfaip3* is a regulatory mechanism employed by the epithelium to limit the TNF-α-induced inflammatory response.

As the quality control of the obtained data revealed the clustering of samples by replicate in one case, it is likely that some of the observed variations in the dataset were caused by technical rather than biological effects. This has to be considered when deriving conclusions from these data. For future experiments, using a larger sample size would be advisable to have the option to exclude samples that exhibit technical rather than biological variability.

Finally, we attempted to replicate the effect of AHR loss on the inflammatory response to *H. pylori* infection in human primary epithelial cells using an air-liquid interface model, termed mucosoids. Human primary cells from the antrum region of the stomach were infected in the presence or absence of AHR inhibitors and the resulting activation of AHR signalling and NF-κB signalling was assessed via RT-qPCR. While the infection induced AHR and NF-κB signalling, inhibition of AHR failed to increase the NF-κB-mediated expression of *IL8*. As we observed a difference in AHR expression levels between antrum and corpus in human patient samples, infections were repeated using human primary corpus cells and an inhibitor specifically inhibiting ligand binding to AHR. Again, no increase *in IL8* expression could be observed when AHR signalling was inhibited. We therefore hypothesized that rather than activation of AHR by bacterial ligands, the presence of AHR was important for the regulation of NF-κB signalling.

To investigate this, we generated $AHR^{-/-}$ cells and infected wild-type and $AHR^{-/-}$ AGS cell lines in the presence or absence of AHR inhibitor. While inhibition of AHR did not lead to an increase in IL-8 expression, $AHR^{-/-}$ AGS cells showed a significant increase in IL-8 expression in the absence of infection and after infection with a low MOI for 24 h, compared to wild-type AGS cells. Finally, analysis of *TNF* expression in infected AGS cells revealed no significant difference between wild-type and AHR-deficient AGS cells. As relatively high variability was observed between experiments, it is possible that repeating this particular experiment would result in a significant difference, especially as there was a trend visible suggesting a higher expression of *TNF* in AHR-deficient cells. It is also conceivable that the observed increase in

Tnf expression in the murine epithelial cells is a species-specific effect that is less pronounced or absent in human cells. The results suggest that the difference between wild-type and AHR-deficient cells is more pronounced at the later time point; it is possible that the experiments were stopped too early, and as the dynamics of the inflammatory response in this setting are not known, increasing the duration of the infection might be beneficial and yield a clearer difference between the genotypes.

We then tested if overexpression of AHR would have the inverse effect and decrease expression of *IL8* compared to wild-type cells, but did not find this to be the case.

Due to the high variability observed in the data between experiments, these should be repeated to assess if a difference between wild-type and AHR-overexpressing cells can be observed.

There are two possible explanations for these findings, the first one being that expression of CYP1A1 is already very high in AGS cells and overexpression of AHR did not lead to even higher expression of CYP1A1; the second explanation is that the expression level of AHR and its activity are not directly correlated. This could be the case if the regulation of NF-κB by AHR is exerted through a mechanism that involves other cofactors that would be a limiting factor for this activity, such as CUL4B in the CUL4B-AHR ubiquitinase complex, for example. Activation of overexpressed AHR is unlikely to be limited by availability of AHR ligands, as they are abundant in cell culture medium (Wincent, Bengtsson *et al.*, 2012).

For all experiments that were analysed by RT-qPCR, it should be mentioned that efficiency of the selected primer pairs was not tested. The $\Delta\Delta C_T$ method assumes 100% efficiency for both gene of interest and reference gene. If this is not the case, the true gene expression is likely to be different from the one calculated with the $\Delta\Delta C_T$ method. For future experiment, a better approach would be to determine reaction efficiencies for each primer pair and calculate gene expression using the Pfaffl method, which takes efficiencies into account (Pfaffl, 2001).

Overall, these experiments support the hypothesis that the differential inflammatory response observed in *Ahr*-deficient murine samples was not due to an activation of AHR by *H. pylori* in the wild-type cells, but rather caused by the absence of AHR in the knockout cells.

Chapter 5 – Discussion

The aim of this thesis was to answer the questions, if the aryl hydrocarbon receptor is activated during infection of gastric epithelial cells with *H. pylori*, if this activation leads to modulation of the inflammatory response to the infection and if inhibition of the AHR would in turn lead to an increase in pro-inflammatory signalling. As the AHR has been found to interact with members of and regulate the NF-κB-driven inflammatory response, and it has been found to be activated during bacterial infection and regulate the host immune response, we hypothesized that activation of the AHR by the bacterium might be a mechanism by which *H. pylori* is able to locally evade the strong NF-κB-driven host response to infection, contributing to its ability to chronically infect the host stomach.

We found that AHR-deficient mice showed improved ability to suppress infection with *H. pylori* compared to wild-type mice, evidenced by a significantly decreased bacterial burden after 8 weeks of infection with the mouse colonizing strain PMSS1. Analysis of the tissue for evidence of gastric pathology revealed no differences between genotypes at either timepoint.

We then investigated the role of AHR in the epithelial immune response to *H. pylori* infection using human epithelial cancer cell lines as well as human primary epithelial cell models. AHR signalling was found to be activated in epithelial cells upon *H. pylori* infection. While NF-κB signalling, assessed by expression levels of *IL8* was significantly increased in an AHR-deficient AGS cell line compared to wild-type cells, this effect could not be replicated by inhibition of AHR using different inhibitors, neither in AGS cells nor in primary human gastric epithelial cells. Overexpression of AHR in AGS cells did not lead to decreased NF-κB signalling in infected cells compared to wild-type AGS cells.

To understand if the findings made *in vivo* could be replicated in epithelial cells, murine primary gastric epithelial cells from the corpus were cultured as organoids and showed increased expression of the NF-κB target gene *Cxcl1* in AHR-deficient cells; this was independent of the presence of *H. pylori*. Mice do not express *IL8*, but *Cxcl1* and *Cxcl2* are functional homologues

in mice (Lee, Cacalano *et al.*, 1995). As infection did induce neither NF-κB signalling nor AHR signalling, the primary cells were instead cultured in a mucosoid-like liquid-liquid interface culture. While this was different from air-liquid interface cultures used for human primary cells, it still enabled formation of a monolayer and infection of cells with *H. pylori* PMSS1. Transcriptome analysis was carried out using RNA-sequencing. Expression of AHR was not increased or decreased following infection with *H. pylori*. Here, we found that AHR-deficient cells showed increased activation of NF-κB signalling in absence of infection, however this difference disappeared once cells had been infected. When we investigated expression of NF-κB target genes in more detail, we found that *Tnf* and a number of TNF-α-dependent genes were more highly expressed in *Ahr*-deficient cells. Quality control of this data set revealed that variability observed in the data was at least partially due to technical reason. The experiment should ideally be repeated including more replicates to confirm the findings.

We also analysed tissue collected from infected mice for evidence of gastric pathology, such as mucosal hyperplasia. We found a significant increase in epithelial thickness in wild-type, but not AHR-deficient mice after 8 weeks of infection, suggesting a progression in gastric disease in agreement with the precancerous cascade outlined by Correa and Piazuelo (Correa and Piazuelo, 2012). However, due to the low number of mice in the control groups, this experiment was likely underpowered and we therefore were not able to draw any definitive conclusions.

In order to understand what drove the observed differences between AHR-deficient and wild-type mice, we performed RNA-sequencing to analyse the transcriptome of the mice in bulk tissue samples from both the antrum and corpus of the stomach. Analysis of the antrum transcriptome suggested a stronger NF-κB and interferon-driven pro-inflammatory immune response in AHR-deficient mice, that was most prominent at 2 weeks p.i. and seemingly equalised at eight weeks of infection. However, quality control of the dataset revealed that the data were of relatively low quality, thereby making these findings less reliable. RNA-sequencing of the corpus samples showed a clearer effect of the treatment, although it was

stronger than the effect caused by the genotype, which was unexpected. Again, the quality of the data set was not satisfactory, and any conclusions drawn from these data should be confirmed in future experiments.

As Zhu and colleagues found downregulation of AHR in stomach tissue from *H. pylori* infected patients (Zhu, Gao *et al.*, 2018), we analysed expression of the *AHR* gene in cDNA samples obtained from *H. pylori*-positive gastritis patients and a healthy, *H. pylori*-negative control group. We found expression of *AHR* to be increased in *H. pylori*-positive patients, but only in the corpus, while it did not change in the antrum. As was the case in the *in vivo* infection experiment, due to the low number of samples in the respective control groups, the experiment was likely underpowered and cannot definitely rule out a decrease in *AHR* expression following *H. pylori* infection.

Changes in AHR expression could not be observed in mice.

As we hypothesized that *H. pylori* might exploit a potential immunomodulatory role of AHR by activating it, we were interested in understanding how this activation could be triggered during infection. Apart from direct activation of AHR through a ligand, inhibition of CYP1A1 is a way of inducing AHR by only small amounts of ligands present in normal cell culture medium (Wincent, Bengtsson *et al.*, 2012). This was tested by concurrent treatment of cells with an AHR ligand and *H. pylori*, however no significant difference could be observed between this treatment and treatment with AHR ligand alone. The high variability in some of the conditions might have been the reason for this result; the experiment should therefore be repeated. To avoid activation of AHR by compounds introduced from culturing medium, bacteria were washed several times in PBS; however, contamination with external AHR ligands derived from plastic tubes and pipettes cannot be excluded. This could be avoided by using glass dishes, tubes and pipettes for culturing and suspension preparation but this is outside the scope of this project and could be relevant for future attempts to identify AHR ligands in *H. pylori*.

Keeping the mentioned limitations in mind, the data suggested that the inflammatory response to infection was stronger in AHR-deficient mice over the entire duration of the experiment and

that it was mainly driven by NF-κB, likely involving TNF-α. Furthermore, we could observe that in the absence of infection, NF-κB signalling seemed to be more active in wild-type mice, suggesting that AHR is required for basal activity of NF-κB as well as for limiting the extent of activation during infection; judging from the data on bacterial colonisation, this modulation of NF-κB seemed to hinder complete clearance of bacteria from the host.

Assuming that differences in bacterial clearance are exerted by the AHR through NF-κB is only based on correlation, however. To prove causation, further experiments are needed, showing that removing AHR leads to increase in NF-κB signalling and that this in turn directly causes decreased bacterial load, for example through induction of bacterial cell death. This is difficult to prove *in vivo* as in the complete organism, a multitude of other factors can compound any findings, such as the presence of immune cells during infection and the influence of the stroma on the epithelial inflammatory response. Our approach was to reduce the complexity by investigating the effect of loss of AHR on a single cell compartment, in this case the epithelium. Overall, these findings suggested that loss of AHR was beneficial for the host in that it enabled clearance of the bacteria through an unknown mechanism.

As discussed, since downregulation of AHR in stomach tissue from *H. pylori* infected patients has been described previously (Zhu, Gao *et al.*, 2018), we analysed expression of the *AHR* gene in our samples and found that our results contradict the previously published findings. There is no obvious reason for that; one possible explanation could be that while our data are of *AHR* gene expression, the publication by Zhu et al. investigated expression of AHR protein. It is possible that the protein expression was inhibited also in the patients whose cDNA we analysed. However, as we did not have access to protein or tissue samples, we will not be able to confirm this. Another more speculative explanation is that the samples analysed by Zhu et al. were collected from Chinese patients, while our samples had originally been collected in Europe. One can assume that the strain or strains infecting the Chinese cohort was different from the ones found in German patients and that strain-specific differences could lead to differential regulation of AHR expression.

One interesting finding was that the pro-inflammatory cytokine *Tnf* was strongly overexpressed in AHR-deficient murine epithelial cells, both before and during infection. This could be a key effector protein driving the increased inflammatory response to infection. To confirm this, an important future experiment would be to show that increased expression of the *Tnf* gene in AHR-deficient cells also leads to increased expression of TNF-α and that this induces inflammation in other cells. Detection of the secreted protein via ELISA could support this hypothesis, as well as treating non-infected wild-type cells with cell culture supernatants collected from AHR-deficient cells and subsequent investigation of NF-κB signalling. In that case, another assumption would be that AHR inhibits expression of TNF-α at the transcriptional level. To investigate this, a chromatin immunoprecipitation (ChIP) assay could be performed. Binding of AHR to regulatory regions of *Tnf* would support this hypothesis. Additionally, inhibition of TNF-α knockdown of *Tnf* using siRNA in AHR-deficient cells should reduce or remove the difference in NF-κB signalling between wild-type and AHR-deficient cells.

Ripk2 expression was also found to be significantly higher in infected AHR-deficient cells compared to wild-type cells. RIPK-2 is an important adaptor molecule for pro-inflammatory effectors, including NOD1, TNFR1 and TLR. Repression of this gene by AHR could be another intriguing modulatory mechanism. Similar to the experiments suggested for TNF/*Tnf*, knockdown of *Ripk2* could be attempted to understand if it decreases the NF-κB signalling activity in AHR-deficient cells to the level of wild-type cells. Regulation of this gene by AHR could also be tested via ChIP assay.

When investigating the effect of inhibitor treatment of infected cells on NF-κB signalling, no difference was observed between treated and untreated cells, at different time points, suggesting lack of differential gene expression was not due to the inhibitor or the duration of infection. This was unexpected as almost all known AHR signalling pathways in higher developed organisms require binding of a ligand to AHR. Few ligand-independent AHR signalling mechanisms have been described (Singh, Hord *et al.*, 1996; Chang, Fan *et al.*, 2007; Xiao, Son *et al.*, 2015), although it should be kept in mind that AHR ligands are abundant in cell culture medium and creating a truly AHR ligand-free environment is challenging (Wincent,

Bengtsson *et al.*, 2012). However, this does not rule out that further, yet undiscovered mechanisms can exist.

The fact that we could not observe a difference in *H.pylori*-induced NF-κB signalling when increasing AHR expression is only unexpected when assuming that a positive correlation exists between the level of AHR protein and its inhibitory effect on NF-κB signalling. If it exerts this effect through a multi-protein complex or more generally through a mechanism involving more factors than only AHR, abundance of these other interaction partners is likely to be a limiting factor. The logical next step would have been to perform a rescue experiment by using the AHR-overexpressing vector to re-introduce AHR into the AHR-deficient AGS cells. However, our knockout cell line constitutively expresses the CRISPR/Cas9 system targeting wild-type AHR and it would therefore not be possible to use the same plasmid to express wild-type AHR in these cells. To remedy this, the PAM sequence targeted by the gRNA expressed in the AHR-knockout cells needs to be mutated first. Re-expression of AHR in the AHR-deficient cells should then return *IL8* expression to a similar level as in the parental AGS cells. Another, more direct analysis of NF-κB activation is the preparation of nuclear extracts and analysis of phosphorylated p65 levels by Western blot, which could be added as further proof of active NF-κB signalling.

To investigate the aforementioned potential limitations further, future experiments should aim to identify binding partners of AHR during infection, for example by co-immunoprecipitation followed by mass spectrometry analysis of the protein complex. This would also be critical to understand if the immunomodulatory effect of AHR is carried out at the level of protein-protein interactions.

We did not make a functional connection between increased NF-κB signalling and antibacterial response in epithelial cells yet. This is an important open question and the next step to prove this connection would be bacterial survival assays using mucus produced by mucosoids, as shown by Boccellato and colleagues (Boccellato, Woelffling *et al.*, 2019). If loss of AHR in the epithelium is sufficient to promote bacterial clearance, decreased bacterial survival should be

observed as a result. It is also possible that this is the result of synergism between epithelial cells and other cell types, for example immune cells, where loss of AHR would re-sensitize epithelial cells to pro-inflammatory cytokines produced by immune cells, leading to expression of antimicrobial effector molecules.

The data presented in this thesis suggest inhibition of NF-κB signalling in epithelial cells by AHR, and that this is potentially mediated through differential expression of *Tnf* and regulation of TNF-dependent signalling pathways. Which mechanism is responsible for this inhibition is still not known, it is conceivable that AHR directly binds in regulatory regions of differentially expressed genes such as *Tnf* or *Ripk2* or that it regulates the half-life of members of the NF-κB signalling pathway via its function as a E3 ubiquitin protein ligase. Crucially, the effect of NF-κB modulation seems not to be dependent on ligand binding, and it is therefore important to understand, which functional region of the AHR protein is involved in this mechanism. To this end, a site-directed mutagenesis experiment could be performed, inactivating distinct regions of the protein to target DNA binding, subcellular localisation, ARNT heterodimerisation and ligand binding, and testing if re-expression of mutant AHR forms can return *IL8* expression to a similar level as in the parental AGS cells expressing wild-type AHR.

The findings presented in this thesis show that AHR signalling is involved in the inflammatory response to *H. pylori* infection and that loss of AHR improved bacterial clearance in mice, suggesting that in the wild-type mouse, AHR inhibits the pro-inflammatory response to infection, likely through modulation of NF-κB signalling. As inhibition of AHR and knock-out of AHR led to observation of different phenotypes, inhibition of AHR is not likely to be a viable strategy to promote clearance of *H. pylori*.

References

Abdullah, A., M. Maged, M. I. Hairul-Islam, I. A. Osama, H. Maha, A. Manal and H. Hamza (2019). "Activation of aryl hydrocarbon receptor signaling by a novel agonist ameliorates autoimmune encephalomyelitis." PLoS One **14**(4): e0215981.

Abron, J. D., N. P. Singh, M. K. Mishra, R. L. Price, M. Nagarkatti, P. S. Nagarkatti and U. P. Singh (2018). "An endogenous aryl hydrocarbon receptor ligand, ITE, induces regulatory T cells and ameliorates experimental colitis." Am J Physiol Gastrointest Liver Physiol **315**(2): G220-g230.

Akira, S., S. Uematsu and O. Takeuchi (2006). "Pathogen recognition and innate immunity." Cell **124**(4): 783-801.

Arnold, I. C., J. Y. Lee, M. R. Amieva, A. Roers, R. A. Flavell, T. Sparwasser and A. Muller (2011). "Tolerance rather than immunity protects from Helicobacter pylori-induced gastric preneoplasia." Gastroenterology **140**(1): 199-209.

Backert, S. and M. Naumann (2010). "What a disorder: proinflammatory signaling pathways induced by Helicobacter pylori." Trends Microbiol **18**(11): 479-486.

Banerjee, A., S. Thamphiwatana, E. M. Carmona, B. Rickman, K. S. Doran and M. Obonyo (2014). "Deficiency of the myeloid differentiation primary response molecule MyD88 leads to an early and rapid development of Helicobacter-induced gastric malignancy." Infect Immun **82**(1): 356-363.

Bankhead, P., M. B. Loughrey, J. A. Fernandez, Y. Dombrowski, D. G. McArt, P. D. Dunne, S. McQuaid, R. T. Gray, L. J. Murray, H. G. Coleman, J. A. James, M. Salto-Tellez and P. W. Hamilton (2017). "QuPath: Open source software for digital pathology image analysis." Sci Rep **7**(1): 16878.

Bansil, R., J. P. Celli, J. M. Hardcastle and B. S. Turner (2013). "The Influence of Mucus Microstructure and Rheology in Helicobacter pylori Infection." Front Immunol **4**: 310.

Barker, N., M. Huch, P. Kujala, M. van de Wetering, H. J. Snippert, J. H. van Es, T. Sato, D. E. Stange, H. Begthel, M. van den Born, E. Danenberg, S. van den Brink, J. Korving, A. Abo, P. J. Peters, N. Wright, R. Poulsom and H. Clevers (2010). "Lgr5(+ve) stem cells drive self-renewal in the stomach and build long-lived gastric units in vitro." Cell Stem Cell **6**(1): 25-36.

Barranco, S. C., C. M. Townsend, Jr., C. Casartelli, B. G. Macik, N. L. Burger, W. R. Boerwinkle and W. K. Gourley (1983). "Establishment and characterization of an in vitro model system for human adenocarcinoma of the stomach." Cancer Res **43**(4): 1703-1709.

Barranco, S. C., C. M. Townsend, Jr., M. A. Quraishi, N. L. Burger, H. C. Nevill, K. H. Howell and W. R. Boerwinkle (1983). "Heterogeneous responses of an in vitro model of human stomach cancer to anticancer drugs." Invest New Drugs **1**(2): 117-127.

Bartfeld, S., T. Bayram, M. van de Wetering, M. Huch, H. Begthel, P. Kujala, R. Vries, P. J. Peters and H. Clevers (2015). "In vitro expansion of human gastric epithelial stem cells and their responses to bacterial infection." Gastroenterology **148**(1): 126-136 e126.

Bartfeld, S. and H. Clevers (2015). "Organoids as Model for Infectious Diseases: Culture of Human and Murine Stomach Organoids and Microinjection of Helicobacter Pylori." J Vis Exp(105).

Basset, C., J. Holton, R. O'Mahony and I. Roitt (2003). "Innate immunity and pathogen-host interaction." Vaccine **21 Suppl 2**: S12-23.

Bauer, B. and T. F. Meyer (2011). "The Human Gastric Pathogen Helicobacter pylori and Its Association with Gastric Cancer and Ulcer Disease." Ulcers **2011**: 1-23.

Bauer, B., E. Pang, C. Holland, M. Kessler, S. Bartfeld and T. F. Meyer (2012). "The Helicobacter pylori virulence effector CagA abrogates human β-defensin 3 expression via inactivation of EGFR signaling." Cell Host Microbe **11**(6): 576-586.

Bauer, B., T. Wex, D. Kuester, T. Meyer and P. Malfertheiner (2013). "Differential Expression of Human Beta Defensin 2 and 3 in Gastric Mucosa of Helicobacter pylori-Infected Individuals." Helicobacter **18**(1): 6-12.

Bauerfeind, P., R. Garner, B. E. Dunn and H. L. Mobley (1997). "Synthesis and activity of Helicobacter pylori urease and catalase at low pH." Gut **40**(1): 25-30.

Bessede, A., M. Gargaro, M. T. Pallotta, D. Matino, G. Servillo, C. Brunacci, S. Bicciato, E. M. Mazza, A. Macchiarulo, C. Vacca, R. Iannitti, L. Tissi, C. Volpi, M. L. Belladonna, C. Orabona, R. Bianchi, T. V. Lanz, M. Platten, M. A. Della Fazia, D. Piobbico, T. Zelante, H. Funakoshi, T. Nakamura, D. Gilot, M. S. Denison, G. J. Guillemin, J. B. DuHadaway, G. C. Prendergast, R. Metz, M. Geffard, L. Boon, M. Pirro, A. Iorio, B. Veyret, L. Romani, U. Grohmann, F. Fallarino and P. Puccetti (2014). "Aryl hydrocarbon receptor control of a disease tolerance defence pathway." Nature **511**(7508): 184-190.

Beswick, E. J., I. V. Pinchuk, S. Das, D. W. Powell and V. E. Reyes (2007). "Expression of the programmed death ligand 1, B7-H1, on gastric epithelial cells after Helicobacter pylori exposure promotes development of CD4+ CD25+ FoxP3+ regulatory T cells." Infect Immun **75**(9): 4334-4341.

Beswick, E. J., I. V. Pinchuk, R. B. Earley, D. A. Schmitt and V. E. Reyes (2011). "Role of gastric epithelial cell-derived transforming growth factor beta in reduced CD4+ T cell proliferation and development of regulatory T cells during Helicobacter pylori infection." Infect Immun **79**(7): 2737-2745.

Bimczok, D., R. H. Clements, K. B. Waites, L. Novak, D. E. Eckhoff, P. J. Mannon, P. D. Smith and L. E. Smythies (2010). "Human primary gastric dendritic cells induce a Th1 response to H. pylori." Mucosal Immunology **3**(3): 260-269.

Blighe, K. and A. Lun (2023). PCAtools: Everything Principal Components Analysis.

Boccellato, F., S. Woelffling, A. Imai-Matsushima, G. Sanchez, C. Goosmann, M. Schmid, H. Berger, P. Morey, C. Denecke, J. Ordemann and T. F. Meyer (2019). "Polarised epithelial monolayers of the gastric mucosa reveal insights into mucosal homeostasis and defence against infection." Gut **68**(3): 400-413.

Brandt, S., T. Kwok, R. Hartig, W. Konig and S. Backert (2005). "NF-kappaB activation and potentiation of proinflammatory responses by the Helicobacter pylori CagA protein." Proc Natl Acad Sci U S A **102**(26): 9300-9305.

Bunaciu, R. P. and A. Yen (2011). "Activation of the Aryl hydrocarbon receptor ahr promotes retinoic acid–induced differentiation of myeloblastic leukemia cells by restricting expression of the stem cell transcription factor Oct4." Cancer research **71**(6): 2371-2380.

Burke, M. D. and R. T. Mayer (1974). "Ethoxyresorufin: direct fluorimetric assay of a microsomal O-dealkylation which is preferentially inducible by 3-methylcholanthrene." Drug Metab Dispos **2**(6): 583-588.

Carney, J. A. (2010). "Gastric Mucosal Lymphoid Follicles: Histology, Distribution, Frequency, and Etiologic Features." The American Journal of Surgical Pathology **34**(7).

Carver, L. A. and C. A. Bradfield (1997). "Ligand-dependent interaction of the aryl hydrocarbon receptor with a novel immunophilin homolog in vivo." J Biol Chem **272**(17): 11452-11456.

Celli, J. P., B. S. Turner, N. H. Afdhal, S. Keates, I. Ghiran, C. P. Kelly, R. H. Ewoldt, G. H. McKinley, P. So, S. Erramilli and R. Bansil (2009). "Helicobacter pylori moves through mucus by reducing mucin viscoelasticity." Proceedings of the National Academy of Sciences of the United States of America **106**(34): 14321-14326.

Chang, C.-C., Y.-M. Sue, N.-J. Yang, Y.-H. Lee and S.-H. Juan (2014). "3-Methylcholanthrene, an AhR Agonist, Caused Cell-Cycle Arrest by Histone Deacetylation through a RhoA-Dependent Recruitment of HDAC1 and pRb2 to E2F1 Complex." PLOS ONE **9**(3): e92793.

Chang, X., Y. Fan, S. Karyala, S. Schwemberger, C. R. Tomlinson, M. A. Sartor and A. Puga (2007). "Ligand-independent regulation of transforming growth factor beta1 expression and cell cycle progression by the aryl hydrocarbon receptor." Mol Cell Biol **27**(17): 6127-6139.

Chen, Y., A. Lun and G. Smyth (2016). "From reads to genes to pathways: differential expression analysis of RNA-Seq experiments using Rsubread and the edgeR quasi-likelihood pipeline [version 2; peer review: 5 approved]." F1000Research **5**(1438).

Cildir, G., K. C. Low and V. Tergaonkar (2016). "Noncanonical NF-kappaB Signaling in Health and Disease." Trends Mol Med **22**(5): 414-429.

Correa, P. and M. B. Piazuelo (2012). "The gastric precancerous cascade." J Dig Dis **13**(1): 2-9.

Crew, K. D. and A. I. Neugut (2006). "Epidemiology of gastric cancer." World J Gastroenterol **12**(3): 354-362.

Croxen, M. A., G. Sisson, R. Melano and P. S. Hoffman (2006). "The Helicobacter pylori chemotaxis receptor TlpB (HP0103) is required for pH taxis and for colonization of the gastric mucosa." J Bacteriol **188**(7): 2656-2665.

Cullen, T. W., D. K. Giles, L. N. Wolf, C. Ecobichon, I. G. Boneca and M. S. Trent (2011). "Helicobacter pylori versus the host: remodeling of the bacterial outer membrane is required for survival in the gastric mucosa." PLoS Pathog **7**(12): e1002454.

D'Costa, K., M. Chonwerawong, L. S. Tran and R. L. Ferrero (2018). "Mouse Models Of Helicobacter Infection And Gastric Pathologies." J Vis Exp(140): e56985.

de Bernard, M., B. Arico, E. Papini, R. Rizzuto, G. Grandi, R. Rappuoli and C. Montecucco (1997). "Helicobacter pylori toxin VacA induces vacuole formation by acting in the cell cytosol." Mol Microbiol **26**(4): 665-674.

de Waal Malefyt, R., J. Abrams, B. Bennett, C. G. Figdor and J. E. de Vries (1991). "Interleukin 10(IL-10) inhibits cytokine synthesis by human monocytes: an autoregulatory role of IL-10 produced by monocytes." J Exp Med **174**(5): 1209-1220.

Degiuli, M. and F. Calvo (2006). "Survival of early gastric cancer in a specialized European center. Which lymphadenectomy is necessary?" World J Surg **30**(12): 2193-2203.

Di Meglio, P., João H. Duarte, H. Ahlfors, Nick D. L. Owens, Y. Li, F. Villanova, I. Tosi, K. Hirota, Frank O. Nestle, U. Mrowietz, Michael J. Gilchrist and B. Stockinger (2014). "Activation of the Aryl Hydrocarbon Receptor Dampens the Severity of Inflammatory Skin Conditions." Immunity **40**(6): 989-1001.

DiDonato, J. A., F. Mercurio and M. Karin (2012). "NF-kappaB and the link between inflammation and cancer." Immunol Rev **246**(1): 379-400.

Dixon, M. F., R. M. Genta, J. H. Yardley and P. Correa (1996). "Classification and grading of gastritis. The updated Sydney System. International Workshop on the Histopathology of Gastritis, Houston 1994." Am J Surg Pathol **20**(10): 1161-1181.

Domínguez-Acosta, O., L. Vega, E. Estrada-Muñiz, M. S. Rodríguez, F. J. Gonzalez and G. Elizondo (2018). "Activation of aryl hydrocarbon receptor regulates the LPS/IFNγ-induced inflammatory response by inducing ubiquitin-proteosomal and lysosomal degradation of RelA/p65." Biochemical Pharmacology **155**: 141-149.

Elitsur, Y., S. Jackman, S. Keerthy and W. E. Triest (1999). "T and B Cells Repertoire in Gastric Lymph Follicles in Children with Helicobacter Pylori Infection." Pediatric Research **45**(7): 110-110.

Enan, E. and F. Matsumura (1996). "Identification of c-Src as the integral component of the cytosolic Ah receptor complex, transducing the signal of 2,3,7,8-tetrachlorodibenzo-p-dioxin (TCDD) through the protein phosphorylation pathway." Biochemical Pharmacology **52**(10): 1599-1612.

Eslick, G. D., L. L. Lim, J. E. Byles, H. H. Xia and N. J. Talley (1999). "Association of Helicobacter pylori infection with gastric carcinoma: a meta-analysis." Am J Gastroenterol **94**(9): 2373-2379.

Fehlings, M., L. Drobbe, V. Moos, P. Renner Viveros, J. Hagen, M. Beigier-Bompadre, E. Pang, E. Belogolova, Y. Churin, T. Schneider, T. F. Meyer, T. Aebischer and R. Ignatius (2012). "Comparative analysis of the interaction of Helicobacter pylori with human dendritic cells, macrophages, and monocytes." Infect Immun **80**(8): 2724-2734.

Feige, M. H., M. Vieth, O. Sokolova, C. Tager and M. Naumann (2018). "Helicobacter pylori induces direct activation of the lymphotoxin beta receptor and non-canonical nuclear factor-kappa B signaling." Biochim Biophys Acta Mol Cell Res **1865**(4): 545-550.

Feldman, R. A., A. J. P. Eccersley and J. M. Hardie (1998). "Epidemiology of Helicobacter pylori : acquisition, transmission, population prevalence and disease-to-infection ratio." British Medical Bulletin **54**(1): 39-53.

Fischbach, W., M. E. Goebeler-Kolve, B. Dragosics, A. Greiner and M. Stolte (2004). "Long term outcome of patients with gastric marginal zone B cell lymphoma of mucosa associated lymphoid tissue (MALT) following exclusive Helicobacter pylori eradication therapy: experience from a large prospective series." Gut **53**(1): 34-37.

Flach, C. F., M. Mozer, M. Sundquist, J. Holmgren and S. Raghavan (2012). "Mucosal vaccination increases local chemokine production attracting immune cells to the stomach mucosa of Helicobacter pylori infected mice." Vaccine **30**(9): 1636-1643.

Fogh, J., J. M. Fogh and T. Orfeo (1977). "One Hundred and Twenty-Seven Cultured Human Tumor Cell Lines Producing Tumors in Nude Mice23." JNCI: Journal of the National Cancer Institute **59**(1): 221-226.

Ford, A. C., Y. Yuan, D. Forman, R. Hunt and P. Moayyedi (2020). "Helicobacter pylori eradication for the prevention of gastric neoplasia." Cochrane Database Syst Rev **7**(7): Cd005583.

Fueldner, C., S. Riemschneider, J. Haupt, H. Jungnickel, F. Schulze, K. Zoldan, C. Esser, S. Hauschildt, J. Knauer, A. Luch, S. Kalkhof and J. Lehmann (2022). "Aryl Hydrocarbon Receptor Activation by Benzo[a]pyrene Prevents Development of Septic Shock and Fatal Outcome in a Mouse Model of Systemic Salmonella enterica Infection." Cells **11**(4).

Fukunaga, B. N., M. R. Probst, S. Reisz-Porszasz and O. Hankinson (1995). "Identification of functional domains of the aryl hydrocarbon receptor." J Biol Chem **270**(49): 29270-29278.

Garcia, G. R., B. C. Goodale, M. W. Wiley, J. K. La Du, D. A. Hendrix and R. L. Tanguay (2017). "In vivo characterization of an AHR-dependent long noncoding RNA required for proper Sox9b expression." Molecular pharmacology **91**(6): 609-619.

Gebert, B., W. Fischer, E. Weiss, R. Hoffmann and R. Haas (2003). "Helicobacter pylori vacuolating cytotoxin inhibits T lymphocyte activation." Science **301**(5636): 1099-1102.

Genta, R. M., H. W. Hamner and D. Y. Graham (1993). "Gastric lymphoid follicles in Helicobacter pylori infection: Frequency, distribution, and response to triple therapy." Human Pathology **24**(6): 577-583.

Gewirtz, A. T., Y. Yu, U. S. Krishna, D. A. Israel, S. L. Lyons and R. M. Peek, Jr. (2004). "Helicobacter pylori flagellin evades toll-like receptor 5-mediated innate immunity." J Infect Dis **189**(10): 1914-1920.

Giovannoni, F., I. Bosch, C. M. Polonio, M. F. Torti, M. A. Wheeler, Z. Li, L. Romorini, M. S. Rodriguez Varela, V. Rothhammer, A. Barroso, E. C. Tjon, L. M. Sanmarco, M. C. Takenaka, S. M. S. Modaresi, C. Gutiérrez-Vázquez, N. G. Zanluqui, N. B. dos Santos, C. D. Munhoz, Z. Wang, E. B. Damonte, D. Sherr, L. Gehrke, J. P. S. Peron, C. C. Garcia and F. J. Quintana (2020). "AHR is a Zika virus host factor and a candidate target for antiviral therapy." Nature Neuroscience **23**(8): 939-951.

Girardin, S. E., R. Tournebize, M. Mavris, A.-L. Page, X. Li, G. R. Stark, J. Bertin, P. S. DiStefano, M. Yaniv and P. J. Sansonetti (2001). "CARD4/Nod1 mediates NF-κB and JNK activation by invasive Shigella flexneri." EMBO reports **2**(8): 736-742.

Gobert, A. P., D. J. McGee, M. Akhtar, G. L. Mendz, J. C. Newton, Y. Cheng, H. L. Mobley and K. T. Wilson (2001). "Helicobacter pylori arginase inhibits nitric oxide production by eukaryotic cells: a strategy for bacterial survival." Proc Natl Acad Sci U S A **98**(24): 13844-13849.

Graham, F. L., J. Smiley, W. C. Russell and R. Nairn (1977). "Characteristics of a human cell line transformed by DNA from human adenovirus type 5." J Gen Virol **36**(1): 59-74.

Grimaldi, G., S. Rajendra and J. Matthews (2018). "The aryl hydrocarbon receptor regulates the expression of TIPARP and its cis long non-coding RNA, TIPARP-AS1." Biochemical and biophysical research communications **495**(3): 2356-2362.

Grivennikov, S. I., F. R. Greten and M. Karin (2010). "Immunity, Inflammation, and Cancer." Cell **140**(6): 883-899.

Grunewald, M. E., M. G. Shaban, S. R. Mackin, A. R. Fehr and S. Perlman (2020). "Murine coronavirus infection activates the aryl hydrocarbon receptor in an indoleamine 2, 3-dioxygenase-independent manner, contributing to cytokine modulation and proviral TCDD-inducible-PARP expression." Journal of virology **94**(3): 10.1128/jvi. 01743-01719.

Gutierrez-Vazquez, C. and F. J. Quintana (2018). "Regulation of the Immune Response by the Aryl Hydrocarbon Receptor." Immunity **48**(1): 19-33.

Haas, R., T. F. Meyer and J. P. M. van Putten (1993). "Aflagellated mutants of Helicobacter pylori generated by genetic transformation of naturally competent strains using transposon shuttle mutagenesis." Molecular Microbiology **8**(4): 753-760.

Hanieh, H. and A. Alzahrani (2013). "MicroRNA-132 suppresses autoimmune encephalomyelitis by inducing cholinergic anti-inflammation: A new Ahr-based exploration." European Journal of Immunology **43**(10): 2771-2782.

Hanyu, H., K. A. Engevik, A. L. Matthis, K. M. Ottemann, M. H. Montrose and E. Aihara (2019). "Helicobacter pylori Uses the TlpB Receptor To Sense Sites of Gastric Injury." Infection and Immunity **87**(9): 10.1128/iai.00202-00219.

Hase, K., M. Murakami, M. Iimura, S. P. Cole, Y. Horibe, T. Ohtake, M. Obonyo, R. L. Gallo, L. Eckmann and M. F. Kagnoff (2003). "Expression of LL-37 by human gastric epithelial cells as a potential host defense mechanism against Helicobacter pylori." Gastroenterology **125**(6): 1613-1625.

Hatz, R. A., G. Meimarakis, E. Bayerdörffer, M. Stolte, T. Kirchner and G. Enders (1996). "Characterization of Lymphocytic Infiltrates in Helicobacter pylori-Associated Gastritis." Scandinavian Journal of Gastroenterology **31**(3): 222-228.

Hessey, S. J., J. Spencer, J. I. Wyatt, G. Sobala, B. J. Rathbone, A. T. Axon and M. F. Dixon (1990). "Bacterial adhesion and disease activity in Helicobacter associated chronic gastritis." Gut **31**(2): 134-138.

Heyninck, K. and R. Beyaert (1999). "The cytokine-inducible zinc finger protein A20 inhibits IL-1-induced NF-κB activation at the level of TRAF6." FEBS letters **442**(2-3): 147-150.

Heyninck, K., D. De Valck, W. V. Berghe, W. Van Criekinge, R. Contreras, W. Fiers, G. Haegeman and R. Beyaert (1999). "The zinc finger protein A20 inhibits TNF-induced NF-κB–dependent gene expression by interfering with an RIP-or TRAF2-mediated transactivation signal and directly binds to a novel NF-κB–inhibiting protein ABIN." The Journal of cell biology **145**(7): 1471-1482.

Hirata, Y., S. Maeda, T. Ohmae, W. Shibata, A. Yanai, K. Ogura, H. Yoshida, T. Kawabe and M. Omata (2006). "Helicobacter pylori Induces IκB Kinase α Nuclear Translocation and Chemokine Production in Gastric Epithelial Cells." Infection and Immunity **74**(3): 1452-1461.

Holokai, L., J. Chakrabarti, T. Broda, J. Chang, J. A. Hawkins, N. Sundaram, L. E. Wroblewski, R. M. Peek, Jr., J. Wang, M. Helmrath, J. M. Wells and Y. Zavros (2019). "Increased Programmed Death-Ligand 1 is an Early Epithelial Cell Response to Helicobacter pylori Infection." PLoS Pathog **15**(1): e1007468.

Hou, X. X., G. Chen, A. M. Hossini, T. Hu, L. Wang, Z. Pan, L. Lu, K. Cao, Y. Ma, C. C. Zouboulis, L. Xia and Q. Ju (2019). "Aryl Hydrocarbon Receptor Modulates the Expression of TNF-α and IL-8 in Human Sebocytes via the MyD88-p65NF-κB/p38MAPK Signaling Pathways." J Innate Immun **11**(1): 41-51.

Huang, J. Q., S. Sridhar, Y. Chen and R. H. Hunt (1998). "Meta-analysis of the relationship between Helicobacter pylori seropositivity and gastric cancer." Gastroenterology **114**(6): 1169-1179.

Huang, Julie Y., Emily G. Sweeney, M. Sigal, H. C. Zhang, S. J. Remington, Michael A. Cantrell, Calvin J. Kuo, K. Guillemin and Manuel R. Amieva (2015). "Chemodetection and Destruction of Host Urea Allows Helicobacter pylori to Locate the Epithelium." Cell Host & Microbe **18**(2): 147-156.

IARC (1994). "Schistosomes, liver flukes and Helicobacter pylori." IARC Monogr Eval Carcinog Risks Hum **61**: 1-241.

Ikuta, T., H. Eguchi, T. Tachibana, Y. Yoneda and K. Kawajiri (1998). "Nuclear Localization and Export Signals of the Human Aryl Hydrocarbon Receptor*." Journal of Biological Chemistry **273**(5): 2895-2904.

Inohara, N., T. Koseki, J. Lin, L. del Peso, P. C. Lucas, F. F. Chen, Y. Ogura and G. Núñez (2000). "An Induced Proximity Model for NF-κB Activation in the Nod1/RICK and RIP Signaling Pathways *." Journal of Biological Chemistry **275**(36): 27823-27831.

Isaacson, P. G. (1994). "Gastrointestinal lymphoma." Human Pathology **25**(10): 1020-1029.

Isomoto, H., M. Miyazaki, Y. Mizuta, F. Takeshima, K. Murase, K. Inoue, K. Yamasaki, I. Murata, T. Koji and S. Kohno (2000). "Expression of nuclear factor-kappaB in Helicobacter pylori-infected gastric mucosa detected with southwestern histochemistry." Scand J Gastroenterol **35**(3): 247-254.

Isomoto, H., Y. Mizuta, M. Miyazaki, F. Takeshima, K. Omagari, K. Murase, T. Nishiyama, K.-i. Inoue, I. Murata and S. Kohno (2000). "Implication of NF-κB in Helicobacter pylori-associated gastritis." The American Journal of Gastroenterology **95**(10): 2768-2776.

Janeway, C. A., Jr. (1989). "Approaching the asymptote? Evolution and revolution in immunology." Cold Spring Harb Symp Quant Biol **54 Pt 1**: 1-13.

Jinek, M., K. Chylinski, I. Fonfara, M. Hauer, J. A. Doudna and E. Charpentier (2012). "A Programmable Dual-RNA–Guided DNA Endonuclease in Adaptive Bacterial Immunity." Science **337**(6096): 816-821.

Jost, P. J. and J. Ruland (2007). "Aberrant NF-κB signaling in lymphoma: mechanisms, consequences, and therapeutic implications." Blood **109**(7): 2700-2707.

Karam, S. M. and C. P. Leblond (1992). "Identifying and counting epithelial cell types in the “corpus” of the mouse stomach." The Anatomical Record **232**(2): 231-246.

Karttunen, R., T. Karttunen, H. P. Ekre and T. T. MacDonald (1995). "Interferon gamma and interleukin 4 secreting cells in the gastric antrum in Helicobacter pylori positive and negative gastritis." Gut **36**(3): 341-345.

Kawai, T. and S. Akira (2009). "The roles of TLRs, RLRs and NLRs in pathogen recognition." Int Immunol **21**(4): 317-337.

Kazlauskas, A., L. Poellinger and I. Pongratz (1999). "Evidence That the Co-chaperone p23 Regulates Ligand Responsiveness of the Dioxin (Aryl Hydrocarbon) Receptor*." Journal of Biological Chemistry **274**(19): 13519-13524.

Kim, D. W., L. Gazourian, S. A. Quadri, R. Romieu-Mourez, D. H. Sherr and G. E. Sonenshein (2000). "The RelA NF-kappaB subunit and the aryl hydrocarbon receptor (AhR) cooperate to transactivate the c-myc promoter in mammary cells." Oncogene **19**(48): 5498-5506.

Kimura, A., T. Naka, T. Nakahama, I. Chinen, K. Masuda, K. Nohara, Y. Fujii-Kuriyama and T. Kishimoto (2009). "Aryl hydrocarbon receptor in combination with Stat1 regulates LPS-induced inflammatory responses." J Exp Med **206**(9): 2027-2035.

Kneidinger, B., C. Marolda, M. Graninger, A. Zamyatina, F. McArthur, P. Kosma, M. A. Valvano and P. Messner (2002). "Biosynthesis pathway of ADP-L-glycero-beta-D-manno-heptose in Escherichia coli." J Bacteriol **184**(2): 363-369.

Kopp, E. B. and R. Medzhitov (1999). "The Toll-receptor family and control of innate immunity." Current Opinion in Immunology **11**(1): 13-18.

Korotkevich, G., V. Sukhov, N. Budin, B. Shpak, M. N. Artyomov and A. Sergushichev (2021). "Fast gene set enrichment analysis." bioRxiv: 060012.

Krzyżek, P., D. Pawełka, B. Iwańczak, R. Kempiński, K. Leśniakowski, F. Mégraud, Ł. Łaczmański, M. Biernat and G. Gościniak (2020). "High Primary Antibiotic Resistance of Helicobacter pylori Strains Isolated from Pediatric and Adult Patients in Poland during 2016-2018." Antibiotics (Basel) **9**(5).

Kudo, I., M. Hosaka, A. Haga, N. Tsuji, Y. Nagata, H. Okada, K. Fukuda, Y. Kakizaki, T. Okamoto, E. Grave and H. Itoh (2018). "The regulation mechanisms of AhR by molecular chaperone complex." J Biochem **163**(3): 223-232.

Kurbel, S., B. Kurbel, B. Dmitrović and A. Vcev (2001). "A model of the gastric gland ejection cycle: low ejection fractions require reduction of the glandular dead space." J Theor Biol **210**(3): 337-343.

Laemmli, U. K. (1970). "Cleavage of Structural Proteins during the Assembly of the Head of Bacteriophage T4." Nature **227**(5259): 680-685.

Lamb, A., X. D. Yang, Y. H. Tsang, J. D. Li, H. Higashi, M. Hatakeyama, R. M. Peek, S. R. Blanke and L. F. Chen (2009). "Helicobacter pylori CagA activates NF-kappaB by targeting TAK1 for TRAF6-mediated Lys 63 ubiquitination." EMBO Rep **10**(11): 1242-1249.

Lee, J., G. Cacalano, T. Camerato, K. Toy, M. W. Moore and W. I. Wood (1995). "Chemokine binding and activities mediated by the mouse IL-8 receptor." Journal of immunology (Baltimore, Md.: 1950) **155**(4): 2158-2164.

Lee, Y. C., T. H. Chiang, C. K. Chou, Y. K. Tu, W. C. Liao, M. S. Wu and D. Y. Graham (2016). "Association Between Helicobacter pylori Eradication and Gastric Cancer Incidence: A Systematic Review and Meta-analysis." Gastroenterology **150**(5): 1113-1124.e1115.

Lehours, P. and R. L. Ferrero (2019). "Review: Helicobacter: Inflammation, immunology, and vaccines." Helicobacter **24**(S1).

Lello, E., B. Furnes and T. H. Edna (2007). "Short and long-term survival from gastric cancer. A population-based study from a county hospital during 25 years." Acta Oncol **46**(3): 308-315.

Lemaitre, B., E. Nicolas, L. Michaut, J. M. Reichhart and J. A. Hoffmann (1996). "The dorsoventral regulatory gene cassette spätzle/Toll/cactus controls the potent antifungal response in Drosophila adults." Cell **86**(6): 973-983.

Li, J.-X., M. Zeng, X.-H. Mao, Q.-M. Zou and F.-C. Zhu (2016). "Helicobacter pylori vaccination – Authors' reply." The Lancet **387**(10020): 749.

Li, L., N. Soetandyo, Q. Wang and Y. Ye (2009). "The zinc finger protein A20 targets TRAF2 to the lysosomes for degradation." Biochim Biophys Acta **1793**(2): 346-353.

Li, Q. and I. M. Verma (2002). "NF-kappaB regulation in the immune system." Nat Rev Immunol **2**(10): 725-734.

Link, A., C. Langner, W. Schirrmeister, W. Habendorf, J. Weigt, M. Venerito, I. Tammer, D. Schluter, P. Schlaermann, T. F. Meyer, T. Wex and P. Malfertheiner (2017). "Helicobacter pylori vacA genotype is a predominant determinant of immune response to Helicobacter pylori CagA." World J Gastroenterol **23**(26): 4712-4723.

Liu, C., M. Xia, Y. Zhang, P. Jin, L. Zhao, J. Zhang, T. Li, X. Zhou, Y. Tu and F. Kong (2018). "Micro124-mediated AHR expression regulates the inflammatory response of chronic rhinosinusitis (CRS) with nasal polyps." Biochemical and biophysical research communications **500**(2): 145-151.

Livak, K. J. and T. D. Schmittgen (2001). "Analysis of Relative Gene Expression Data Using Real-Time Quantitative PCR and the 2−ΔΔCT Method." Methods **25**(4): 402-408.

Lun, A. T., Y. Chen and G. K. Smyth (2016). "It's DE-licious: A Recipe for Differential Expression Analyses of RNA-seq Experiments Using Quasi-Likelihood Methods in edgeR." Methods Mol Biol **1418**: 391-416.

Ma, A. and B. A. Malynn (2012). "A20: linking a complex regulator of ubiquitylation to immunity and human disease." Nat Rev Immunol **12**(11): 774-785.

Malaty, H. M., N. D. Logan, D. Y. Graham and J. E. Ramchatesingh (2001). "Helicobacter pylori infection in preschool and school-aged minority children: effect of socioeconomic indicators and breast-feeding practices." Clin Infect Dis **32**(10): 1387-1392.

Mantovani, A., P. Allavena, A. Sica and F. Balkwill (2008). "Cancer-related inflammation." Nature **454**(7203): 436-444.

Maradana, M. R., N. B. Marzook, O. E. Diaz, T. Mkandawire, N. L. Diny, Y. Li, A. Liebert, K. Shah, M. Tolaini, M. Kváč, B. Stockinger and A. Sateriale (2023). "Dietary environmental factors shape the immune defense against Cryptosporidium infection." Cell Host Microbe **31**(12): 2038-2050.e2034.

Marshall, B. J., J. A. Armstrong, D. B. McGechie and R. J. Glancy (1985). "Attempt to fulfil Koch's postulates for pyloric Campylobacter." Med J Aust **142**(8): 436-439.

Marshall, B. J. and J. R. Warren (1984). "Unidentified curved bacilli in the stomach of patients with gastritis and peptic ulceration." Lancet **1**(8390): 1311-1315.

Matsumura, F. (2009). "The significance of the nongenomic pathway in mediating inflammatory signaling of the dioxin-activated Ah receptor to cause toxic effects." Biochemical Pharmacology **77**(4): 608-626.

McBerry, C., R. M. Gonzalez, N. Shryock, A. Dias and J. Aliberti (2012). "SOCS2-induced proteasome-dependent TRAF6 degradation: a common anti-inflammatory pathway for control of innate immune responses." PLoS One **7**(6): e38384.

McCarthy, D. J., Y. Chen and G. K. Smyth (2012). "Differential expression analysis of multifactor RNA-Seq experiments with respect to biological variation." Nucleic Acids Research **40**(10): 4288-4297.

McCarthy, J. V., J. Ni and V. M. Dixit (1998). "RIP2 Is a Novel NF-κB-activating and Cell Death-inducing Kinase *." Journal of Biological Chemistry **273**(27): 16968-16975.

McGuckin, M. A., S. K. Lindén, P. Sutton and T. H. Florin (2011). "Mucin dynamics and enteric pathogens." Nature Reviews Microbiology **9**(4): 265-278.

Medzhitov, R. (2007). "Recognition of microorganisms and activation of the immune response." Nature **449**(7164): 819-826.

Medzhitov, R., P. Preston-Hurlburt and C. A. Janeway, Jr. (1997). "A human homologue of the Drosophila Toll protein signals activation of adaptive immunity." Nature **388**(6640): 394-397.

Meireson, A., M. Devos and L. Brochez (2020). "IDO Expression in Cancer: Different Compartment, Different Functionality?" Front Immunol **11**: 531491.

Mejia-Garcia, A., E. González-Barbosa, C. Martínez-Guzmán, M. Torres-Ramos, M. Rodríguez, S. Guzmán-León and G. Elizondo (2015). "Activation of AHR mediates the ubiquitination and proteasome degradation of c-Fos through the induction of Ubcm4 gene expression." Toxicology **337**: 47-57.

Mejias-Luque, R., J. Zoller, F. Anderl, E. Loew-Gil, M. Vieth, T. Adler, D. B. Engler, S. Urban, J. L. Browning, A. Muller, M. Gerhard and M. Heikenwalder (2017). "Lymphotoxin beta receptor signalling executes Helicobacter pylori-driven gastric inflammation in a T4SS-dependent manner." Gut **66**(8): 1369-1381.

Menaker, R. J., P. J. Ceponis and N. L. Jones (2004). "Helicobacter pylori induces apoptosis of macrophages in association with alterations in the mitochondrial pathway." Infect Immun **72**(5): 2889-2898.

Metidji, A., S. Omenetti, S. Crotta, Y. Li, E. Nye, E. Ross, V. Li, M. R. Maradana, C. Schiering and B. Stockinger (2018). "The Environmental Sensor AHR Protects from Inflammatory Damage by Maintaining Intestinal Stem Cell Homeostasis and Barrier Integrity." Immunity **49**(2): 353-362.e355.

Meyer, B. K. and G. H. Perdew (1999). "Characterization of the AhR-hsp90-XAP2 core complex and the role of the immunophilin-related protein XAP2 in AhR stabilization." Biochemistry **38**(28): 8907-8917.

Meyer, B. K., J. R. Petrulis and G. H. Perdew (2000). "Aryl hydrocarbon (Ah) receptor levels are selectively modulated by hsp90-associated immunophilin homolog XAP2." Cell Stress Chaperones **5**(3): 243-254.

Michetti, P., C. Kreiss, K. L. Kotloff, N. Porta, J. L. Blanco, D. Bachmann, M. Herranz, P. F. Saldinger, I. Corthésy-Theulaz, G. Losonsky, R. Nichols, J. Simon, M. Stolte, S. Ackerman, T. P. Monath and A. L. Blum (1999). "Oral immunization with urease and Escherichia coli heat-labile enterotoxin is safe and immunogenic in Helicobacter pylori-infected adults." Gastroenterology **116**(4): 804-812.

Mitchell, D. J., H. Q. Huynh, P. J. M. Ceponis, N. L. Jones and P. M. Sherman (2004). "Helicobacter pylori Disrupts STAT1-Mediated Gamma Interferon-Induced Signal Transduction in Epithelial Cells." Infection and Immunity **72**(1): 537-545.

Modlin, R. L., H. D. Brightbill and P. J. Godowski (1999). "The Toll of Innate Immunity on Microbial Pathogens." New England Journal of Medicine **340**(23): 1834-1835.

Morey, P., L. Pfannkuch, E. Pang, F. Boccellato, M. Sigal, A. Imai-Matsushima, V. Dyer, M. Koch, H. J. Mollenkopf, P. Schlaermann and T. F. Meyer (2018). "Helicobacter pylori Depletes Cholesterol in Gastric Glands to Prevent Interferon Gamma Signaling and Escape the Inflammatory Response." Gastroenterology **154**(5): 1391-1404.e1399.

Moura-Alves, P., K. Fae, E. Houthuys, A. Dorhoi, A. Kreuchwig, J. Furkert, N. Barison, A. Diehl, A. Munder, P. Constant, T. Skrahina, U. Guhlich-Bornhof, M. Klemm, A. B. Koehler, S. Bandermann, C. Goosmann, H. J. Mollenkopf, R. Hurwitz, V. Brinkmann, S. Fillatreau, M. Daffe, B. Tummler, M. Kolbe, H. Oschkinat, G. Krause and S. H. Kaufmann (2014). "AhR sensing of bacterial pigments regulates antibacterial defence." Nature **512**(7515): 387-392.

Moura-Alves, P., A. Puyskens, A. Stinn, M. Klemm, U. Guhlich-Bornhof, A. Dorhoi, J. Furkert, A. Kreuchwig, J. Protze, L. Lozza, G. Pei, P. Saikali, C. Perdomo, H. J. Mollenkopf, R. Hurwitz, F. Kirschhoefer, G. Brenner-Weiss, J. Weiner, H. Oschkinat, M. Kolbe, G. Krause and S. H. E. Kaufmann (2019). "Host monitoring of quorum sensing during Pseudomonas aeruginosa infection." Science **366**(6472): eaaw1629.

Münzenmaier, A., C. Lange, E. Glocker, A. Covacci, A. Moran, S. Bereswill, P. A. Baeuerle, M. Kist and H. L. Pahl (1997). "A secreted/shed product of Helicobacter pylori activates transcription factor nuclear factor-kappa B." J Immunol **159**(12): 6140-6147.

Muzio, M. and A. Mantovani (2000). "Toll-like receptors." Microbes and Infection **2**(3): 251-255.

Newton, K. and V. M. Dixit (2012). "Signaling in innate immunity and inflammation." Cold Spring Harb Perspect Biol **4**(3).

NICE. (2014, 18/10/2019). "Gastro-oesophageal reflux disease and dyspepsia in adults: investigation and management." from https://www.nice.org.uk/guidance/cg184.

Nielsen, H. and L. P. Andersen (1992). "Chemotactic activity of Helicobacter pylori sonicate for human polymorphonuclear leucocytes and monocytes." Gut **33**(6): 738-742.

Nuding, S., M. Gersemann, Y. Hosaka, S. Konietzny, C. Schaefer, J. Beisner, B. O. Schroeder, M. J. Ostaff, K. Saigenji, G. Ott, M. Schaller, E. F. Stange and J. Wehkamp (2013). "Gastric antimicrobial peptides fail to eradicate Helicobacter pylori infection due to selective induction and resistance." PLoS One **8**(9): e73867.

O'Reilly, L. A., T. L. Putoczki, L. A. Mielke, J. T. Low, A. Lin, A. Preaudet, M. J. Herold, K. Yaprianto, L. Tai, A. Kueh, G. Pacini, R. L. Ferrero, R. Gugasyan, Y. Hu, M. Christie, S. Wilcox, R. Grumont, M. D. W. Griffin, L. O'Connor, G. K. Smyth, M. Ernst, P. Waring, S. Gerondakis and A. Strasser (2018). "Loss of NF-κB1 Causes Gastric Cancer with Aberrant Inflammation and Expression of Immune Checkpoint Regulators in a STAT-1-Dependent Manner." Immunity **48**(3): 570-583.e578.

Odenbreit, S., J. Püls, B. Sedlmaier, E. Gerland, W. Fischer and R. Haas (2000). "Translocation of Helicobacter pylori CagA into gastric epithelial cells by type IV secretion." Science **287**(5457): 1497-1500.

Ohtake, F., A. Baba, I. Takada, M. Okada, K. Iwasaki, H. Miki, S. Takahashi, A. Kouzmenko, K. Nohara, T. Chiba, Y. Fujii-Kuriyama and S. Kato (2007). "Dioxin receptor is a ligand-dependent E3 ubiquitin ligase." Nature **446**(7135): 562-566.

Ohtake, F., K.-i. Takeyama, T. Matsumoto, H. Kitagawa, Y. Yamamoto, K. Nohara, C. Tohyama, A. Krust, J. Mimura and P. Chambon (2003). "Modulation of oestrogen receptor signalling by association with the activated dioxin receptor." Nature **423**(6939): 545-550.

Ostaff, M. J., E. F. Stange and J. Wehkamp (2013). "Antimicrobial peptides and gut microbiota in homeostasis and pathology." EMBO Mol Med **5**(10): 1465-1483.

Øvrevik, J., M. Låg, V. Lecureur, D. Gilot, D. Lagadic-Gossmann, M. Refsnes, P. E. Schwarze, T. Skuland, R. Becher and J. A. Holme (2014). "AhR and Arnt differentially regulate NF-κB signaling and chemokine responses in human bronchial epithelial cells." Cell Communication and Signaling **12**(1): 48.

Pachathundikandi, S. K., N. Tegtmeyer, I. C. Arnold, J. Lind, M. Neddermann, C. Falkeis-Veits, S. Chattopadhyay, M. Brönstrup, W. Tegge, M. Hong, H. Sticht, M. Vieth, A. Müller and S. Backert (2019). "T4SS-dependent TLR5 activation by Helicobacter pylori infection." Nat Commun **10**(1): 5717.

Palframan, S. L., T. Kwok and K. Gabriel (2012). "Vacuolating cytotoxin A (VacA), a key toxin for Helicobacter pylori pathogenesis." Front Cell Infect Microbiol **2**: 92.

Pan, K. F., L. Zhang, M. Gerhard, J. L. Ma, W. D. Liu, K. Ulm, J. X. Wang, L. Zhang, Y. Zhang, M. Bajbouj, L. F. Zhang, M. Li, M. Vieth, R. Y. Liu, M. Quante, L. H. Wang, S. Suchanek, T. Zhou, W. X. Guan, R. Schmid, M. Classen and W. C. You (2016). "A large randomised controlled intervention trial to prevent gastric cancer by eradication of Helicobacter pylori in Linqu County, China: baseline results and factors affecting the eradication." Gut **65**(1): 9-18.

Pappas, B., Y. Yang, Y. Wang, K. Kim, H. J. Chung, M. Cheung, K. Ngo, A. Shinn and W. K. Chan (2018). "p23 protects the human aryl hydrocarbon receptor from degradation via a heat shock protein 90-independent mechanism." Biochem Pharmacol **152**: 34-44.

Parsonnet, J., G. D. Friedman, D. P. Vandersteen, Y. Chang, J. H. Vogelman, N. Orentreich and R. K. Sibley (1991). "Helicobacter pylori infection and the risk of gastric carcinoma." N Engl J Med **325**(16): 1127-1131.

Patel, S. R., K. Smith, D. P. Letley, K. W. Cook, A. A. Memon, R. J. Ingram, E. Staples, S. Backert, A. M. Zaitoun, J. C. Atherton and K. Robinson (2013). "Helicobacter pylori downregulates expression of human β-defensin 1 in the gastric mucosa in a type IV secretion-dependent fashion." Cell Microbiol **15**(12): 2080-2092.

Peek, R. M., Jr. and J. E. Crabtree (2006). "Helicobacter infection and gastric neoplasia." J Pathol **208**(2): 233-248.

Petrulis, J. R., G. Chen, S. Benn, J. LaMarre and N. J. Bunce (2001). "Application of the ethoxyresorufin-O-deethylase (EROD) assay to mixtures of halogenated aromatic compounds." Environ Toxicol **16**(2): 177-184.

Petrulis, J. R., A. Kusnadi, P. Ramadoss, B. Hollingshead and G. H. Perdew (2003). "The hsp90 Co-chaperone XAP2 alters importin beta recognition of the bipartite nuclear localization signal of the Ah receptor and represses transcriptional activity." J Biol Chem **278**(4): 2677-2685.

Pfaffl, M. W. (2001). "A new mathematical model for relative quantification in real-time RT-PCR." Nucleic Acids Res **29**(9): e45.

Pfannkuch, L., R. Hurwitz, J. Traulsen, J. Sigulla, M. Poeschke, L. Matzner, P. Kosma, M. Schmid and T. F. Meyer (2019). "ADP heptose, a novel pathogen-associated molecular pattern identified in Helicobacter pylori." FASEB J **33**(8): 9087-9099.

Plummer, M., S. Franceschi, J. Vignat, D. Forman and C. de Martel (2015). "Global burden of gastric cancer attributable to Helicobacter pylori." Int J Cancer **136**(2): 487-490.

Quintana, F. J., G. Murugaiyan, M. F. Farez, M. Mitsdoerffer, A.-M. Tukpah, E. J. Burns and H. L. Weiner (2010). "An endogenous aryl hydrocarbon receptor ligand acts on dendritic cells and T cells to suppress experimental autoimmune encephalomyelitis." Proceedings of the National Academy of Sciences **107**(48): 20768-20773.

Ramarao, N., S. D. Gray-Owen and T. F. Meyer (2000). "Helicobacter pylori induces but survives the extracellular release of oxygen radicals from professional phagocytes using its catalase activity." Mol Microbiol **38**(1): 103-113.

Robinson, M. D., D. J. McCarthy and G. K. Smyth (2010). "edgeR: a Bioconductor package for differential expression analysis of digital gene expression data." Bioinformatics **26**(1): 139-140.

Robinson, M. D. and A. Oshlack (2010). "A scaling normalization method for differential expression analysis of RNA-seq data." Genome Biology **11**(3): R25.

Rodrigues, A. D. and R. A. Prough (1991). [40] Induction of cytochromes P450IA1 and P450IA2 and measurement of catalytic activities. Methods in Enzymology, Academic Press. **206:** 423-431.

Rolig, A. S., C. Cech, E. Ahler, J. E. Carter and K. M. Ottemann (2013). "The degree of Helicobacter pylori-triggered inflammation is manipulated by preinfection host microbiota." Infect Immun **81**(5): 1382-1389.

Rothhammer, V., D. M. Borucki, E. C. Tjon, M. C. Takenaka, C. C. Chao, A. Ardura-Fabregat, K. A. de Lima, C. Gutiérrez-Vázquez, P. Hewson, O. Staszewski, M. Blain, L. Healy, T. Neziraj, M. Borio, M. Wheeler, L. L. Dragin, D. A. Laplaud, J. Antel, J. I. Alvarez, M. Prinz and F. J. Quintana (2018). "Microglial control of astrocytes in response to microbial metabolites." Nature **557**(7707): 724-728.

Rothhammer, V. and F. J. Quintana (2019). "The aryl hydrocarbon receptor: an environmental sensor integrating immune responses in health and disease." Nature Reviews Immunology **19**(3): 184-197.

Sachs, G., D. R. Scott and Y. Wen (2011). "Gastric infection by Helicobacter pylori." Curr Gastroenterol Rep **13**(6): 540-546.

Sakurai, S., T. Shimizu and U. Ohto (2017). "The crystal structure of the AhRR-ARNT heterodimer reveals the structural basis of the repression of AhR-mediated transcription." J Biol Chem **292**(43): 17609-17616.

Sarma, V., F. W. Wolf, R. M. Marks, T. B. Shows and V. M. Dixit (1992). "Cloning of a novel tumor necrosis factor-alpha-inducible primary response gene that is differentially expressed in development and capillary tube-like formation in vitro." Journal of immunology (Baltimore, Md. : 1950) **148**(10): 3302-3312.

Schiering, C., E. Wincent, A. Metidji, A. Iseppon, Y. Li, A. J. Potocnik, S. Omenetti, C. J. Henderson, C. R. Wolf, D. W. Nebert and B. Stockinger (2017). "Feedback control of AHR signalling regulates intestinal immunity." Nature **542**(7640): 242-245.

Schmidt, J. V., G. H. Su, J. K. Reddy, M. C. Simon and C. A. Bradfield (1996). "Characterization of a murine Ahr null allele: involvement of the Ah receptor in hepatic growth and development." Proc Natl Acad Sci U S A **93**(13): 6731-6736.

Schnekenburger, M., L. Peng and A. Puga (2007). "HDAC1 bound to the Cyp1a1 promoter blocks histone acetylation associated with Ah receptor-mediated trans-activation." Biochimica et Biophysica Acta (BBA) - Gene Structure and Expression **1769**(9): 569-578.

Schwarz, S., G. Morelli, B. Kusecek, A. Manica, F. Balloux, R. J. Owen, D. Y. Graham, S. van der Merwe, M. Achtman and S. Suerbaum (2008). "Horizontal versus familial transmission of Helicobacter pylori." PLoS Pathog **4**(10): e1000180.

Schweitzer, K., O. Sokolova, P. M. Bozko and M. Naumann (2010). "Helicobacter pylori induces NF-kappaB independent of CagA." EMBO Rep **11**(1): 10-11; author reply 11-12.

Sepe, L. P., K. Hartl, A. Iftekhar, H. Berger, N. Kumar, C. Goosmann, S. Chopra, S. C. Schmidt, R. K. Gurumurthy, T. F. Meyer and F. Boccellato (2020). "Genotoxic Effect of Salmonella Paratyphi A Infection on Human Primary Gallbladder Cells." mBio **11**(5).

Serrano, C., M. I. Diaz, A. Valdivia, A. Godoy, A. Peña, A. Rollan, A. Kirberg, E. Hebel, J. Fierro, G. Klapp, A. Venegas and P. R. Harris (2007). "Relationship between Helicobacter pylori virulence factors and regulatory cytokines as predictors of clinical outcome." Microbes and Infection **9**(4): 428-434.

Shah, K., M. R. Maradana, M. Joaquina Delàs, A. Metidji, F. Graelmann, M. Llorian, P. Chakravarty, Y. Li, M. Tolaini, M. Shapiro, G. Kelly, C. Cheshire, D. Bhurta, S. B. Bharate and B. Stockinger (2022). "Cell-intrinsic Aryl Hydrocarbon Receptor signalling is required for the resolution of injury-induced colonic stem cells." Nature Communications **13**(1): 1827.

Sharma, S. A., M. K. Tummuru, M. J. Blaser and L. D. Kerr (1998). "Activation of IL-8 gene expression by Helicobacter pylori is regulated by transcription factor nuclear factor-kappa B in gastric epithelial cells." J Immunol **160**(5): 2401-2407.

Sigal, M., M. D. M. Reines, S. Mullerke, C. Fischer, M. Kapalczynska, H. Berger, E. R. M. Bakker, H. J. Mollenkopf, M. E. Rothenberg, B. Wiedenmann, S. Sauer and T. F. Meyer (2019). "R-spondin-3 induces secretory, antimicrobial Lgr5(+) cells in the stomach." Nat Cell Biol **21**(7): 812-823.

Sigal, M., M. E. Rothenberg, C. Y. Logan, J. Y. Lee, R. W. Honaker, R. L. Cooper, B. Passarelli, M. Camorlinga, D. M. Bouley, G. Alvarez, R. Nusse, J. Torres and M. R. Amieva (2015). "Helicobacter pylori Activates and Expands Lgr5(+) Stem Cells Through Direct Colonization of the Gastric Glands." Gastroenterology **148**(7): 1392-1404.e1321.

Singh, S. S., N. G. Hord and G. H. Perdew (1996). "Characterization of the Activated Form of the Aryl Hydrocarbon Receptor in the Nucleus of HeLa Cells in the Absence of Exogenous Ligand." Archives of Biochemistry and Biophysics **329**(1): 47-55.

Smyth, E. C., M. Nilsson, H. I. Grabsch, N. C. T. van Grieken and F. Lordick (2020). "Gastric cancer." The Lancet **396**(10251): 635-648.

Song, H. Y., M. Rothe and D. V. Goeddel (1996). "The tumor necrosis factor-inducible zinc finger protein A20 interacts with TRAF1/TRAF2 and inhibits NF-kappaB activation." Proc Natl Acad Sci U S A **93**(13): 6721-6725.

Soutto, M., N. Bhat, S. Khalafi, S. Zhu, J. Poveda, M. Garcia-Buitrago, A. Zaika and W. El-Rifai (2021). "NF-kB-dependent activation of STAT3 by H. pylori is suppressed by TFF1." Cancer Cell International **21**(1): 444.

Stathis, A., C. Chini, F. Bertoni, I. Proserpio, C. Capella, L. Mazzucchelli, E. Pedrinis, F. Cavalli, G. Pinotti and E. Zucca (2009). "Long-term outcome following Helicobacter pylori eradication in a retrospective study of 105 patients with localized gastric marginal zone B-cell lymphoma of MALT type." Ann Oncol **20**(6): 1086-1093.

Stelzner, K., N. Vollmuth and T. Rudel (2023). "Intracellular lifestyle of Chlamydia trachomatis and host–pathogen interactions." Nature Reviews Microbiology **21**(7): 448-462.

Su, C., M. Padra, M. A. Constantino, S. Sharba, A. Thorell, S. K. Lindén and R. Bansil (2018). "Influence of the viscosity of healthy and diseased human mucins on the motility of Helicobacter pylori." Scientific Reports **8**(1): 9710.

Subramanian, A., P. Tamayo, V. K. Mootha, S. Mukherjee, B. L. Ebert, M. A. Gillette, A. Paulovich, S. L. Pomeroy, T. R. Golub, E. S. Lander and J. P. Mesirov (2005). "Gene set enrichment analysis: A knowledge-based approach for interpreting genome-wide expression profiles." Proceedings of the National Academy of Sciences **102**(43): 15545-15550.

Sun, S.-C. (2017). "The non-canonical NF-κB pathway in immunity and inflammation." Nature Reviews Immunology **17**(9): 545-558.

Sundrud, M. S., V. J. Torres, D. Unutmaz and T. L. Cover (2004). "Inhibition of primary human T cell proliferation by Helicobacter pylori vacuolating toxin (VacA) is independent of VacA effects on IL-2 secretion." Proceedings of the National Academy of Sciences **101**(20): 7727-7732.

Sutton, P. and J. M. Boag (2019). "Status of vaccine research and development for Helicobacter pylori." Vaccine **37**(50): 7295-7299.

Sutton, P. and Y. T. Chionh (2013). "Why can't we make an effective vaccine against Helicobacter pylori?" Expert Rev Vaccines **12**(4): 433-441.

Swanson, H. I., K. Tullis and M. S. Denison (1993). "Binding of transformed Ah receptor complex to a dioxin responsive transcriptional enhancer: evidence for two distinct heteromeric DNA-binding forms." Biochemistry **32**(47): 12841-12849.

Tan, S., L. S. Tompkins and M. R. Amieva (2009). "Helicobacter pylori Usurps Cell Polarity to Turn the Cell Surface into a Replicative Niche." PLOS Pathogens **5**(5): e1000407.

Thomas, T., D. Stefanoni, J. A. Reisz, T. Nemkov, L. Bertolone, R. O. Francis, K. E. Hudson, J. C. Zimring, K. C. Hansen, E. A. Hod, S. L. Spitalnik and A. D'Alessandro (2020). "COVID-19 infection alters kynurenine and fatty acid metabolism, correlating with IL-6 levels and renal status." JCI Insight **5**(14).

Torok, A. M., A. H. Bouton and J. B. Goldberg (2005). "Helicobacter pylori induces interleukin-8 secretion by Toll-like receptor 2- and Toll-like receptor 5-dependent and -independent pathways." Infect Immun **73**(3): 1523-1531.

Torti, M. F., F. Giovannoni, F. J. Quintana and C. C. Garcia (2021). "The Aryl Hydrocarbon Receptor as a Modulator of Anti-viral Immunity." Front Immunol **12**: 624293.

Traulsen, J., C. Zagami, A. A. Daddi and F. Boccellato (2021). "Molecular modelling of the gastric barrier response, from infection to carcinogenesis." Best Pract Res Clin Gastroenterol **50-51**: 101737.

Tsay, T. B., P. H. Chen and L. W. Chen (2019). "Aryl hydrocarbon receptor ligands enhance lung immunity through intestinal IKKbeta pathways." J Transl Med **17**(1): 304.

Uehata, T. and O. Takeuchi (2020). "RNA Recognition and Immunity-Innate Immune Sensing and Its Posttranscriptional Regulation Mechanisms." Cells **9**(7).

Uemura, N., S. Okamoto, S. Yamamoto, N. Matsumura, S. Yamaguchi, M. Yamakido, K. Taniyama, N. Sasaki and R. J. Schlemper (2001). "Helicobacter pylori infection and the development of gastric cancer." N Engl J Med **345**(11): 784-789.

Vaidyanathan, B., A. Chaudhry, W. T. Yewdell, D. Angeletti, W.-F. Yen, A. K. Wheatley, C. A. Bradfield, A. B. McDermott, J. W. Yewdell and A. Y. Rudensky (2017). "The aryl hydrocarbon receptor controls cell-fate decisions in B cells." Journal of Experimental Medicine **214**(1): 197-208.

van Den Brink, G. R., F. J. ten Kate, C. Y. Ponsioen, M. M. Rive, G. N. Tytgat, S. J. van Deventer and M. P. Peppelenbosch (2000). "Expression and activation of NF-kappa B in the antrum of the human stomach." J Immunol **164**(6): 3353-3359.

Velin, D., K. Straubinger and M. Gerhard (2016). "Inflammation, immunity, and vaccines for Helicobacter pylori infection." Helicobacter **21 Suppl 1**: 26-29.

Venerito, M., A. Link, T. Rokkas and P. Malfertheiner (2016). "Gastric cancer – clinical and epidemiological aspects." Helicobacter **21**(S1): 39-44.

Viala, J., C. Chaput, I. G. Boneca, A. Cardona, S. E. Girardin, A. P. Moran, R. Athman, S. Mémet, M. R. Huerre, A. J. Coyle, P. S. DiStefano, P. J. Sansonetti, A. Labigne, J. Bertin, D. J. Philpott and R. L. Ferrero (2004). "Nod1 responds to peptidoglycan delivered by the Helicobacter pylori cag pathogenicity island." Nat Immunol **5**(11): 1166-1174.

Vogel, C. F., E. M. Khan, P. S. Leung, M. E. Gershwin, W. L. Chang, D. Wu, T. Haarmann-Stemmann, A. Hoffmann and M. S. Denison (2014). "Cross-talk between aryl hydrocarbon receptor and the inflammatory response: a role for nuclear factor-kappaB." J Biol Chem **289**(3): 1866-1875.

Vogel, C. F. and F. Matsumura (2009). "A new cross-talk between the aryl hydrocarbon receptor and RelB, a member of the NF-kappaB family." Biochem Pharmacol **77**(4): 734-745.

Vogel, C. F. A., E. Sciullo, W. Li, P. Wong, G. Lazennec and F. Matsumura (2007). "RelB, a New Partner of Aryl Hydrocarbon Receptor-Mediated Transcription." Molecular Endocrinology **21**(12): 2941-2955.

Wang, Y.-C., C.-L. Chen, B.-S. Sheu, Y.-J. Yang, P.-C. Tseng, C.-Y. Hsieh and C.-F. Lin (2014). "Helicobacter pylori Infection Activates Src Homology-2 Domain–Containing Phosphatase 2 To Suppress IFN-γ Signaling." The Journal of Immunology **193**(8): 4149-4158.

Warren, J. R. and B. Marshall (1983). "Unidentified curved bacilli on gastric epithelium in active chronic gastritis." Lancet **1**(8336): 1273-1275.

Weddle, E. and H. Agaisse (2018). "Principles of intracellular bacterial pathogen spread from cell to cell." PLoS Pathog **14**(12): e1007380.

Weighardt, H., M. Shapiro, M. Mayer, I. Förster, B. Stockinger and N. L. Diny (2024). "The aryl hydrocarbon receptor (AHR) repressor limits expression of antimicrobial genes but not AHR-dependent genes in intestinal eosinophils." Journal of Leukocyte Biology: qiae105.

Wertz, I. E., K. M. O'rourke, H. Zhou, M. Eby, L. Aravind, S. Seshagiri, P. Wu, C. Wiesmann, R. Baker and D. L. Boone (2004). "De-ubiquitination and ubiquitin ligase domains of A20 downregulate NF-κB signalling." Nature **430**(7000): 694-699.

Wilson, S. R., A. D. Joshi and C. J. Elferink (2013). "The Tumor Suppressor Kruppel-Like Factor 6 Is a Novel Aryl Hydrocarbon Receptor DNA Binding Partner." Journal of Pharmacology and Experimental Therapeutics **345**(3): 419-429.

Wincent, E., J. Bengtsson, A. Mohammadi Bardbori, T. Alsberg, S. Luecke, U. Rannug and A. Rannug (2012). "Inhibition of cytochrome P4501-dependent clearance of the endogenous agonist FICZ as a mechanism for activation of the aryl hydrocarbon receptor." Proc Natl Acad Sci U S A **109**(12): 4479-4484.

Wu, J. Y., Y. C. Lee and D. Y. Graham (2019). "The eradication of Helicobacter pylori to prevent gastric cancer: a critical appraisal." Expert Rev Gastroenterol Hepatol **13**(1): 17-24.

Wu, T., E. Hu, S. Xu, M. Chen, P. Guo, Z. Dai, T. Feng, L. Zhou, W. Tang, L. Zhan, X. Fu, S. Liu, X. Bo and G. Yu (2021). "clusterProfiler 4.0: A universal enrichment tool for interpreting omics data." The Innovation **2**(3): 100141.

Xia, H. X., X. G. Fan and N. J. Talley (1999). "Clarithromycin resistance in Helicobacter pylori and its clinical relevance." World J Gastroenterol **5**(3): 263-266.

Xiao, W., J. Son, S. U. Vorrink, F. E. Domann and P. C. Goswami (2015). "Ligand-independent activation of aryl hydrocarbon receptor signaling in PCB3-quinone treated HaCaT human keratinocytes." Toxicol Lett **233**(3): 258-266.

Xie, F., J. Wang and B. Zhang (2023). "RefFinder: a web-based tool for comprehensively analyzing and identifying reference genes." Functional & Integrative Genomics **23**(2): 125.

Xie, F., P. Xiao, D. Chen, L. Xu and B. Zhang (2012). "miRDeepFinder: a miRNA analysis tool for deep sequencing of plant small RNAs." Plant Mol Biol.

Yamada, T., H. Horimoto, T. Kameyama, S. Hayakawa, H. Yamato, M. Dazai, A. Takada, H. Kida, D. Bott, A. C. Zhou, D. Hutin, T. H. Watts, M. Asaka, J. Matthews and A. Takaoka (2016). "Constitutive aryl hydrocarbon receptor signaling constrains type I interferon–mediated antiviral innate defense." Nature Immunology **17**(6): 687-694.

Yan, L., Y. Chen, F. Chen, T. Tao, Z. Hu, J. Wang, J. You, B. C. Y. Wong, J. Chen and W. Ye (2022). "Effect of Helicobacter pylori Eradication on Gastric Cancer Prevention: Updated Report From a Randomized Controlled Trial With 26.5 Years of Follow-up." Gastroenterology **163**(1): 154-162.e153.

Yang, L., C. Kartsonaki, P. Yao, C. de Martel, M. Plummer, D. Chapman, Y. Guo, S. Clark, R. G. Walters, Y. Chen, P. Pei, J. Lv, C. Yu, R. Jeske, T. Waterboer, G. M. Clifford, S. Franceschi, R. Peto, M. Hill, L. Li, I. Y. Millwood and Z. Chen (2021). "The relative and attributable risks of cardia and non-cardia gastric cancer associated with Helicobacter pylori infection in China: a case-cohort study." Lancet Public Health **6**(12): e888-e896.

Yao, E. F. and M. S. Denison (1992). "DNA sequence determinants for binding of transformed Ah receptor to a dioxin-responsive enhancer." Biochemistry **31**(21): 5060-5067.

Yeste, A., M. C. Takenaka, I. D. Mascanfroni, M. Nadeau, J. E. Kenison, B. Patel, A. M. Tukpah, J. A. Babon, M. DeNicola, S. C. Kent, D. Pozo and F. J. Quintana (2016). "Tolerogenic nanoparticles inhibit T cell-mediated autoimmunity through SOCS2." Sci Signal **9**(433): ra61.

Yin, X., P. Krikorian, T. Logan and V. Csizmadia (2010). "Induction of RIP-2 kinase by proinflammatory cytokines is mediated via NF-kappaB signaling pathways and involves a novel feed-forward regulatory mechanism." Mol Cell Biochem **333**(1-2): 251-259.

Yoda, T., T. Tochitani, T. Usui, M. Kouchi, H. Inada, T. Hosaka, Y. Kanno, I. Miyawaki and K. Yoshinari (2022). "Involvement of the CYP1A1 inhibition-mediated activation of aryl hydrocarbon receptor in drug-induced hepatotoxicity." The Journal of Toxicological Sciences **47**(9): 359-373.

Yoshimatsu, Y., T. Sujino, K. Miyamoto, Y. Harada, S. Tanemoto, K. Ono, S. Umeda, K. Yoshida, T. Teratani, T. Suzuki, Y. Mikami, N. Nakamoto, N. Sasaki, K. Takabayashi, N. Hosoe, H. Ogata, K. Sawada, T. Imamura, A. Yoshimura and T. Kanai (2022). "Aryl hydrocarbon receptor signals in epithelial cells govern the recruitment and location of Helios+ Tregs in the gut." Cell Reports **39**(6): 110773.

Young, D. F., T. S. Carlos, K. Hagmaier, L. Fan and R. E. Randall (2007). "AGS and other tissue culture cells can unknowingly be persistently infected with PIV5; a virus that blocks interferon signalling by degrading STAT1." Virology **365**(1): 238-240.

Yun, C. H., A. Lundgren, J. Azem, Å. Sjöling, J. Holmgren, A.-M. Svennerholm and B. S. Lundin (2005). "Natural Killer Cells and Helicobacter pylori Infection: Bacterial Antigens and Interleukin-12 Act Synergistically To Induce Gamma Interferon Production." Infection and Immunity **73**(3): 1482-1490.

Zeng, M., X. H. Mao, J. X. Li, W. D. Tong, B. Wang, Y. J. Zhang, G. Guo, Z. J. Zhao, L. Li, D. L. Wu, D. S. Lu, Z. M. Tan, H. Y. Liang, C. Wu, D. H. Li, P. Luo, H. Zeng, W. J. Zhang, J. Y. Zhang, B. T. Guo, F. C. Zhu and Q. M. Zou (2015). "Efficacy, safety, and immunogenicity of an oral recombinant Helicobacter pylori vaccine in children in China: a randomised, double-blind, placebo-controlled, phase 3 trial." Lancet **386**(10002): 1457-1464.

Zhang, Q., Y. Zhu, C. Lv, Y. Fang, M. Liao, Y. Xia, Z. Wei and Y. Dai (2023). "AhR activation promotes Treg cell generation by enhancing Lkb1-mediated fatty acid oxidation via the Skp2/K63-ubiquitination pathway." Immunology **169**(4): 412-430.

Zheng, P. Y. and N. L. Jones (2003). "Helicobacter pylori strains expressing the vacuolating cytotoxin interrupt phagosome maturation in macrophages by recruiting and retaining TACO (coronin 1) protein." Cell Microbiol **5**(1): 25-40.

Zhou, P., Y. She, N. Dong, P. Li, H. He, A. Borio, Q. Wu, S. Lu, X. Ding, Y. Cao, Y. Xu, W. Gao, M. Dong, J. Ding, D.-C. Wang, A. Zamyatina and F. Shao (2018). "Alpha-kinase 1 is a cytosolic innate immune receptor for bacterial ADP-heptose." Nature.

Zhou, Z., G. Xia, Z. Xiang, M. Liu, Z. Wei, J. Yan, W. Chen, J. Zhu, N. Awasthi, X. Sun, K. M. Fung, Y. He, M. Li and C. Zhang (2019). "A C-X-C Chemokine Receptor Type 2-Dominated Cross-talk between Tumor Cells and Macrophages Drives Gastric Cancer Metastasis." Clin Cancer Res **25**(11): 3317-3328.

Zhu, J., L. Luo, L. Tian, S. Yin, X. Ma, S. Cheng, W. Tang, J. Yu, W. Ma, X. Zhou, X. Fan, X. Yang, J. Yan, X. Xu, C. Lv and H. Liang (2018). "Aryl Hydrocarbon Receptor Promotes IL-10 Expression in Inflammatory Macrophages Through Src-STAT3 Signaling Pathway." Front Immunol **9**: 2033.

Zhu, R., C. Gao, L. Wang, G. Zhang, W. Zhang, Z. Zhang, L. Shen and S. Wang (2018). "Involvement of Aryl Hydrocarbon Receptor and Aryl Hydrocarbon Receptor Repressor in Helicobacter Pylori-related Gastric Pathogenesis." J Cancer **9**(15): 2757-2764.

Zimmermann, S., L. Pfannkuch, M. A. Al-Zeer, S. Bartfeld, M. Koch, J. Liu, C. Rechner, M. Soerensen, O. Sokolova, A. Zamyatina, P. Kosma, A. P. Maurer, F. Glowinski, K. P. Pleissner, M. Schmid, V. Brinkmann, A. Karlas, M. Naumann, M. Rother, N. Machuy and T. F. Meyer (2017). "ALPK1- and TIFA-Dependent Innate Immune Response Triggered by the Helicobacter pylori Type IV Secretion System." Cell Rep **20**(10): 2384-2395.

Appendix

7.1 Supplementary data

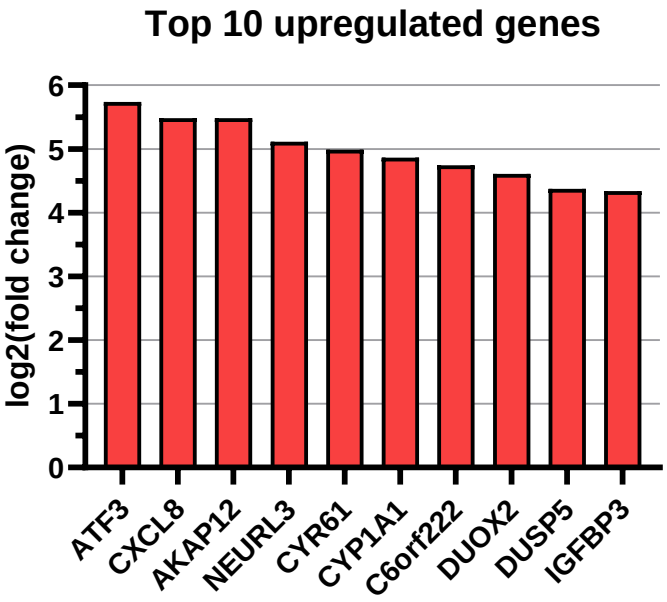

Figure 7.1.1 | Microarray analysis of gene expression in human primary mucosoid cultures infected with *H. pylori*.
Fold change was calculated as ratio of gene expression after infection to gene expression in non-infected cells. Differences in gene expression between infected and non-infected cells were tested for statistical significance by paired t-test. All genes shown passed the threshold of $p<0.05$.

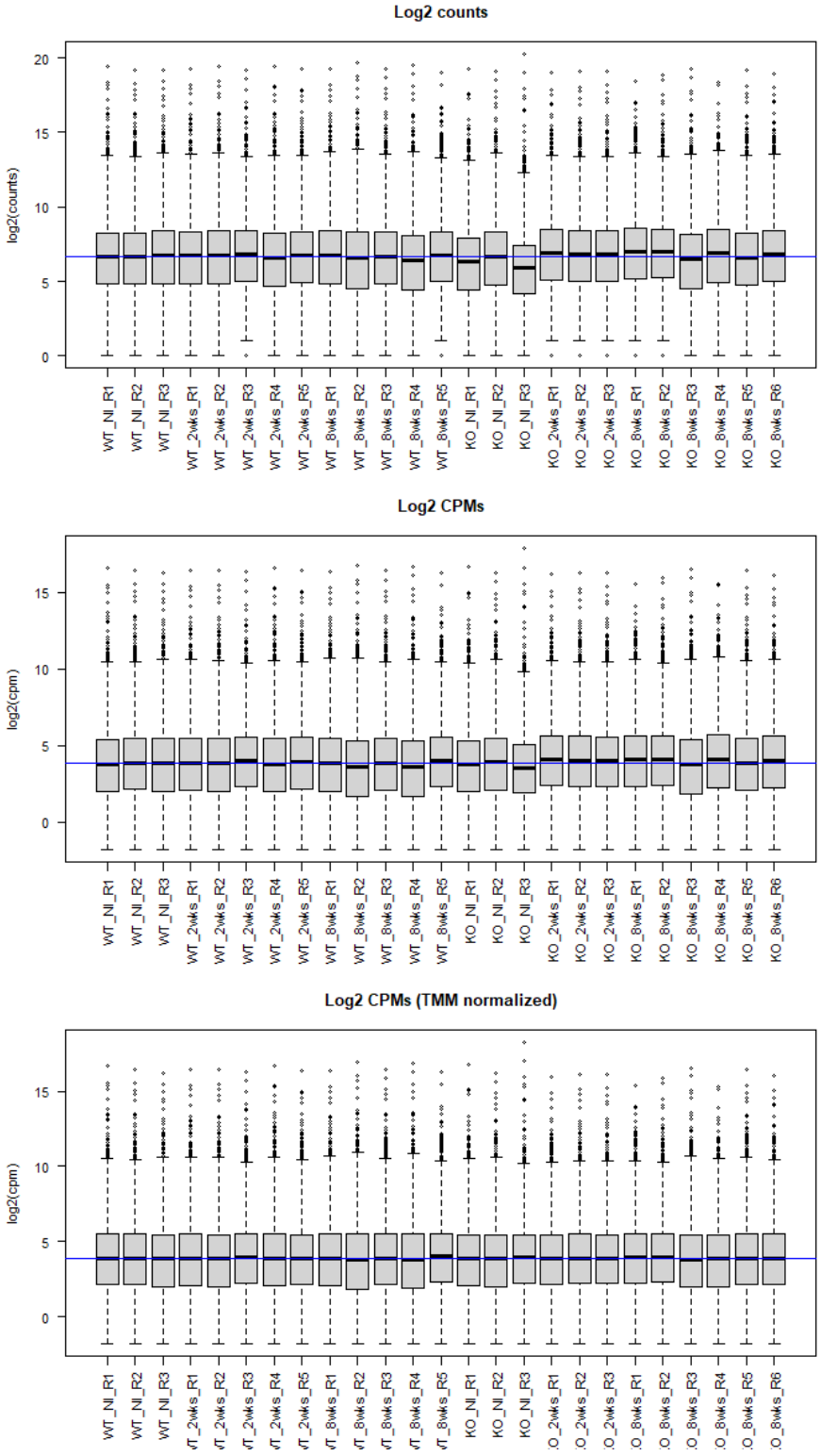

Figure 7.1.2 | Normalisation of library sizes after RNA sequencing to correct for sequencing depth and compositional bias (antrum).
Sequencing of RNA from mouse stomach antrum tissue. Top: Log2 of raw counts before normalisation. Middle: Log2 of counts per million counts (CPM), normalised for sequencing depth. Bottom: Log2 of CPM values, normalised for compositional bias using the TMM method (Robinson and Oshlack, 2010)

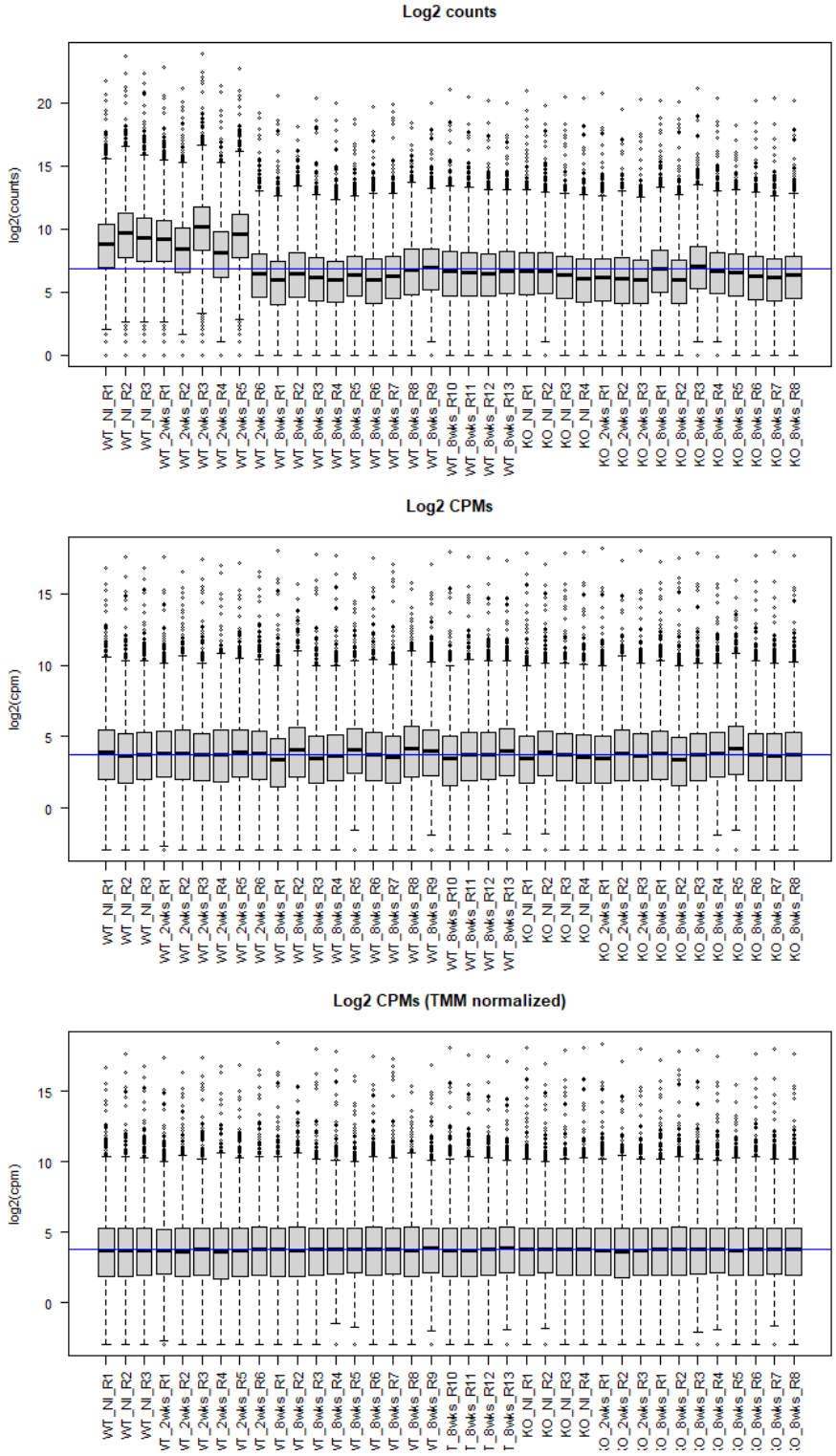

Figure 7.1.3 | Normalisation of library sizes after RNA sequencing to correct for sequencing depth and compositional bias (corpus).
Sequencing of RNA from mouse stomach corpus tissue. Top: Log2 of raw counts before normalisation. Middle: Log2 of counts per million counts (CPM), normalised for sequencing depth. Bottom: Log2 of CPM values, normalised for compositional bias using the TMM method (Robinson and Oshlack, 2010)

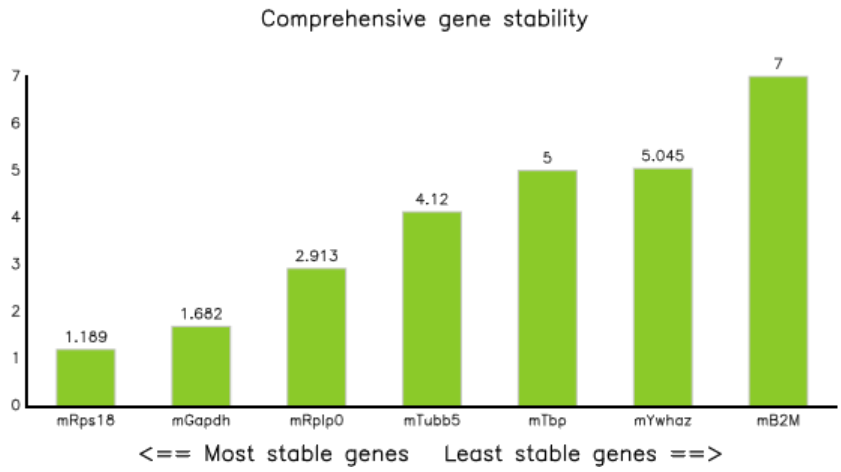

Figure 7.1.4 | Ranking of candidate reference genes for qPCR of murine cell samples.

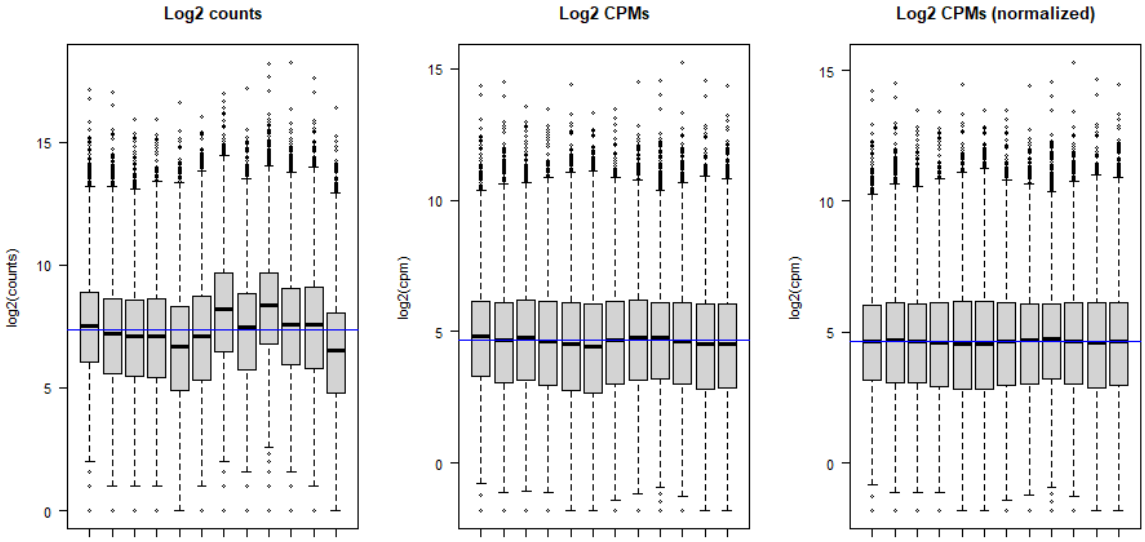

Figure 7.1.5 | Normalisation of library sizes after RNA sequencing to correct for sequencing depth and compositional bias (mucosoids).
Sequencing of RNA from mouse mucosoids. Left: Log2 of raw counts before normalisation. Middle: Log2 of counts per million counts (CPM), normalised for sequencing depth. Right: Log2 of CPM values, normalised for compositional bias using the TMM method (Robinson and Oshlack, 2010).

7.1.1 GSEA results mouse (antrum)

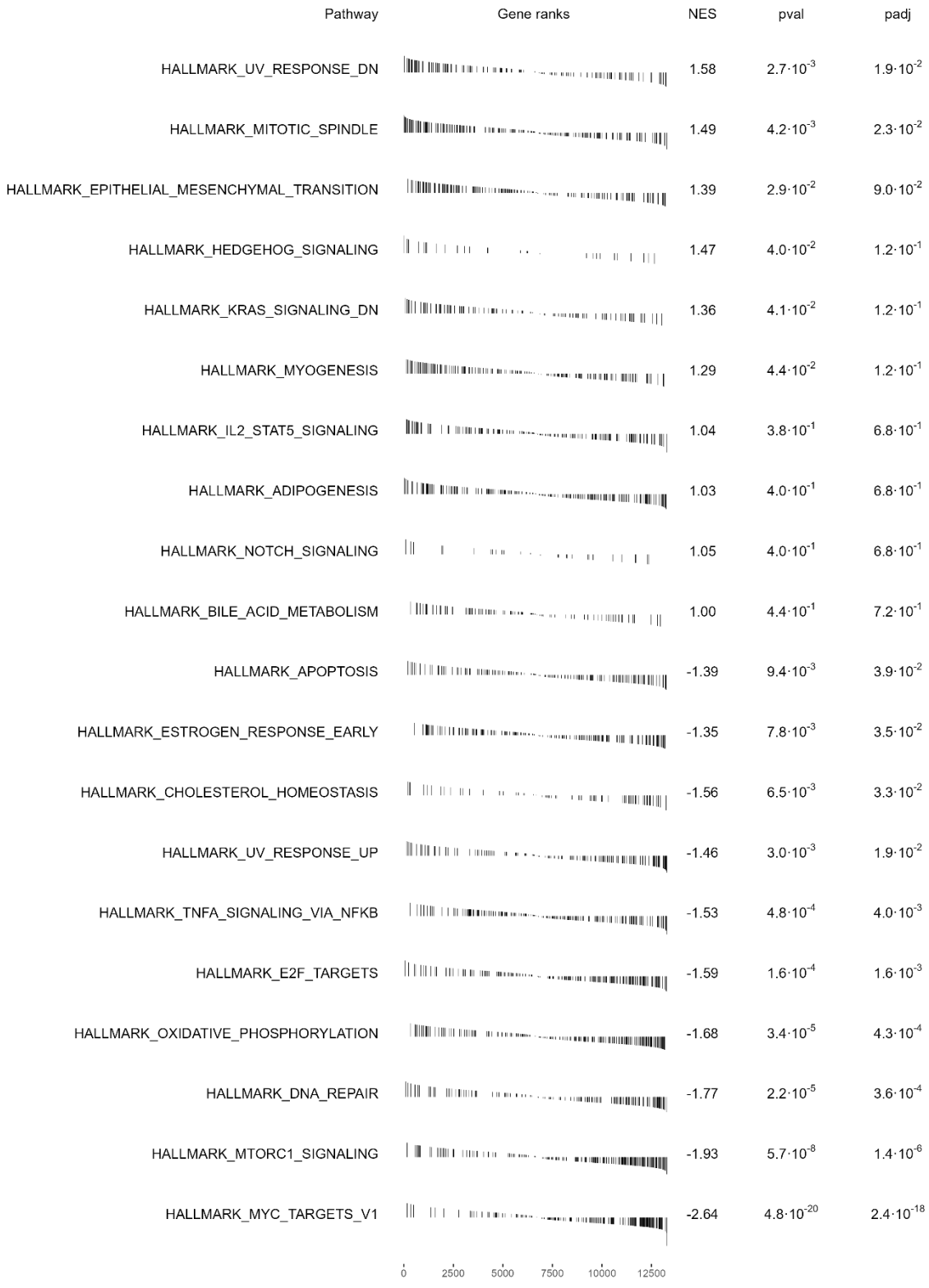

Figure 7.1.6 | GSEA results KO NI vs wild-type NI mouse (antrum)

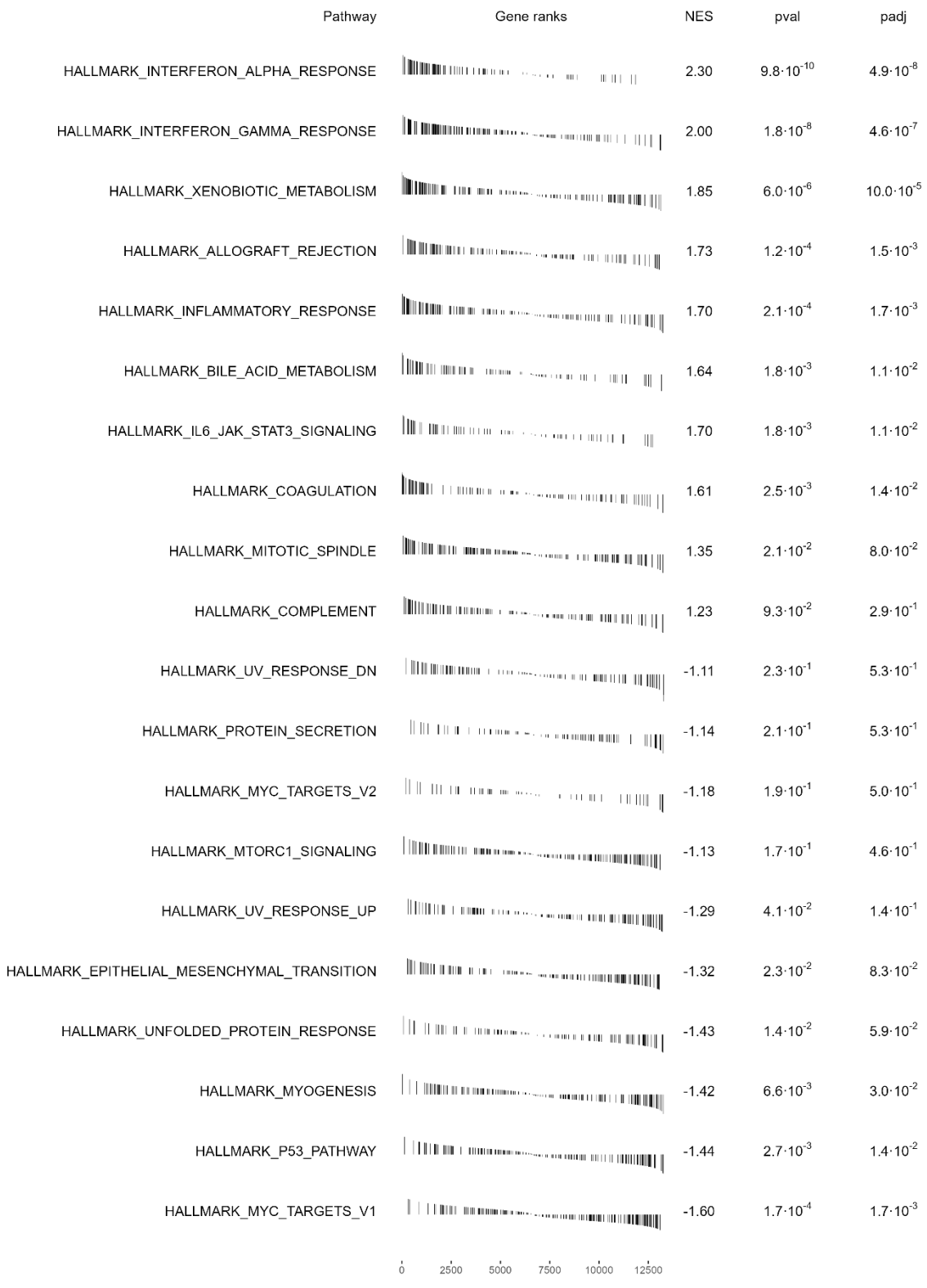

Figure 7.1.7 | GSEA results wild-type 2 weeks vs NI mouse (antrum)

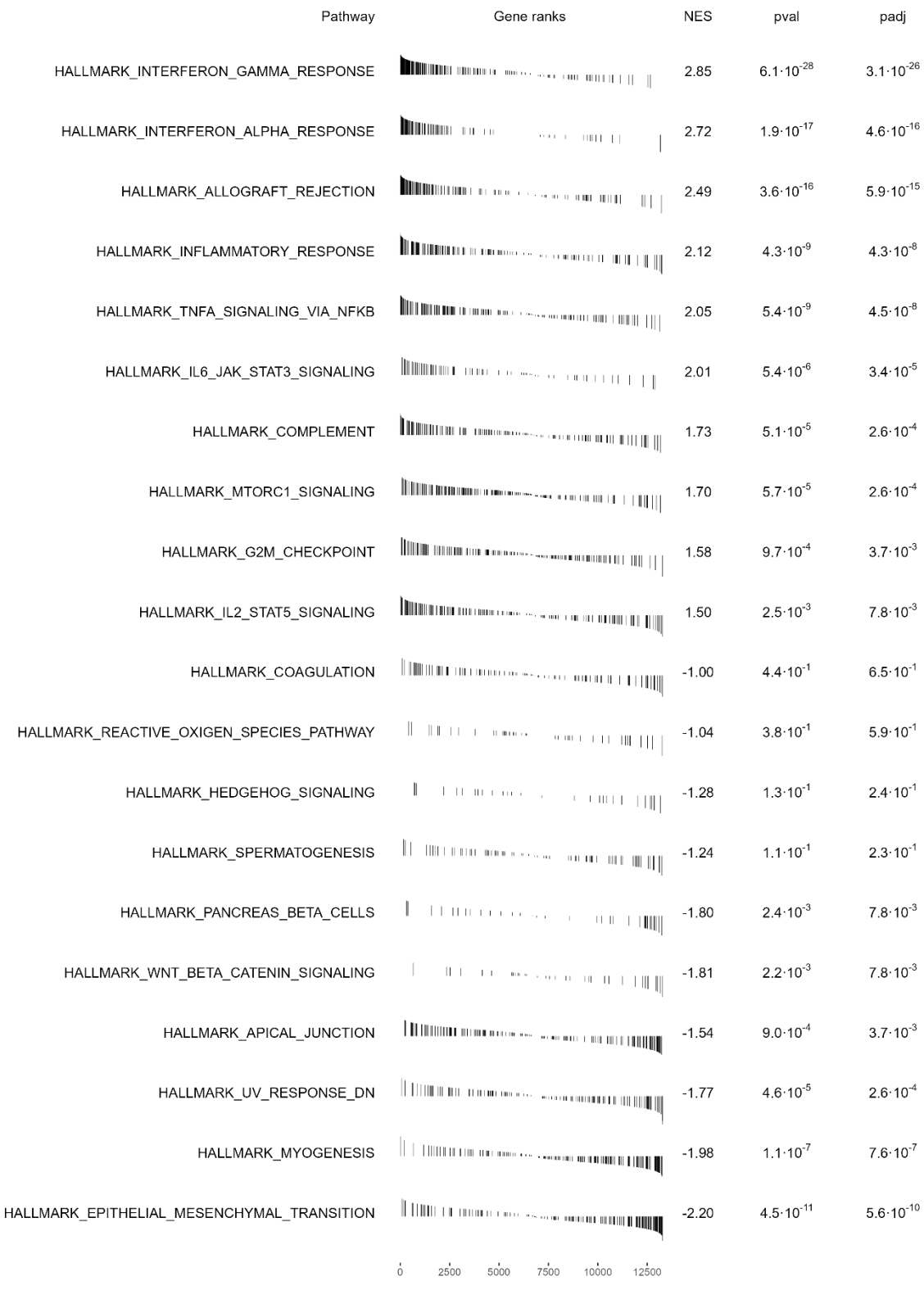

Figure 7.1.8 | GSEA results wild-type 8 weeks vs NI mouse (antrum)

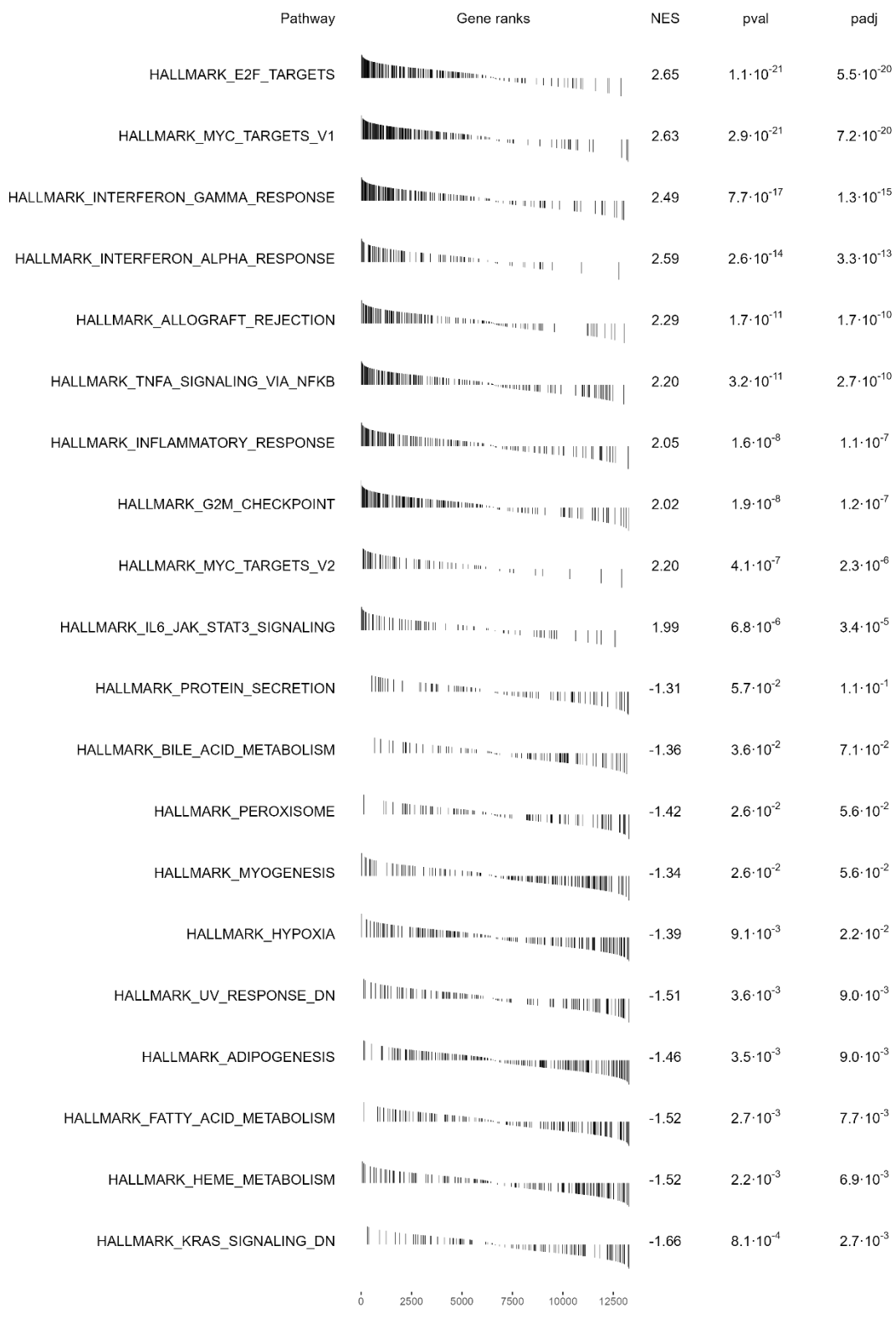

Figure 7.1.9 | GSEA results KO 2 weeks vs NI mouse (antrum)

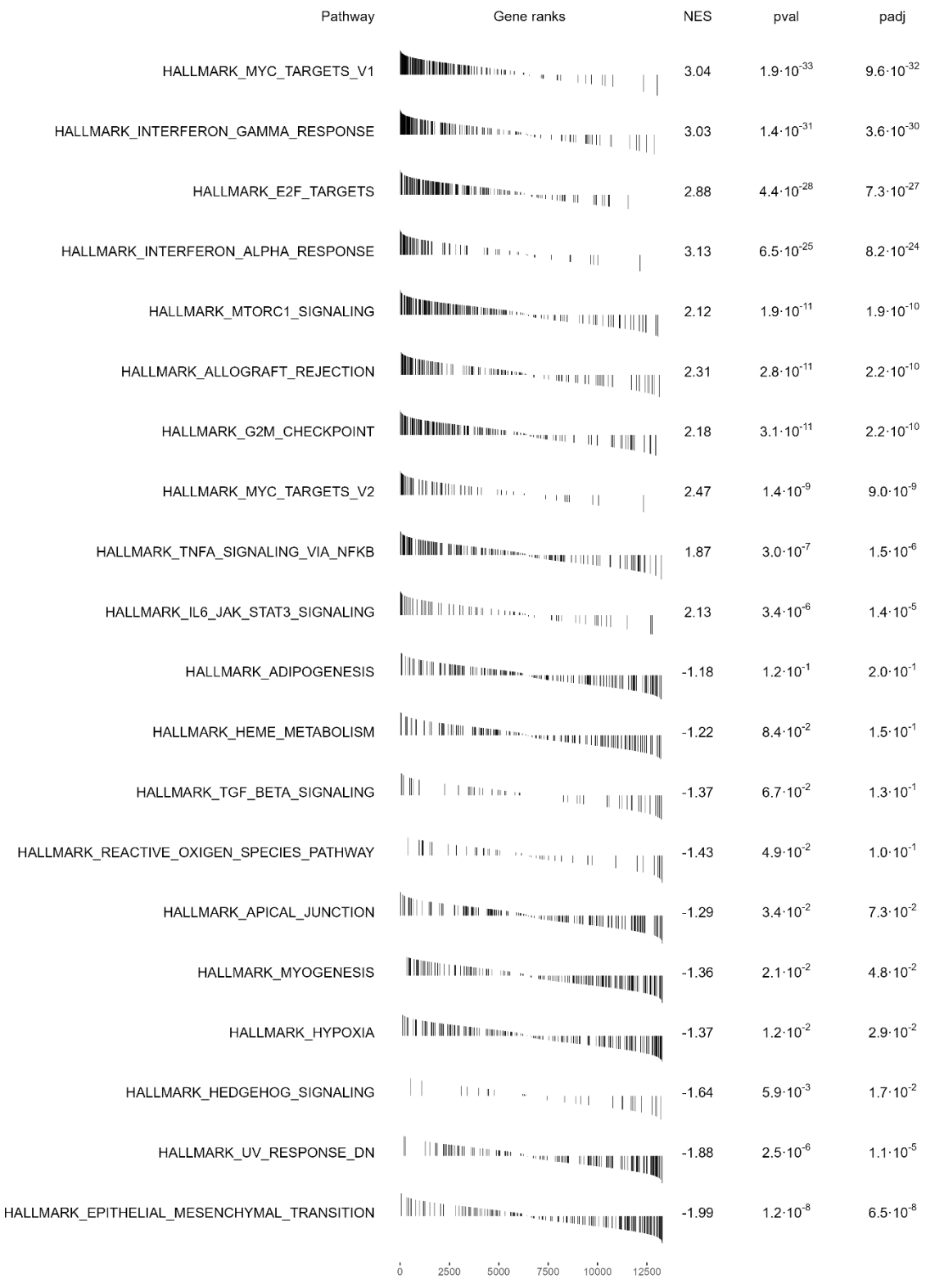

Figure 7.1.10 | GSEA results KO 8 weeks vs NI mouse (antrum)

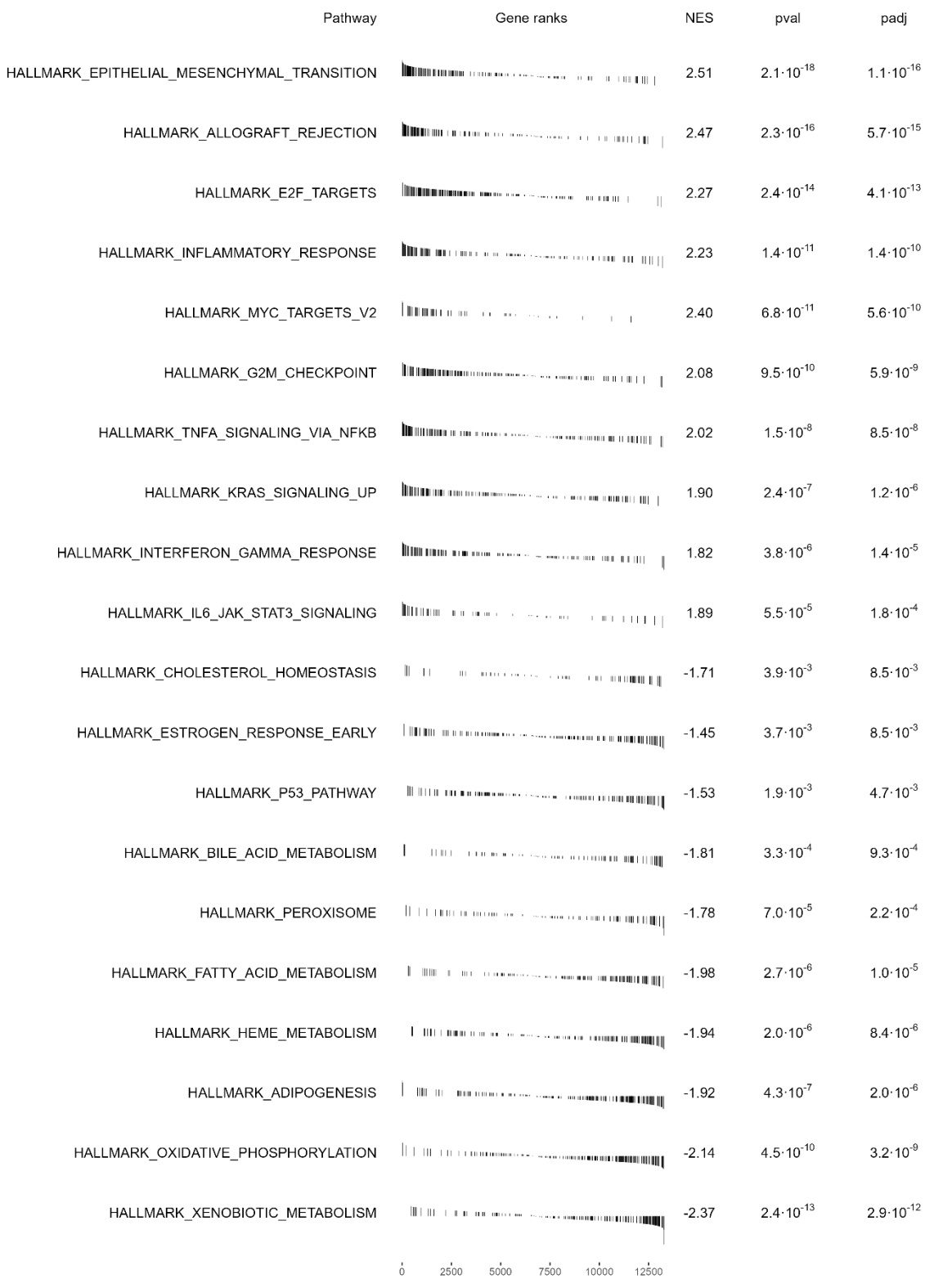

Figure 7.1.11 | GSEA results KO vs wild-type 2 weeks (antrum)

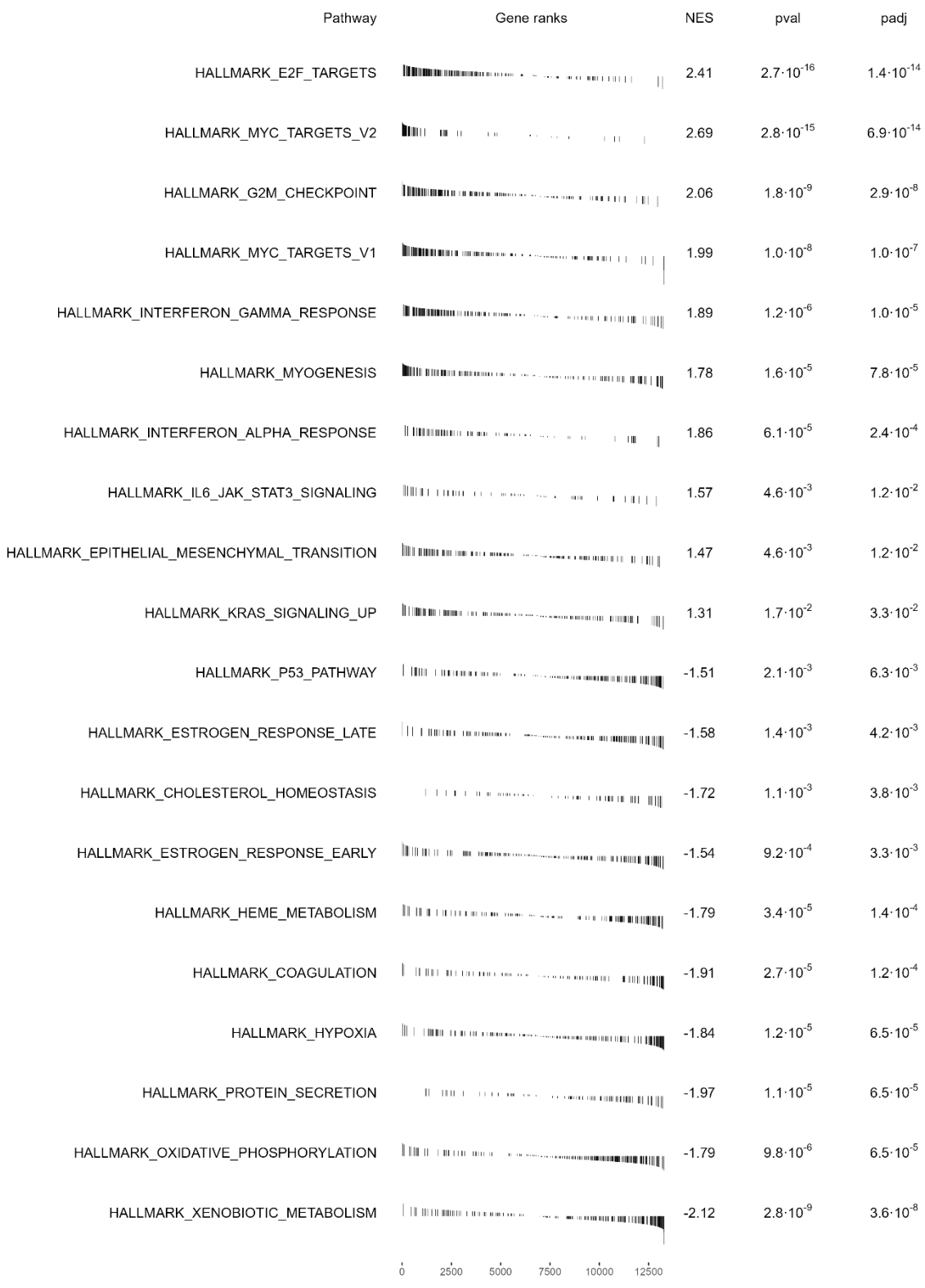

Figure 7.1.12 | GSEA results KO vs wild-type 8 weeks (antrum)

7.1.2 GSEA results mouse (corpus)

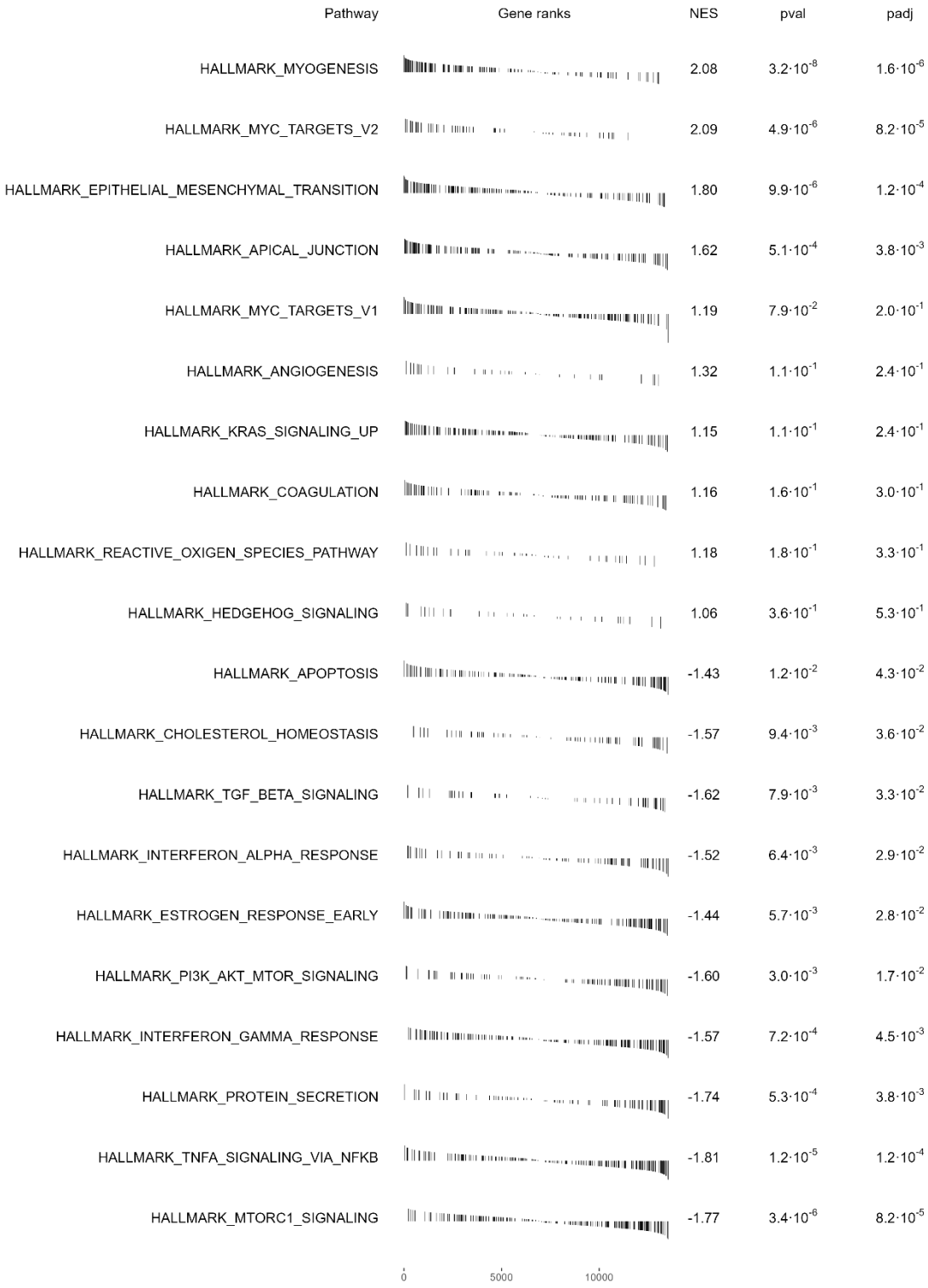

Figure 7.1.13 | GSEA results KO NI vs wild-type NI mouse (corpus)

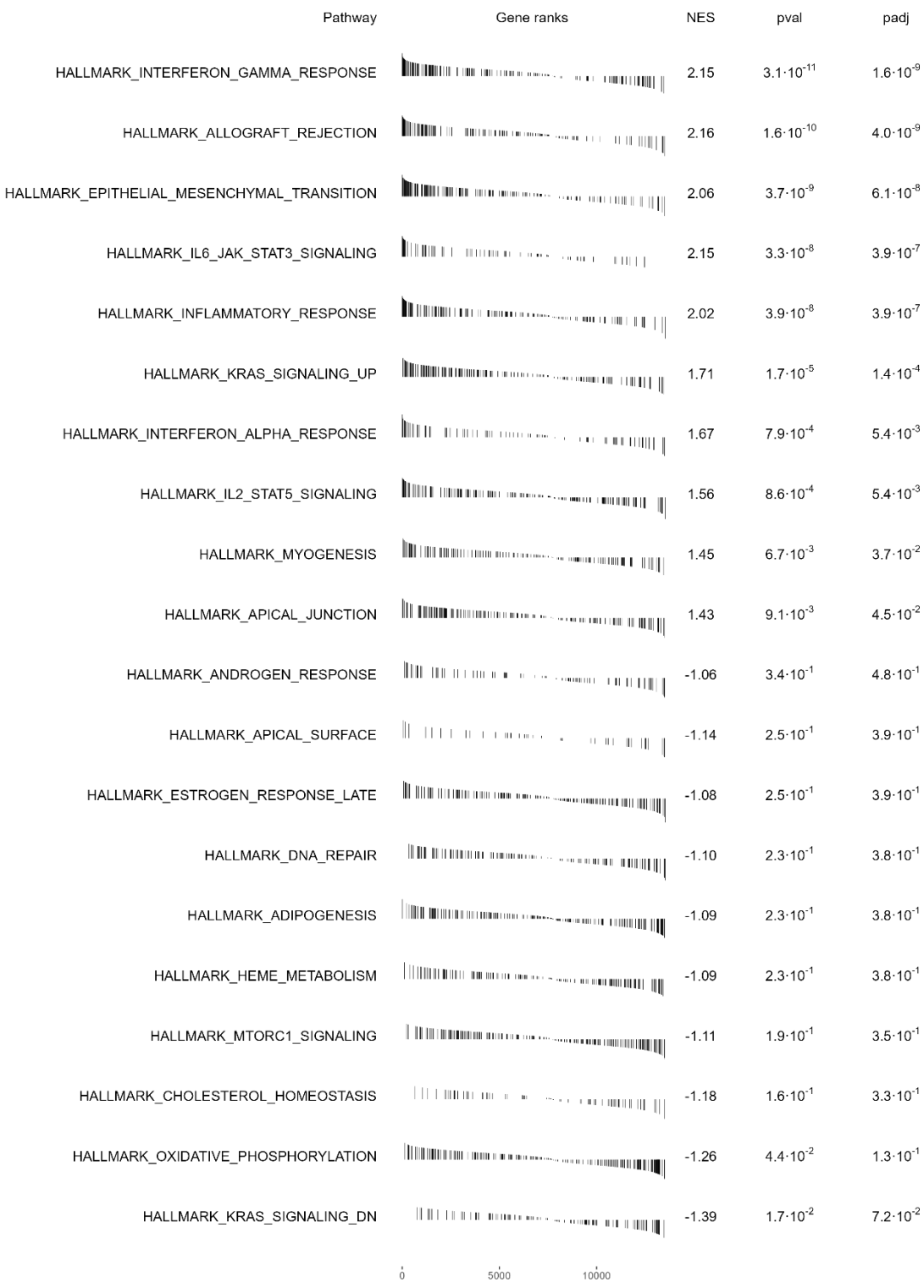

Figure 7.1.14 | GSEA results wild-type 2 wks vs wild-type NI mouse (corpus)

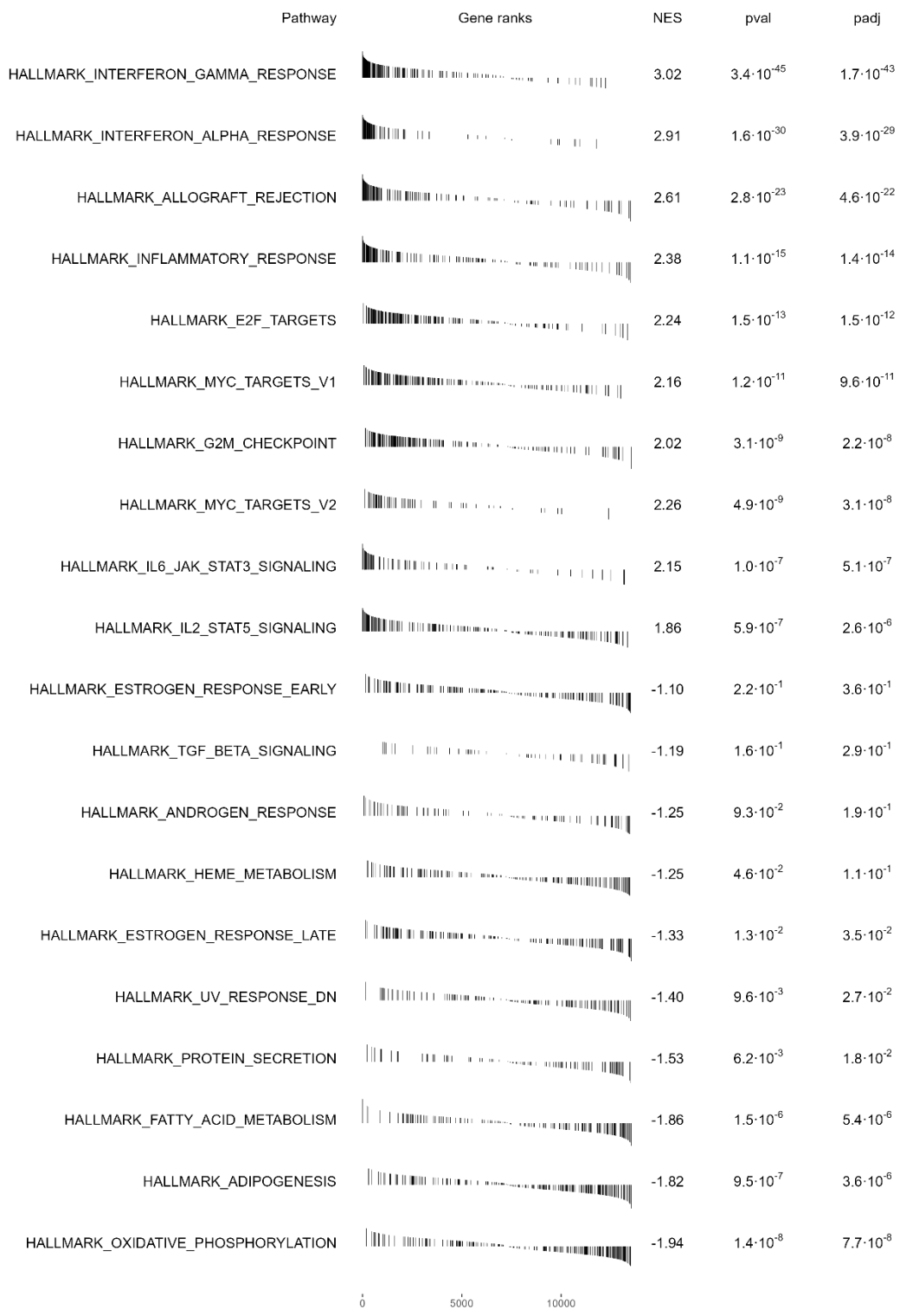

Figure 7.1.15 | GSEA results wild-type 8 wks vs wild-type NI mouse (corpus)

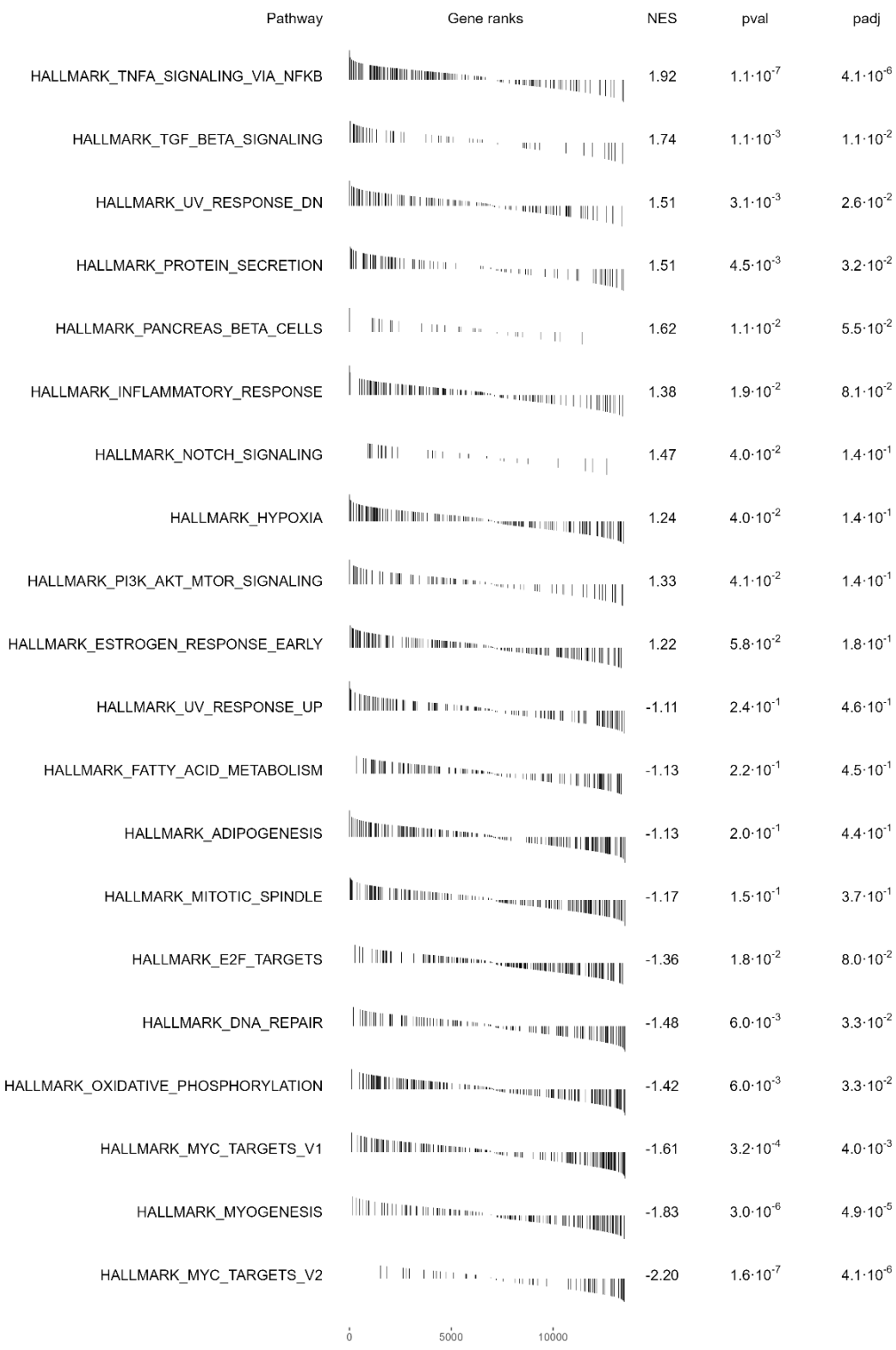

Figure 7.1.16 | GSEA results KO 2 wks vs KO NI mouse (corpus)

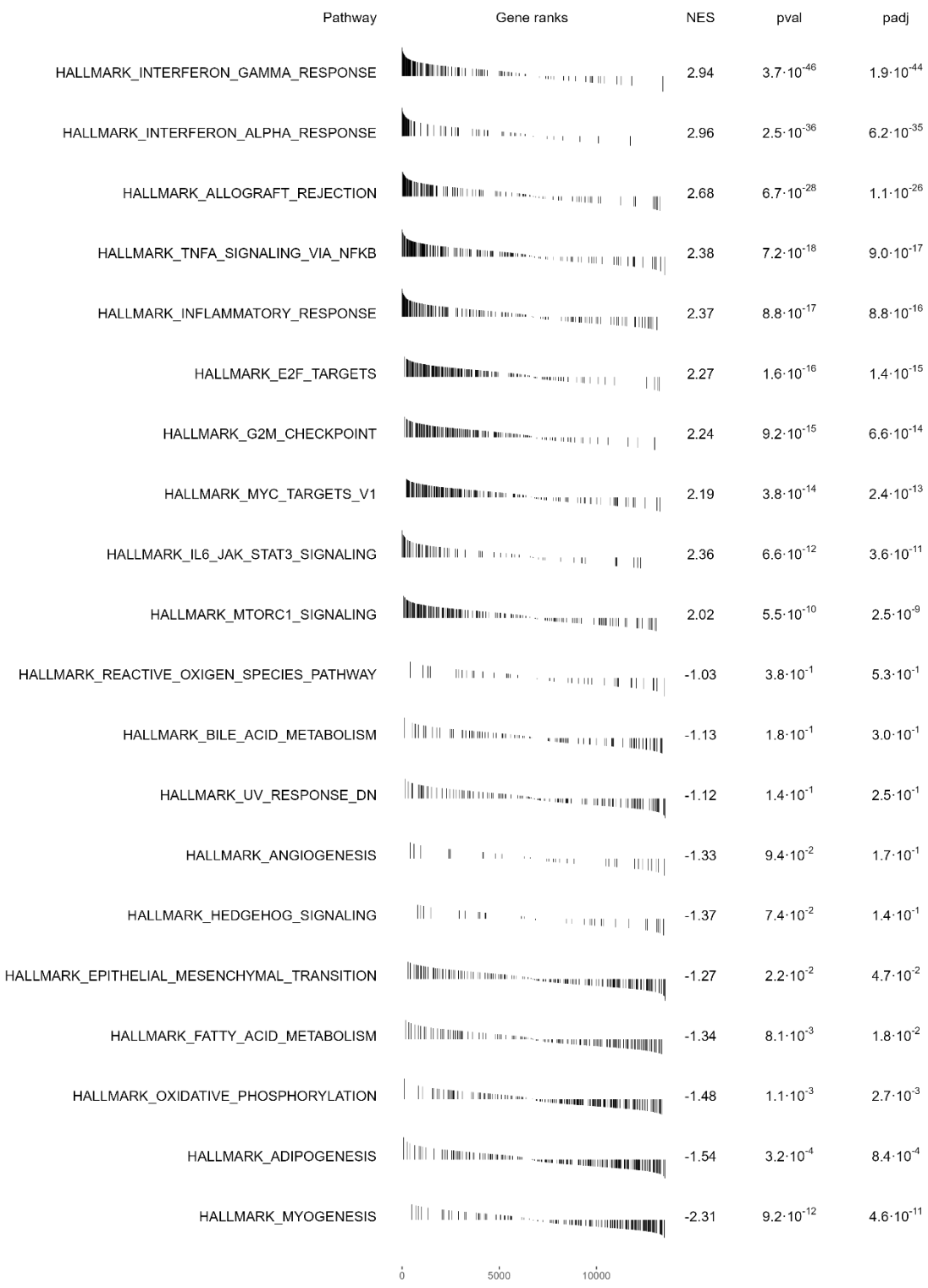

Figure 7.1.17 | GSEA results KO 8 wks vs KO NI mouse (corpus)

7.1.3 GSEA results mouse (mucosoids)

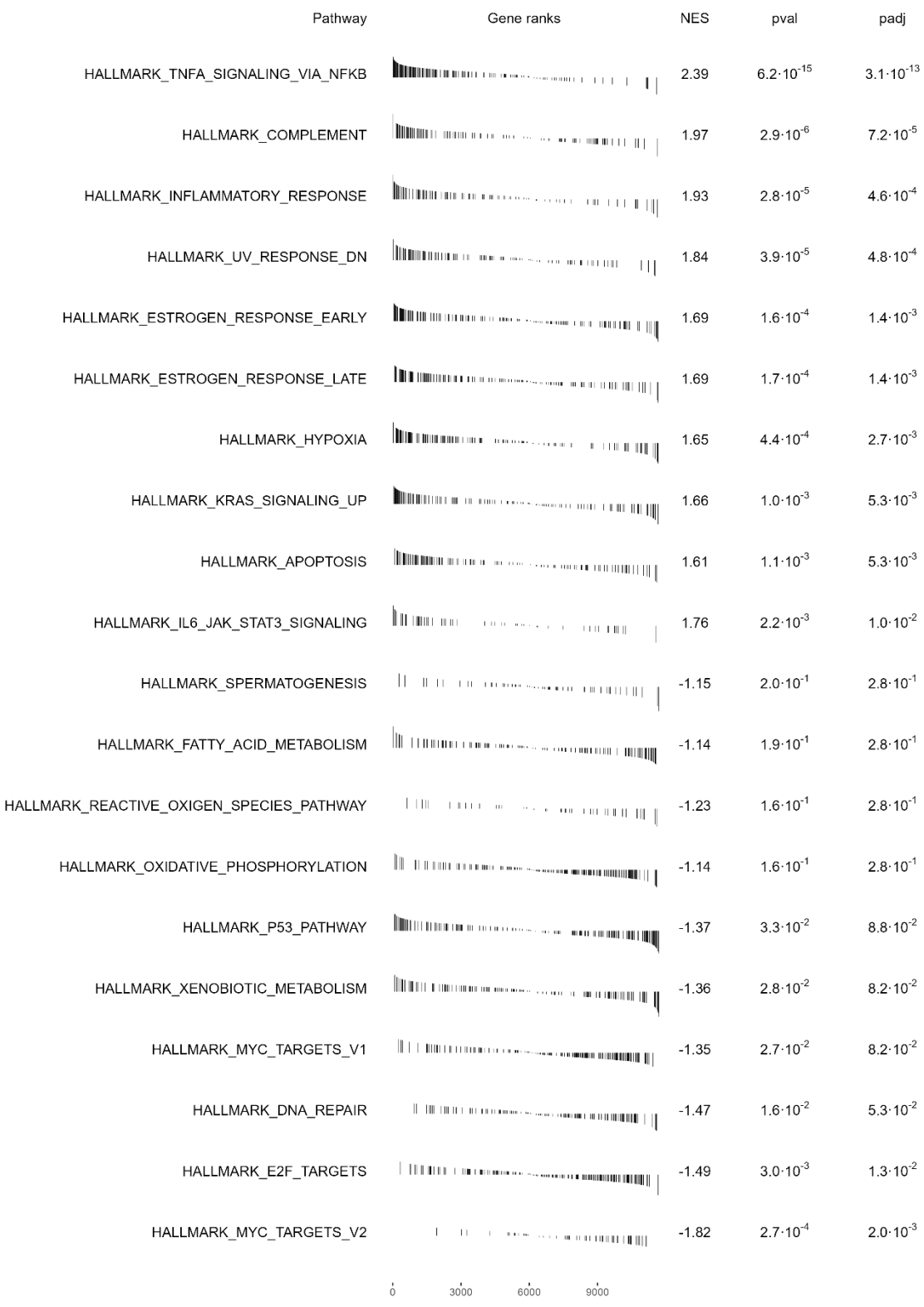

Figure 7.1.18 | GSEA results non-infected knockout vs wild-type cells (mucosoids)

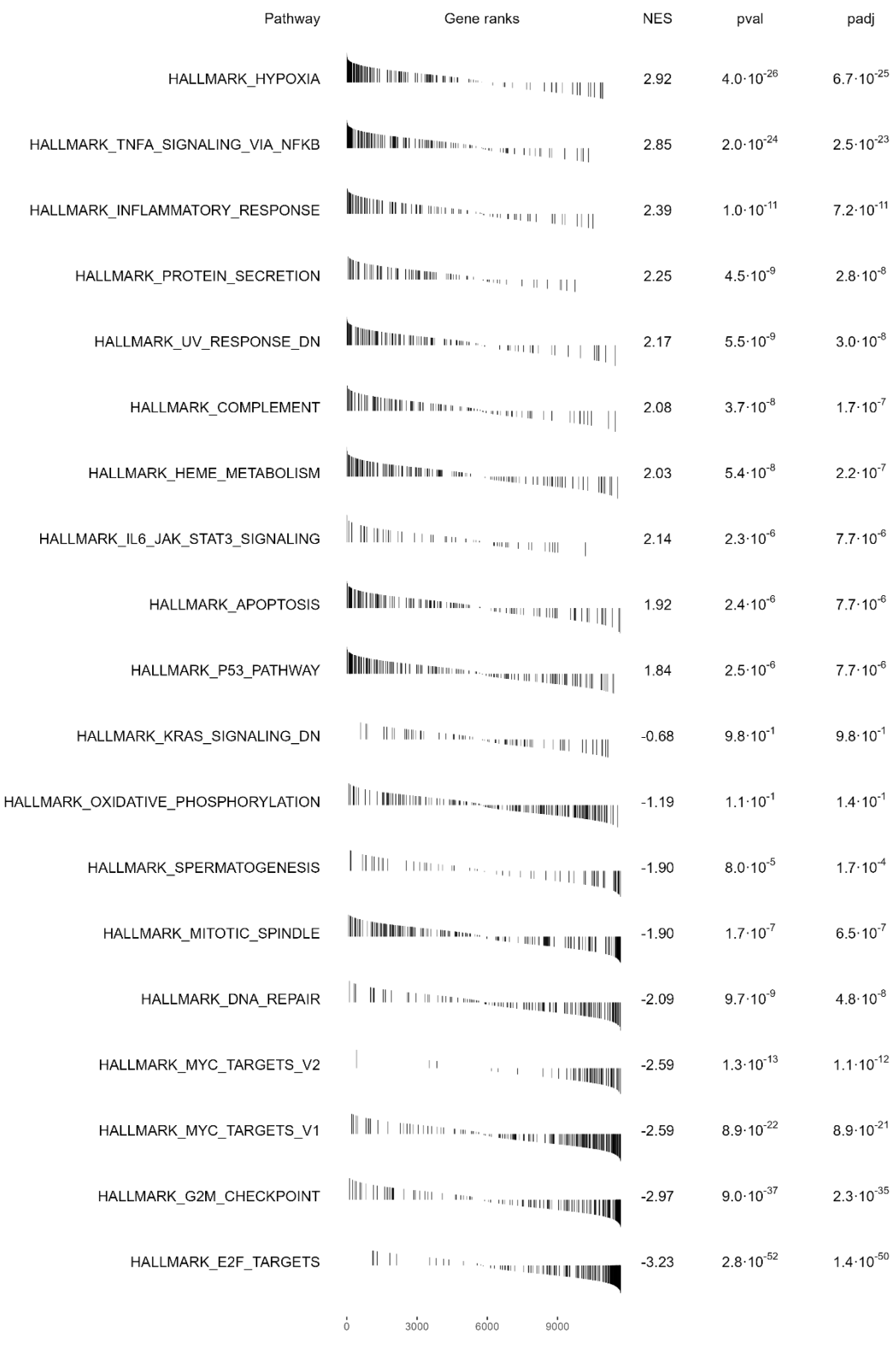

Figure 7.1.19 | GSEA results infected vs non-infected wild-type cells (mucosoids)

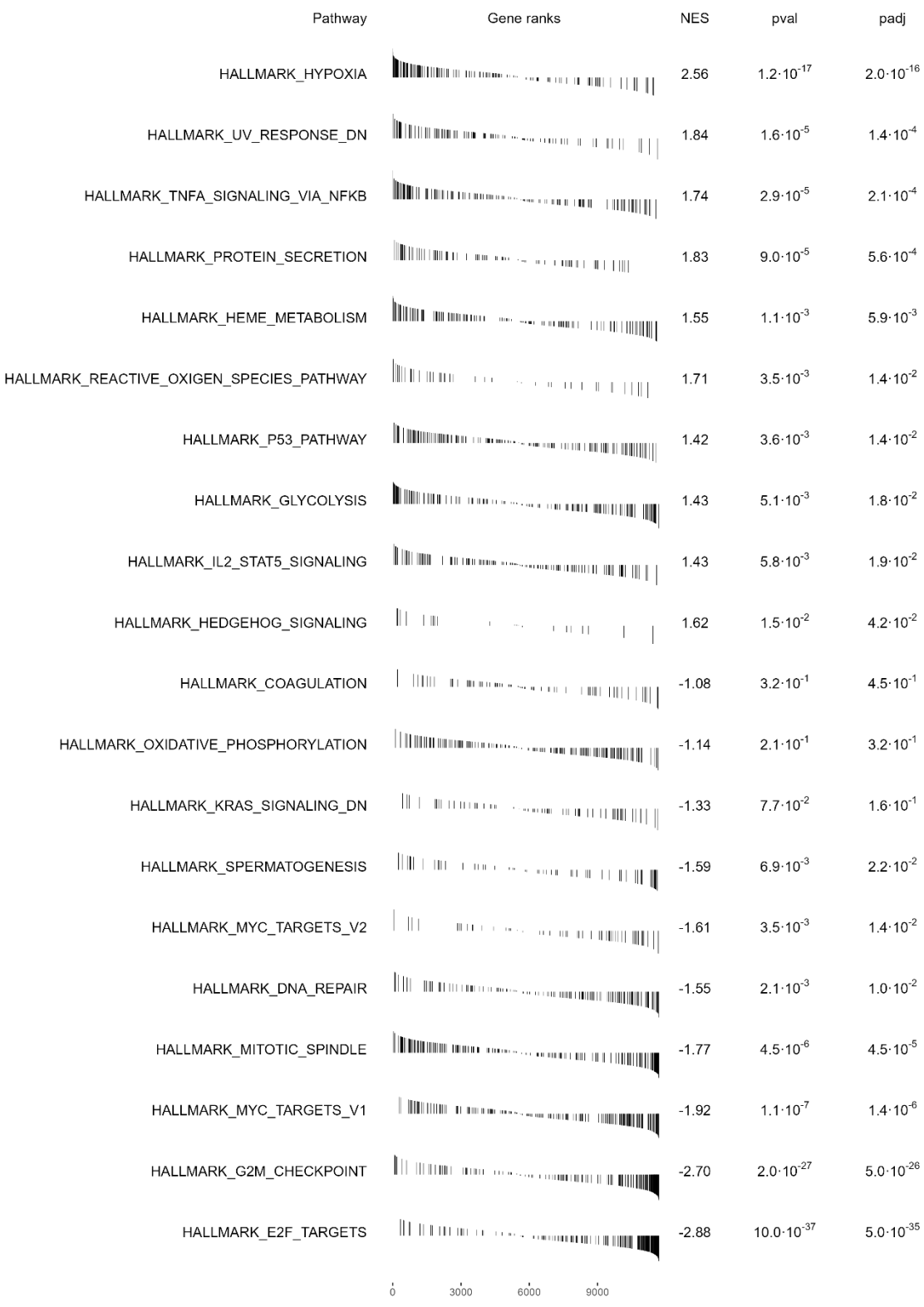

Figure 7.1.20 | GSEA results infected vs non-infected knockout cells (mucosoids)

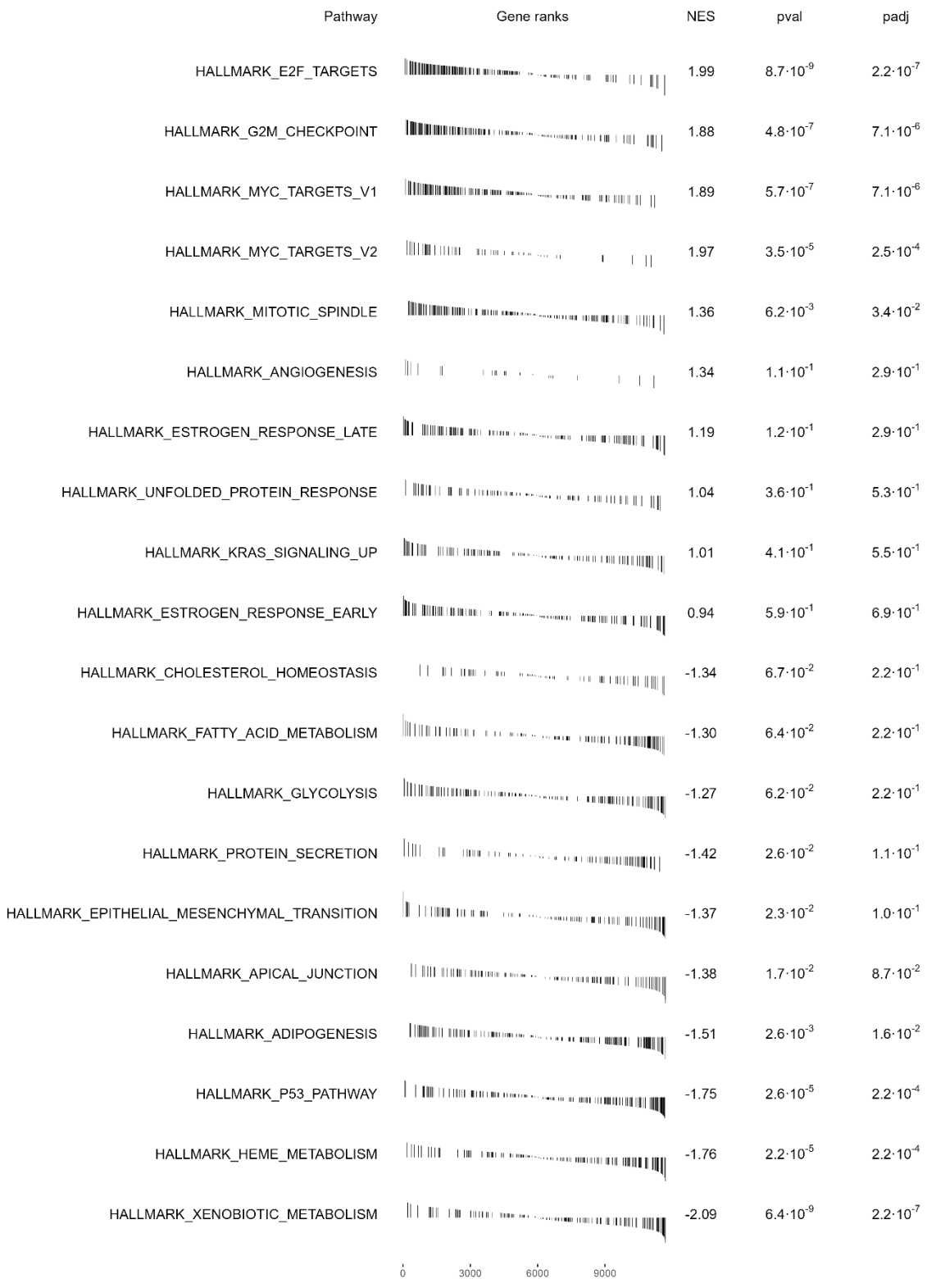

Figure 7.1.21 | GSEA results infected knockout vs wild-type cells (mucosoids)

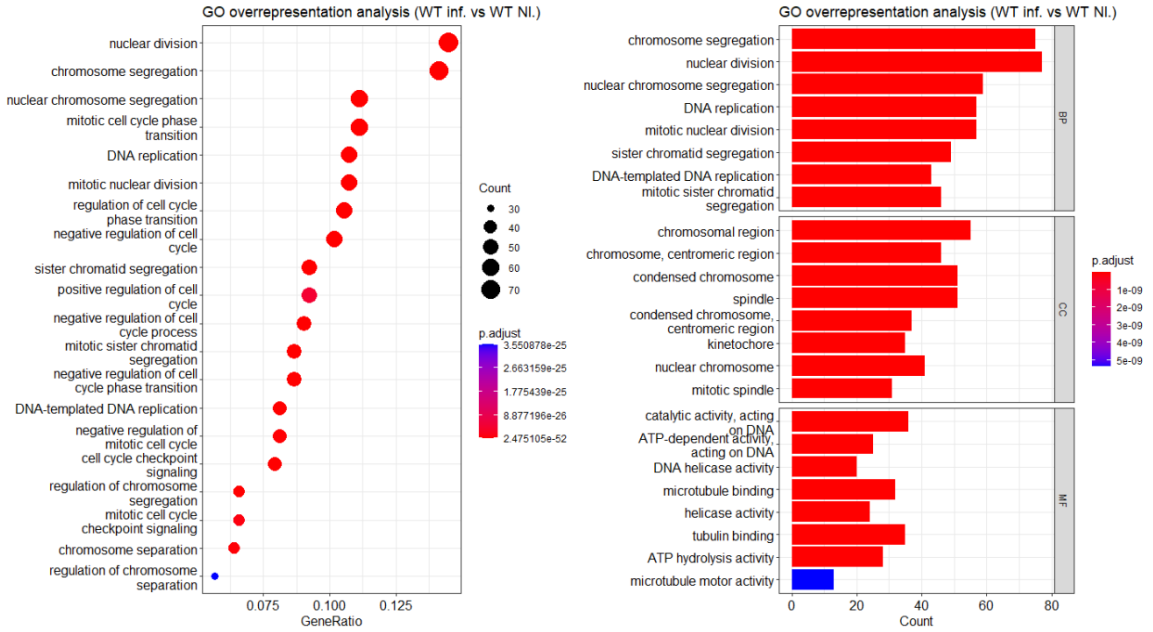

Figure 7.1.22 | GO overrepresentation analysis (wild-type inf vs wild-type NI) mucosoids

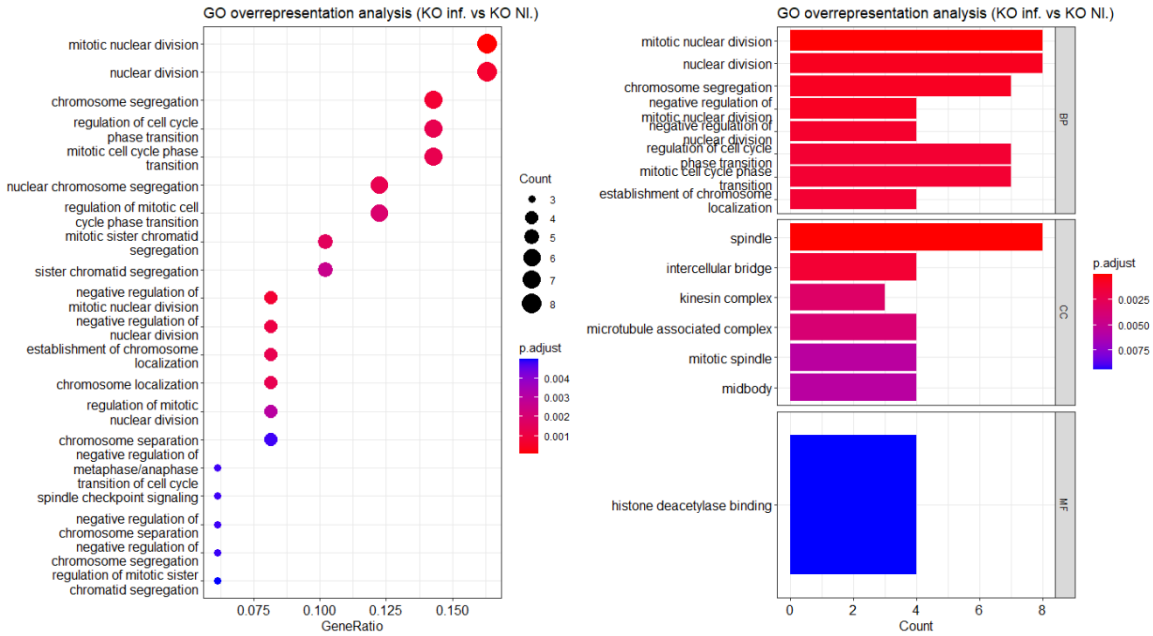

Figure 7.1.23 | GO overrepresentation analysis (KO inf. vs KO NI) mucosoids

7.2 Vector Maps

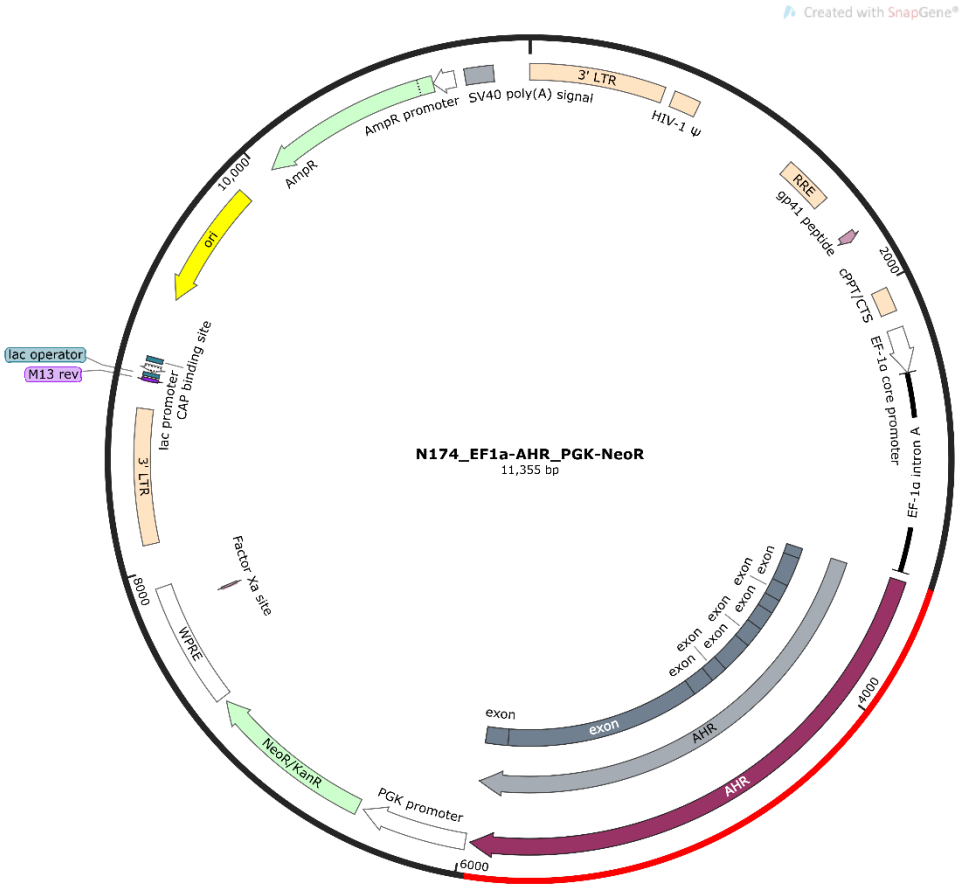

Figure 7.2.1 | N174_EF1a-AHR_PGK-NeoR.
Lentiviral vector used for AHR overexpression, based on the N174-MCS plasmid. Highlighted in red is the inserted AHR coding sequence.

Figure 7.2.2 | MISSION LV01 plasmid (U6-gRNA:ef1a-puro-2A-Cas9-2A-tGFP).
Lentiviral vector used for expression of Cas9 and an AHR-specific gRNA, used for knockout of AHR.